Science

30 July 2010 | $10

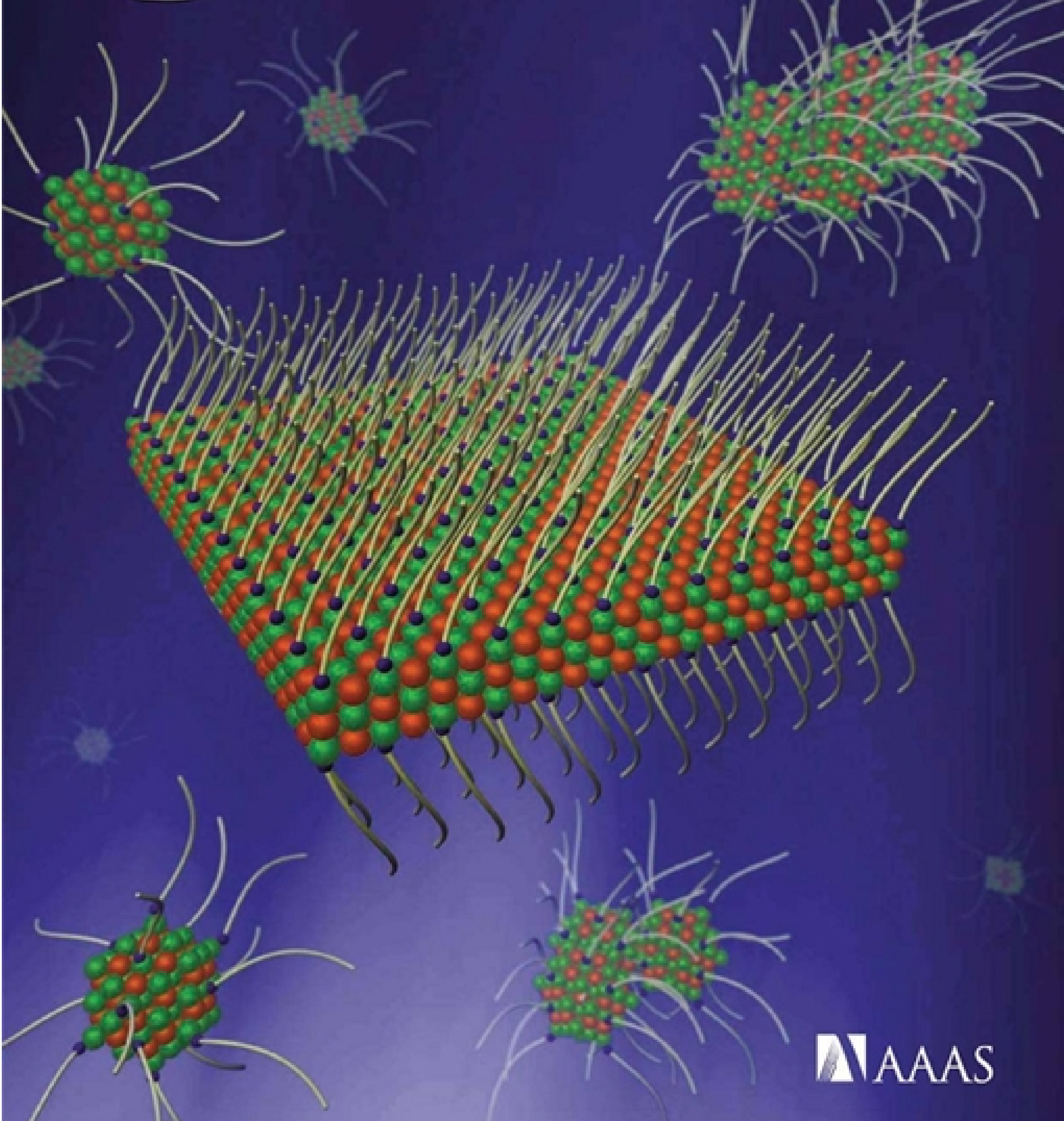

AAAS

CONTENTS continued >>

page 505

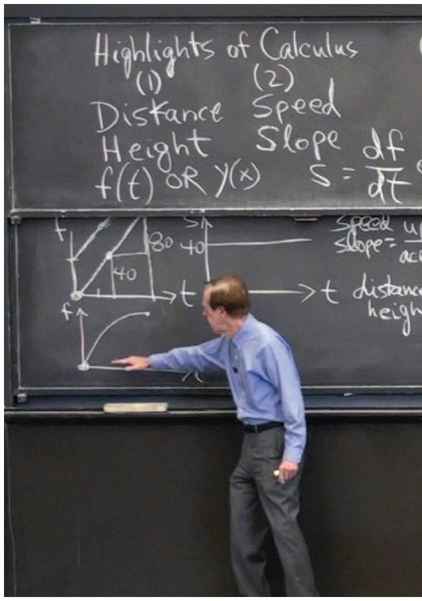

page 525

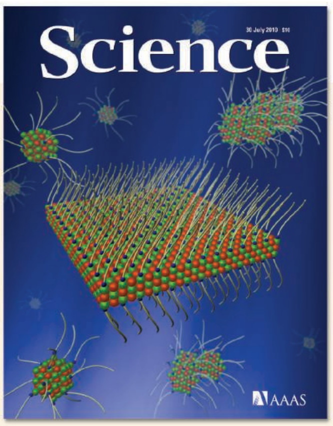

COVER

Lead sulfide nanocrystals (green, lead; orange, sulfur) self-assemble in solution, forming two-dimensional aggregates and ultrathin single-crystal sheets on the micrometer scale. The formation of dense and highly ordered oleic acid monolayers (dark blue spheres with long projections) on the sheets' surfaces helps drive the oriented attachment of the nanocrystals, resulting in a material with outstanding photoconductive properties. See page 550.

Image: Christian Klinke/Hamburg University, Germany

DEPARTMENTS

CONTENTS continued >>

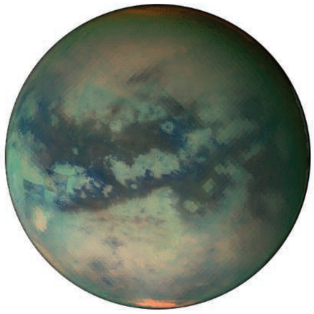

page 519

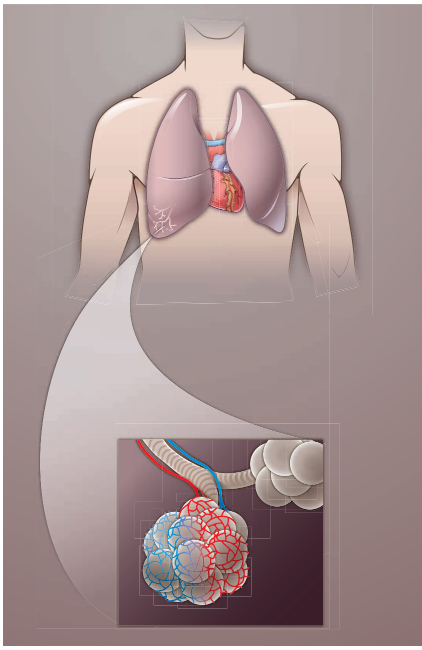

pages 520 & 538

page 556

Published by AAAS

SCIENCEONLINE

SCIENCEXPRESS

www.sciencexpress.org

PTIP Promotes Chromatin Changes Critical for Immunoglobulin Class Switch Recombination
J. A. Daniel et al.
A factor that regulates chromatin accessibility and recombination during immunoglobulin rearrangements is identified.
10.1126/science.1187942

FAN1 Acts with FANCI-FANCD2 to Promote DNA Interstrand Cross-Link Repair
T. Liu et al.
The nuclease FAN1 acts with Fanconi anemia proteins to help repair damaged DNA.
10.1126/science.1192656

Planar Cell Polarity Acts Through Septins to Control Collective Cell Movement and Ciliogenesis
S. K. Kim et al.
A gene involved in morphogenesis and ciliogenesis is mutated in patients with Bardet-Biedl syndrome.
10.1126/science.1191184

Quantum Oscillations and Hall Anomaly of Surface States in the Topological Insulator Bi_2Te_3
D.-X. Qu et al.
Quantum oscillations are used to detect the surface current of a topological insulator, yielding high carrier mobilities.
10.1126/science.1189792

Land-Level Changes Produced by the M_w 8.8 2010 Chilean Earthquake
M. Farías et al.
The 2010 M_w 8.8 Chilean earthquake ruptured ~500 kilometers and vertically displaced over three meters.
10.1126/science.1192094

TECHNICALCOMMENTS

Comment on "Patterns of Diversity in Marine Phytoplankton"
J. Huisman
Full text at www.sciencemag.org/cgi/content/full/329/5991/512-c

Response to Comment on "Patterns of Diversity in Marine Phytoplankton"
A. D. Barton et al.
Full text at www.sciencemag.org/cgi/content/full/329/5991/512-d

SCIENCENOW

www.sciencenow.org
Highlights From Our Daily News Coverage

'Locked-In' Patients Can Follow Their Noses
New technology could allow paralyzed patients to type and move a wheelchair by sniffing.

'Mind Meld' Enables Good Conversation
When two people talk, similar areas of their brains activate.

Obscure Immune Cells Thwart Ticks
New technique for deleting cells allows researchers to pin down their function.

CREDIT: MING LIU, TIT MENG LIM, YU CAI/TEMASEK LIFE SCIENCES LABORATORY AND DEPARTMENT OF BIOLOGICAL SCIENCES, NATIONAL UNIVERSITY OF SINGAPORE

SCIENCESIGNALING

www.sciencesignaling.org
The Signal Transduction Knowledge Environment

RESEARCH ARTICLE: Autocrine Purinergic Receptor Signaling Is Essential for Macrophage Chemotaxis
M. Kronlage et al.
Amplification of outside-in chemotactic signaling by inside-out purinergic signaling drives macrophage migration.

RESEARCH ARTICLE: Decoupling of Receptor and Downstream Signals in the Akt Pathway by Its Low-Pass Filter Characteristics
K. A. Fujita et al.
The Akt pathway can serve as a signal decoupler, converting a weak receptor signal into a strong effector signal.

RESEARCH ARTICLE: The *Drosophila* Female Germline Stem Cell Lineage Acts to Spatially Restrict DPP Function Within the Niche
M. Liu et al.
Drosophila ovarian stem cells communicate with somatic cells to define the size of the stem cell niche.

PERSPECTIVE: Inhibiting the Inhibitor of the Inhibitor—Blocking PKC-θ to Enhance Regulatory T Cell Function
K. T. Roybal and C. Wülfing
PKC-θ functions differently in regulatory T cells, which may be linked to its exclusion from immune synapses.

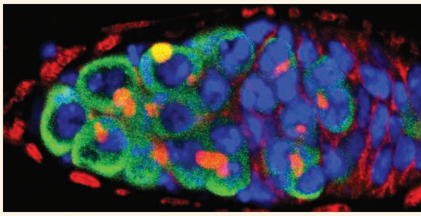

SCIENCESIGNALING
Defining the size of the stem cell niche.

RESEARCH ARTICLE: Function of an Implanted Tissue Glucose Sensor for More Than 1 Year in Animals
D. A. Gough et al.
An implanted tissue glucose sensor can provide stable readings of glucose concentrations for more than a year.

RESEARCH ARTICLE: A Human-Specific Deletion in Mouse *Cmah* Increases Disease Severity in the mdx Model of Duchenne Muscular Dystrophy
K. Chandrasekharan et al.
A mouse model for Duchenne muscular dystrophy engineered to produce humanlike glycosylation mimics the human disease better than existing models.

SCIENCECAREERS

www.sciencecareers.org/career_magazine
Free Career Resources for Scientists

Feeding Your Research Into the Policy Debate
E. Pain
Early-career scientists who want their research to inform policymaking need to learn how to navigate the public arena and communicate effectively.

Answering Biomedical Questions With Information Technology
N. Volkers
Harvard physician-scientist Lynn Bry has developed an informatics system for matching biological samples to research needs.

SCIENCETRANSLATIONAL MEDICINE

www.sciencetranslationalmedicine.org
Integrating Medicine and Science

PERSPECTIVE: The Wnt Signaling Pathway as a Potential Target for Therapies to Enhance Bone Repair
T. A. Einhorn
Modulating Wnt signaling may be an effective means of stimulating skeletal healing after fractures or surgery.

PERSPECTIVE: Channelopathies—Decoding Disease Pathogenesis
A. Terzic and C. Perez-Terzic
Tissue-specific potassium channel dysfunction has been implicated in a complex multiorgan syndrome.

SCIENCEPODCAST

www.sciencemag.org/multimedia/podcast
Free Weekly Show

Download the 30 July *Science* Podcast to hear about how dopamine influences human impulsivity, the stalling of psychiatric drug development, your letters to *Science*, and more.

SCIENCEINSIDER

news.sciencemag.org/scienceinsider
Science Policy News and Analysis

SCIENCE (ISSN 0036-8075) is published weekly on Friday, except the last week in December, by the American Association for the Advancement of Science, 1200 New York Avenue, NW, Washington, DC 20005. Periodicals Mail postage (publication No. 484460) paid at Washington, DC, and additional mailing offices. Copyright © 2010 by the American Association for the Advancement of Science. The title SCIENCE is a registered trademark of the AAAS. Domestic individual membership and subscription (51 issues): $146 ($74 allocated to subscription). Domestic institutional subscription (51 issues): $910; Foreign postage extra: Mexico, Caribbean (surface mail) $55; other countries (air assist delivery) $85. First class, airmail, student, and emeritus rates on request. Canadian rates with GST available upon request, GST #1254 88122. Publications Mail Agreement Number 1069624. **Printed in the U.S.A.**

Change of address: Allow 4 weeks, giving old and new addresses and 8-digit account number. **Postmaster:** Send change of address to AAAS, P.O. Box 96178, Washington, DC 20090–6178. **Single-copy sales:** $10.00 current issue, $15.00 back issue prepaid includes surface postage; bulk rates on request. **Authorization to photocopy** material for internal or personal use under circumstances not falling within the fair use provisions of the Copyright Act is granted by AAAS to libraries and other users registered with the Copyright Clearance Center (CCC) Transactional Reporting Service, provided that $20.00 per article is paid directly to CCC, 222 Rosewood Drive, Danvers, MA 01923. The identification code for *Science* is 0036-8075. *Science* is indexed in the *Reader's Guide to Periodical Literature* and in several specialized indexes.

AAAS
ADVANCING SCIENCE, SERVING SOCIETY

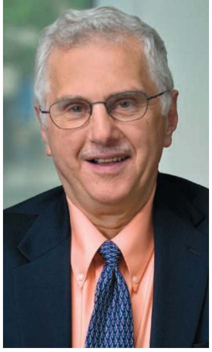

Reframing Science Standards

Bruce Alberts is Editor-in-Chief of *Science*

A PROMISING DRAFT *FRAMEWORK FOR SCIENCE EDUCATION* WAS RECENTLY POSTED BY THE U.S. National Academies for public comment (until 2 August) and review (see www7.nationalacademies.org/bose). Its goal is to define the science that all students should be taught from age 5 through precollege in the United States, building on lessons learned from the 1996 National Science Education Standards (NSES). Will this new effort, initiated to help produce a common core for science education across states,* be more successful than the last one?

In 1989, the governors of all 50 states issued a call for "voluntary national standards" in each of the major academic disciplines. In response, the NSES were issued by the National Academy of Sciences in 1996. The results have been disappointing. In particular, the requirement for students to master a large number of facts and concepts took precedence over the strong emphasis on "science as inquiry" in the NSES. The new *Framework* attempts to overcome this problem in several interesting ways.

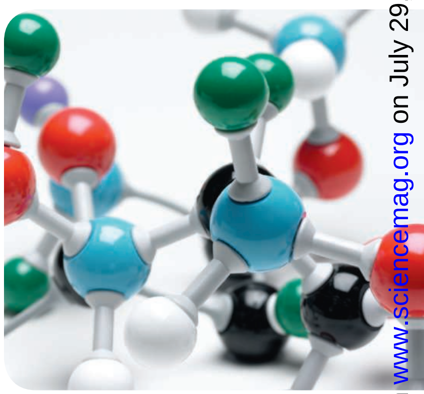

First, the draft *Framework* focuses on only four core concepts in each of four disciplines: life sciences, physical sciences, earth and space sciences, and engineering and technology. And differing from the NSES, each core concept extends over all years of schooling. The intention is to leave room during the school day for three important strands of science learning that have been systematically ignored in favor of the traditional content strand, which focuses on knowing, using, and interpreting scientific explanations of the natural world. The critical strands that have been missing are generating and evaluating scientific evidence and explanations, understanding the nature and development of scientific knowledge, and participating in scientific practices and discourse.†

Second, the *Framework* supplements the dominant theme of inquiry in the NSES with a greatly expanded discussion of why any definition of science education must center around active participation in scientific practices and extensive experience with evaluating evidence. The current focus on transmitting only the knowledge that scientists have discovered fails to provide students with the thinking and problem-solving skills that are essential for life in our complex societies, and it also fails to give them a sound understanding of why science has been so successful as a special way of knowing about the world. Thus, the draft *Framework* contains a powerful chapter containing 16 useful tables entitled Scientific and Engineering Practices. (The inclusion of engineering itself represents a major, positive break with tradition.)

The *Framework* also stresses the importance of building coherence into the science curriculum from year to year through reference to the ongoing research on "learning progressions." As an example, the recognition that any object is composed of specific materials, and has certain properties because of those materials, is known to be an important first step toward understanding atomic-molecular theory. To guide curriculum design, the last half of the draft document presents prototype learning progressions for each of the core concepts to be learned, expanding on the landmark *Atlas for Science Literacy* produced by the American Association for the Advancement of Science.

The *Framework* will be finalized in response to the feedback received on the public draft, and then, because responsibility for education is assigned to each state by the U.S. Constitution, the final standards will be developed through a coalition of states led by the nonprofit organization Achieve. The worst thing that scientists could do would be to insist that the core disciplinary ideas be expanded to include their specialties. Instead, the scientific community should focus on preparing college students to "ask questions; collect, analyze, and interpret data; construct and critique arguments; communicate and interpret scientific and technical texts; and apply and use scientific knowledge"—precisely as the *Framework* specifies for the precollege years.

– Bruce Alberts

10.1126/science.1195444

*A. I. Leshner, S. Malcom, J. E. Roseman, *Science* **328**, 1075 (2010). †B. Alberts, *Science* **323**, 437 (2009).

CREDITS: (TOP) TOM KOCHEL; (RIGHT) THINKSTOCK

www.sciencemag.org

Science

1200 New York Avenue, NW
Washington, DC 20005
Editorial: 202-326-6550, FAX 202-289-7562
News: 202-326-6581, FAX 202-371-9227
Bateman House, 82-88 Hills Road
Cambridge, UK CB2 1LQ
+44 (0) 1223 326500, FAX +44 (0) 1223 326501

Subscription Services For change of address, missing issues, new orders and renewals, and payment questions: 866-434-AAAS (2227) or 202-326-6417, FAX 202-842-1065. Mailing addresses: AAAS, P.O. Box 96178, Washington, DC 20090-6178 or AAAS Member Services, 1200 New York Avenue, NW, Washington, DC 20005

Institutional Site Licenses please call 202-326-6755 for any questions or information

Reprints: Author Inquiries 800-635-7181
Commercial Inquiries 803-359-4578

Permissions 202-326-7074, FAX 202-682-0816

Member Benefits AAAS/Barnes&Noble.com bookstore www.aaas.org/bn; AAAS Online Store www.apisource.com/aaas/ code MKB6; AAAS Travels: Betchart Expeditions 800-252-4910; Apple Store www.apple.com/eppstore/aaas; Bank of America MasterCard 1-800-833-6262 priority code FAA3YU; Cold Spring Harbor Laboratory Press Publications www.cshlpress.com/affiliates/aaas.htm; GEICO Auto Insurance www.geico.com/landingpage/go51.htm?logo=17624; Hertz 800-654-2200 CDP#343457; Office Depot https://bsd.officedepot.com/portalLogin.do; Seabury & Smith Life Insurance 800-424-9883; Subaru VIP Program 202-326-6417; VIP Moving Services www.vipmayflower.com/domestic/index.html; Other Benefits: AAAS Member Services 202-326-6417 or www.aaasmember.org.

science_editors@aaas.org	(for general editorial queries)
science_letters@aaas.org	(for queries about letters)
science_reviews@aaas.org	(for returning manuscript reviews)
science_bookrevs@aaas.org	(for book review queries)

Published by the American Association for the Advancement of Science (AAAS), *Science* serves its readers as a forum for the presentation and discussion of important issues related to the advancement of science, including the presentation of minority or conflicting points of view, rather than by publishing only material on which a consensus has been reached. Accordingly, all articles published in *Science*—including editorials, news and comment, and book reviews—are signed and reflect the individual views of the authors and not official points of view adopted by AAAS or the institutions with which the authors are affiliated.

AAAS was founded in 1848 and incorporated in 1874. Its mission is to advance science, engineering, and innovation throughout the world for the benefit of all people. The goals of the association are to: enhance communication among scientists, engineers, and the public; promote and defend the integrity of science and its use; strengthen support for the science and technology enterprise; provide a voice for science on societal issues; promote the responsible use of science in public policy; strengthen and diversify the science and technology workforce; foster education in science and technology for everyone; increase public engagement with science and technology; and advance international cooperation in science.

Information for Authors
See pages 352 and 353 of the 15 January 2010 issue or access www.sciencemag.org/about/authors

Editor-in-Chief **Bruce Alberts**
Executive Editor **Monica M. Bradford**
News Editor **Colin Norman**
Managing Editor, Research Journals **Katrina L. Kelner**
Deputy Editors **R. Brooks Hanson, Barbara R. Jasny, Andrew M. Sugden**

Editorial senior editors/commentary Lisa D. Chong, Brad Wible; **senior editors** Gilbert J. Chin, Pamela J. Hines, Paula A. Kiberstis (Boston), Marc S. Lavine (Toronto), Beverly A. Purnell, L. Bryan Ray, Guy Riddihough, H. Jesse Smith, Phillip D. Szuromi (Tennessee), Valda Vinson, Jake S. Yeston; **associate editors** Kristen L. Mueller, Jelena Stajic, Nicholas S. Wigginton, Laura M. Zahn; **research associate** Alexis Wynne Mogul; **book review editor** Sherman J. Suter; **associate letters editor** Jennifer Sills; **editorial manager** Cara Tate; **senior copy editors** Jeffrey E. Cook, Cynthia Howe, Harry Jach, Lauren Kmec, Barbara P. Ordway, Trista Wagoner; **copy editor** Chris Filiatreau; **editorial coordinators** Carolyn Kyle, Beverly Shields; **publications assistants** Ramatoulaye Diop, Joi S. Granger, Emily Guise, Jeffrey Hearn, Michael Hicks, Lisa Johnson, Scott Miller, Jerry Richardson, Jennifer A. Seibert, Brian White, Anita Wynn; **editorial assistants** Emily C. Horton, Patricia M. Moore, Miriam Weinberg; **executive assistant** Alison Crawford; **administrative support** Maryrose Madrid; **editorial fellow** Melissa R. McCartney

Editorial director, web and new media Stewart Wills; **senior web editor** Tara S. Marathe; **web editor** Robert Frederick; **web development manager** Martyn Green; **web developer** Andrew Whitesell

News deputy news editors Robert Coontz, Eliot Marshall, Jeffrey Mervis, Leslie Roberts; **contributing editors** Elizabeth Culotta, Polly Shulman; **news writers** Yudhijit Bhattacharjee, Adrian Cho, Jennifer Couzin, David Grimm, Jocelyn Kaiser, Richard A. Kerr, Eli Kintisch, Greg Miller, Elizabeth Pennisi, Lauren Schenkman, Robert F. Service (Pacific NW), Erik Stokstad, Jue Wang; **interns** Kristen Minogue, Nezile Mthembu, Dolly Krishnaswamy; **contributing correspondents** Jon Cohen (San Diego, CA), Daniel Ferber, Ann Gibbons, Sam Kean, Robert Koenig, Andrew Lawler, Mitch Leslie, Charles C. Mann, Virginia Morell, Gary Taubes; **copy editors** Linda B. Felaco, Melvin Gatling, Melissa Raimondi; **administrative support** Scherraine Mack; **bureaus** San Diego, CA: 760-942-3252, FAX 760-942-4979; Pacific Northwest: 503-963-1940

Production director James Landry; **senior manager** Wendy K. Shank; **assistant manager** Rebecca Doshi; **senior specialists** Steve Forrester, Chris Redwood, Anthony Rosen; **Preflight director** David M. Tompkins; **manager** Marcus Spiegler; **specialist** Jason Hillman

Art director Yael Kats; **associate art director** Laura Creveling; **senior illustrators** Chris Bickel, Katharine Sutliff; **illustrator** Yana Greenman; **senior art associates** Holly Bishop, Preston Huey, Nayomi Kevitiyagala; **art associates** Kay Engman, Matthew Twombly; **photo editor** Leslie Blizard

***Science* International**

Europe (science@science-int.co.uk) **editorial: international managing editor** Andrew M. Sugden; **senior editor/commentary** Julia Fahrenkamp-Uppenbrink; **senior editors** Caroline Ash, Stella M. Hurtley, Ian S. Osborne, Peter Stern; **associate editor** Maria Cruz; **locum editor** Helen Pickersgill; **editorial support** Rachel Roberts, Alice Whaley; **administrative support** John Cannell, Janet Clements, Louise Hartwell; **news: europe news editor** John Travis; **deputy news editor** Daniel Clery; **contributing correspondents** Michael Balter (Paris), John Bohannon (Vienna), Martin Enserink (Amsterdam and Paris), Gretchen Vogel (Berlin); **intern** Sarah Reed

Latin America contributing correspondent Antonio Regalado

Asia Japan Office: Asca Corporation, Tomoko Furusawa, Rustic Bldg. 7F, 77 Tenjin-cho, Shinjuku-ku, Tokyo 162-0808, Japan; +81 3 6802 4616, FAX +81 3 6802 4615, inquiry@sciencemag.jp; **asia news editor** Richard Stone (Beijing: rstone@aaas.org); **contributing correspondents** Dennis Normile [Japan: +81 (0) 3 3391 0630, FAX +81 (0) 3 5936 3531; dnormile@gol.com]; Hao Xin [China: cindyhao@gmail.com]; Pallava Bagla [South Asia: +91 (0) 11 2271 2896; pbagla@vsnl.com]

Executive Publisher **Alan I. Leshner**
Publisher **Beth Rosner**

Fulfillment Systems and Operations (membership@aaas.org); **director** Waylon Butler; **customer service supervisor** Pat Butler; **specialists** Latoya Casteel, LaVonda Crawford, Vicki Linton, April Marshall; **data entry supervisor** Cynthia Johnson; **specialists** Shirlene Hall, Tarrika Hill, William Jones

Business Operations and Administration director Deborah Rivera-Wienhold; **business systems and financial analysis director** Randy Yi; **manager, business analysis** Eric Knott; **manager, business operations** Jessica Tierney; **financial analysts** Priti Pamnani, Celeste Troxler; **rights and permissions: administrator** Emilie David; **associate** Elizabeth Sandler; **marketing director** Ian King; **marketing managers** Allison Pritchard, Alison Chandler, Julianne Wielga; **marketing associates** Aimee Aponte, Mary Ellen Crowley, Wendy Wise; **senior marketing executive** Jennifer Reeves; **director, site licensing** Tom Ryan; **director, corporate relations** Eileen Bernadette Moran; **publisher relations, eresources specialist** Kiki Forsythe; **senior publisher relations specialist** Catherine Holland; **publisher relations, east coast** Phillip Smith; **publisher relations, west coast** Philip Tsolakidis; **fulfillment supervisor** Iquo Edim; **fulfillment coordinator** Carrie MacDonald; **marketing manager** Christina Schlecht; **marketing associate** Laura Tutino; **electronic media: manager** Lizabeth Harman; **project manager** Trista Snyder; **assistant manager** Lisa Stanford; **senior production specialists** Ryan Atkins, Christopher Coleman, **computer specialist** Walter Jones, Kai Zhang; **production specialists** Angela Forest, Nichele Johnston, Kimberly Oster; **director, web and new media** Will Collins

advertising director, worldwide ad sales Bill Moran
commercial editor Sean Sanders: 202-326-6430
assistant commercial editor Tianna Hicklin 202-326-6463
project director, outreach Brianna Blaser

Product (science_advertising@aaas.org); **midwest** Rick Bongiovanni: 330-405-7080, FAX 330-405-7081; **east coast/e. canada** Laurie Faraday: 508-747-9395, FAX 617-507-8189; **west coast/w. canada** Lynne Stickrod: 415-931-9782, FAX 415-520-6940; **uk/europe/asia** Roger Goncalves: TEL/FAX +41 43 243 1358; **japan** ASCA Corporation, Nanako Ide +81 (0) 3 6802 4616, FAX +81 (0) 3 6802 4615; ads@sciencemag.jp; **senior traffic associate** Deiandra Simms

worldwide associate director of *Science* Careers Tracy Holmes: +44 (0) 1223 326525, FAX +44 (0) 1223 326532

Classified (advertise@sciencecareers.org); **u.s.: midwest/west coast/south central/canada** Tina Burks: 202-326-6577; **east coast/industry** Elizabeth Early: 202-326-6578; **advertising operations manager** Kate Panganiban **sales coordinators** Rohan Edmonson, Shirley Young; **europe/row sales:** Susanne Kharraz, Dan Pennington, Alex Palmer; **sales assistant** Lisa Patterson; **japan** ASCA Corporation, Jie Chin +81 (0) 3 6802 4616, FAX +81 (0) 3 6802 4615; careerads@sciencemag.jp; **advertising support manager** Karen Foote: 202-326-6740; **advertising production operations manager** Deborah Tompkins; **senior production specialist/graphic designer** Amy Hardcastle; **senior production specialist** Robert Buck; **senior traffic associate** Christine Hall

Paying for HIV/AIDS drugs
500

Neuropharma's medicine cabinet
502

ARCHAEOLOGY

Copper Mine Threatens Ancient Monastery in Afghanistan

VIENNA—A decade after the Taliban destroyed the famous Bamiyan Buddhas—two massive statues that have stood sentry in an Afghan valley for 1500 years—archaeologists are warning that Afghan antiquities are again at risk. This time the threat comes from a venture blessed by the Western-backed Afghan government. A Chinese company intends to blow up an ancient Buddhist monastery south of Kabul to make way for a massive copper mine. The plan has sparked outrage among Afghan and French archaeologists, who have recently uncovered more than 100 statues within a large religious complex that includes seven *stupas*, or tombs built to house the relics of saints.

In their first public talk on the finds at a recent meeting here,* excavation leaders called for an international meeting to galvanize support for the site. And French officials intended to raise concerns about the impending demolition at a meeting of foreign ministers from around the world in Kabul last week. The controversy pits Afghanistan's desperate need for revenue against its ancient heritage as an Asian crossroads. "This will have to be decided by [Afghan President Hamid] Karzai," says Philippe Marquis, head of the French archaeological mission to Afghanistan.

Marquis says plans to dynamite the monastery in April were postponed but have not been canceled. The United States and its allies are pushing for increased foreign investment in Afghanistan, and a 14 June report issued by the U.S. Defense Department estimated that $1 trillion of minerals such as copper, iron, cobalt, and lithium lie under eastern Afghanistan alone. Some geologists think Mes Aynak holds the world's second largest deposit of copper, and the $3 billion contract with Beijing's China Metallurgical Group Corp. to mine it is the most lucrative in Afghanistan's history.

Located in a mountainous region 40 kilometers southeast of the capital, Mes Aynak is a hill topped by a 4500-square-meter monastery. Although the site was spotted by archaeologists in the 1960s, it was never excavated. During the late 1990s, the hill was home to an al-Qaida training camp, according to the 2004 report by the National Commission on Terrorist Attacks Upon the United States. In recent years, looters have damaged much of the monastery complex in the search for antiquities, says Nader Rassouli, director of Afghanistan's National Institute of Archaeology in Kabul, which is also participating in the current excavations.

"The site is huge, and we have amazing remains," he said at the meeting. The monastery flourished from as early as the 2nd century B.C.E. until at least the 6th century C.E., although it may have continued as a settlement until as late as the 9th century C.E., says Marquis. The joint Afghan-French team began salvage work last summer, halting in November due to the severe winter at the 2400-meter altitude. Among the finds are three dozen clay statues, including a reclining Buddha 5 meters long, as well as dozens of wooden and stone Buddhas. Rassouli estimates that the site covers 100 to 400 hectares, including two areas yet to be excavated. As the archaeologists work, Chinese engineers are busy building a railroad, housing, and a power plant nearby, in preparation for mining, according to Afghan government statements on the project.

Two millennia ago, this region served as a critical conduit in the spread of Buddhism to Central Asia and China, says T. Richard Blurton, an archaeologist and curator at London's British Museum who has excavated in Afghanistan. He says Mes Aynak could provide new data on both the origin and demise of the religion here. Researchers now believe that as late as the 7th century C.E., when Islam arrived in the area, Buddhism was still making inroads as far west as Iran and as far north as Turkmenistan. "It's quite tantalizing to consider how Buddhism coexisted with the new religion," Blurton says. There are also Hindu deities from that late period at Tepe Sardar, a large monastery located in the eastern Afghan city of Ghazni. Further evidence from Mes Aynak could help provide a new picture of religious blending at an important historical juncture, says Blurton.

The ancient monks of Mes Aynak apparently knew they were sitting on a large copper deposit, because there are signs of mining throughout the monastery's long history, says Marquis. Soviet geological surveys in the 1970s rediscovered the mineral deposit, but the outbreak of war in 1979 prevented its development. In May 2008, the state-owned China Metallurgical Group signed a contract

*European Association for South Asian Archaeology and Art, 4–9 July 2010.

Mine over matter. These statues south of Kabul may face destruction.

CREDITS: DAFA/AFGHANISTAN NATIONAL INSTITUTE OF ARCHAEOLOGY

Europe's
eel crusade
505

Robots with
high IQs
508

to begin extracting copper. "This project provides high levels of income for the government and opportunities for more than 6000 people and for thousands of others indirectly," said Ibrahim Adel, the Afghan minister of mines at the time of the signing ceremony. *The Washington Post* reported in November that Adel was suspected of taking a $30 million bribe from the Chinese company. Adel denied the allegation but resigned in January; no charges have been filed.

Geologists estimate that there are 13 million tons of ore at Mes Aynak. A feasibility study will not be completed until early next year, but Afghan officials estimate that the Chinese will extract 200,000 tons of copper and provide Afghanistan with up to $400 million in annual revenues. Requests for comment about the monastery demolition from both the Afghan Ministry of Mines and the Chinese company went unanswered. Marquis compares the plan to destroy Mes Aynak with the Taliban's infamous 2001 destruction of the Bamiyan Buddhas. "Karzai is the only one who can say no," he says. In Marquis's view, copper mining and the monastery can coexist by creating a protected archaeological area that eventually could generate tourism income. That compromise may prove a tough sell in a country under intense pressure to produce short-term revenue.

Meanwhile, Rassouli hopes to sponsor an international meeting to drum up support for the ruin. "Time is running short," he says. "This place is going to be destroyed in a few months, and we need to find another solution—or the site is doomed."

–ANDREW LAWLER

2011 BUDGET

NSF Funding Request Faring Well in Congress

Last week, a Senate committee declared the U.S. National Science Foundation (NSF) to be "the finest science foundation in the world." And federal legislators seem prepared to back up their kind words with hard cash. While the 2011 budget requests of other U.S. research agencies are struggling to stay afloat in choppy fiscal seas, so far NSF's is sailing through Congress largely intact.

Last week, the Senate appropriations committee gave NSF all but $71 million of the $498 million increase that it had requested for 2011. A few weeks earlier, a House of Representatives spending panel endorsed the entire 7.2% increase, which would boost NSF's budget next year to $7.4 billion. That's also the target for the first of a 3-year reauthorization of the 2007 America COMPETES Act adopted in late May by the House and approved last week by the Senate Commerce, Science, and Transportation Committee, which threw the above verbal bouquet to the science agency. Both NSF and the Department of Energy's (DOE's) Office of Science are included in the COMPETES reauthorization, which would keep their budgets on a 10-year doubling path as well as give them program guidance. But Senate appropriators have provided the DOE office with only half of a much smaller (4.4%) increase it has requested. What's more, a House spending panel earlier this month told DOE to make do in 2011 with its current budget of $4.9 billion (see graphic).

Both NSF and DOE are still a long way from the finish line. Their spending bills must move through each house and then be reconciled, most likely after the November elections. That timetable may also apply to the reauthorization bills. Although the House version (H.R. 5116) is a top priority for the retiring chair of the House science committee, Representative Bart Gordon (D–TN), the Senate may run out of time before it completes work on its bill (S. 3605).

In the meantime, NSF is riding high in the eyes of key legislators from both parties. An expanding budget would be no small accomplishment at a time when Republicans and many Democrats are demanding that Congress slash federal spending to reduce the $1.4 trillion deficit. "The one thing that might keep us from passing a bill is concern over the level of authorization," Senator Kay Bailey Hutchison (R–TX), the ranking member of the Senate science panel, told *Science* after last week's markup of S. 3605. "I think we should authorize basically level funding. But I think that NSF deserves a higher level than the others because of its excellent record of supporting basic research." Adds committee chair Senator Jay Rockefeller (D–WV), "I like our authorization levels. [That level of support is] vital to our country's future."

To be sure, NSF has taken a few lumps this year. Its clumsy handling of employees found to be using their computers to view and circulate pornography triggered a sharp rebuke in the House version of the COMPETES bill (*Science*, 21 May, p. 960). And last week, Senate appropriators told the agency to abandon its plan to fold three programs aimed at boosting the number of minority students in science and engineering into one initiative (*Science*, 23 July, p. 376). "One size will not fit all," notes the report accompanying the spending bill.

Science lobbyists are keeping their fingers crossed that the good vibrations will continue once Congress returns from its August recess. "I am very pleased with the numbers and the accolades for NSF," says Samuel Rankin of the Coalition for National Science Funding in Washington, D.C. "I will remain cautious, however, until an [appropriations] bill is signed."

–JEFFREY MERVIS

A Tale of Two Agencies

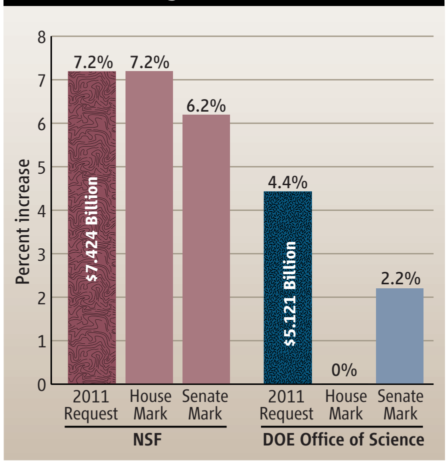

Congressional favorite. NSF's budget request for 2011 is faring much better than those for DOE science programs. The Administration has promised to double the budgets of both agencies over 10 years.

SOURCE: OMB, CONGRESS

VOLCANOLOGY

Is China's Riskiest Volcano Stirring Or Merely Biding Its Time?

CHANGBAI MOUNTAIN, CHINA—On the north slope of Changbai Mountain, throngs of tourists jostle at a precipice to catch a glimpse of Sky Pond, the volcano's huge caldera lake several hundred meters below. For Koreans who revere this mountain on the border of China and North Korea as the birthplace of the Korean nation, no pilgrimage is complete without a peek at Sky Pond.

They'd better enjoy the view while it lasts.

Last month, a South Korean geologist declared that the 2744-meter-tall volcano, known as Mount Paektu to Koreans and Tianchi caldera to Chinese, is showing signs of waking from a century-long slumber. North Korean scientists, too, are worried about recent geophysical anomalies observed at the mountain, *Science* has learned. But Chinese volcanologists, who have a sophisticated monitoring system set up at Changbai, discount the threat and insist that the volcano is quiet. South Korea plans to hold a meeting with China and Japan in November to "get to the bottom of the matter," says an official with the Korean Meteorological Administration (KMA) in Seoul who requested anonymity because of the issue's sensitivity.

An eruption of Changbai could have devastating consequences. Of China's 14 active volcanoes, "Changbai poses the biggest hazard and therefore is our most dangerous one," says Xu Jiandong, director of the China Earthquake Administration's (CEA's) Active Volcano Research Center in Beijing. Part of the risk is the threat of lahars from the huge lake in the 5-kilometer-wide caldera. About 100,000 people live on or near Changbai's slopes, and in summertime the region is packed with tourists.

As volcanoes go, Changbai is in the big leagues. In a violent, explosive eruption around 1000 C.E.—dating is not precise, so it's called the "millennium eruption"—the volcano disgorged up to 30 cubic kilometers of magma, or 10 times as much as the famed Krakatoa eruption in 1883. Pyroclastic flows covered an area extending roughly 50 kilometers from Tianchi caldera. In the past 2000 years, only the 1815 eruption of Tambora in Indonesia rivals Changbai, which dumped ash as far away as northern Japan, says Tsuyoshi Miyamoto, a geologist at Tohoku University in Miyagi, Japan, who has studied past eruptions at Changbai. Smaller eruptions have occurred at roughly 100-year intervals since then, with the last one in 1903.

At a KMA seminar in Seoul last month, Yun Sung-hyo, a geologist at Pusan National University, citing Chinese data, said signs indicate "that Mount Paektu may have an eruption in the near future," according to a report by Yonhap News Agency. And in recent months, North Korean geologists who monitor the volcano have sought cooperation with Western volcanologists, including a joint expedition to the volcano, training abroad for North Korean scientists, and upgrades to a research station at Paektu, says a North Korean official who requested anonymity. No cooperation has yet gotten off the ground.

Chinese volcanologists keep a close eye on Changbai; they say an eruption does not seem imminent. From 2002 to 2005, the volcano's magma chamber evidently was filling, says Xu. In quiet periods, seismometers register about 100 small tremors a year around the mountain, he says. In 2003, Changbaishan Tianchi Volcano Observatory recorded 1293 tremors. By 2006, the frequency had receded to background rate, and in the first 6 months of 2010 the station recorded 58 tremors. The mountain rose about 6.8 centimeters in 2003 and 2004, and the ratio of helium-3 to helium-4—"a good indication

HIGH ENERGY PHYSICS

Fermilab Physicists Don't See Higgs, Argue They Should Keep Looking

PARIS—This year's International Conference on High Energy Physics was a case study in irony. The meeting was billed as the coming-out party for the Large Hadron Collider (LHC), the gigantic European atom smasher that started taking data in March, but the buzz surrounded results from the older Tevatron collider at Fermi National Accelerator Laboratory (Fermilab) in Batavia, Illinois. Quelling rumors, Fermilab physicists said they had *not* yet spotted a long-sought particle called the Higgs boson. Nevertheless, their improved nonobservation has them pushing to run the Tevatron three extra years, through 2014—a plan that officials at Fermilab itself do not necessarily favor.

Higgs bosons lurking "virtually" in the vacuum are thought to drag on other particles to give them mass. But physicists' standard model of the fundamental particle does not predict how much the Higgs itself will weigh, so scientists must search for it. Physicists know from previous experiments that the Higgs most likely weighs between 114 and 185 giga-electron volts (GeV), or between 121 and 197 times as much as a proton. Last year, Fermilab researchers showed that it likely does not weigh between 162 GeV and 166 GeV. Now, they've widened that "exclusion window" to between 158 GeV and 175 GeV (see figure).

That advance suggests that Fermilab researchers have nearly enough data and sensitivity to spot the Higgs if it's anywhere in the 114-to-185-GeV range, says Fermilab's Dmitri Denisov, co-spokesperson for the 500-member team working with the D0 particle detector. "Everywhere, we are very, very close," he says. If the Tevatron smashed protons into antiprotons through 2014, researchers would collect 65% more data than they will have by the end of next year. That should be enough to glimpse the Higgs—if it's there—before physicists at the LHC can. "There's definitely a window of opportunity here," Denisov says.

That's because the LHC, housed at the European particle physics laboratory CERN near Geneva, Switzerland, will shut down at the end of 2011 to repair thousands of unreliable solder connections between its superconducting magnets. In September 2008, the LHC broke down during preliminary tests when one of those connections melted. After 14 months of repairs, CERN officials decided to run the accelerator at no more than

Search for the Higgs Particle

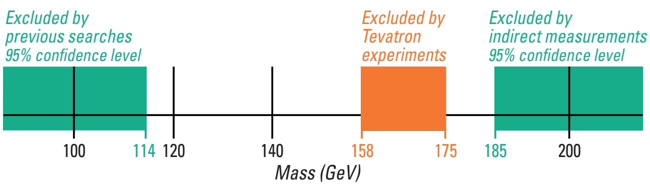

Where it's not. Fermilab's new limits on the mass of the Higgs boson.

CREDIT: ADAPTED FROM FERMILAB

Living dangerously. Tourists peer over the rim of Tianchi's caldera.

of magma activity because the source is the mantle," Xu says—nearly doubled during that time. Changbai has been largely quiet since 2005, says Xu, who expects it to kick into another "active phase" again in the next few years. "But that doesn't mean it will erupt," he says. Miyamoto agrees and notes that it is extremely unlikely that the next eruption would rival the millennium eruption.

Korean scientists are wary. One bone of contention is data sharing. "We can only get earthquake data from China, and it's not real-time," says the KMA official. Data sharing will be a main topic at the tripartite meeting, he says. Xu says that data sharing "is a sensitive question." China will allow foreigners access to data if they "can ensure CEA that it will be used for scientific purposes only," he says. Part of the problem is the proximity to the North Korean border. During a visit to Changbaishan Tianchi Volcano Observatory on the north slope of Changbai last week, a staff member declined to answer questions from *Science* on the grounds that "the observatory's work is a state secret."

CEA has proposed a major upgrade of its Tianchi caldera monitoring network to begin next year. One dark spot is the Korean side of the volcano. A few years ago, China proposed building a seismic station for North Korea and integrating observations, says Xu. The offer was declined. "They even didn't want us to build more observatory stations on *our* side of the border," Xu says. In the meantime, Changbai's magma chamber continues to fill.

–RICHARD STONE

---

half-energy—still 3.5 times the Tevatron's energy—until all of the suspect connections could be resoldered (*Science*, 12 February, p. 766). That shutdown will stretch to 15 months to allow workers to make other modifications as well, says Stephen Myers, CERN's director of accelerators and technology.

Physicists working with the two biggest particle detectors at the LHC, ATLAS and CMS, say they can overtake the Tevatron experiments with the data they hope to collect by the end of next year. Marat Gataullin, a CMS member from the California Institute of Technology in Pasadena, showed projections that CMS alone would surpass D0 and Fermilab's other particle detector, CDF, in their combined sensitivity to a Higgs weighing more than 135 GeV. But Giampiero Passarino, a theorist at the University of Turin in Italy, says he's skeptical. "By the shutdown? I doubt it."

Running the Tevatron through 2014 would cost about $100 million, says Robert Roser, co-spokesperson for the 600-member team working with CDF. But finding the money would be tough, especially as the lab is building a new $260 million neutrino experiment called NOνA and is developing plans for other projects, says Young-Kee Kim, Fermilab's deputy director: "If we run the Tevatron, then there's a clear impact on NOνA immediately." Still, Kim says, lab officials are taking the proposal seriously.

Some European physicists say they favor running the Tevatron longer. "In an ideal world, I think it would be good to have the Tevatron running in parallel with the LHC," says Guido Tonelli of the University of Pisa in Italy, spokesperson for the 3170-member CMS team. "For the next 2 or 3 years, the two machines will be complementary."

The price may be too high, some Americans say. "I don't see anybody coming along with a check for the $100 million or whatever it costs to run the Tevatron for 3 years," says Melvyn Shochet, a physicist at the University of Chicago in Illinois and chair of the U.S. government's High Energy Physics Advisory Panel. "So Fermilab has to consider what it's going to give up" to run the Tevatron. Fermilab's physics advisory committee should weigh in next month.

–ADRIAN CHO

CREDIT: R. STONE/SCIENCE

*Science*Insider

From the *Science* Policy Blog

Senate Majority Leader Harry Reid (D–NV) declared the effort to pass **a mandatory cap on comprehensive greenhouse gas emissions dead** as he couldn't muster a bipartisan supermajority of 60 lawmakers. *Science*Insider interviewed a pollster whose data suggested one reason was ignorance: Many Americans didn't even know what **cap and trade**, the central element of such a limit, was. *Science*Insider included posthumous remarks of climatologist Stephen Schneider on the long effort to pass such a law. And it reviewed a study that said that **federal and state rules already on the books**—if enforced aggressively—would get the United States close to President Barack Obama's stated goal of cutting emissions by 17% by 2005. bit.ly/climatebillcoverage

Italian archaeologists were furious after **archaeological samples turned blue** during storage in a former military facility near Verona. Now a new analysis by mineralogist Gilberto Artioli of the University of Padua in Italy suggests an organic molecule is responsible. He had been asked to analyze the stone tools by archaeologist Laura Longo, the former curator of Verona's Natural History Museum. Longo was suspended without salary recently after she complained about the handling of the artifacts. bit.ly/blueartifacts

Duke University has **suspended three cancer clinical trials** after allegations that a university scientist on the studies embellished his resume, … while the National Institutes of Health seeks to **close a loophole on a conflict-of-interest rule** that covers scientists changing jobs.
bit.ly/trials_halted
bit.ly/looph_nih

A group of scientists who study the coasts have lobbied Thad Allen, who heads the federal response to the gulf oil spill, to halt **coastal engineering projects** intended to protect ecosystems there. Sand berms built in the water to stop oil from striking wetlands have started to erode. A plan to "armor" the berms to halt that problem could be even more disruptive, the scientists say in a letter. bit.ly/oilfixes

For more science policy news, visit **news.sciencemag.org/scienceinsider**.

Published by AAAS

About face. South African National AIDS Council head Nono Simelela (*center*) calls shift in HIV/AIDS policy "profound."

INTERNATIONAL CONFERENCE

Money Woes Cast Shadow Over HIV/AIDS, But Ray of Light in South Africa

VIENNA—When Nelson Mandela was inaugurated as the president of postapartheid South Africa, he promised that never again would his country "suffer the indignity of being the skunk of the world." At the 18th International AIDS Conference held here last week, the South African government—which from 1999 to 2008 had a president who questioned whether HIV even caused disease and a health minister who advocated lemons and garlic for treatment—declared that it is no longer the skunk of the AIDS world. "In the past, South Africa has been the subject of much criticism at these conferences for being a highly divided country on its approach to the HIV and AIDS pandemic," South African Minister of Health Aaron Motsoaledi told the attendees. "Today, we are guided by science."

"All of us are thrilled by the new direction in South Africa," said former U.S. President Bill Clinton, echoing the sentiments of the nearly 20,000 participants. Indeed, the news from South Africa was a bright spot in what was otherwise a gloomy discussion of the funding shortfalls that threaten to slow the remarkable progress against HIV/AIDS made during the past 6 years.

The sea change in South Africa—which has an estimated 5.5 million infected people, more than any other country—was especially welcomed because of a growing sentiment that the hardest hit nations must do more to help themselves. As Motsoaledi explained, under the leadership of President Jacob Zuma, last April South Africa launched an ambitious effort to test 15 million people for HIV and expects to start a half-million new people on antiretroviral treatment by June 2011. The HIV/AIDS budget last year increased by 30%, and, he stressed, 83% of the \$2.33 billion spent on all related efforts in the country comes from government coffers.

Michel Sidibé, head of the Joint United Nations Programme on HIV/AIDS (UNAIDS), urged Zuma last September at the U.N. General Assembly to attack HIV/AIDS aggressively. "I told him the major challenge for any leader is legacy," Sidibé told *Science*. "What could be more compelling to your people than saying that during my period, I want to make sure that no babies are born with HIV and no mothers will die from HIV?" But Sidibé didn't expect his lobbying to work, especially because Zuma is married to several women and in 2006 was put on trial (and acquitted) for allegedly raping an HIV-infected woman. Sidibé says he was "amazed" by Zuma's response.

South African researchers also unveiled what was widely seen as the meeting's most important scientific finding, which was simultaneously reported online in *Science* (www.sciencemag.org/cgi/content/abstract/science.1193748). A large clinical study by South African researchers found that a vaginal microbicide for the first time unequivocally protected women from becoming infected by HIV. The gel, which contains the anti-HIV drug tenofovir, also unexpectedly halved the risk of becoming infected by herpes simplex virus-2. HSV-2 infection eases transmission of HIV, so the microbicide packs a one-two punch. (The co-authors said the HSV-2 results were left out of the *Science* paper for space reasons.)

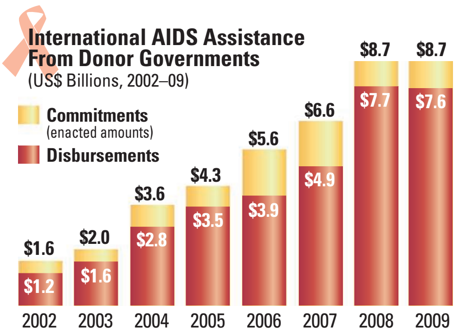

Flat lined. After 6 years of steep increases in aid from donor countries, HIV/AIDS funding plateaued, leading to a growing gap between resources and opportunities.

But for most of the weeklong conference, money woes ruled the day. According to UNAIDS, the effort to combat HIV/AIDS in resource-limited countries in 2008 cost \$15.6 billion, 70% of which came from international aid. As a result, more than 5 million people now receive lifesaving anti-HIV drugs. But the global financial crisis flattened budgets (see graph) and forced treatment programs to stop enrolling new people, raising concerns about sustaining—let alone expanding—the efforts under way. UNAIDS now calculates that 10 million people urgently need treatment, which would cost an additional \$10 billion each year to provide. "The challenge is not finding the money; the challenge is to find the priorities," said conference chair Julio Montaner of the University of British Columbia in Canada. "When there is a Wall Street emergency or an oil spill, billions upon billions of dollars are quickly mobilized."

Montaner and others say the most immediate way to address the funding shortfall is to increase efficiency by cost-saving tactics such as shifting tasks from doctors to nurses, better integrating HIV/TB care, and starting treatment earlier so people don't require hospitalization. But Kevin De Cock, head of the Center for Global Health at the U.S. Centers for Disease Control and Prevention, warned that efficiencies alone can't solve the problem. "You squeeze and you squeeze and then no more juice comes out," said De Cock.

No one had a concrete plan for finding new funds, but many hope that wealthy countries will contribute more to the main multilateral financing mechanism, the independent Global Fund to Fight AIDS, Tuberculosis and Malaria. Austria, the meeting's host, especially took a drubbing for not being more generous.

Some conference goers were deeply disappointed that U.S. President Barack Obama had not done more to address the funding

Published by AAAS

shortfall and worry that he is shifting funds away from HIV/AIDS to maternal and child health in his new $63 billion, 6-year Global Health Initiative. The concern stems in part from a 2008 article in the *Journal of the American Medical Association* that argues for just such a shift, co-authored by Ezekiel Emanuel, a medical ethicist, brother to Obama chief of staff Rahm Emanuel, and a special adviser to the president's Office of Management and Budget.

"The president didn't write that article," Emanuel told *Science*, noting that he penned it before joining the Administration. "And the president submitted budgets that obviously were very different." Indeed, Obama's budget increases global HIV/AIDS funding for fiscal year 2011 by 3.5%, and a new UNAIDS/Kaiser Family Foundation analysis shows that the United States is the world's largest donor to AIDS efforts, contributing 58% of all disbursements to developing countries in 2009.

Many innovative ideas were bandied about, foremost among them the financial transaction, or Robin Hood, tax that would take a tiny percentage of funds from banks each time they moved large sums to another institution. UNAIDS's Sidibé, an economist by training, and Michel Kazatchkine, who heads the Global Fund, both strongly backed the idea. But Bill Gates expressed doubts. "I know a lot of experts who say it's not workable," said Gates at a press conference, noting that it would be difficult to enforce. Kazatchkine disagreed, saying it could be organized by currency, so that, say, the euro group did its own policing. "The technical feasibility is there," he said.

One obvious cost-saving idea that has been much discussed in the backrooms of Washington and Geneva didn't make it onto the meeting agenda: merging the two biggest players, the Global Fund and the U.S. President's Emergency Plan for AIDS Relief (PEPFAR). Kazatchkine and U.S. Ambassador Eric Goosby, who heads PEPFAR, told *Science* that they think the strategy makes sense. "We're working hard on making that perhaps ultimately happen some day, but happening on some scale as soon as possible," said Kazatchkine, contending that the structure of the Global Fund is better in the long run than that of PEPFAR because it responds to proposals from affected countries. Goosby says they have already begun to mesh projects in some countries. "People are beginning to take down the walls between these efforts," said Goosby.

Washington, D.C., will host the meeting in July 2012, which will take these money woes literally to the White House's doorstep.

–JON COHEN

*Science*NOW

From *Science*'s Online Daily News Site

Bacteria Bring Leaves Back From the Dead

When the leaves they depend on turn a deathly yellow in the fall, leaf miner moths (*Phyllonorycter blancardella*) perform CPR. Even as the rest of the leaf wilts, the patch surrounding a leaf miner larva stays a photosynthetically active green. A new study shows that this green island effect is thanks to bacteria within the grubs.

Ecologist David Giron of the Université François Rabelais in Tours, France, and colleagues dosed some female leaf miners with oral antibiotics to kill their internal microbes. Then the insects laid eggs. Larvae from untreated mothers were able to form green islands, but larvae from dosed moms were not, the team reported in the *Proceedings of the Royal Society B.* The hero could be a microbe of the genus *Wolbachia*, which carries a gene that, in plants, makes death-delaying hormones called cytokinins. bit.ly/stay-green

Earth as an Extrasolar Planet

Astronomers have vetted a new method for finding habitable planets—by testing it on Earth. When a planet transits, or passes between its star and Earth, components of the planet's atmosphere subtract some wavelengths from the star's light and add others. By training a spectrograph on this light, scientists can tease out the composition of the planet's atmosphere and look for life-sustaining elements.

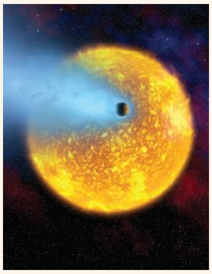

To see if this approach could work on a small, Earth-like world, astrophysicist Alfred Vidal-Madjar and colleagues at the Institut d'Astrophysique de Paris decided to try it on a likely candidate: Earth. Taking the moon's-eye-view, the researchers looked at the sunlight filtered through Earth's atmosphere as it passed between the sun and moon during a lunar eclipse. The method was a success: The researchers detected ozone, oxygen, nitrogen, and sodium in the reflected light from Earth's atmosphere, they report in a paper accepted for publication in *Astronomy & Astrophysics*. bit.ly/like-earth

'Locked-In' Patients Can Follow Their Noses

Patients who can't move, speak, or even control their blinking—known as "locked-in"—could communicate with the outside world through sniffing, thanks to a new technology.

Neurobiologist Noam Sobel of the Weizmann Institute of Science in Rehovot, Israel, and colleagues developed a device that looks like an oxygen delivery tube and detects various types of sniffing. Computer programs then translate the sniffs into typing and wheelchair movement. The team found that healthy subjects could use the device to type sentences and navigate a wheelchair by sniffing, as well (though not as fast) as they were able to using their hands.

With the wheelchair program, a quadriplegic patient moved the wheelchair as well as a healthy, nonparalyzed person could. When quadriplegic and locked-in patients tried the typing program, all used the typing program without much difficulty, increasing their speed and accuracy with each use, the researchers reported in the *Proceedings of the National Academy of Sciences*. bit.ly/sniff-tech

Read the full postings, comments, and more at **news.sciencemag.org/sciencenow**.

CREDITS (TOP TO BOTTOM): DAVID GIRON; ESA/HUBBLE

Is Pharma Running Out of Brainy Ideas?

Recent cutbacks raise concerns about the future of drug development for nervous system disorders

WHEN EMILIANGELO RATTI FOUND OUT late last year that GlaxoSmithKline (GSK) planned to pull the plug on drug discovery in some areas of neuroscience, including pain and depression, he knew he had to do something. As a senior vice president and head of the pharmaceutical company's center for drug discovery in neuroscience, Ratti oversaw work at two centers that were targeted for closure, one in Harlow, U.K., and one in Verona, Italy. Ratti scrambled to arrange a deal with an American contract research organization called Aptuit, which took over the Verona facility on 1 July and will provide research for hire for GSK and other companies. "I'm very proud of that because I've been able to secure the future of my 500 people," Ratti says. At the Harlow facility, hundreds of employees have been laid off, while many others have been transferred within GSK, Ratti says.

In announcing the move to investors and analysts on 4 February, GSK Chief Executive Andrew Witty explained that pain, depression, and anxiety were areas where "we believe the probability of success is relatively low, [and] we think the cost of attaining success is disproportionately high." Ceasing research in these areas would save GSK £250 million ($387 million) by 2012. A few weeks later, news came that AstraZeneca was closing research facilities in the United States and Europe and ceasing drug-discovery work in schizophrenia, bipolar disorder, depression, and anxiety.

Online
sciencemag.org
Podcast interview with author Greg Miller.

These cutbacks by two of the top players in drug development for disorders of the central nervous system (CNS) have raised concerns that the pharmaceutical industry is pulling out, or at least pulling back, in this area. In direct response to the cuts at GSK and AstraZeneca, the Institute of Medicine (IOM) Forum on Neuroscience and Nervous System Disorders organized a meeting in late June that brought together leaders from government, academia, and private foundations to take stock. (The forum's chair, Alan Leshner, is also the executive publisher of *Science*.)

"The biggest problem isn't the announcements by GSK and AstraZeneca, it's when you look at the pipeline and see what companies are actually doing in psychiatric drug development," says Thomas Insel, director of the National Institute of Mental Health. "There are very few new molecular entities, very few novel ideas, and almost nothing that gives any hope for a transformation in the treatment of mental illness."

That's worrying, Insel and others say, because the need for better treatments for neurological and psychiatric disorders is vast. Hundreds of millions of people are afflicted worldwide. Yet for some common disorders, like Alzheimer's disease, no truly effective treatments exist; for others, like depression, the existing drugs have limited efficacy and substantial side effects.

What's in the pipeline?

At first glance, the situation doesn't appear to be so dire. A report released 14 July by the Pharmaceutical Research and Manufacturers of America (PhRMA) touts a record-high 313 drugs in the pipeline for mental health disorders such as depression, anxiety, and addiction. Another report, commissioned by IOM for the June meeting and prepared by the Tufts Center for the Study of Drug Development, identified 1747 drugs in development for a much longer list of disorders, including degenerative diseases like multiple sclerosis and neurological conditions like epilepsy. Indeed, the Tufts report suggests that the pipeline has expanded rapidly for many conditions in recent years (see graph, p. 503). But a closer look tells a different story, says Steven Hyman, a psychiatrist and former NIMH director who is now provost at Harvard University. Many of the drugs in clinical trials have long been approved and are now being tested for a new indication, Hyman says. Looking over the Tufts and PhRMA reports' lists of drugs in

late-stage clinical trials for depression, he notes that both are loaded with antipsychotic drugs, including Risperdal (risperidone) and Seroquel (quetiapine), two of the first "atypical antipsychotics" approved by the Food and Drug Administration in the 1990s. "People with depression can have anxiety and agitation, and low doses of antipsychotics seem to improve those symptoms," Hyman says. "But they don't necessarily have an independent effect on the core depressive symptoms, and they come with a real side-effect burden."

Other treatment candidates have limitations as well. Both lists include Corlux (mifepristone, better known as RU-486, the abortion drug). Even if it proves effective for depression, it couldn't be prescribed for women of reproductive age, Hyman notes. The Tufts list includes Agomelatine, a drug that boosts the effects of the hormone melatonin and blocks receptors for the neurotransmitter serotonin. Hyman says there's little compelling evidence that boosting melatonin has antidepressant effects, and he notes that the drug has had mixed results in European trials for depression. "This is hardly a rich pipeline," Hyman says. "It suggests a sad dearth of ideas and involves lots of attempts at patent extensions and new indications for old drugs."

Risky business

The reasons for the seeming lack of innovation are partly historical, says William Potter, who retired in January from Merck, where he was vice president for neuroscience. In the 1980s and '90s, drug companies realized that they could make billions of dollars a year off drugs that were slightly modified versions of already-approved medications, particularly the SSRI antidepressants like Prozac, Potter says: "The investment in truly innovative projects was not as deep as it might have been because you could make so much money from 'me, too,' drugs."

The current climate for innovation may be even worse. Companies will soon lose billions of dollars in revenue as patents expire on dozens of blockbuster drugs (see figure, below). Meanwhile, the costs of research and development are rising. "Most companies don't see where they're going to be getting the cash flow, so they're having to be more conservative," Potter says. "You can't just ask companies to throw money at something that might not pay off."

The Tufts report suggests that pharma executives have good reason to see investments in CNS drug development as riskier

$$$ Expiring Patents and Rising Research Costs

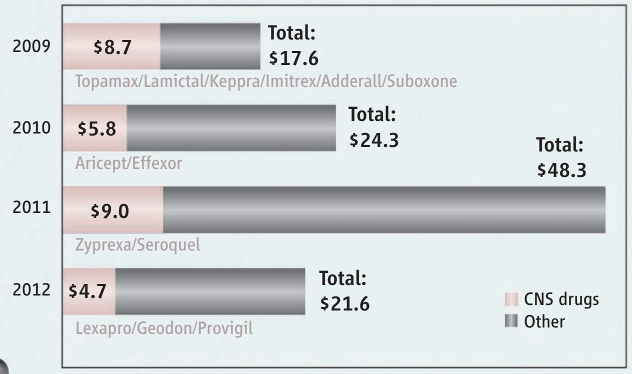

U.S. sales (in billions) for top 10 selling drugs with expiring patents

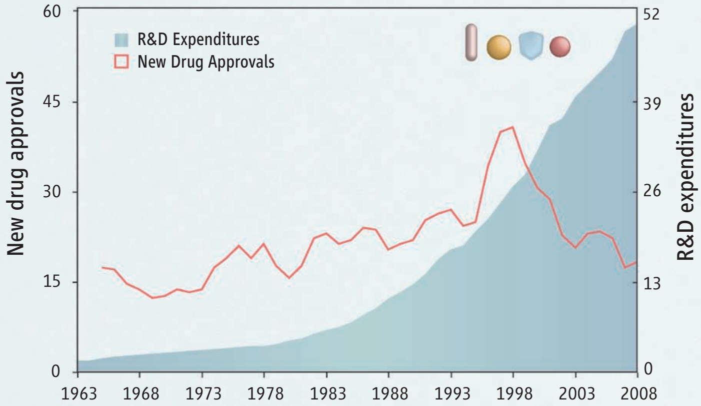

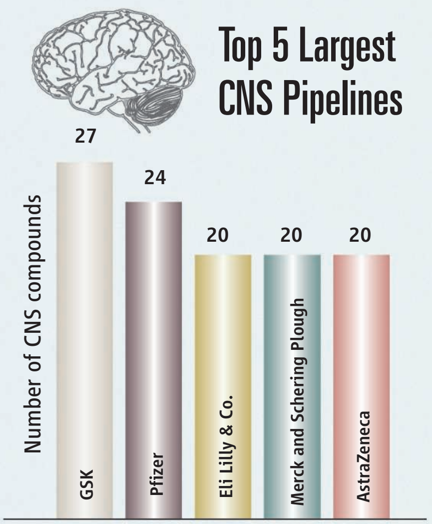

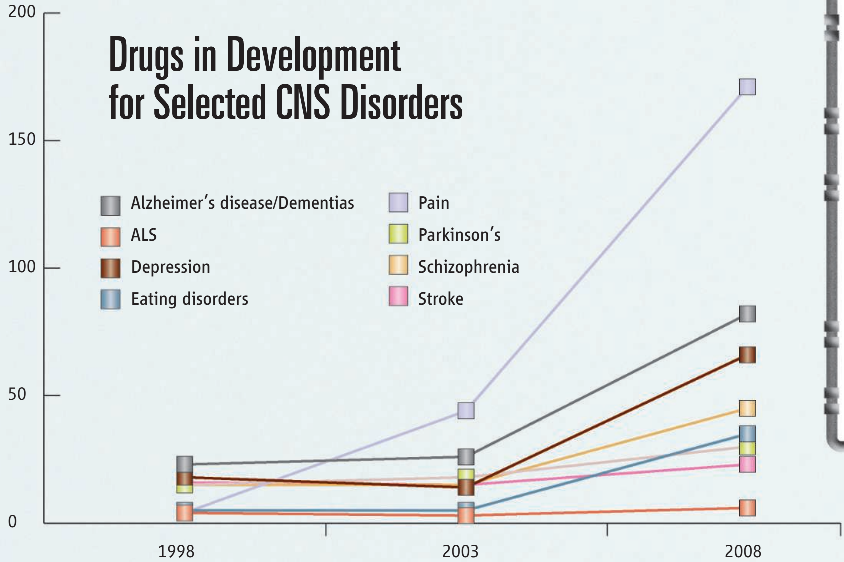

CREDIT: ADAPTED BY PERMISSION OF THE INSTITUTE OF MEDICINE; (SOURCE) TUFTS CENTER FOR THE STUDY OF DRUG DEVELOPMENT

than investments in other areas. CNS drugs cost more and take longer to bring to market than other types of drugs (see figure, right). And only 8% of CNS drugs that make it to clinical trials end up being approved, about half the average success rate across all therapeutic areas. Moreover, when CNS drugs fail, they tend to do so in late-stage clinical trials, after a significant investment has been made, says Kenneth Kaitin, director of the Tufts center.

Adding to those troubles, the animal models, particularly for psychiatric disorders, are far from perfect at predicting which compounds will be effective in humans, and the clinical trials are often more complicated for CNS disorders, says Ratti. These disorders tend to be complex and intermittent, and their symptoms often defy objective measurement. "All these things together are making discovery and development in neuroscience significantly risky," he says.

Many companies see areas like oncology and autoimmune disorders as safer bets, says Steven Paul, who stepped down in February as executive vice president for science and technology for Eli Lilly and Co. "Their perception is that the science is a little richer and the odds are less daunting in some of these other areas," he says. Even within neuroscience, Paul says, some companies may see psychiatric drugs as a bigger gamble than drugs for neurological conditions. Paul, who is a psychiatrist, says he doesn't necessarily agree with that assessment: "I personally believe there are compelling pathways and new targets to pursue."

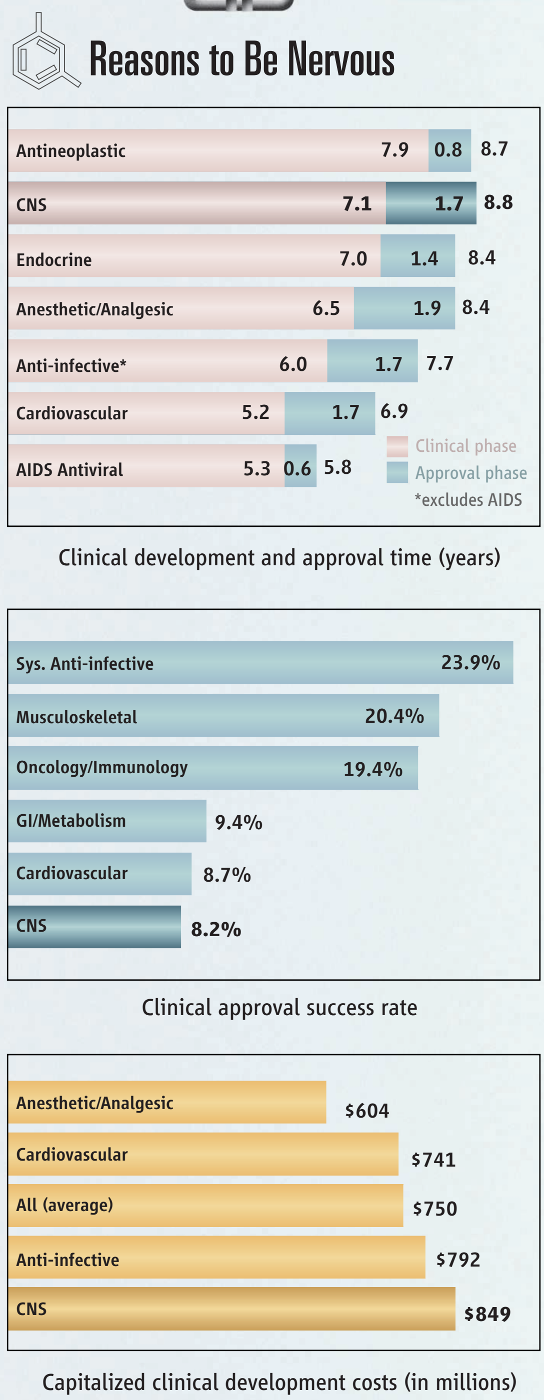

Seeking a new model

Given the economic challenges, experts inside and outside pharma say the old model of drug development, in which companies assume all the risks and costs of searching for new drugs and shepherding them from test tube to clinic, is no longer viable. "Traditionally, they would have significant internal research groups that would be as good as anyone at doing some of the basic research that might lead to new targets," says Adrian Ivinson, who directs the Harvard NeuroDiscovery Center. "We're seeing less and less of that."

Many companies are trying to reduce costs by outsourcing R&D. AstraZeneca and GSK both set up R&D centers in Shanghai, China, in 2007, for example. The GSK center focuses on developing treatments for multiple sclerosis, Parkinson's, and Alzheimer's diseases; its work on those disorders will continue despite the recent cutbacks in other areas of neuroscience. Another outsourcing strategy involves contracting with biotech companies and academic researchers to do some of the early drug-discovery work that was previously done in-house. "They are sending scouts out into the community to talk to groups like ours and many others to identify projects with potential for drug discovery," Ivinson says. In a typical arrangement, a company funds a research project in exchange for the right to license any resulting compounds that show therapeutic potential.

At the IOM meeting, there was much discussion about public-private partnerships. Insel notes that the U.S. National Institutes of Health (NIH) already has a drug-discovery effort that might serve as a model, the Therapeutics for Rare and Neglected Diseases project launched last year. A measure in the new U.S. health-care legislation could expand NIH's role: It authorizes up to $500 million a year for a "Cures Acceleration Network" aimed at speeding drug development (*Science*, 26 March, p. 1562). "It's a strong message from Congress that they would like to see NIH more involved in drug discovery and drug development," says Insel.

Another possibility might be a shared repository of compounds. "Pharma has thousands and thousands of compounds that are leads they've decided not to follow," Insel says. "Would it make sense to put those into a resource that other people could begin to mine?" In May, GSK made public a library of potential malaria drugs, but neurology and psychiatry are far more lucrative markets. An open-access library of compounds would involve a host of challenges, not the least of which are questions about intellectual property, Insel says. "These are big and thorny issues, but we have got to grapple with them so that 10 years from now we're not looking at the same list of compounds that we know don't work well enough and hoping that if we just give them to a different group of patients we'll get a better outcome."

–GREG MILLER

CREDITS: ADAPTED BY PERMISSION OF THE INSTITUTE OF MEDICINE; SOURCE: TUFTS CENTER FOR THE STUDY OF DRUG DEVELOPMENT

ECOLOGY

Europe Tries to Save Its Eels

New national efforts to save the European eel face political and scientific challenges

Eel rescuer? German agriculture minister Ilse Aigner releases young eels into the Havel River.

BERLIN—On a sunny morning this spring, German agriculture minister Ilse Aigner waded into the controversy over how to save the European eel. With several Berlin fishers, she helped release 65,000 young eels, called elvers, into the Havel River, which flows through Germany's capital city. Sporting rubber boots and a smile, Aigner gamely emptied her net of writhing fish into the cloudy river water. She then posed with the fishers, holding up a T-shirt that read "Eel Rescuer" and "Thank you for stocking eels!"

But whether Aigner's actions helped the long-term prospects for *Anguilla anguilla*, better known as the European eel, is hotly debated. Stocking eels in the Berlin river "is useless," says Heike Vesper, fisheries officer for the conservation organization WWF Germany in Hamburg. "It's essentially a waste."

Although the eels Aigner released have a good chance of thriving in the Havel, it is an open question whether any of them will reproduce. To contribute to the next generation, European eels must ultimately migrate back to the species' presumed spawning grounds in the Atlantic Ocean. From Berlin, that is a journey of more than 5000 kilometers, through dammed rivers, past deadly power plant turbines, and around fishing nets. Stocking young eels on the inland side of such barriers gives them only the slimmest chance of becoming a parent, say many conservationists and scientists.

No one disputes that eel rescuers are badly needed. Once abundant in European waters, the numbers of European eels have fallen drastically since the 1970s, by as much as 99% according to some estimates (*Science*, 10 October 2003, p. 221). Besides dams, turbines, and fishing, a number of factors, including a recently introduced parasite, chemical pollutants, and possible changes in ocean currents, are all suspected of playing a role in the eel's decline.

Sorting out the impact of each is difficult, because much about the eel's complex life cycle remains a mystery to scientists. "We are looking for life on Mars, but we still don't know where [European] eels spawn," says fish physiologist Arjan Palstra of the University of Barcelona in Spain. The recent population crash, however, has stimulated innovative research on eels, from complex tracking experiments to simulations of their marathon migration in the lab, as scientists try to understand why the eel is disappearing—and to come up with ways that politicians and others might be able to make a difference.

Politicians are at least paying attention. In 2007, the European Union issued a regulation requiring each of its member countries to develop an "eel management plan." The measure calls for limits on eel mortality based on a theoretical estimate of eel survival called the pristine rate: the number of eels that would have migrated back out to the open ocean in the absence of human impacts. The plans must ensure that at least 40% of this amount really do make the trip.

Precious commodity. The number of glass eels reaching European shores has plummeted, and prices have skyrocketed.

CREDITS (TOP TO BOTTOM): PERCY VOGEL; CREUX THIERRY/NEWSCOM

Nationwide conservation efforts based on the regulation are finally coming into effect; plans for two of the largest countries, Germany and the United Kingdom, were approved in April. But eel experts worry that many of the plans don't go far enough and fail to address some of the eels' most crucial problems. "From the perspective of the eel population, there's room for improvement," says Kim Aarestrup of the National Institute of Aquatic Resources in Silkeborg, Denmark.

Elusive eels

European eels apparently start and, if they survive long enough, end their lives in the deep, clear, calm, and featureless waters of the Atlantic Ocean's Sargasso Sea, a region bounded by major ocean currents and roughly the size of the continental United States. However, no one has seen a spawning European eel or its eggs in the wild.

The main evidence pointing to the Sargasso as the eels' spawning ground is that the smallest eel larvae have been spotted there. (One early observation was described in *Nature* in 1923, and that report is still regularly cited, notes David Righton of the Centre for Environment, Fisheries & Aquaculture Science in Lowestoft, U.K.) These larvae seem to grow from approximately 5 mm in the Sargasso to roughly 5 cm as they drift toward the European coast with the Gulf Stream. Scientists don't know whether larvae direct their course by actively swimming, and what they ate was a mystery too until recently—a study of larvae stomach contents reported in June indicate the eels consume zooplankton. By the time the animals get close to the coast, they have grown into 7-cm-long transparent eels.

These so-called glass eels enter estuaries from Morocco to Iceland. Unlike salmon, which return to their natal river or stream to spawn, eels seem to let ocean currents steer

them by chance to their freshwater habitat. Some eels end up in Ireland, whereas others reach Greece; no genetic differences among these populations have been found.

The glass eels swim upstream and, once they enter fresh water, turn gray, becoming so-called elvers. Elvers gradually change color again, becoming yellow eels. The animals spend most of their lives in this form, living in rivers, lakes, and swamps and storing up energy, primarily as fat, for their final journey back to the Sargasso. Males spend roughly a decade as yellow eels, and females spend significantly longer—perhaps because egg production requires more energy than making sperm. Eventually, reacting to a trigger that scientists have yet to identify, they begin the long trip back to their birthplace to spawn.

To prepare for the journey, yellow eels undergo a radical transformation. They toughen their skin, alter their gills, and develop a black back and silver underside that helps them hide from open-ocean predators. The animals, called silver eels, rely entirely on their fat stores to make the long swim back to the Sargasso, ingesting only water on the way.

An average silver eel is more than 20% fat, making them a favorite target of fishers across northern Europe, where smoked, fried, and jellied eel are traditional favorites. (Yellow eels are also eaten in significant numbers.) In southern Europe, the fishers concentrate on the younger glass eels found in coastal waters. Some are shipped to Asia, where the spaghetti-thin eels are eaten as a delicacy or farmed for later harvesting as yellow eels. Others are sent to European aquaculture farms, where they are later sold to restocking programs—like the one Aigner highlighted in Berlin—or directly to fish farms where they are raised for European consumption. It is the number of glass eels that has fallen most dramatically over the past 30 years, arriving at less than 10% of the rate recorded in the 1970s. Once a cheap food, a kilo of glass eels now goes for about €500 ($640).

Planning a comeback

Conservationists worry that both silver and glass eel fisheries are unsustainable, given the dearth of incoming glass eels. But in political circles, there is some rivalry between the northern and southern fisheries. The tension—and the relative power of fishing interests—is reflected in the countries' different management plans as well.

Ireland has taken the strictest approach, closing the commercial fishery at least through 2012. But some eel fishers can still make a living: Ireland pays them to "catch and carry" live eels over barriers, both on their inward and outward migrations. The Netherlands and the United Kingdom have shortened their eel-fishing seasons, banning fishers from catching glass eels especially in the last stages of their upstream migration and prohibiting fishing for silver eels during their autumn downstream migration.

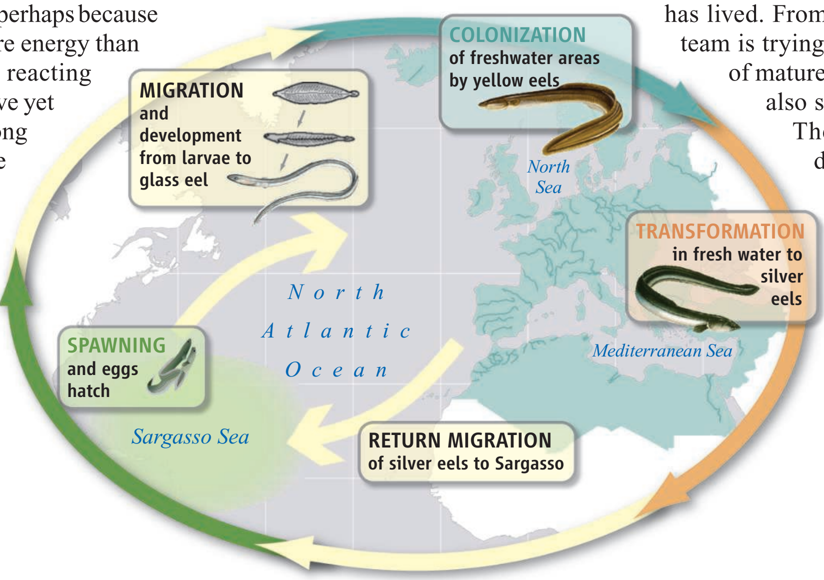

Mysterious journey. Eels travel thousands of kilometers from their apparent Atlantic Ocean spawning grounds to Europe—and back again.

CREDIT: K. ENGMAN/SCIENCE

Germany's plan has been especially disappointing to conservationists, says WWF's Vesper. It relies primarily on stocking: transferring young eels from coastal regions—often from southern Europe—to habitats upriver. The strategy is based on fishing interests, not the eels' survival, Vesper charges. German stocking programs have been going on at least since the early 20th century and are traditionally paid for by fishing organizations. So as not to discourage those efforts, the German plan puts few new restrictions on eel fishing. Instead, it calls for the temporary shutdown of dam turbines and for an open season on another protected species: cormorants. Fishers blame the birds for eating a significant portion of the available eels.

But some worry that stocking programs, although increasing the number of eels in Germany, may be detrimental to the species as a whole. No one knows exactly how successful stocked eels are at making their way back out to sea. Transporting young eels across the continent may disrupt their navigational imprinting and leave them unable to find their way back to the Sargasso, Palstra says.

Reinhold Hanel of the Institute of Fisheries Ecology in Hamburg, Germany, and his colleagues are addressing that issue by analyzing eels' otoliths, structures in the inner ear that help animals maintain balance. Scientists can study the composition of the otoliths to determine where an eel has lived. From such information, Hanel's team is trying to determine what fraction of mature eels entering the Baltic Sea also spent their early years there. The project "should help us determine whether stocking is worthwhile or counterproductive," Hanel says.

Farther south, France has a plan to reduce fishing mortality by 30% and improve eel habitat and migration routes, but it does not ban the (very lucrative) export of eels to Asia, a step recommended by the International Council for the Exploration of the Sea. E.U. officials have not yet given the green light to plans submitted by Greece, Portugal, Spain, and Italy. Because the Mediterranean countries have little historical data available to estimate how many adult eels should be migrating out each year, regulators have been arguing over how many outgoing eels will fulfill the mandate.

A fish odyssey

A major weakness of all the European plans, say Palstra and others, is that they do not take into account the variable quality of silver eels leaving each country on their reproductive migration. "[Potential] spawners are leaving everywhere from Morocco to Iceland. We don't know which of those really contribute to the next generation," says Russell Poole of Ireland's Marine Institute in Furnace. The target rate of outgoing eels may need to be adjusted upward if the viable breeding fraction is low.

To try to help answer that question, Righton, Aarestrup, Poole, and colleagues from seven countries across Europe are cooperating on a 4-year, €4 million ($5.2 million) project called the "eeliad," which is tagging migrating silver eels as they start

their journey. The eels carry 12-centimeter-long satellite tags to record water depth, temperature, sunrise, and sunset. The tags release at a preset time, rise to the surface, and transmit their stored data. No tags have yet made it all the way to the Sargasso, but an earlier tagging project found that migrating eels spend the night in shallow, warmer water and dive during the day to depths of up to 1000 meters. Such dives might help the animals regulate their temperature, allowing females to postpone maturation of their eggs until they reach the Sargasso Sea (*Science*, 25 September 2009, p. 1660).

Difficulty moving up and down in the water column may be one reason the European eel is in trouble. Eels use an organ called the swim bladder to regulate buoyancy. This organ is attacked by a nematode parasite, called *Anguillicola crassus*, that started appearing in European waters in the 1980s, presumably imported from Asia along with Asian eels used in aquaculture. The parasite has since spread across Europe, given a lift by stocking efforts. Whereas Asian eels have some natural resistance to the parasite, usually hosting just five or six per animal, infected European eels frequently have dozens. To better ascertain how the parasites affect this migration, eeliad researchers last year tagged eels known to be infected, Righton says.

The parasite problem can also be explored in the laboratory thanks to 22 eel "swim tunnels," a complex of tubes filled with 7000 liters of water that allows the fish to swim thousands of kilometers as if they were returning to the ocean. Using this device, Palstra, his Ph.D. supervisor, Guido van den Thillart of Leiden University in the Netherlands, and their colleagues found in 2007 that eels infected with the parasites swim 20% slower while using 20% more energy than uninfected eels—perhaps using up their fat reserves before they reach the Sargasso or causing them to have little left over to devote to egg production once they arrive.

The international eel trade has also spread a suite of viruses that render eels less fit for their epic journey. Van den Thillart and Vincent van Ginneken, also of Leiden University, have found that eels infected with so-called Eel Virus European X developed hemorrhages and anemia during their simulated migration in the swim tubes and died after swimming roughly 1000 kilometers.

So it is possible that even if the management plans allow significant numbers of silver eels to escape back into the Atlantic, relatively few are able to complete their biological mission. Palstra suspects that in the long term, Europe may need to raise wild-caught young eels in clean habitats—free of viruses, parasites, and chemicals such as PCBs—and ensure that they are able to leave for the open ocean.

Breeding eels in captivity would be one way to reduce fishing pressure on the wild population, but for now, this is still just a research goal. Scientists have had some success: They can use hormone treatments to prompt European eels to produce sperm and eggs in the lab. The eggs fertilize and hatch, but the larvae die after a few days, in part because no one has yet figured out what to feed them. Japanese researchers announced in April that they had produced offspring from Asian eels that had been bred and raised in captivity, for the first time completing an eel's life cycle in captivity. They apparently feed their larvae a slurry of shark egg powder, Palstra says, but their success rate is still very low. He and colleagues from 15 institutes from Norway to Tunisia are part of a new E.U.-funded project, PRO-EEL, that aims to replicate the Japanese success with European eels.

Endangered delicacy. European and Asian gourmands enjoy fried, jellied, and smoked eels.

CREDITS (TOP TO BOTTOM): ARJAN P. PALSTRA/UNIVERSITAT DE BARCELONA; CORBIS; J. DADDY/WIKIMEDIA COMMONS; HOLGER HOLLEMANN/CORBIS

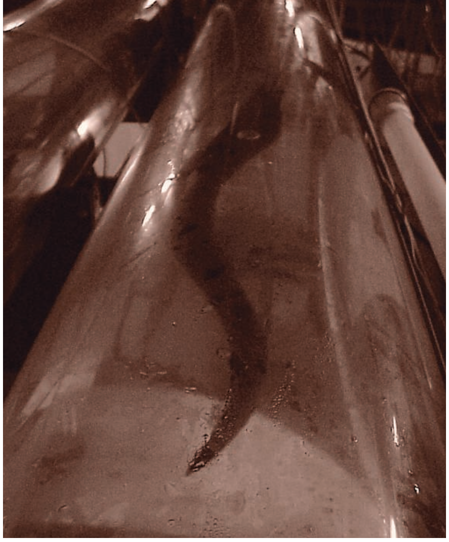

Virtual voyage. Swim tunnels allow scientists to study eel migration in the lab.

Blame it on nature?

A few scientists question whether humans are really at fault for the crash of the European eel. The decline could be part of a natural cycle, says Brian Knights, a retired eel biologist from the University of Westminster. Perhaps changes in the Gulf Stream are driving the larvae off course or changes in water temperature or food availability are affecting the animals' survival. "It might be that the major cause of change is beyond our control," he says.

Most eel experts, however, don't hesitate to point the finger at people's appetite for the fish. "If you look at the exploitation of eels, habitat loss, and disease, … it's hard to argue that human impact has nothing to do with it," counters Aarestrup. "But because we know so little, it's hard to make the argument" that particular interventions will make a difference, he admits.

And eel watchers agree that there will not be any quick payoffs from Europe's conservation plans. In many regions, it can take female eels 20 years to mature into migration-ready silver eels. "You're looking at a very slow recovery process for the population," says Poole. "You're not going to see anything obvious in the next 20 to 50 years."

At the same time, it is unlikely that the European eel will go completely extinct. "Anyone who talks about extinction is alarmist," Poole says. "You're talking about fish that spawn multiple millions of eggs." The fisheries, however, may face real danger. "You can't continue to exploit a stock where current recruitment is less than 10% of previous levels," Poole says.

The political decisions are not easy ones, Aarestrup admits. "We know less about eels than we know about climate changes," he says. "But the question is, can we afford to do nothing?"

–GRETCHEN VOGEL

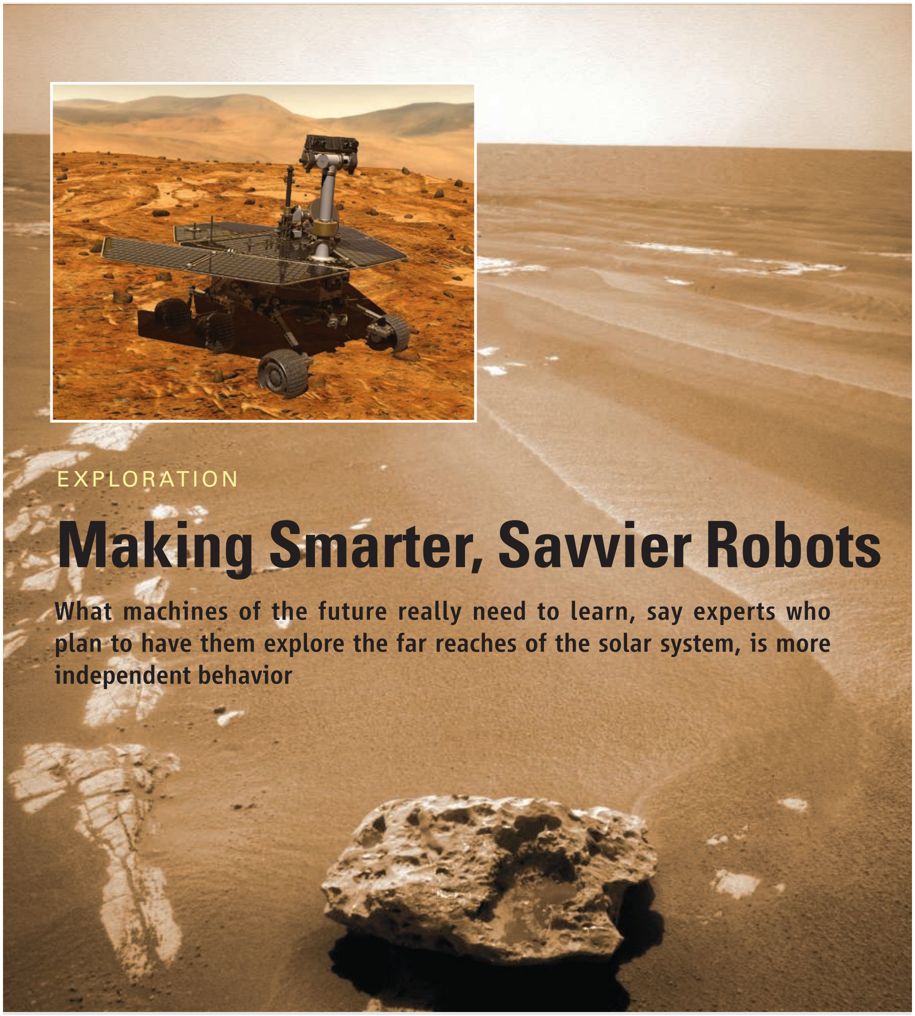

Which rock? On Mars, the robot Opportunity needed some human help to spot this meteorite.

EXPLORATION

Making Smarter, Savvier Robots

What machines of the future really need to learn, say experts who plan to have them explore the far reaches of the solar system, is more independent behavior

On 18 July 2009, the Mars rover Opportunity was scooting toward a distant martian crater when it spied an anomaly amid the ripples of red soil: a bruise-colored rock the size of a watermelon. It looked like a meteorite—potential evidence that the ancient atmosphere of Mars, like today's, was thin enough for such rocks to pass through without exploding.

The strange rock was exactly the kind of thing NASA sent Opportunity to find. But because Mars and Earth are millions of kilometers apart and rotate out of sync, NASA scientists didn't see it until Opportunity had driven 200 meters beyond it. They hit reverse but had to wait three full days for Opportunity to backtrack to the spot.

The researchers got their meteorite. But the near miss—and the frustrating delay—underscored a defect of current exploration technology: Basically, robots are pretty dumb. Now scientists across the world are striving to change that by developing intelligent robots that can circumvent danger and spot enticing features on their own.

Hundreds of scientists, mostly at NASA and at universities, are working on improving robot explorers. But only a few dozen specialize in developing robots with true, high-level independence. The main NASA lab, at the Jet Propulsion Laboratory (JPL) in Pasadena, California, has a dozen people and a budget of about $4 million—a lower figure than in the past. But scientists there see promising signs. For one, NASA chief technologist Robert Braun has begun a new, general Space Technology Program that lists "machine intelligence" as one thrust.

"There are compelling reasons to send humans into deep space," says Steve Chien, who develops autonomous space systems for JPL. "A smart scientist can do much better experiments. But it's very expensive. By making the spacecraft much smarter, we can reduce the gap between human exploration and robotic exploration."

Where to go

Robots with an IQ boost will be essential for fully exploring some locations in the solar system—including hostile spots. On Venus, for example, 450°C surface temperatures and pressures comparable to those a kilometer deep in the ocean will destroy the onboard computers of any lander within 5 hours, tops. To get anything done, the lander will need to perform experiments, such as sampling soil, without human input.

Rendezvous missions with comets or asteroids and landings on distant moons would also benefit from more autonomous robots, researchers say. On Saturn's moon Titan, radio waves carrying scientists' instructions take 90 minutes to arrive from Earth. Yet a probe flying through Titan's atmosphere would have to negotiate hazards in real time, notes Wolfgang Fink, a computer scientist working at the California Institute of Technology and the University of Arizona. "If it's about to fly into a mountain range, it can't say, 'I'm flying into a mountain range. Please advise,' and wait 1½ hours."

Scientists also hope that greater intelligence will make robots more efficient, improving their "energy storage, memory, computational throughput, communication downlink bandwidth, and heating and cooling capability," says Larry Matthies, a computer scientist at JPL. Opportunity (and its companion on Mars, Spirit) travel at such pokey paces—28 kilometers total in 6 years—partly because they rely on humans to spot dangerously loose sand or steep slopes. A smarter robot could zip around obstacles by itself and travel up to 10 times as far each day, Matthies estimates. And the more work the rover can do alone, the more time it will have to collect good samples.

Recipes for "eureka"

In December and January, NASA took the first steps toward making a spacecraft autonomous when it uploaded four pieces of software to Opportunity. Tara Estlin, a senior engineer at JPL, explains that, with the new software, "scientists can give us a single property or combination of properties—the largest rock you can find, or the darkest rock," and Opportunity will zero in on them. In March, the software passed its first test by discovering, all on its own, an angular, football-size rock—ejected from a nearby impact crater—in a field of rounder boulders. (Paradoxically, though, Estlin's team still has to tell the rover a day in advance when to be autonomous and when not to.)

Earth-based systems have already demonstrated significant independence, within limits. Chien works on the Earth Observing

CREDITS: (MAIN) NASA/JPL-CALTECH; NASA/JPL

Sensorweb, a group of half a dozen NASA satellites that monitor Earth's atmosphere. Some scan large sections of Earth's surface and pick out a flood or a volcanic plume from space. They beam the data to ground-based computers, which in turn direct higher-resolution satellites to focus on the event—all without human input. Chien hopes to expand the work to other planets. But the instruments can spot only a short list of predefined events; they cannot find anything interesting or new on their own. Asked whether the system could shift its attention on its own between the two most notable geological events of the past few months, the Eyjafjallajökull volcano eruption in March and the BP oil slick in the Gulf of Mexico in April, Chien groans: "I wish, I wish."

To solve problems of data filtering and interpretation, some researchers are working to cultivate a robot's taste for the unusual. Sometimes scientists want to study the most representative feature around, but more often they are intrigued by anomalies. "If the whole desert is smooth and one area is rough, that's interesting," says Chien. "If the whole desert is rough and one area is smooth, that's interesting. If you really don't know about the environment, you have to fall back on something like outliers."

Patrick McGuire, a computer scientist and geologist at the University of Chicago in Illinois, has developed a simple setup that can detect novel features in a landscape. A netbook laptop hooked up to a cell phone with a camera snaps a picture and compares its colors, textures, and shapes with other pictures in its memory. The computer then compresses the image with an algorithm. If the compression process is very similar to that of an earlier image, the computer concludes that the new image doesn't contain much novel information and throws it out.

McGuire has tested this system at rock outcrops in Utah and Spain that resemble the barren landscape a probe might encounter on a distant planet. He reported late last year that the software performed equally well in both locations. In one case, the software immediately recognized a patch of lichen as novel—and then, with the next picture, threw out an image of lichen on another rock as too similar to bother remembering, demonstrating that it is a quick study.

Curious future

Some scientists, including Fink, say better programming alone won't turn robots into independent explorers. "In planetary exploration, you're in for surprises," Fink argues, "and you will not always have a rule" on how to proceed. He dreams of robots that can experiment with their own "neural networks"—their internal architectures for taking inputs, processing information, and producing outputs—and can, like humans, form their own rules for exploring.

McGuire says certain architectures have advantages in different applications. With a so-called Hopfield neural network, for example, a computer can recognize an entire picture stored in memory after seeing only a fraction. Many robots come equipped with multiple lenses and cameras that take pictures on different scales, so the capability to tag small snippets as familiar would help make the robot more efficient in selecting which scenes to shoot or not shoot.

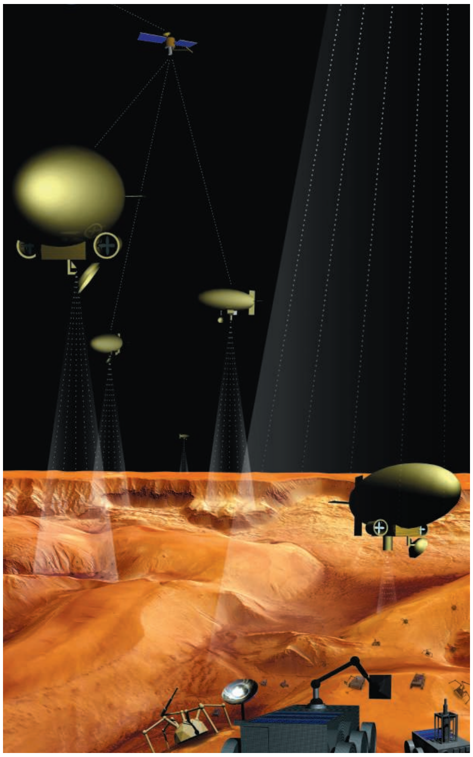

Mechanized teamwork. Caltech's Wolfgang Fink foresees robots exploring in tiered ranks.

CREDIT: DR. WOLFGANG FINK AND WAYNE WALLER, VISUAL AND AUTONOMOUS EXPLORATION SYSTEMS RESEARCH LABORATORY, CALIFORNIA INSTITUTE OF TECHNOLOGY

Even more ambitiously, Fink is developing systems to give robots freedom to change their logical architecture—essentially to "rewire" their brains. A robot might make a rule more complicated or simpler by adding or cutting steps, or combining the binary code of two rules and trying out their "offspring." If the new rules worked well, it adds them to its problem-solving repertoire.

Fink published a paper last year on a self-configuring neural network to sort odd numbers from even numbers. Working with numbers 24 bits long—in the tens of millions in decimal notation—the network hit upon the solution (look at the final digit) with no guidance. And by focusing on one bit, the computer freed 23 other bits for different tasks. In other contexts, such self-configuring networks have helped scientists design circuits and new drugs.

Ultimately, Fink says, he hopes to instill something like curiosity in robots. That kind of programming would go far beyond algorithms his team has developed to help robots calculate the best angle to stretch out an arm to grasp an object or scoop soil. "We're after the *intent* to deploy the arm. How does the spacecraft know where it wants to dig? This is of interest to me."

The first test?

Smart, curious robot explorers wouldn't have to work alone. Fink envisions a multitier scheme of robots with satellites, blimps or balloons, and platoons of ground rovers. An intelligent satellite would direct the blimps to canvass certain areas. The blimps, in turn, would direct surface rovers to scout hydrothermal vents or rappel down cliff faces with a cable. Based on feedback between each tier, the satellite would decide which sites to concentrate on and how best to deploy the other machines. It would judge when to risk sending rovers into dangerous areas like active volcanoes, and when to stop collecting data, Fink says. "A spacecraft could even leave a place and tell you, 'There's nothing interesting here. I'll go somewhere else and I'll tell you when I get there.' " Fink and his team have started building a test site in Arizona with rovers, boats, and blimps for field experiments with rudimentary versions of such robotic expeditions.

Chien imagines a different sort of teamwork: human explorers with fast-learning robot assistants. A group led by David Akin at the University of Maryland, College Park, is testing a golf cart–size three-wheeled rover, named Raven, to help astronauts explore planets. On tricky terrain such as loose soil or slopes, Akin says, the astronaut can simply say, "Follow my path," and the robot will.

President Barack Obama's stated goals of sending humans to an asteroid in the 2020s and to Mars in the 2030s could help foster such partnerships. Chien says human-and-robot teams could do a better job together than either could alone. Humans would make plans and be in charge, while robots slogged through the important but routine technician work. "It's the classic apprentice thing," Chien says. "You want the biggest brainpower worrying about the biggest problems."

–SAM KEAN

LETTERS

edited by Jennifer Sills

Immigration Law Jeopardizes University Collaboration

RECENTLY, THE ARIZONA LEGISLATURE PASSED AN AGGRESSIVE IMMIgration law requiring that local police ask individuals for proof of citizenship or immigration status if there is reasonable suspicion that they are in the United States illegally. We believe that this law increases the likelihood of race-based inquiry by police and the possibility that individuals will be treated differently solely because of their appearance. The consequences of this law can be profound.

The passage of the law has led to similar apprehension in Mexican institutions of higher learning. Many Mexican faculty and students have expressed serious concerns about traveling to Arizona to work on collaborative projects. Four Mexican universities so far have also canceled or placed on hold programs that required Mexican students to attend Arizona universities (*1*). Sadly, this means that innovative collaborative programs in fields such as medicine, toxicology, and biotechnology, as well as a binational economic development initiative (Advanced Technology Transfer Program) aimed at increasing the quality of life of citizens of Mexico and Arizona, are now in jeopardy.

The faculty and students that comprise an educational community, whether on a single university campus or across international borders, represent a social model built upon diversity of culture, ethnicity, and ideas. Indeed, institutions of higher learning exist to educate and enlighten our population precisely so that practices such as racial stereotyping are recognized as destructive forces that are contrary to basic principles of human dignity. As faculty and students of Mexico and the universities of the state of Arizona, we must continue to work hard to celebrate the richness of the diversity of our border, work across fiscal and cultural boundaries, and strive to better our ways of life. We will continue to work in a collaborative spirit, which is the hallmark of all great societies.

Unintended consequences. Concerns about Arizona's new law have led Mexican universities to cancel collaborative programs.

JOSÉ ANTONIO DE LA PEÑA,[1] MEREDITH HAY,[2] CARLOS ARÁMBURO DE LA HOZ,[3] JOAQUIN RUIZ[4]*

[1]Deputy Director General for Science, Consejo Nacional de Ciencia y Tecnología, México D.F., 03940, México. [2]Executive Vice President/Provost, The University of Arizona, Tucson, AZ 85721, USA. [3]Coordinator of Scientific Research, Universidad Nacional Autónoma de México, Circuito de la Investigación Científica S/N, Ciudad Universitaria, Mexico D.F., 04510, México. [4]Executive Dean of the Colleges of Letters, Arts and Science, The University of Arizona, Tucson, AZ 85721, USA.

*To whom correspondence should be addressed. E-mail: jruiz@email.arizona.edu

Note

1. Canceled programs include a mobility program for bachelors of arts students at the Universidad Nacional Autónoma de México, a Technology Transfer summer program at the Centro de Investigación Científica y de Educación Superior de Ensenada, all collaboration programs at the Universidad de Guanajuato (UG), and all collaboration Programs at the Universidad Autónoma de San Luis Potosí.

Graduate Education: The Future Is Now

AS CHAIR AND VICE CHAIR OF THE COMMISSION on the Future of Graduate Education, we appreciated J. Mervis's detailed News of the Week story on the Commission's report, *The Path Forward: The Future of Graduate Education in the United States* ("Report seeks expansion in a time of belt-tightening," 7 May, p. 678). We would like to address the issue it raised about the timing of the report's recommendations.

It is clear that the United States faces serious fiscal challenges. The Obama Administration has begun to address reducing the federal deficit, which will help ensure our long-term prosperity. Every effort must be made to spend public dollars wisely, focusing on those investments that will yield enhanced productivity in the future.

The Commission's recommendations are designed to be an integral part of a national innovation strategy to ensure that the United States will have the intellectual leadership, along with the innovative technology, necessary to be successful in the 21st century global economy. A central theme of the Commission's report is how graduate education plays an essential role in strengthening our national competitiveness and innovation capacity, especially given the projected 17 to 18% increases over the next decade in the number of jobs requiring a doctoral or master's degree (*1*).

Our proposed investment of $10 billion over the next 5 years for a graduate education training initiative will yield substantial benefits to our country in the future. We must be—and we are—ready with a plan that charts a path forward.

WILLIAM B. RUSSEL[1]* AND SUZANNE ORTEGA[2]

[1]Dean of the Graduate School, Princeton University, Princeton, NJ 08544, USA. [2]Executive Vice President and Provost, University of New Mexico, Albuquerque, NM 87131, USA.

*To whom correspondence should be addressed. E-mail: wbrussel@princeton.edu

Reference

1. U.S. Bureau of Labor Statistics, "Employment projections: 2008–2018 summary" (2009); www.bls.gov/news.release/ecopro.nr0.htm.

CREDIT: ROSS D. FRANKLIN/AP PHOTO

Sustainability: A Household Word

I THANK Q. WANG AND G. P. PETERS *ET AL.* ("China's environmental civilian activism" and "Effects of China's economic growth," Letters, 14 May, p. 824) for responding to my Policy Forum, "China's road to sustainability" (2 April, p. 50). Their Letters reiterated important forces affecting sustainability, which I have previously addressed (*1*–*3*).

In contrast to Peters *et al.*, I maintain that the direct and indirect impacts of households on the environment (*4*) are important and deserve much more attention. For example, the household sector is the major direct and indirect consumer of energy (*5*). From 1980 to 2006, direct residential electricity usage in China increased 31-fold, whereas electricity usage in other sectors increased only 8-fold (*6*). In 2005, households' indirect energy usage (e.g., energy usage by other sectors that produce and transport products for households) was 4.5 times as high as their direct energy usage; between 1992 and 2005, indirect energy usage increased 6.3 times as fast as direct energy usage (*7*). CO_2 emissions from households increased over time (*5*, *8*). With increasing domestic demand and household proliferation (rapid increase in the number of households) in China, household impacts on the environment may continue to rise in the future.

I agree with Wang that more people in China have been involved in environmental civilian activism against environmental damage from industries, but it is essential to consider their own increasing environmental impacts that result from lifestyle changes such as increasing consumption, increasing demand for household products, and increasing divorces (*9*). To minimize the environmental impacts of industries, it is important to reduce household demand for industrial products.

JIANGUO LIU
Center for Systems Integration and Sustainability, Michigan State University, East Lansing, MI 48823, USA. E-mail: jliu@panda.msu.edu

References

1. J. Liu, J. Diamond, *Science* **319**, 37 (2008).
2. J. Liu, J. Diamond, *Nature* **435**, 1179 (2005).
3. J. Liu, P. Raven, *Crit. Rev. Environ. Sci. Technol*. **40**, 823 (2010).
4. J. Liu *et al.*, *Nature* **421**, 530 (2003).
5. Z. Lu, R. Matsuhashi, Y. Yoshida, *Environ. Informatics Archives* **5**, 214 (2007).
6. China Energy Group, China Energy Databook v. 7.0 (2008); http://china.lbl.gov/research/china-energy-databook.
7. H. Liu *et al.*, *Energ. Pol*. **37**, 3194 (2009).
8. Y. Wang, M. Shi, *Chin. J. Pop. Res. Environ*. **7**, 11 (2009).
9. E. Yu, J. Liu, *Proc. Natl. Acad. Sci. U.S.A.* **104**, 20629 (2007).

CORRECTIONS AND CLARIFICATIONS

Reports: "Climate change will affect the Asian water towers" by W. W. Immerzeel *et al.* (11 June, p. 1382). In Fig. 3, the superscript minus signs in the units along the *y* axis were mistakenly omitted. The units should have read Q ($m^3 s^{-1}$). The corrected figure is shown here.

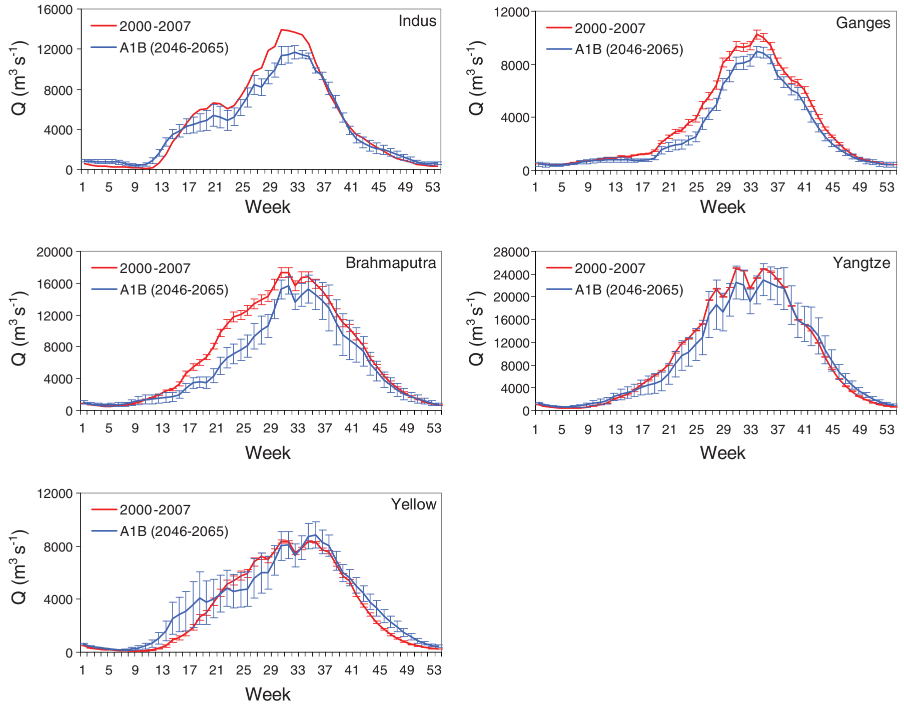

TECHNICAL COMMENT ABSTRACTS

Comment on "Patterns of Diversity in Marine Phytoplankton"

Jef Huisman

Barton *et al.* (Reports, 19 March 2010, p. 1509) argued that stable conditions enable neutral coexistence of many phytoplankton species in the tropical oceans, whereas seasonal variation causes low biodiversity in subpolar oceans. However, their model prediction is not robust. A minor deviation from the neutrality assumption favors coexistence in fluctuating rather than stable environments.

Full text at www.sciencemag.org/cgi/content/full/329/5991/512-c

Response to Comment on "Patterns of Diversity in Marine Phytoplankton"

Andrew D. Barton, Stephanie Dutkiewicz, Glenn Flierl, Jason Bragg, Michael J. Follows

Huisman argues that environments of intermediate variability promote coexistence of model phytoplankton, apparently contrasting our hypothesis that stability allows for greater diversity of equivalent competitors in the ocean. We argue that our original interpretations of the mechanisms governing model diversity patterns remain valid and that Huisman's results are complementary to our hypotheses.

Full text at www.sciencemag.org/cgi/content/full/329/5991/512-d

Studies Support Probable Long-Term Safety of MRI

F. S. PRATO *ET AL.*'S LETTER ("MRI SAFETY NOT scientifically proven," 30 April, p. 568), and the News story to which it referred (*1*), questioned the safety of exposure to strong magnetic fields associated with magnetic resonance imaging (MRI) scans. However, neither the Letter nor the related News story provides new evidence of risk from MRI. Prato *et al.*'s reference to a study that used functional MRI (fMRI) does not address the issue of MRI safety (*2*).

The literature on MRI safety focuses on the demonstrated risks of (i) physical injury from ferromagnetic objects and (ii) magnetic fields in connection to implanted medical devices (*3*). The limited prospective studies on the bioeffects of MRI have not identified significant biological or neurocognitive risks, even at fields up to 8 T in humans (*4*)

and 9.4 T in animals (*5*). Because of the low magnetic susceptibility of biological tissues, exposure to static magnetic fields alone produces no measurable long-term effects (*6*). A recent review of the health effects of static magnetic fields by Feychting concludes that the available evidence from epidemiological studies is not sufficient to draw any conclusions about potential health effects of static magnetic field exposure (*7*).

Risks associated with MRI are recognized and documented. The FDA has published guidelines that recommend limits for exposure to static magnetic fields below 8 T, magnetic field gradients below 6 T/s, and radio frequency fields in order to protect tissues from heating (*8–10*). Operating within these guidelines, our own longitudinal fMRI study in healthy children who underwent five scans over the course of 5 years found no decline in IQ scores, which were in the average range or better (*11*).

Proving the absence of harm is difficult, but these studies support the probable long-term safety of MRI. If evidence can be found for an adverse effect, scientists using MRI as a tool to study brain development in healthy children must pause to consider the implications. Meanwhile, it is not factually correct to state that "no study to date has shown that CT [x-ray computed tomography] increases cancer risk" as Prato *et al*. have done; drawing such parallels between MRI and x-ray exposure is inappropriate and may foment unfounded fear (*12*).

SCOTT K. HOLLAND,[1]* ANNA W. BYARS,[1,2] ELENA PLANTE,[3] JERZY P. SZAFLARSKI,[1,4] KIM DIETRICH,[5] MEKIBIB ALTAYE[1,6]

[1]Pediatric Neuroimaging Research Consortium, Department of Pediatric Radiology, Cincinnati Children's Hospital Medical Center, Cincinnati, OH 45229, USA. [2]Department of Pediatric Neurology, Cincinnati Children's Hospital Medical Center, Cincinnati, OH 45229, USA. [3]Department of Speech and Hearing Sciences and Disorders, University of Arizona, Tucson, AZ 85721, USA. [4]Department of Neurology, University of Cincinnati Academic Health Center, Cincinnati, OH 45267, USA. [5]Department of Environmental Health, University of Cincinnati, Cincinnati, OH 45267, USA. [6]Department of Pediatrics, Division of Biostatistics and Epidemiology, University of Cincinnati College of Medicine, Cincinnati, OH 45267, USA.

*To whom correspondence should be addressed. E-mail: Scott.Holland@cchmc.org

References

1. L. Jiao, *Science* **327**, 931 (2010).
2. J. A. Robertson *et al.*, *J. R. Soc. Interface* **7**, 467 (2010).
3. F. G. Shellock, J. V. Crues, *Radiology* **232**, 635 (2004).
4. D. W. Chakeres, F. de Vocht, *Prog. Biophys. Mol. Biol.* **87**, 255 (2005).
5. W. B. High, J. Sikora, K. Ugurbil, M. Garwood, *J. Magnet. Reson. Imaging* **12**, 122 (2000).
6. A. K. A. Silva, E. L. Silva, E. S. T. Egito, A. S. Carrico, *Radiat. Environ. Biophys.* **45**, 245 (2006).
7. M. Feychting, *Prog. Biophys. Mol. Biol.* **87**, 241 (2005).
8. K. H. Ng, O. Faust, R. Acharya, *J. Med. Syst.*, 10.1007/s10916-010-9460-9, published online 30 March 2010.
9. L. A. Zaremba, "Guidance for industry and FDA staff: Criteria for significant risk investigations of magnetic resonance diagnostic devices" (U.S. Department of Health and Human Services, Food and Drug Administration, 14 July 2003).
10. T. O. Woods, "Guidance for industry and FDA staff: Establishing safety and compatibility of passive implants in the magnetic resonance (MR) environment" (U.S. Department of Health and Human Services, Food and Drug Administration, 21 August 2008).
11. J. P. Szaflarski *et al.*, *Ann. Neurol.* **59**, 796 (2006).
12. M. Mazonakis, A. Tzedakis, J. Damilakis, N. Gourtsoyiannis, *Eur. Radiol.* **17**, 1352 (2007).

Letters to the Editor

Letters (~300 words) discuss material published in *Science* in the previous 3 months or issues of general interest. They can be submitted through the Web (www.submit2science.org) or by regular mail (1200 New York Ave., NW, Washington, DC 20005, USA). Letters are not acknowledged upon receipt, nor are authors generally consulted before publication. Whether published in full or in part, letters are subject to editing for clarity and space.

SCIENCE POLICY

Trapped in the Lower Left Quadrant?

Michael Stampfer

Life can be a series of hardships for those who are professionally involved with European research policy and politics: We are confronted with loads of goals, actors, and programs; conflicting games; and managerial overload. These institutional settings are shaping not only the funding (and, thus, the outcome) of European research but also mindsets, even moods, and certainly policy documents. The situation reflects a dichotomy in official European discourses on science and innovation: Undeniable successes are cherished while we are continually told that something fundamental is going wrong with research policy on our continent.

It is particularly worrying to see the swings in the dominant discourse. Is our main weakness that we are unable to carry out excellent fundamental research, or do we squander fantastic scientific results through an inability to properly develop them into innovative technologies? Are Europeans not bowing deeply enough to help small firms, or are we unwilling to stretch ambitiously to grasp the grand challenges ahead? The most constant term in European discourse is paradox, and official policy documents over nearly 30 years produce a paradoxical big picture. Where are we standing? A famous illustration from Donald Stokes's *Pasteur's Quadrant* (*1*) offers a helpful analogy. Stokes defined Pasteur's quadrant as "use-inspired basic research," his optimal goal for research policies. Research seeking a fundamental understanding of nature (the Bohr quadrant) builds scientific reputation, and developing technological solutions for immediate problems (the Edison quadrant) leads to short-term commercial success. The fourth quadrant, however, can be interpreted as a place not worth inhabiting. Tracking European science and research policy may leave the impression that it has been meandering across the whole of Stokes's matrix.

Claus Madsen's *Scientific Europe* fuels my suspicion that European policy discourse and the author himself have sometimes been trapped in this fourth quadrant. I do not mean the book is overly pessimistic about the history and perspectives of the place now known as the European Research Area (ERA). On the contrary, Madsen pays ample attention to the continent's postwar and contemporary developments.

Scientific Europe
Policies and Politics of the European Research Area

by Claus Madsen
Multi-Science, Brentwood, Essex, UK, 2010. 252 pp. Paper, £37.50, €45.
ISBN 9781907132155.

The author, affiliated with the European Southern Observatory, comes from a scientific community that has been able to develop large infrastructures, held together by intergovernmental treaties. The book's first major strand tells how Europe's great science missions had to be organized collectively (and on equal footing) because no country was strong enough alone. This precommunity approach proved both successful and resilient. Success came with scientific results but also through Europe becoming the home of big machines: the Large Hadron Collider was built while the U.S. supercollider was not, and the International Thermonuclear Experimental Reactor is being built in France. For resilience, take a recent example from my home country: Last year, the Austrian science ministry unwisely planned to quit CERN. Within days of the announcement, after foreign policy protests from other governments, Austria's chancellor overturned the decision.

Efforts toward European Community research funding, from the 1980s on, form the book's second major strand. Here Madsen focuses mainly on the Framework Programmes, as they spread from an original mission of fostering industrial competitiveness to ever-expanding goals and fields of action. Great achievements stand against an inability to leave chosen trajectories, catch-all instruments, controlling bureaucracies, and huge difficulties in evaluating impact. A world of its own had developed, apart from the original ways of working together.

The third strand deals with broader research policy efforts to overcome political fragmentation in Europe. In 2000, the European Council boldly introduced the ERA concept: a long-term vision to create a common market for European research matters, using new policy instruments within the Framework Programmes. Through accompanying "Lisbon" and "Barcelona" promises, the member states pledged to become supercompetitive and to spend more on research. The European Commission has been the principal driving force, with some notable exceptions—energy and guiding principles for the new European Research Council came from the scientific community and from smaller member states.

Although quantitative goals have been missed, there has been progress, albeit at a slow pace and ever accompanied by gloomy analyses. Some of the challenges ahead include questions the book is deeply concerned about, especially the future and governance of infrastructures. Madsen rightly acknowledges the Commission (eager to take over) as the most dynamic ERA actor and infrastructures as perhaps the key ERA element. Also correctly, he fears that today's Brussels practices could lead to policy deadlocks.

Remedy will be difficult. Unlike in the United States, there is no single principal, and Madsen's recipe to build more bottom-up, multiactor settings could lead to unmanageable complexity. He argues for a stronger role of member states in the ERA, a wake up of the scientific community, distinct forms of European infrastructure policies, and systems thinking. However, he correctly notes that when it comes to generic policy questions, calls "for much stronger involvement" have never been answered by the scientific communities, and member states will probably not go beyond their interests of national competitiveness, interests encouraged by the official European policy discourse.

The book's strengths include Madsen's command of the official and semiofficial sources and his descriptions of the different historical trajectories and their interactions. Madsen's point on simpler, trust-based rules is urgent. Readers will find his depiction of the complex settings of European science policy valuable. With his constructive approach, the author cannot be blamed as an iconoclast: his main concern is the rearrangement of existing players and elements.

The reviewer is at the Vienna Science and Technology Fund, Waehringer Strasse 3/15a, A-1090 Vienna, Austria. E-mail: stampfer@wwtf.at

PHOTO CREDITS: WIKIMEDIA COMMONS

Prospective readers should be aware that *Scientific Europe* is strongly dominated by descriptive elements, the author having been present at all major events. Over long stretches, it reads like a veiled autobiography with the rich material collected personally over time. Illustrations show many big names and machines. Madsen presents the story without strong underlying hypotheses or basic theoretical assumptions. The latter are imported with the many policy papers to which he extensively refers, which leads to a mix of explanatory approaches. The author is not the first "hard" scientist who in writing about politics and policy analysis seems to stick to the way of thinking he has used throughout his life. He should not be blamed for doing so, but social scientists can and will use his book for the material portrayed and not for the conceptual approaches presented. In any event, the book largely looms around big machines, and authors should not be overly criticized for the things they love dearly.

References

1. D. Stokes, *Pasteur's Quadrant: Basic Science and Technological Innovation* (Brookings, Washington, DC, 1997).

10.1126/science.1192324

ART EXHIBITION

Shared Resources

Andreas Keller

The belief that a dialogue between science and the arts could benefit both sides has led to numerous projects that look beyond the differences in approach to find some commonality between these two creative endeavors. A good starting point for interdisciplinary communication is the shared objects and materials that can be and are used in artistic as well as in scientific projects. *Dead or Alive*, an exhibition at the Museum of Arts and Design in New York, offers diverse and interesting works made from biological materials by 37 artists from 12 countries. Among other materials, the installations incorporate seeds, leaves, spices, horse hair, anchovies, moth cocoons, eggs, bones, feathers, and thousands of dried insects.

Dead or Alive
Nature Becomes Art

David Revere McFadden, Lowery Sims, and Elizabeth Edwards Kirrane, Curators
Museum of Arts and Design, New York. Through 24 October 2010. Catalog, 2010. 133 pp. $29.95. ISBN 9781890385200. www.madmuseum.org

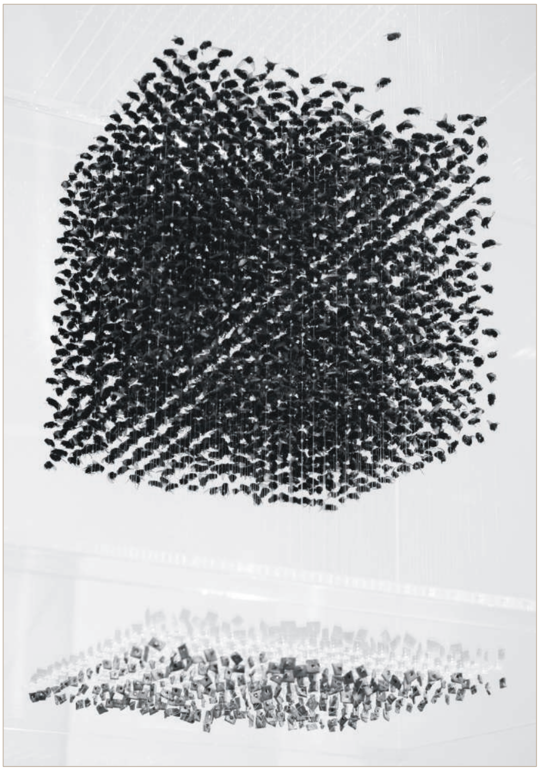

Claire Morgan's *On Top of the World* (bluebottle flies, spider, nylon, lead, acrylic; 2009).

The exhibition reflects the cultural history of the curiosity cabinets (Wunderkammern) of Renaissance Europe, where intricate shells, colorful bird feathers, and stuffed exotic animals were displayed for their aesthetic value and to satisfy scientific curiosity. In the 18th century, the acceptance of the Linnaean taxonomy put all living organisms in categories; from then on, a display of biological samples was considered scientific only if a taxonomical order was enforced on it.

The distinction between artistic and scientific use of natural objects remains superficial at best, however: New York's Metropolitan Museum of Art displays *The Physical Impossibility of Death in the Mind of Someone Living* (1992), a tiger shark in formaldehyde by British artist Damien Hirst (who also contributed to *Dead or Alive*). Similar sharks in formaldehyde can be seen in natural history museums around the world. Presented as art, biological material can be idiosyncratic and endorse ambiguity, whereas a scientific context requires that the same material be presented with objectivity that excludes personal bias. Nonetheless, these differences are small compared to the powerful emotions—like fear or awe—that the spectacle of a 14-foot shark will evoke in any context.

Dead or Alive explores the gray area of biological objects that is shared by scientists and artists as the starting point of their respective processes. Some works would not be out of place in a Renaissance curiosity cabinet. Jan Fabre, the Belgian artist whose *Heaven of Delight* (2002) previously covered parts of the ceiling of the Hall of Mirrors in the Royal Palace of Brussels with over one million jewel beetle wing cases, contributed *Skull* (2001): a flying humanoid skull made from iridescent golden and green beetles, which carries a limp stuffed pigeon in its jaws. Other installations are less literal in how they arrange or transform their animalic subjects. In Claire Morgan's *On Top of the World* (2009), 3375 black flies with red eyes and a single spider are tangling on nylon threads to form a cubic swarm of fly carcasses. Some of the flies are missing wings, legs, or their head, and the faint but distinct smell of dead flies frames the sculpture. Morgan tries to tame the constant movement and the decay of the natural world by arranging it in idealistic geometrical structures. The German artist Jochem Hendricks goes one step further by reducing entire animal bodies to their principal chemical constituent: carbon. In *Hansi* and *Bubi*, two works from his Cold Bird series (2002–2005), Hendricks presents two diamonds on black velvet cushions surrounded by yellow (*Bubi*) or blue (*Hansi*) feathers and fluffy white down. The tiny, yellowish diamonds were made from two pet parakeets, whose bodies were transformed under pressure, allegedly in "two former Soviet research institutes"—the same institutes that, the artist reports, transformed the amputated right leg of a soccer player into a diamond for his *Left Defender Right Leg* (2002–5).

The other installations in this fascinating exhibition deal with biological material in similar ways. Animal and plant parts are taken out of their normal context and arranged or transformed for various effects. At no point will visitors feel like they accidentally wandered into a natural history museum. The power of biological materials in the hand of artists to evoke emotions from disgust to empathy—and sometimes both—is present throughout *Dead or Alive*.

10.1126/science.1193016

The reviewer is at the Laboratory of Neurogenetics and Behavior, Rockefeller University, 1230 York Avenue, Box 63, New York, NY 10065, USA. E-mail: kellera@mail.rockefeller.edu

HEALTH-CARE POLICY

To Reform U.S. Health Care, Start with Systematic Reviews

Before initiating new research, a formal synthesis of currently available knowledge should determine whether it is necessary.

Kay Dickersin

With passage of The Patient Protection and Affordable Care Act (Public Law 111-148), the United States has taken an important step toward health care for all. But can "good" health care for all be achieved? The United States has lagged behind Canada, Europe, Australia, and now China (*1*) in making a national commitment to creating and utilizing research evidence on "what works" as an integral part of clinical practice and health policy (*2*). This approach, termed "evidence-based health care," has been defined as "the integration of best research evidence with clinical expertise and patient values" (*3*). Evidence-based health care is not without its critics. Some have rejected it as "cookbook medicine" (*4*, *5*), apparently ignoring that evidence is not the only ingredient in the approach and that the alternative ignores the scientific underpinnings of medicine.

Evidence We Need, Evidence We Have

For good health care, the research evidence we need most is from studies of interventions aimed at treatment, prevention, diagnosis, and screening. Sometimes the evidence we seek, for example, from randomized trials, is scarce or difficult to identify or its findings are inconclusive. We can solve these problems, which together constitute a research "evidence gap," but first we have to acknowledge them and work in a coordinated fashion with our international colleagues so that we get the answers we need quickly, without unnecessary duplication of effort.

We have plenty of research, published in over 22,000 biomedical journals, so why do we not have the answers we need? When evidence is unreliable, does not exist, or is insufficient to address important questions, we must generate new evidence. But some have argued that, before we initiate new research, we should be required to show whether it is needed by conducting a formal synthesis of currently available knowledge and that similar credit should be accorded to those synthesizing research as to those performing primary research (*6*–*8*).

"Systematic reviews" are a scientific approach being used across the sciences (*11*–*15*) to synthesize existing evidence. When it appears that studies are similar enough in the questions they are addressing and that they are of sufficient quality, results of the studies may be combined quantitatively in a "meta-analysis" (*12*, *14*). Meta-analysis is an optional quantitative synthesis within a systematic review. There are agreed-upon criteria for designing high-quality primary studies (e.g., control group, adequate sample sizes, and transparent reporting). Ought we not to insist on the same for review articles?

Synthesizing research evidence is challenging and requires training (*2*). In addition, even proponents of systematic reviews are concerned that poor-quality primary studies result in unreliable synthesized results and that combining results of studies that are too dissimilar (e.g., in population, interventions, and outcomes assessed) can lead to erroneous conclusions (*14*). At the direction of the U.S. Congress, the Institute of Medicine is currently producing standards for systematic reviews, an important step (*15*).

When there are coordinated U.S. efforts for performing systematic reviews, funding agencies have focused mainly on federal programs and have used internal agency staff or contractual investigators (*18*). These programs [e.g., (*19, 20*)], although critically important, lack capacity and were never intended to cover the full range and depth of health-related questions.

Addressing the Research Evidence Gap

One alternative approach, which might both increase capacity and reduce duplication of effort, would be for the United States to increase its investment in international activities aimed at synthesizing the available evidence. The Cochrane Collaboration (*21*) engages people from more than 100 countries to conduct and maintain systematic reviews of the best current evidence to address important questions relating to clinical care and health policy. Since its beginnings in 1993, Cochrane has also played an important role in developing standards for conducting and reporting systematic reviews (*21*–*24*). The global, nonprofit Cochrane effort has been likened to the health services equivalent of the Human Genome Project (*25*).

…research synthesis must be recognized as a methodology and field in its own right.

As far as I know, no NIH institute is prepared to take on a large-scale, deliberate, coordinated effort to generate evidence and to conduct systematic reviews across health fields and topics. The National Institutes of Health (NIH), with few exceptions, has focused on funding the generation of evidence, not its synthesis, which is arguably equally important because it reliably identifies areas where new evidence is needed. It is not clear that any NIH institute has required a comprehensive systematic review of evidence before a clinical trial is funded, beyond the literature review requested as a part of the grant application. Given the high cost of clinical trials, it seems fair to ask applicants for a systematic accounting of what is known before funding is approved, such as is required by the UK Medical Research Council (*16*) and others (*17*).

The decision to conduct a Cochrane review may emanate from an author's interest in the topic ("voluntary"), from a prioritization exercise ("commissioned"), or a combination of the two (e.g., prioritized topics are made public and authors volunteer). Cochrane reviews are made publicly available through an electronic journal, *The Cochrane Library*, updated monthly and currently made freely available to more than half of the world's population, through national subscriptions or other provisions, for example, to low-income countries (*26*). The collaboration has long-standing, freely available standards for conducting reviews (*12*); is among the most productive groups in the world, in terms of number of reviews produced and updated; and is often cited (*27*). As of July 2010, *The Cochrane Library* includes 4309 completed reviews and 1935 protocols of reviews in

Director Center for Clinical Trials, Director U.S. Cochrane Center, Johns Hopkins Bloomberg School of Public Health, Baltimore, MD 21205, USA. E-mail: kdickers@jhsph.edu

preparation. The Cochrane Collaboration also enlists a well-trained workforce, with more than 1500 of its affiliated systematic review authors based in the United States.

In addition to investments federal funding agencies are already making in their own programs, they can and ought to invest in a coordinated way in infrastructure for Cochrane systematic reviews and to encourage cooperative work between knowledge producers to increase efficiencies. Although the Cochrane Collaboration itself does not pay for salary support for review authors, all are supported indirectly by the collaboration infrastructure, which provides centralized management, standardized guidance on methods, quality control, education, and support for consumer engagement. No commercial funding of Cochrane reviews is permitted. Furthermore, because Cochrane entities are funded through many sources and governments, any single funding source (such as the NIH) can leverage its own investment against global investment.

However, federal funders may want more control over the project than that which appears possible through an existing global, not-for-profit effort. Related to this, there can be a misperception that Cochrane is a European organization, and a concern that a non-U.S. focus could dilute U.S.-based goals (*28*). Although a few promising efforts have taken place [e.g., Cochrane support provided by the National Institute of Child Health and Human Development (*29*) and the National Eye Institute], it is not clear that appropriate grant mechanisms are in place that would allow a broad-based, coordinated investment in the existing U.S.-based Cochrane infrastructure; the newer Common Fund (*30*) and Blueprint (*31*) mechanisms that support trans-NIH initiatives may be useful models for such a broad-based initiative. The Cochrane Collaboration may have to change too, perhaps to be better able to understand and respond to funder priorities.

Most systematic reviews have been done poorly in the past (*32*), which indicates a need for skilled faculty and educational programs that will yield a capable and dedicated workforce. The United States can tap into Cochrane reviewers' existing, underutilized expertise. In addition, research groups doing systematic reviews must be developed and sustained so that a group's knowledge and skills are not lost with the completion of a review. Furthermore, to attract and retain creative and productive investigators, research synthesis must be recognized as a methodology and field in its own right, and systematic reviewers must be given adequate credit for their research (*33*).

The Way Forward

The Patient Protection and Affordable Care Act mandates creation of a new, nonprofit corporation, the Patient-Centered Outcomes Research Institute (PCORI), and a funding stream for "comparative clinical effectiveness research" (CER)—both new primary research and research synthesis—comparing the benefits and harms of interventions to prevent, diagnose, treat, and monitor health conditions. The institute holds promise to coordinate efforts to produce good science and to serve as the flagship for collaborative, productive research. Specific targets of investment would be as follows:

• Take advantage of being late to the game and test the most promising approaches to health care identified elsewhere. The United States cannot afford a "not invented here" mindset, ignoring lessons and promising models from outside the United States and, instead, building from scratch.

• Provide support for a coordinated approach to performing high-quality systematic reviews, both commissioned and voluntary.

• Develop, expand, adapt, or clarify federal funding mechanisms to ensure that support is sustained so research groups do not disband as systematic reviews are completed, and so reviews are kept up-to-date.

• Provide federal infrastructure support to external scientific organizations, such as the Cochrane Collaboration, so as to leverage international collaboration.

• Commit substantial and sustained resources to training grants specifically aimed at educating and expanding the professional workforce required to synthesize the evidence and keep reviews up-to-date.

• Increase federal support for research on methods for more efficient and informative trials and systematic reviews.

• Provide support for knowledge translation research, to learn how best to translate research evidence so that it is useful to decision-makers. Although PCORI provides a budget for "dissemination" of CER findings, it is not clear that there are funds for research to identify effective ways to do this.

• Involve health-care decision-makers (e.g., consumers, policy-makers, and doctors) throughout the research process so that the evidence generated is likely to be useful.

Synthesis of what we know from primary research, using up-to-date systematic reviews, is critical to each step in the process, from prioritizing research to implementing high-quality, cost-effective clinical care. Changes in the federal funding and academic reward systems could help attract, educate, and retain talented researchers and support high-quality research and infrastructure that will help lead to evidence-based health care.

References and Notes

1. C. Zhu, *Science* **327**, 1429 (2010).
2. J. Eden, B. Wheatley, B. McNeil, H. Sox, Eds., *Knowing What Works in Health Care: A Roadmap for the Nation* (National Academies Press, Washington, DC, 2008).
3. D. Sackett, S. E. Straus, W. S. Richardson, W. Rosenberg, R. B. Haynes, *Evidence-Based Medicine: How to Practice and Teach EBM* (Churchill Livingstone, New York, ed. 2, 2000).
4. D. L. Sackett, W. M. C. Rosenberg, J. A. M. Gray, R. B. Haynes, W. S. Richardson, *BMJ* **312**, 71 (1996).
5. M. B. Kapp, *Arch. Intern. Med.* **150**, 496 (1990).
6. R. J. Light, D. B. Pillemer, *Summing Up: The Science of Reviewing Research* (Harvard Univ. Press, Cambridge MA, 1984).
7. J. M. Ziman, *Nature* **224**, 318 (1969).
8. S. Clark, R. Horton, *Lancet* **376**, 10 (2010).
9. L. V. Hedges, *Am. Psychol.* **42**, 443 (1987).
10. K. M. Richardson, H. R. Rothstein, *J. Occup. Health Psychol.* **13**, 69 (2008).
11. J. Gurevitch, J. A. Morrison, L. V. Hedges, *Am. Nat.* **155**, 435 (2000).
12. J. P. T. Higgins, S. Green, Eds., *Cochrane Handbook for Systematic Reviews of Interventions* (Wiley-Blackwell, Hoboken, NJ, 2008).
13. C. Mann, *Science* **249**, 476 (1990).
14. M. Borenstein, L. V. Hedges, J. P. T. Higgins, H. R. Rothstein, Eds., *Introduction to Meta-Analysis* (Wiley and Sons, Hoboken, NJ, 2009).
15. Standards for Systematic Reviews of Clinical Effectiveness Research, www.iom.edu/Activities/Quality/SystemReviewCER.aspx.
16. Efficacy and Mechanism Evaluation Review, preliminary application guidance, www.eme.ac.uk/funding/pdfs/EME_PAGuidance_March2010_PA2.5.pdf.
17. U.K. Department of Health, *Research Governance Framework for Health and Social Care* (Department of Health, London, ed. 2, 2005); www.dh.gov.uk/prod_consum_dh/groups/dh_digitalassets/@dh/@en/documents/digitalasset/dh_4122427.pdf.
18. U.S. Government Accountability Office, *Program Evaluation: A Variety of Rigorous Methods Can Help Identify Effective Interventions* (GAO-10-30, Government Printing Office, Washington, DC, 2009).
19. Centers for Disease Control and Prevention (CDC), The Guide to Community Preventive Services, www.thecommunityguide.org/index.html.
20. Agency for Health Care Research and Quality (AHRQ), Evidence-Based Practice Centers (EPCs); www.ahrq.gov/clinic/epc/.
21. The Cochrane Collaboration, www.cochrane.org/.
22. I. Chalmers, K. Dickersin, T. C. Chalmers, *BMJ* **305**, 786 (1992).
23. K. Dickersin, E. Manheimer, *Clin. Obstet. Gynecol.* **41**, 315 (1998).
24. A. Ault, *Science* **300**, 2024 (2003).
25. C. D. Naylor, *Lancet* **345**, 840 (1995).
26. The Cochrane Library, www.thecochranelibrary.com/view/0/FreeAccess.html.
27. R. Horton, *Lancet* **376**, 80 (2010).
28. L. Newman, *Lancet* **356**, 1990 (2000).
29. W. McGuire, P. W. Fowlie, R. F. Soll, *Arch. Dis. Child. Fetal Neonatal Ed.* **95**, F2 (2010).
30. The NIH Common Fund, http://nihroadmap.nih.gov/.
31. NIH Blueprint for Neuroscience Research, http://neuroscienceblueprint.nih.gov/.
32. D. Moher, J. Tetzlaff, A. C. Tricco, M. Sampson, D. G. Altman, *PLoS Med.* **4**, e78 (2007).
33. C. Garritty, A. Tsertsvadze, A. C. Tricco, M. Sampson, D. Moher, *PLoS ONE* **5**, e9914 (2010).

34. K.D. gratefully acknowledges comments by M. Redford, K. Robinson, and D. Tovey and contributions of Cochrane data from N. Royle and L. Jones.

10.1126/science.1189330

GENOMICS

E. coli, What a Noisy Bug

Investigators detail striking genome-wide variation in gene expression between individual cells.

Sanjay Tyagi

To study gene expression, researchers often grind up a large number of cells grown under the same conditions and then measure the amounts of gene products, such as messenger RNAs (mRNAs) and proteins, in the soup. Many recent studies, however, have pointed out that beneath such average measurements lies great variation among individual cells, sometimes referred to as "noise" (*1*, *2*).

In multicellular organisms, studies of noise have raised questions about how tissue specificity is maintained in the face of great variation (*2*). In unicellular organisms, researchers have found that noise can give rise to groups of cells within a genetically homogenous population that behave differently (*3*). By measuring noise in the genomes of different organisms, researchers can explore its evolutionary and functional importance (*4*). On page 533 of this issue, Taniguchi *et al*. (*5*) contribute to this effort by reporting the absolute numbers of, and cell-to-cell variation in, protein molecules present in single *Escherichia coli* cells for a set of 1018 genes covering about one-fourth of the genome. They also provide simultaneous counts of mRNA molecules for a smaller set of 137 genes that are abundantly expressed.

The authors used a combination of fluorescence microscopy and a library of genes tagged with fluorescent labels in a system automated for high through-put to count molecules in individual cells. They found that, depending on the gene, each cell contained 0.1 to 10,000 copies of each protein and 0.05 to 5 copies of each mRNA species. The ratio of mRNA to protein ranged from 1:100 to 1:10,000. At a given moment, a fraction of *E. coli* cells will not have even a single molecule of certain proteins or mRNAs. Essential genes are expressed at higher levels, so that cells have at least one molecule of a protein that they cannot live without. These numbers may be counterintuitive, but they generally conform to earlier ensemble measurements (*6*). What is truly intriguing is the high level of noise in gene expression that the researchers discovered across the whole genome.

For low-abundance proteins (<10 copies per cell), the level of noise decreased as abundance increased. For more abundant proteins, the noise level remained stationary above a certain limit. One component of this noise—dubbed "intrinsic" noise—arises because a cell typically holds just one copy of each gene and very few molecules of gene-activating proteins. Under such conditions, the interaction of the two is subject to chance, resulting in stochastic (random) synthesis of mRNA and protein (*7*). Although intrinsic noise nicely explains noise trends in low-abundance proteins, it is not obvious why noise does not continue to decrease as proteins become more abundant. One hypothesis is that cells have variable "metabolic capacities" to produce proteins, perhaps due to variations in the number of RNA polymerases, ribosomes or other factors that globally affect the synthesis of proteins. These factors—called "extrinsic" noise—might create a floor below which noise levels do not fall (*5*, *8*, *9*). One prediction generated by this hypothesis, confirmed by Taniguchi *et al*., is that the levels of two proteins subjected to extrinsic noise will fluctuate over time in a correlated manner.

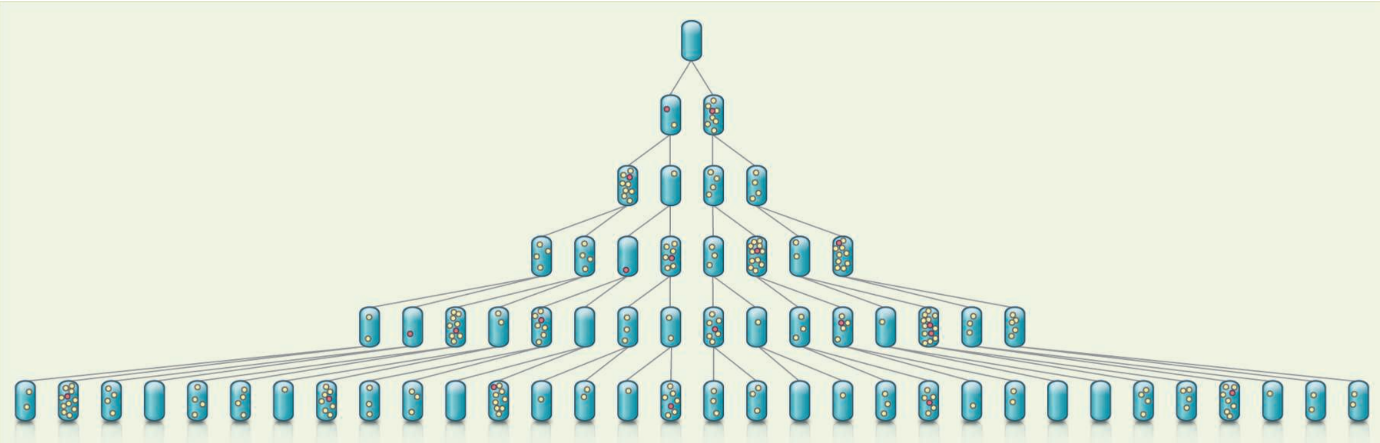

Noisy inheritance. For a given gene, the number of molecules of mRNA (red dots) and corresponding protein (yellow dots) can vary greatly among genetically identical cells in a population at a given moment in time. This high level of "noise" is due, in part, to differences in the life spans of mRNAs, which are relatively short-lived, and proteins, which can persist for longer than the time required for cell division. Surviving protein molecules are passed to daughter cells by random assortment, resulting in unequal distribution when the number of molecules of a protein is small. As a result, some cells have many copies of mRNA and proteins for a given gene, whereas other cells can have relatively few or none, and the number of mRNAs and proteins within a cell may not correlate.

A striking observation is that, although the numbers of molecules of mRNAs and proteins for any given gene correlate well at the ensemble level, they do not correlate at all within individual cells. How is it that, in an organism in which the processes of transcription and translation are coupled, the number of mRNAs does not relate to the number of proteins within each cell? The explanation lies in the different lifetimes of mRNAs and proteins. The mRNAs survive for only a few minutes within cells, whereas proteins persist for hours—exceeding the duration of the cell cycle (*5*, *10*). Furthermore, for many cells the only source of some proteins is those that are inherited from the mother cell, as mRNA is produced relatively rarely (see the figure). This results in unequal inheritance of the limited number of molecules of a given protein

Public Health Research Institute, University of Medicine and Dentistry of New Jersey, 225 Warren Street, Newark, NJ 07103, USA. E-mail: tyagisa@umdnj.edu

CREDIT: ADAPTED BY P. HUEY/SCIENCE

Published by AAAS

during cell division (*8*, *10*), a phenomenon that also occurs in mammalian cells (*11*).

Another consequence of differences in the lifetimes of mRNAs and proteins is that noise is higher for mRNAs than it is for their corresponding proteins. The mRNAs are produced in short random bursts and degrade soon after being used as templates for the synthesis of a few protein molecules, whereas the synthesized proteins are added to a pre-existing pool. Protein levels are thus relatively "buffered" from fluctuations in the level of the corresponding mRNA. Similar buffering has been observed in mammalian cells (*12*).

Are there any differences in noise characteristics between bacteria and eukaryotes? Investigators have performed a pair of genome-wide studies in yeast (*4*, *9*) that are similar to the study reported here. A comparison of the results suggests that gene expression in bacteria is noisier than in yeast (*5*). Although researchers have yet to perform a genome-wide study of higher eukaryotes, the results of several studies with reporter genes and with natural genes suggest that mRNA expression in mammalian cells is noisier than in both yeast and bacteria (*2*). A possible reason is that, in the higher eukaryotes, the control regions of genes are sequestered within tightly packed chromatin and the gene activating proteins can gain access to these regions only during random episodes in which local chromatin becomes loose (*12*).

Now that there is reliable knowledge of the levels of expression and the underlying variation of mRNAs and proteins for a considerable portion of the *E. coli* genome, it is possible to explore how noise propagates along gene expression pathways, in which the amount of one protein can influence the expression of another. Investigators can also investigate how cells coordinate the expression of proteins that need to work together, such as multisubunit proteins or proteins that serve within metabolic cycles. Genome-wide studies of noise in related organisms, or in the same organism under different conditions, such as stress or aging, will allow researchers to determine whether noise is simply a limitation of the gene expression apparatus or an essential trait subject to evolutionary selection and refinement.

References and Notes

1. M. B. Elowitz, A. J. Levine, E. D. Siggia, P. S. Swain, *Science* **297**, 1183 (2002).
2. A. Raj, A. van Oudenaarden, *Cell* **135**, 216 (2008).
3. H. Maamar, A. Raj, D. Dubnau, *Science* **317**, 526 (2007).
4. J. R. Newman *et al.*, *Nature* **441**, 840 (2006).
5. Y. Taniguchi *et al.*, *Science* **329**, 533 (2010).
6. P. Lu, C. Vogel, R. Wang, X. Yao, E. M. Marcotte, *Nat. Biotechnol.* **25**, 117 (2006).
7. A. Becskei, B. B. Kaufmann, A. van Oudenaarden, *Nat. Genet.* **37**, 937 (2005).
8. N. Rosenfeld, J. W. Young, U. Alon, P. S. Swain, M. B. Elowitz, *Science* **307**, 1962 (2005).
9. A. Bar-Even *et al.*, *Nat. Genet.* **38**, 636 (2006).
10. I. Golding, J. Paulsson, S. M. Zawilski, E. C. Cox, *Cell* **123**, 1025 (2005).
11. A. Sigal *et al.*, *Nature* **444**, 643 (2006).
12. A. Raj, C. S. Peskin, D. Tranchina, D. Y. Vargas, S. Tyagi, *PLoS Biol.* **4**, e309 (2006).

13. Supported by the National Institute of Mental Health grant MH079197.

10.1126/science.1194036

PLANETARY SCIENCE

Winds of Change on Titan

Ralph D. Lorenz

Periodic strong winds blowing opposite to the prevailing wind may explain the dune orientation on Titan.

On Saturn's moon Titan, giant sand dunes cover more than 20% of the surface. The orientation of thousands of dunes (*1*, *2*) within Titan's equatorial belt indicates transport of sand from west to east (by "westerly" winds), whereas all the atmospheric circulation models suggest that the winds should be in the opposite direction. A new model by Tokano (*3*) may have found the resolution: Although the winds are usually easterlies (as in other work), there is a blast of wind from the west for a brief interval around each equinox, and it is these stronger winds that dominate the dune orientation.

The discovery of dunes on Titan (*4*) in Cassini radar imagery was itself something of a surprise (and only possible because Titan's dunes are so large—a kilometer or so wide, tens to hundreds of kilometers long, and often more than 100 m high), and it is not clear where all this sand comes from. The term "sand" in geology is a particle size range (0.06 to 2 mm), not a composition. For example, dunes on Earth and Mars are not always made of quartz sand; there are the black basaltic sands of Hawaii and Iceland, or the white sands of gypsum in New Mexico; Mars has these too, plus some striking green sands of olivine. On Titan, the dark dune sands make up an inventory (*5*) of ~0.5 million km^3 of material—apparently of an organic composition, as spectroscopic mapping (*6*) by Cassini's infrared spectrometer shows a signature, concentrated in the sand, of aromatic molecules such as benzene. This makes the dunes the largest carbon sink on Titan (larger than the polar seas of liquid hydrocarbons, and 1000 times the carbon in all the coal known on Earth). The dune organic inventory com-

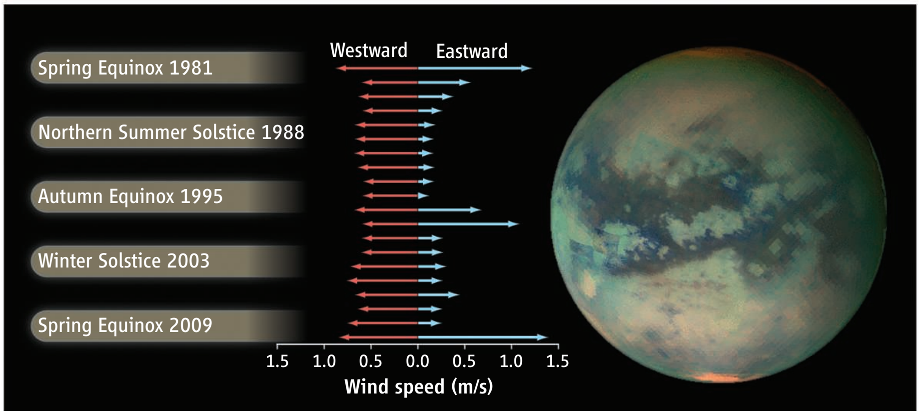

Going against the flow. The annual range of near-surface equatorial zonal winds on Titan in Tokano's model (*3*): The strongest westerly (eastward) wind in an interval is shown as a blue arrow, the strongest easterly in red. The winds are predominantly easterlies, and if the sand transport threshold were as low as 0.5 m/s, easterlies would drive the dune orientation. However, if the threshold is higher (e.g., 1.0 m/s), only the westerlies at equinox are fast enough to form dunes, which therefore indicate this direction even though easterlies are more common overall.

PHOTO CREDIT: NASA/JPL/UNIVERSITY OF ARIZONA

Applied Physics Laboratory, Johns Hopkins University, Laurel, MD 20723, USA. E-mail: ralph.lorenz@jhuapl.edu

pares reasonably well with the result of 4.5 billion years of production of heavy organic molecules, a rate recently measured (*7*) at 10^5 to 10^6 tonnes/year as Cassini flew through the ionosphere where these compounds form.

The fact that the dunes are confined to a belt within 30° of the equator is striking. Models of Titan's atmospheric circulation (*8*) predict that low latitudes should dry out, consistent with dunes being found in "dry" places (the moisture on Titan being liquid methane). But the orientation of the dunes themselves indicates that the winds must have a substantial eastward component.

One of the first principles of planetary meteorology [as recognized by Hadley (*9*) in 1735] is that east- and west-wind stresses must on average balance out over the surface of a planet, otherwise its rotation would change. And in particular, because the equatorial surface is farthest from the spin axis of a planet, the low-latitude winds there should be westward (easterlies); otherwise, incredibly fast westerlies would be needed elsewhere to balance them. So numerical models of Titan's circulation tend to produce easterly winds where the dunes are found, contrary to what the dunes suggest.

The trick, it seems, in the new model (*3*) is that although low-latitude surface winds are indeed usually westward (as angular momentum balance would require), there is a brief episode, twice every Titan year, when stronger eastward winds (westerlies) appear. This happens near the equinox, when the Intertropical Convergence Zone (ITCZ) crosses the equator. This region of solar-driven upwelling causes stronger turbulent mixing, which causes the winds to briefly reverse and freshen. It takes some minimum (threshold) wind speed for sand to start moving, so even though winds are more frequently westward, if the sand responds only to the strongest winds, then the orientation of the dunes will reflect that of the rarer but faster eastward winds (see the figure). Indeed, if the model results are correct, the fact that the dunes are eastward-pointing requires that the threshold for sand movement must be >1 m/s.

Debate about such subtleties (*10*) as to whether the dunes grow more than they move will doubtless continue, but the dominant question so far about Titan's dunes may now have been solved just by looking closely at the statistics of the winds. However, some puzzles remain. If the sands are indeed organic, how do the 0.3-μm organic haze particles in the atmosphere transform into ~0.3-mm sand grains that can be blown into dunes? One possibility involves periodic filling and drying (*11*) of Titan's polar seas, but this still leaves the question of how the sand moves from the poles to the equator.

References

1. C. Wald, *Science* **323**, 1418 (2009).
2. R. D. Lorenz, J. Radebaugh, *Geophys. Res. Lett.* **36**, L03202 (2009).
3. T. Tokano, *Aeolian Res.* 10.1016/j.aeolia.2010.04.003 (2010).
4. R. D. Lorenz *et al.*, *Science* **312**, 724 (2006).
5. R. D. Lorenz *et al.*, *Geophys. Res. Lett.* **35**, L02206 (2008).
6. R. N. Clark *et al.*, *J. Geophys. Res.*, 10.1029/2009JE003369 (2010).
7. J.-E. Wahlund *et al.*, *Planet. Space Sci.* **57**, 1857 (2009).
8. J. L. Mitchell, *J. Geophys. Res.* **113**, E08015 (2008).
9. G. Hadley, *Philos. Trans. R. Soc.* **39**, 58 (1735).
10. D. M. Rubin, P. A. Hesp, *Nat. Geosci.* **2**, 653 (2009).
11. O. Aharonson *et al.*, *Nat. Geosci.* **2**, 851 (2009).

10.1126/science.1192840

MEDICINE

Reconstructing the Lung

William R. Wagner[1] and Bartley P. Griffith[2]

Engineering functional lung tissue on the structural scaffold of the native organ in rodents points to a possible strategy for lung regeneration.

From an engineering and materials science perspective, the lung is a paradigm of design efficiency. A gas transfer surface area of approximately 70 m^2 is packed into an elastic, dynamic structure to accomplish efficient oxygen and carbon dioxide transfer. There has been modest success in organizing cells into small-scale structures that mimic pulmonary tissue, but the question of how to scale up and effectively connect such structures has loomed large. Two studies by Petersen *et al.* on page 538 of this issue (*1*) and by Ott *et al.* (*2*) describe an alternative approach by which the structural efficiencies of native lung tissue can be captured while potentially avoiding the immunogenicity barriers associated with nonautologous tissue transplantation.

Temporary reproduction of the gas transfer function of the lungs does not depend on an organized and viable pulmonary tissue, despite early clinical attempts to do this, such as the perfusion of rhesus monkey lungs with patient's blood during open-heart surgery (*3*). Rather, mechanical blood oxygenator designs have advanced to make cardiopulmonary support a routine aspect of such procedures. However, biocompatible artificial lung technology to provide chronic aid for patients in end-stage pulmonary failure remains elusive. Support by synthetic membrane–based lung devices remains limited to a period of days or weeks, requires aggressive therapy to prevent blood clotting (anticoagulation), greatly restricts patient mobility and quality of life, and has high mortality.

The limits of current technology are found at the interface where oxygen and carbon dioxide pass between the blood and gas sides of synthetic hollow-fiber membranes. Blood proteins adsorb to the polymeric membrane surfaces, which can trigger the activation immune cells and deposition of clots onto the fibers. This can result in immune responses and a tendency toward bleeding, respectively, when the blood reenters the patient. Further, to achieve adequate gas transfer, membrane surface areas on the order of 1 m^2 are required. The size of current membrane oxygenators is incompatible with placement within the body. This is in stark contrast to the inherently anticoagulant surfaces of endothelial cell–lined capillaries that provide the 70 m^2 of gas transfer area in the native human lung (see the figure).

Recent approaches to create a more biocompatible artificial lung for extended support have sought to address the surface area per volume limitations of current devices as well as the blood interface bioincompatibility. By reducing fluid boundary layers and optimizing blood flow patterns, blood-contacting synthetic surface areas can be minimized and inhibition of cellular deposition can be improved (*4*). Smaller oxygenators can also be designed to accommodate patients who do not require complete respiratory support (*5*). Microfabrication techniques have generated both branched and densely packed blood-carrying polymeric channels with high gas diffusivity that can be stacked in layers near gas channels (*6*, *7*). The blood pathways of these devices can be lined with autologous endothe-

[1]McGowan Institute for Regenerative Medicine, Departments of Surgery and Bioengineering, University of Pittsburgh, Pittsburgh, PA 15219, USA. [2]Department of Surgery, University of Maryland, Baltimore, MD 21201, USA. E-mail: wagnerwr@upmc.edu

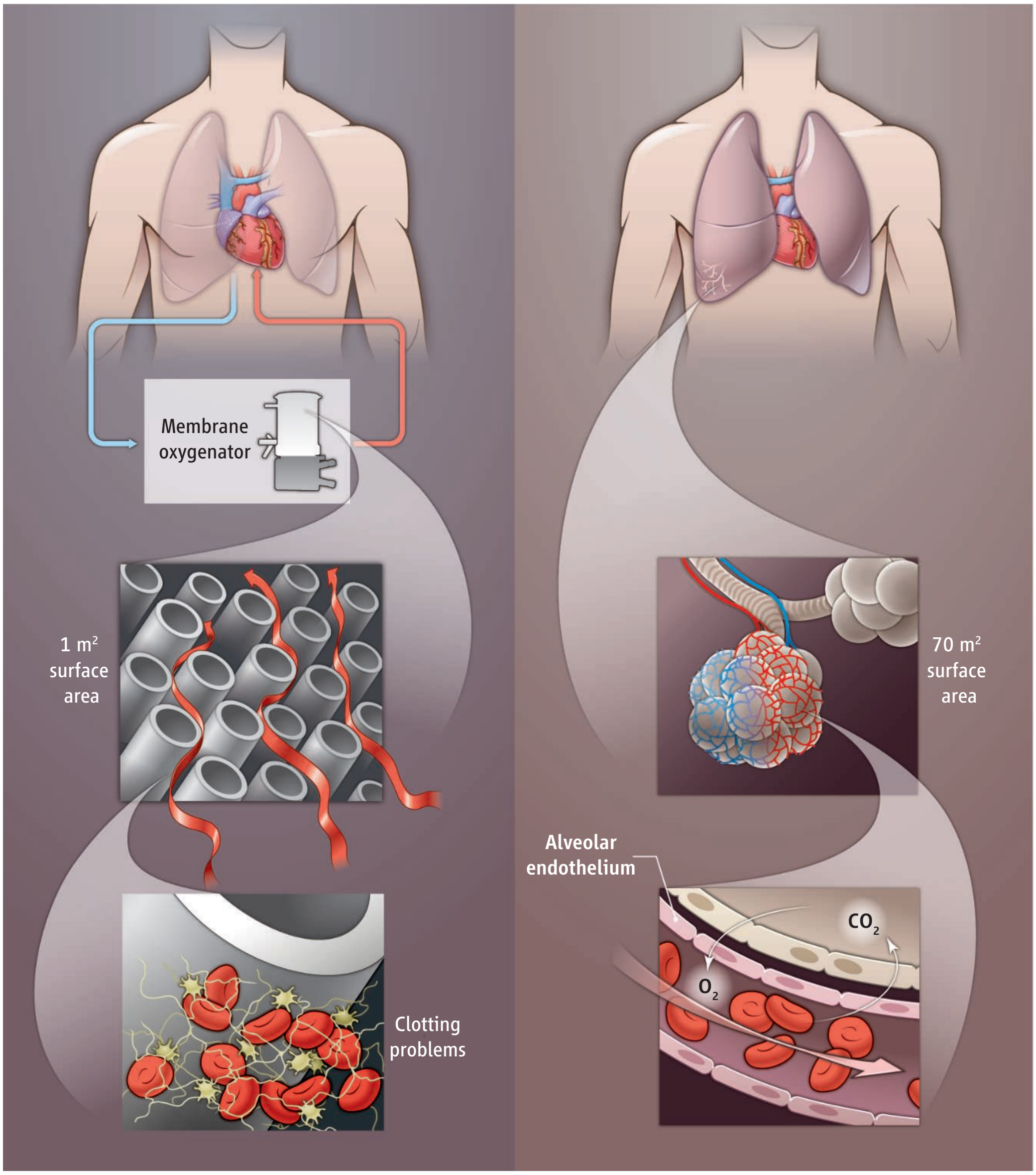

Artificial and limited. Membrane oxygenators currently in clinical use **(left)** commonly use packed hollow-fiber membranes across which blood flows. Protein and cellular deposits on the synthetic surfaces lead to patient complications and the need for anticoagulation therapy. The native lung **(right)** provides approximately 70 m^2 of gas transfer area in alveoli with actively anticoagulant endothelial surfaces lining the blood vessels.

CREDIT: Y. GREENMAN/SCIENCE

lial cells to provide a surface that mimics that of blood vessels and minimizes the need for anticoagulants. In a cell-seed approach, microporous hollow-fiber membranes are chemically modified to support endothelial cell adhesion. These endothelial cell–covered fibers are bundled and rotated in an oxygenator to create mixing and reduce boundary layer limits on gas transfer efficiency (*8*). Such devices create a "bio-hybrid" lung that is primarily synthetic but incorporates patient endothelial cells. If they can simulate native thromboresistant endothelial surfaces, a major goal will be achieved.

Petersen *et al.* and Ott *et al.* apply whole-organ decellularization (removal of all cellular constituents) to the lung, an approach recently explored for heart, liver, and kidney (*9*–*11*). This method has conceptual roots in clinically successful bone marrow transplantation. In vivo tissue devitalization, followed by introduction of a regenerating cell population to reconstruct function, was pioneered by E. Donnall Thomas and colleagues in the 1950s and was the basis of the 1990 Nobel Prize in Physiology or Medicine. Petersen *et al.* and Ott *et al.* removed the cells from isolated adult rat lungs in a manner that preserved the structural characteristics of the organ, notably the vasculature and the airways (including alveoli, the tiny air sacs in which gas transfer occurs). The remaining lung "scaffolds" were maintained in a bioreactor designed to mimic the developmental environment of lung tissue, and repopulated with epithelial and endothelial cells. Lung tissue was successfully regenerated that mimicked native tissue in appearance and could facilitate gas exchange in vitro and when grafted into rodents.

The promise of this tissue-engineering approach lies in its potential to effectively expand the pool of donor organs, particularly if lungs unsuitable for transplant can be processed for seeding with autologous cells for a given patient while the patient is supported with artificial lung technology. More important, if a tissue-engineered lung had the functional profile of an allograft lung, the removal of pharmacologic therapy to combat organ rejection would have a profound effect on the prognosis and quality of life for lung recipients. Other possible applications of this technique include processing of a patient's diseased tissue to remove problematic cellular components followed by regeneration to a healthy state.

Although the reports of Petersen *et al.* and Ott *et al.* open possibilities for treating pulmonary failure and studying mechanisms underlying cell–extracellular matrix interactions, many issues remain to be addressed. Identifying cell sources from the patient that are most effective in repopulating the decellularized lung, achieving a sound blood-gas barrier and a completely endothelialized blood pathway, and providing long-term evaluation of cellularization and differentiation in situ are considerations. The use of extracellular matrix for connective tissue repair is effective in many applications, but there can be failures associated with tissue remodeling that result in mechanically inadequate structures (*12*). How will the lung extracellular matrix ultimately be remodeled? If replacement lung tissue is inappropriately fibrous or weak, long-term outcomes will be insufficient. Also, the level of phenotypic organ recapitulation that can be achieved and is functionally adequate remains open. Like the native organ, will the regenerated lung recruit vascular beds that

will permit increasing blood flows with low resistance? The organ decellularization paradigm has opened a breach where multidisciplinary teams of biologists, clinicians, and engineers can explore new ways to engineer complex tissues. The next generation of artificial or bio-hybrid organs may provide temporary support for patients while patient-specific regenerative solutions are prepared and implanted.

References

1. T. H. Petersen *et al.*, *Science* **329**, 538 (2010); published online 28 June 2010 (10.1126/science.1189345).
2. H. C. Ott *et al.*, *Nat. Med.* 10.1038/nm.2193 (2010).
3. W. S. Stoney, *Circulation* **119**, 2844 (2009).
4. T. Zhang *et al.*, *Artif. Organs* **33**, 36 (2009).
5. S. Fischer *et al.*, *ASAIO J.* **54**, 3 (2008).
6. D. M. Hoganson *et al.*, *J. Thorac. Cardiovasc. Surg.* 10.1016/j.jtcvs.2010.02.062 (2010).
7. K. A. Burgess *et al.*, *Biomed. Microdevices* **11**, 117 (2009).
8. A. A. Polk *et al.*, *Biotechnol. Bioeng.* **106**, 490 (2010).
9. H. C. Ott *et al.*, *Nat. Med.* **14**, 213 (2008).
10. B. E. Uygun *et al.*, *Nat. Med.* **16**, 814 (2010).
11. E. A. Ross *et al.*, *J. Am. Soc. Nephrol.* **20**, 2338 (2009).
12. K. A. Derwin *et al.*, *J. Shoulder Elbow Surg.* **19**, 467 (2010).

10.1126/science.1194087

CHEMISTRY

Connecting Biomass and Petroleum Processing with a Chemical Bridge

Biomass-derived sugars can be converted to fuels via conventional petrochemical processing.

Joseph J. Bozell

Petroleum is not only the primary feedstock for liquid fuels but also the basis for most of the chemicals and polymers that we use (*1*, *2*). Continuing questions about the longevity and stability of petroleum supplies, as well as the environmental impacts of its production and use, have driven the development of alternatives such as agricultural or woody biomass. Biomass could supplement petroleum as the main feedstock for fuel and chemical production (*3*, *4*), but it will be necessary to develop large-scale fermentation infrastructure for fuels, as well as new synthesis routes to chemicals that start with carbohydrates (*5*–*7*). If carbohydrates could be converted to compounds with fewer oxygenated groups that reacted more like petroleum, they could supply the petrochemical industry plants with a renewable feedstock. Two recent papers by Bond *et al.* (*8*) and Lange *et al.* (*9*) now suggest that levulinic acid (LA), a dehydration product of simple sugars like glucose, can meet this need (see the figure). Incorporation of LA as an intermediate allows use of catalytic conversion processes fully compatible with the infrastructure of the chemical industry.

Sugar dehydration, which is performed by treatment with acid, ultimately forms LA and formic acid in an approximately 3:1 weight ratio. This transformation has been known for decades, but has normally been accompanied by the formation of intractable by-products, and it is difficult to separate LA from the mixture. The status of LA as a biorefinery platform chemical was substantially upgraded in the early 1990s by Biofine Renewables and the development of a two-reactor system that enabled the production of LA in high yield (*10*).

The conversion of LA to fuels begins with the well-established, high-yield hydrogenation of LA to γ-valerolactone (GVL). Lange *et al.* optimized this conversion by testing more than 50 hydrogenation catalysts. Reduction of LA with 40-bar H_2 at 200°C, in the presence of a catalyst (1% by weight platinum metal dispersed on titanium oxide), proceeded with 95% conversion efficiency (the fraction of starting material that reacted). The selectivity (the ratio of desired product to all products formed) was nearly the same. The catalyst system showed good stability, with very little deactivation after more than 100 hours of continuous operation. By-products were also minimal; valeric acid (VA) and methyltetrahydrofuran were present at <0.5 mol %.

The subsequent transformations of GVL that removed oxygen and created larger molecules differ in the two studies. Bond *et al.* describe a two-step process that catalytically eliminates CO_2 from GVL in aqueous solution, giving an initial mixture of isomeric butenes. Two or more butene units oligomerize to create higher hydrocarbons (eight or more carbon atoms) of sufficient molecular weight to serve as transportation fuels. After optimization of the individual

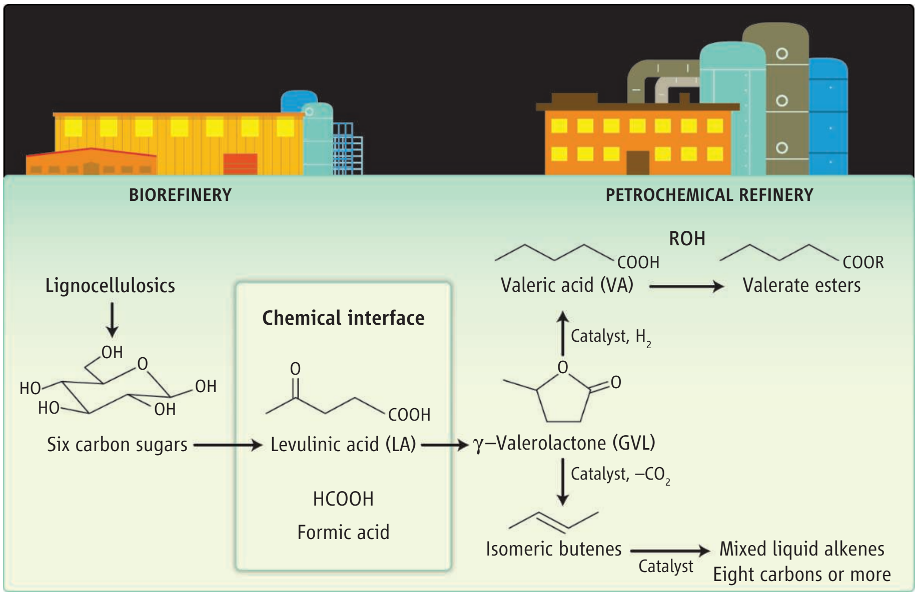

Sugar substitutes for petroleum. Biorefineries can convert biomass to simple six-carbon sugars. Rather than ferment these into alcohols (ROH), they can be converted by acid treatment to levulinic acid, which can serve as initial feedstock for existing petrochemical processing operations. Recent work by Bond *et al.* and Lange *et al.* show how levulinic acid can be converted to fuels and fuel additives through intermediates such as γ-valerolactone (GVL) and valeric acid (VA).

Forest Products Center, Biomass Chemistry Laboratories, University of Tennessee, Knoxville, TN 37996, USA. E-mail: jbozell@utk.edu

steps, they developed an integrated two-reactor system with an interreactor separator, which removes water found to inhibit some of the downstream processes. A 98% yield of butene at 99% GVL conversion was achieved at moderate pressures and temperatures in the presence of a silica-alumina catalyst. After water removal, oligomerization of the butene present in the butane-CO_2 mixture with a macroporous polymeric catalyst converted 90% of the butene with 95% selectivity to liquid alkenes with eight or more carbon atoms. This approach offers the benefit of producing butene fuel precursors without requiring an additional and costly hydrogenation step. Further, the process operates at elevated pressure, sufficient for conversion of CO_2 to chemical products, or for sequestration without need for additional energy-intensive compression.

Unlike the process of Bond *et al*., Lange *et al*. hydrogenated LA to form VA as the main product, which is then reacted with alcohols to form to a family of valerate esters suitable as gasoline- or diesel-fuel additives. This process retains all of the carbon present in LA. The initial 70% conversion of GVL has >90% selectivity for VA with 10-bar H_2 at 250°C. They used a platinum-silica catalyst that was bound inside a porous HZSM-5 zeolite catalyst. In a manner similar to the method reported by Bond *et al*., the reduction proceeds through formation of intermediate pentenoic acid isomers. Although the GVL conversion gradually drops during the reduction, the catalyst can be regenerated by periodic treatment with H_2 at 400°C. Under these conditions, catalyst performance and VA production were maintained for more than 1500 hours of operation. Lange *et al*. also report a single-step conversion of LA and ethanol into ethyl valerate using a catalytic reactive distillation system.

The lower molecular weight esters (methyl, ethyl, and propyl valerate) exhibited performance suitable for use as a gasoline additive at levels of 10 and 20% (by volume). Higher esters (butyl and pentyl valerate) could be used directly as a diesel fuel or as a diesel additive. Road trials using a 15% blend of ethyl valerate in regular gasoline were carried out with 10 vehicles and a total of about 250,000 km of driving. No engine performance issues were noted, but the lower energy density of ethyl valerate resulted in an expected loss of fuel economy per volume.

Thus, functionally useful biorefinery intermediates need not be structurally identical to compounds currently used in the petrochemical industry. Technology development issues must be addressed before a deeply entrenched and established biofuel (ethanol) can be replaced with promising but less recognized alternatives. Research challenges also exist: The initial LA production from sugars is still not highly efficient and has not been tested at scales necessary to ensure viability in a fuel-production scenario.

Finally, the question of what to do with the formic acid produced as an unavoidable LA by-product must be addressed. A similar situation exists within the biodiesel industry, which must deal with the formation of a glycerol co-product. Formic acid can be used to reduce LA to GVL via catalytic transfer hydrogenation, but such processes have yet to be optimized (*11*, *12*). Nonetheless, these demonstrations of a biobased chemical as an intermediate in a process compatible with petrochemical technology will spur the use of renewable biomass as a source of the next generation of biofuels, and as a replacement for traditional raw material supplies.

References

1. K. Weissermel, H.-J. Arpe, *Industrial Organic Chemistry* (Wiley-VCH, Weinheim, Germany, ed. 4, 2003).
2. M. M. Green, H. A. Wittcoff, *Organic Chemistry Principles and Industrial Practice* (Wiley-VCH, Weinheim, Germany, 2003).
3. J. N. Chheda, G. W. Huber, J. A. Dumesic, *Angew. Chem. Int. Ed.* **46**, 7164 (2007).
4. E. de Jong, R. van Ree Rea, R. van Tuil, W. Elbersen, in *Biorefineries—Industrial Processes and Products*, B. Kamm, P. R. Gruber, M. Kamm, Eds. (Wiley-VCH, Weinheim, Germany, 2006), vol. 1, pp. 85–111.
5. R. D. Perlack *et al*., "Biomass as feedstock for a bioenergy and bioproducts industry: The technical feasibility of a billion-ton annual supply" (U.S. Department of Energy, Washington DC, DOE/GO-102995-2135, 2005).
6. J. J. Bozell, *Clean-Soil Air Water* **36**, 641 (2008).
7. J. J. Bozell, G. R. Petersen, *Green Chem.* **12**, 539 (2010).
8. J. Q. Bond, D. M. Alonso, D. Wang, R. M. West, J. A. Dumesic, *Science* **327**, 1110 (2010).
9. J.-P. Lange *et al*., *Angew. Chem. Int. Ed.* **49**, 4479 (2010).
10. S. W. Fitzpatrick, *ACS Symp. Ser.* **921**, 271 (2006).
11. H. Mehdi *et al*., *Top. Catal.* **48**, 49 (2008).
12. H. Heeres *et al*., *Green Chem.* **11**, 1247 (2009).

10.1126/science.1191662

PHYSICS

An Atomic View of Quantum Phase Transitions

The transformation of individual cold atoms between quantum phases has been imaged.

Brian DeMarco

Although it is evident that strong interactions between particles can lead to the formation of quantum-mechanical phases such as high-temperature superconductivity, there are many gaps in our understanding of the underlying physics. Cold atoms trapped in optical lattices have emerged as an ideal model system for understanding the creation of these phases because the strength of the particle interactions can be smoothly tuned and complicating factors in solids such as disorder can be controlled. Although much progress has been made, new techniques are needed if these experiments are to reveal enough detail to verify theoretical models. On page 547 of this issue, Bakr *et al*. (*1*) used their "quantum gas microscope" (*2*) to image and study the dynamics of individual atoms as they transform between different quantum phases.

An artificial solid is created in optical lattice experiments by first cooling atoms trapped as a gas in ultrahigh vacuum to nanokelvin temperatures (*3*). The atoms are then captured in a lattice that is created by slowly turning on a combination of laser beams. The atoms play the role of the electrons or superconducting pairs of electrons in a solid, whereas the light substitutes for the underlying ionic crystal. Different crystal geometries can be produced depending on the arrangement of the lasers. The holographic technique used by Bakr *et al*. to create a square lattice is especially powerful because it can, in principle, produce any two-dimensional crystal geometry.

Optical lattices have been used for a broad spectrum of experiments at the forefront of atomic physics. Strontium atoms trapped in an optical lattice were used to demonstrate the most accurate clock—one that loses a sec-

Department of Physics, University of Illinois at Urbana-Champaign, Urbana, IL 61801, USA. E-mail: bdemarco@illinois.edu

ond every 200 million years—based on neutral atoms (*4*). Optical lattices are also an attractive platform for quantum computing (*5*), in part because a lattice can provide large numbers of properly initialized quantum bits.

The application that has garnered perhaps the most attention uses optical lattices to simulate physics models that we do not completely understand (*6*). One of these is the Hubbard model, which incorporates only two key ideas: Electrons can hop between sites by quantum tunneling, and they interact with each other only if they are on the same site. A key and surprising feature of the Hubbard model is that electrons that would be expected to be mobile can be pinned by strong electronic interactions in a quantum phase known as a Mott insulator. Two versions of this model are realized by cold-atom systems, depending on the atomic species. The Fermi-Hubbard (FH) model is used if the atoms are fermions (*7*, *8*). This model has been applied to materials of key technological importance, such as the high-temperature superconducting cuprates. The Bose-Hubbard (BH) model (*9*) is used if atoms are bosons, such as the rubidium-87 atoms used by Bakr *et al.* in their experiments. Variants of the BH model have been applied to granular superconductors and arrays of Josephson junctions.

Despite the apparent simplicity of Hubbard models, some of their most basic features have confounded physicists. For example, it is not clear how different phases arise in the FH and disordered BH model as parameters such as the interaction energy are varied. The source of this confusion is twofold. Theoretical approaches have failed to produce a complete understanding of these models. In this situation, physicists often resort to numerical simulation to provide answers. Unfortunately, in cases such as the FH model, our most powerful supercomputers can exactly simulate the dynamics of only tens of electrons, and advances consistent with Moore's Law have increased the simulation size by about one electron per decade.

The advantage of replacing computation with optical-lattice simulations is that highly precise atomic physics techniques can be used to coax answers directly from nature. The equivalent of materials parameters in solids can be easily and directly controlled, for example, by tuning the intensity of the lattice lasers. Rather than developing techniques to grow new samples, as in experiments on solids, these adjustments can be made once every experimental cycle (time scales of minutes).

Quantum gas microscopy. At the bottom, atoms (shown in red) in a circular Mott-insulator shell are trapped using lasers. Above this sample, a hemispherical lens that is part of a high-resolution imaging system used by Bakr *et al.* creates an image of this quantum state.

Bakr *et al.* imaged individual atoms transforming from a superfluid into a Mott-insulator phase as the ratio of interaction to tunneling energy was increased (see the figure). Similar studies of this phase transition in an optical lattice probed on the most microscopic scale have also been reported by Sherson *et al.* (*10*). This transformation corresponds to a Mott insulator–superconductor transition in an electronic system; the bosonic Rb atom acts like a superconducting electron pair. In the cold-atom Mott-insulator phase, a fixed number of atoms occupy each lattice site at zero temperature; at any finite temperature the atom number somewhat fluctuates. Fortuitously, unintended ripples present in the atom trap used by Bakr *et al.* revealed that nearly one-dimensional Mott-insulator islands can be prepared with unexpected, ultrahigh fidelity even at finite temperatures. Additional cooling likely occurs when this state ejects thermal excitations into neighboring superfluid or thermal regions. Bakr *et al.* were also able to measure how fast a Mott insulator formed at the single-site level by varying the time over which they increased the lattice laser intensity. Atom-number fluctuations in Mott-insulating sites were suppressed in only a few milliseconds. These measurements provide important new information for ongoing research into equilibrium in lattice experiments (*11*).

The experiments by Bakr *et al.* build on previous work demonstrating optical (*12*) and electron (*13*) imaging of individual optical lattice sites. However, their result provides an atomic view in the strongly correlated regime, in which many-particle states—such as the Mott insulator—exist that cannot be understood qualitatively using a single-particle theory.

This microscopic view of strongly correlated states may be instrumental in achieving a grand challenge for fermion lattice experiments (*14*), that is, cooling the system to low enough temperatures to observe any potential *d*-wave superfluid phase. Such a result would confirm that the FH model is sufficient to explain high-temperature superconductivity. The first step en route to this goal is to cool below the temperature for antiferromagnetic ordering, which so far has been out of reach of experiments (*15*). Microscopy at the single site level will be an important tool for developing and diagnosing new cooling methods. Furthermore, by combining microscopy with holographic potentials, Bakr *et al.* have the means to accomplish entropy segregation through atom-trap engineering (*16*), which may be a viable approach to achieve these exotic quantum states.

References:

1. W. S. Bakr *et al.*, *Science* **329**, 547 (2010).
2. W. S. Bakr, J. I. Gillen, A. Peng, S. Fölling, M. Greiner, *Nature* **462**, 74 (2009).
3. I. Bloch, *Nat. Phys.* **1**, 23 (2005).
4. A. D. Ludlow *et al.*, *Science* **319**, 1805 (2008).
5. C. Monroe, *Nature* **416**, 238 (2002).
6. M. Lewenstein *et al.*, *Adv. Phys.* **56**, 243 (2007).
7. U. Schneider *et al.*, *Science* **322**, 1520 (2008).
8. R. Jördens, N. Strohmaier, K. Günter, H. Moritz, T. Esslinger, *Nature* **455**, 204 (2008).
9. M. Greiner, O. Mandel, T. Esslinger, T. W. Hänsch, I. Bloch, *Nature* **415**, 39 (2002).
10. J. F. Sherson *et al.*, http://arxiv.org/abs/1006.3799 (2010).
11. C.-L. Hung, X. Zhang, N. Gemelke, C. Chin, *Phys. Rev. Lett.* **104**, 160403 (2010).
12. K. D. Nelson, X. Li, D. S. Weiss, *Nat. Phys.* **3**, 556 (2007).
13. P. Würtz, T. Gericke, A. Vogler, F. Etzold, H. Ott, *Appl. Phys. B* **98**, 641 (2010).
14. I. Bloch, *Science* **319**, 1202 (2008).
15. T. Paiva, R. Scalettar, M. Randeria, N. Trivedi, *Phys. Rev. Lett.* **104**, 066406 (2010).
16. J.-S. Bernier *et al.*, *Phys. Rev. A* **79**, 061601 (2009).

10.1126/science.1193401

SPORE* SERIES WINNER

MIT OpenCourseWare: Unlocking Knowledge, Empowering Minds

A collection of more than 2000 course syllabi, lecture notes, assignments, and exams is provided free of charge.

Cecilia d'Oliveira[†], Stephen Carson, Kate James, Jeff Lazarus

As the global economy increasingly demands an educated workforce, school systems in the United States and abroad find themselves overwhelmed by student demand. Particularly in the developing world, there are not enough seats in classrooms with qualified teachers to make high-quality education opportunities available to every student. In places ranging from China to India to Turkey, only a small percentage of qualified students are accepted into university programs, especially those in science and technology fields. Existing institutions are under enormous pressure, and the needs of talented and motivated learners are not being met. Making headway against these formidable challenges will require rethinking traditional educational approaches and will call for the use of innovative technologies to scale up global capacity for providing high-quality education.

In 2000, a faculty committee at Massachusetts Institute of Technology (MIT) was charged with answering two questions: How will the Internet change education? and What should MIT do about it? Many of the Institute's peers were already launching distance-learning ventures, and it was expected that this committee would propose a similar endeavor. Instead, after a summer spent studying options, the committee came forward with a startling proposal. Rather than using the Internet to make money through distance learning, MIT should simply take the core academic materials already created on campus—the syllabi, lecture notes, assignments, and exams—and share them with the world. This suggestion seemed counterintuitive, given the prevailing direction of U.S. higher education at the time, but the profitability of distance learning was unclear, and the committee's proposal was far more consistent with MIT's mission to disseminate knowledge. To facilitate use of this content, they proposed publishing the materials using open licenses like those that had allowed open-source software to flourish (*1*).

Ten years later, MIT OpenCourseWare (OCW), available at http://ocw.mit.edu, contains the core academic content used in ~2000 classes, presenting substantially all the undergraduate and graduate curriculum from MIT's 33 academic departments. A selection of courses, including introductory physics, math, and engineering, contain full video lectures. Partner organizations have created more than 800 translations of OCW courses in five languages. The OCW team has distributed over 200 copies of the entire Web site on hard drives primarily to sub-Saharan Africa, where Internet access is limited. OCW has grown into a global educational resource.

Case study. Haitian entrepreneurs used OCW to bring solar-powered streetlights to Cité Soleil, one of Haiti's poorest shantytowns.

An early challenge for the program was to figure out exactly who was using the site and how. The committee that proposed the project imagined it would largely be used as a resource for educators who would download and adapt the materials for use in their own classes. Even from the beginning, however, it was clear that OCW appealed to wider audiences. Early surveys indicated that educators at other universities represented about 15% of the audience. Students from other universities, another expected audience, made up another 35%. The largest portion of the visitors, however, came from an unanticipated group: 50% of visitors self-identified as independent learners unaffiliated with a university. Although OCW was not structured as a distance-learning program, it became clear that OCW did support independent learning.

OCW currently receives upwards of 1.5 million visits each month from ~900,000 unique individuals (*2*). Students have grown to 42% of the audience, and educators and independent learners now constitute 9% and 43% of visitors, respectively (*3*). Twelve percent of educators responding to a March 2010 visitor survey indicated that they do incorporate OCW materials into their own content as anticipated, but educators more frequently use OCW for personal learning (37%), to adopt new teaching methods (18%), and as a reference for their students (16%). Students were largely expected to use the site as a supplement to materials they received in their own classes, a use identified by 40% of students. Just over 43%, however, indicated that they also use OCW for personal learning beyond the scope of their formal studies, and a further 12% use it as an aid in planning their course of study. Independent learners use OCW in a variety of personal (41%) and professional (50%) contexts, including home-schooling children and keeping up on developments in their professional field. Sixty-six percent of visitors indicate they are mostly or completely successful at meeting their educational goals for visiting the site.

One example of OCW use is that of Professor Triatno Yudo Harjoko, Head of the Architecture Department at the University of Indonesia. Together with his colleagues, Harjoko is redesigning their teaching model. Harjoko describes the main goal in this transition as "encouraging students to learn by themselves, and to be both critical and creative." In the redesign process, OCW, to which Harjoko was introduced by a colleague several years ago, has served as an immense comparative database. Rather than directly transposing OCW syllabi to University of Indonesia courses, Harjoko and his colleagues have been scrutinizing MIT's courses to better understand how they were designed and

MIT OpenCourseWare, Massachusetts Institute of Technology, Cambridge, MA 02142, USA.

*SPORE, Science Prize for Online Resources in Education; www.sciencemag.org/special/spore/. †Author for correspondence. E-mail: cec@mit.edu

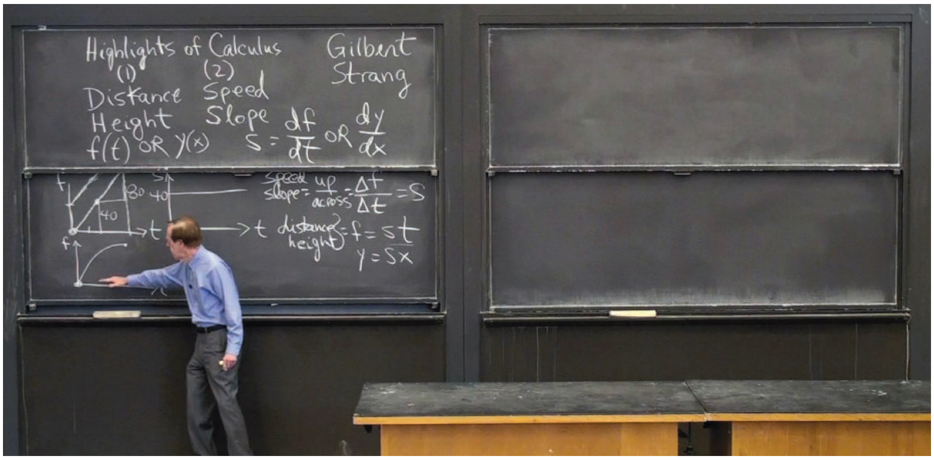

Highlights of Calculus. A series of videos, showing ways in which calculus is important in our lives, are ideal for high school students, college students, and anyone interested in learning the basics of calculus. View the videos at http://ocw.mit.edu/high-school/calculus/.

developed. "We try to understand how the courses are formulated," Harjoko explains, "and what the expected outcomes are. This gives us an important perspective on the learning process."

The impact of OCW also reaches far beyond formal classrooms. Haitian natives Jean-Ronel Noel and Alex Georges provide an example of the many unanticipated ways OCW is generating benefit. Noel and Georges planned to create solar panels to power lighting to serve the needs of their country, but in their research and development process, they required guidance in electrical engineering. Noel found the needed help though OCW. "I was able to use OCW to learn the principles of integrated circuits. It was much better than any other information I found on the Internet." Today their company, Enersa, has made a difference in their community by training and employing 18 people of Cité Soleil and has made a positive impact on the environment by making solar-powered LED lighting available in almost 60 Haitian towns and remote villages (see the first figure).

Perhaps more significant than the direct impact of the site is the global OCW movement MIT helped launch. More than 200 universities worldwide have joined MIT in sharing their own educational materials openly, creating a global body of knowledge that spans many cultures and academic levels. More than 13,000 courses from these schools are available through the OpenCourseWare Consortium portal (http://ocwconsortium.org) (*4*).

MIT has been very successful at attracting a large global audience that uses the OCW materials in a wide variety of ways. The site is a repository of educational resources, a reference for scientific and technical information, an educational planning tool, an informal learning space, and a source of entertainment and inspiration to millions of people. The site has also generated significant benefit for the existing MIT community with more than 90% of students, 84% of faculty, and 50% of alumni accessing the site for a range of academic purposes. In addition, more than a third of incoming freshman who knew of the site before choosing their school say OCW positively influenced their decision to attend MIT.

This variety of uses, however, presents the greatest challenges in developing a vision for the next phase of OCW's development. Although MIT will continue to publish materials from new courses and to update materials from previously published courses, the OCW team is actively seeking new ways to expand the project's global benefit. In 2007, OCW introduced a companion site, Highlights for High School (http://ocw.mit.edu/highschool), which catalogs more than 2600 resources embedded in the main OCW site that correspond to U.S. Advanced Placement curricula for physics, calculus, and biology (see the second figure). The Highlights site has received more than 1 million visits since launch, and 70% of visitors report being mostly or completely successful at meeting their educational goals in accessing the site.

This fall, OCW will begin to introduce course materials designed specifically for use by independent learners, which will include complete sets of content, increased focus on problem-solving, and additional self-assessment opportunities. Through these and other pilot programs, the OCW team hopes to develop a better understanding of how to increase the benefits for this varied global audience.

OCW must also develop a sustainable funding model. MIT currently covers about half the cost of OCW publication, and grant reserves support the rest of the $3.7 million annual budget. As the grant reserves are depleted, OCW expects to transition to a model similar to that used by U.S. National Public Radio, drawing support to complement MIT's direct contributions from a combination of corporate gifts and underwriting, visitor donations, major gifts, and additional grants. In the past year, OCW has received more than $220,000 in small donations from thousands of users around the world, indicating that this model has the potential to generate substantial support.

Despite the global use of OCW materials and the widespread adoption of the OCW model at universities worldwide, we are still in the early stages of understanding the many ways these materials are being used to improve formal and informal learning, and we believe many opportunities lie ahead for increasing the impact of OCW materials from MIT and the many other schools that have chosen to share their educational resources.

About the Authors

Kate James is executive director of OCW. **Cecilia d'Oliveira** is senior manager, User Experience for OCW. **Stephen Carson** is OCW's external relations director, and serves as president of the OCW Consortium board. **Jeff Lazarus** is a special adviser to OCW.

References and Notes

1. OCW content is published under a Creative Commons V3.0 license, www.creativecommons.org.
2. OCW monthly traffic data, http://ocw.mit.edu/about/site-statistics/monthly-reports/.
3. For visitor role and use data, please see: http://ocw.mit.edu/about/site-statistics/.
4. MIT was instrumental in establishing the OCW Consortium and guiding its early collaboration efforts as an informal alliance. In 2009, the Consortium became an independent 501c(3) organization with its own board, officers, and budget. For more information, see http://ocwconsortium.org.

10.1126/science.11826962

FOOD & NUTRITION

Experts Urge Renewed Research to Meet Global Food Needs

Sharing the bounty. The U.S. National Institute of Food and Agriculture is leading new efforts to address U.S. and global food security issues.

Thanks to decades of very successful agricultural science, few Americans ever worry about tomorrow's food, fuel, and fiber. But the world likely will need to double food production by 2050 to meet rising food demand, and past investments alone won't be enough to meet that goal, said experts convened by AAAS.

Agricultural science suffers from a "culture of neglect," said Roger Beachy, director of the National Institute of Food and Agriculture at the U.S. Department of Agriculture. "Because we do not feel the hunger that gnaws at nearly a billion of the world's citizens and because the few American farmers that feed America and much of the world are often out of sight and out of mind of urbanites," he said, "we have become complacent in the support and advocacy for agriculture research."

Beachy delivered the inaugural AAAS Charles Valentine Riley Memorial Lecture at a packed AAAS auditorium on 15 June. The lecture, in memory of the prolific 19th-century writer, artist, and chief of the Federal Entomological Service, was cosponsored by the Charles Valentine Riley Memorial Foundation in collaboration with the World Food Prize Foundation.

With a few exceptions, federal funding for agricultural research has been declining or stagnant for decades, Beachy said, threatening the health and wealth of rural communities and the nation's long-term food security. Industry has picked up some of the slack, he said, but it has "focused on relatively short-term, high-impact outcomes that will support product lines."

As head of the federal government's primary funder of agricultural research, Beachy said he is determined not "to preside over a flat budget and a research paradigm more suited to the 19th century than the 21st century."

Beachy said researchers must be prepared to collaborate widely and share practical results with farmers and consumers. He urged more team-oriented research that combines the talents of engineers, biochemists, crop and animal scientists, and others.

One pressing problem for agricultural scientists is global climate change. Speakers at a 16 June briefing on Capitol Hill, cosponsored by AAAS's Center for Science, Technology and Congress, said it already has shifted growing seasons, threatened water sources, and exacerbated food shortages.

New investment is urgently needed to offset the impact in developing countries, said Gerald Nelson, a senior research fellow at the International Food Policy Research Institute. "If we don't do anything," he said, "projections suggest that unchecked climate change [will result in] a 20% increase in the number of malnourished children in 2050."

Cynthia Rosenzweig, a senior research fellow at NASA Goddard Institute for Space Studies, said climate change is likely to threaten the world's food supply, posing an international security risk. "There is the potential for strong shocks on any nation's agricultural production," she said at the briefing.

But in his lecture at AAAS, Beachy said transformative changes in biotechnology and other sciences "give us a fighting chance to create a world where the world's hunger needs are met while preserving or even restoring our natural resource base."

In a forum following Beachy's talk, Ethiopian-born agronomist Gebisa Ejeta reminded the audience that "with all the breakthroughs that we have made in science around the world, we have not been able to give humanity that fundamental right…to enough food."

Ejeta, 2009 winner of the World Food Prize, said he remains optimistic that scientists can "address issues of agriculture and natural resource management at home and abroad in a more holistic way than ever before."

—Earl Lane, Ginger Pinholster, and Becky Ham

SCIENCE EDUCATION

Young Teachers Hear Importance of Standards

A corps of promising young teachers got expert insight on the drive for the next generation of mathematics and science standards during the annual meeting of the Robert Noyce Teacher Scholarship Program.

In June, a consortium of education and mathematics experts released new standards for K-12 mathematics education in the United States. The standards have already been adopted by 25 states as of mid-July.

Meanwhile, the U.S. National Research Council completed a draft conceptual framework for science education standards and on 12 July submitted it for public comment (see www.aaas.org/go/nas_stds/). Once finalized, the nonprofit education group, Achieve, will coordinate the use of this framework to develop more explicit standards. The National Science Teachers Association and AAAS are supporting partners in these efforts, and the Carnegie Corporation of New York is providing financial support.

The Noyce program, funded by the National Science Foundation, trains students and professionals in science, technology, engineering, and mathematics to be K-12 teachers in high-need school districts. Since the program began in 2002, it has trained 7700 teachers.

Some 475 educators attended the conference, organized by AAAS and held 7 to 9 July in Washington, D.C.

Science Editor-in-Chief Bruce Alberts, in a keynote speech, told them that new standards should emphasize abstract thinking, real-world problem-solving, and communication skills, and that large numbers of creative, dedicated teachers will be crucial.

"Each of you should realize how critical your work is, for our nation's future," he said. "In fact, your work is more important than many of you may recognize."

—Molly McElroy

CREDIT: COURTESY OF USDA AGRICULTURAL RESEARCH SERVICE

New Opportunities for an Ancient Material

Fiorenzo G. Omenetto and David L. Kaplan*

Spiders and silkworms generate silk protein fibers that embody strength and beauty. Orb webs are fascinating feats of bioengineering in nature, displaying magnificent architectures while providing essential survival utility for spiders. The unusual combination of high strength and extensibility is a characteristic unavailable to date in synthetic materials yet is attained in nature with a relatively simple protein processed from water. This biological template suggests new directions to emulate in the pursuit of new high-performance, multifunctional materials generated with a green chemistry and processing approach. These bio-inspired and high-technology materials can lead to multifunctional material platforms that integrate with living systems for medical materials and a host of other applications.

Mechanically, silks are outstanding material systems. The toughness of silk fibers is superior to any of the best synthetic high-performance fibers available today, including Kevlar (Dupont Advanced Fiber Systems). Although important insights into silk protein self-assembly have been achieved over the past 10 years (*1*, *2*), the mechanisms by which these proteins achieve metastable states in the glands of the spinning organisms remain unclear. This is a remarkable processing achievement that allows the concentration of protein in the glands to reach >30 weight % in water (*1*), whereas at this concentration most proteins, globular or fibrous, aggregate and precipitate. In the case of silk, this would result in the premature formation of β sheets (crystallization), resulting in insolubility of the spinning dope and blockage of the spinning apparatus, events that would be catastrophic to the silk-spinning organism (*2*). The lack of full comprehension of these processing steps has limited the ability to spin reconstituted silk solutions into fibers with properties comparable to those of native fibers.

Relationships between silk protein processing and fiber properties suggest that material features are controlled by a combination of the chemistry and the spinning process. Mechanical properties of spider silks are modulated on the basis of spinning conditions, including temperature, reeling rate, and drawing rate, as well as the specific type of silk (Fig. 1) (*3*, *4*). Silkworm silk fibers are also influenced by process conditions such that properties can be achieved to match those of spider silks (*5*). Silks from *Bombyx mori* obtained at different reeling rates result in stronger but more brittle fibers. Wet spinning with postspinning treatments can also be used to generate spider silk–like properties and microstructures from silkworm silks (*6*).

The concentration of silk protein increases during the progression from synthesis to spinning in the glands, with changes in chemistry (cations and decrease in pH) and physical features (sol-gel phase transition), along with mechanical alignment in shear flow (*1*). Chain alignment is involved in later processing stages, and the internal drawdown of fibers—perhaps including active transport of water, addition of hygroscopic polymers such as sericin (in the silkworm), or other unknown mechanisms—plays an important role in the critical final steps that lead to fiber formation. Silks are not "squeezed out" of the glands but are mostly pulled out, either by the legs of the spider or by the "figure eight" movement of the head of the silkworm during spinning. Rheological studies into the different structures in the spinning gel formed in vivo versus in vitro are instructive in terms of how much native silk material (harvested directly from the gland) differs from reprocessed (fibers resolubilized into solution) silks (*7*, *8*). This disparity in solution behavior, as discerned from rheological assessments, suggests that there are still substantial knowledge gaps in understanding how to reverse engineer silk protein fibers. Morphological differences in the fiber cross sections among species originate at the spinerettes of spiders and can provide important clues on how processing within the gland, married to the spinning system, can coexist to control morphological features of the final fibers. Thin ribbons, such as those produced by tarantulas, to circular cross sections and other morphologies have been reported depending on the specific spider species. The influence of gland-specific features and process variables have not been studied in detail related to fiber morphology, yet could provide interesting insight into modes to regulate such fiber features.

Silk chemistries have been selected through evolution, and therefore structure-function relationships have been optimized for survival related to the needs of the silk-producing organisms (*9*–*11*). Among silk variants, particular interest is devoted to the silkworm silk of *B. mori* as the commodity silk protein used in textiles and medical sutures and to the dragline silks of spiders such as *Nephila clavipes* and *Araneus diadematus*. Silks are modular in design, with large internal repeats flanked by shorter (~100 amino acid) terminal domains (N and C termini). Silks have high molecular weight (200 to 350 kD or higher) with transcripts of 10,000 base pairs and higher and >3000 amino acids (*10*, *12*). The larger modular domains are interrupted with relatively short spacers with hydrophilic charge groups in the case of silkworm silk. N and C termini are involved in the assembly and processing of silks, including pH control of assembly (*12*). The N and C termini are highly conserved, in spite of their relatively small size compared with the internal modules (N terminus around 130 amino acids and C terminus around 100 amino acids). Accordingly, the inclusion of such modules in cloned silks may be essential when the emulation of native properties is the goal (Fig. 2).

Because native silkworm and spider populations already display variations in the sizes of silk genes and, as a result, in the proteins generated, it is perhaps important to relate size and modular unit distribution to silk protein assembly and material functions. The roles of the N and C termini in processing related to pH, cations, or protein concentration may be responsible for only a subset of the functional features of these domains (*13*). It is conceivable that their role is to help stabilize silk during synthesis and processing in the gland, further underscoring the critical need to include such domains in genetically engineered silks (*14*, *15*). Some dragline spider silks consist of two key proteins, such as Masp1 and Masp2 in the case of *N. clavipes* or *A. diadematus*, with one of the proteins usually containing proline as a putative entropic spring (*16*). Yet silkworm silks generally have one main protein.

The competition for water between the modular domains in silk proteins has not been quantified. This has implications for processing silks in aqueous and organic solvents. The silk-spinning dope in the glands of spiders and silkworms is stable to perturbations, such as when spiders are flicked off the ceiling by an arachnophobe or during the handling of silkworms. In contrast, high concentrations of silk protein in water readily crystallize from their metastable state, with almost any energy input resulting in rapid crystallization. Under natural conditions, silks can be stored for days and weeks in the producing organisms at ambient temperatures in preparation for spinning without premature crystallization. Conversely, careful control of these processes is essential in laboratory conditions in order to avoid premature crystallization. Many of the above factors lead to questions about how silks can be used as design templates in order to build synthetic polymer chemistry analogs that would recapit-

Department of Biomedical Engineering, Tufts University, Medford, MA 02155, USA.

*To whom correspondence should be addressed. E-mail: david.kaplan@tufts.edu

ulate some or all of the useful functional features that exist in naturally occurring silks (*17*). For example, the ability to design synthetic block copolymers with modular designs that can be processed in water under ambient conditions, and yet achieve water-stable robust mechanical properties without the need for chemical crosslinking, would seem to be an enviable outcome from the lessons offered from the designs of silk chemistries and processing.

The main source of silkworm silk is through sericulture, the domesticated production of silk from *B. mori*. This production approach provides the textile world and the medical suture world with an abundance of material for current demands. Additionally, this production process is a source of support for microeconomies in many parts of the world. In contrast to the established supply chain available for silkworm silk, there are no commercial options for spider silks, largely because of the more aggressive nature of spiders and the more complex and smaller quantities of silk mixtures generated in orb webs. Silks have been cloned and expressed in a variety of heterologous hosts, from bacteria and fungi to plants and mammals, as well as via transgenic silkworms (*18*–*22*), yet the material properties of these cloned silks are inferior to the native materials. This difference can be traced to molecular weight and the modular domains. With few exceptions, most silks when cloned and expressed include only some of the core modular domains; in some cases, these modular domains plus the C terminus are truncated. These truncated silks may be sufficient for some applications, but only where mechanical properties are not critical.

Some silks are encoded by single exons, whereas others have conserved introns, features that are unique because in most eukaryotes it is unusual to have proteins encoded by single exons, particularly when the encoded proteins are so large (>3000 amino acids) (*23*). Silk genetic domains

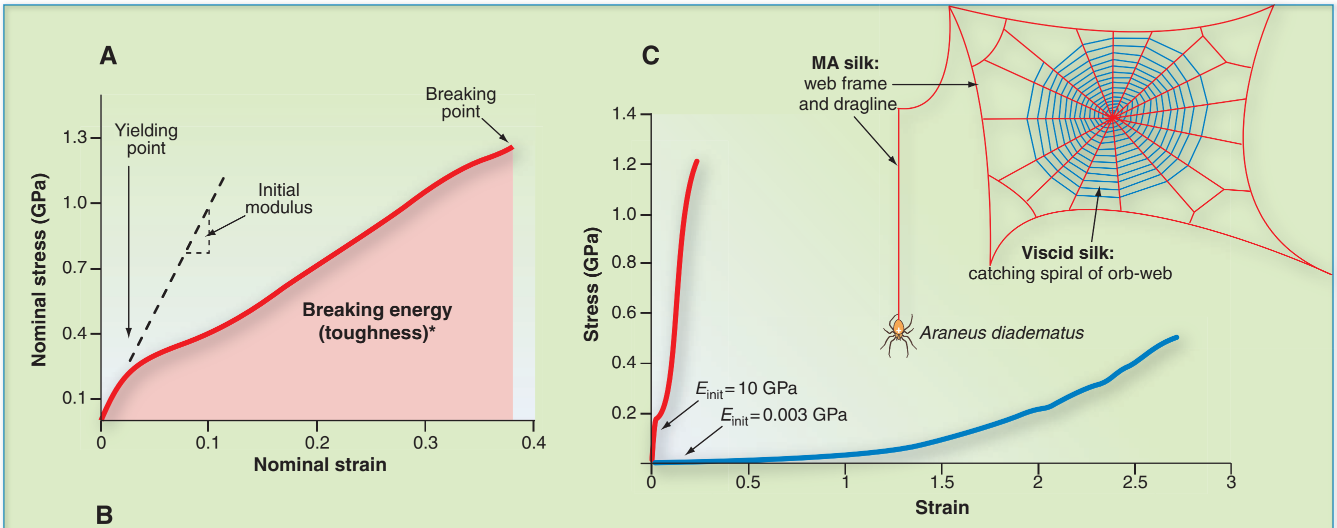

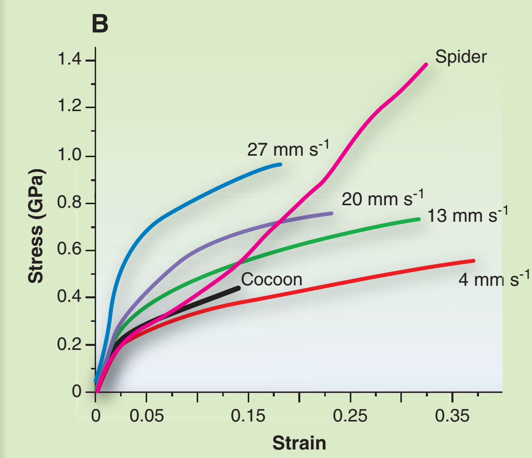

D

Tensile mechanical properties of spider silks and other materials

Material	Stiffness, E_{init} (GPa)	Strength, G_{max} (GPa)	Extensibility ε_{max}	Toughness (MJ m^{-3})	Hysteresis (%)
Araneus MA silk	10	1.1	0.27	160	65
Araneus viscid silk	0.003	0.5	2.7	150	65
Bombyx mori cocoon silk	7	0.6	0.18	70	
Tendon collagen	1.5	0.15	0.12	7.5	7
Bone	20	0.16	0.03	4	
Wool, 100% RH	0.5	0.2	0.5	60	
Elastin	0.001	0.002	1.5	2	10
Resilin	0.002	0.003	1.9	4	6
Synthetic rubber	0.001	0.05	8.5	100	
Nylon fiber	5	0.95	0.18	80	
Kevlar 49 fiber	130	3.6	0.027	50	
Carbon fiber	300	4	0.013	25	
High-tensile steel	200	1.5	0.008	6	

Fig. 1. Mechanical properties of silks. (**A**) Impressive toughness and relative strength of reeled spider dragline silk. The area under the curve shown indicates fiber toughness or the energy taken up by the material before breaking. In terms of strength-to-weight ratio, the spider silk strength (1.1 GPa) is about equivalent to high-tensile engineering steel (1.3 GPa), yet spider silk has a relative density of 1.3 compared with that of steel at 7.8, when reeled at 20 mm s^{-1} at 25°C for *Nephila edulis.* In terms of toughness, spider silk is 165 ± 30 kJ kg^{-1}, which is substantially higher than that of Kevlar 81 (33 kJ kg^{-1}) (*1*, *5*). (**B**) Spinning silk from *B. mori* silkworms at different speeds illustrates control of fiber mechanical properties resulting from processing inputs to complement the importance of chemistry. The data show that the properties can match those of spider silks when spun from the worms at higher rates than native processes. The speeds shown for the lines reflect the rate at which the silk was drawn from the silkworm under controlled conditions at 25°C and are compared with standard degummed silk from cocoons, which are spun from the glands at a natural speed of 4 to 15 mm s^{-1} at 20°C (*3*). (**C**) Stress strain curves for major ampullate (MA) gland silk (red line) and viscid silk (blue line) from the spider *A. diadematus*. E_{init} = initial stiffness (*4*). (**D**) Compilation of data from multiple sources and based on data from the spider *A. diadematus* (*4*). RH indicates relative humidity.

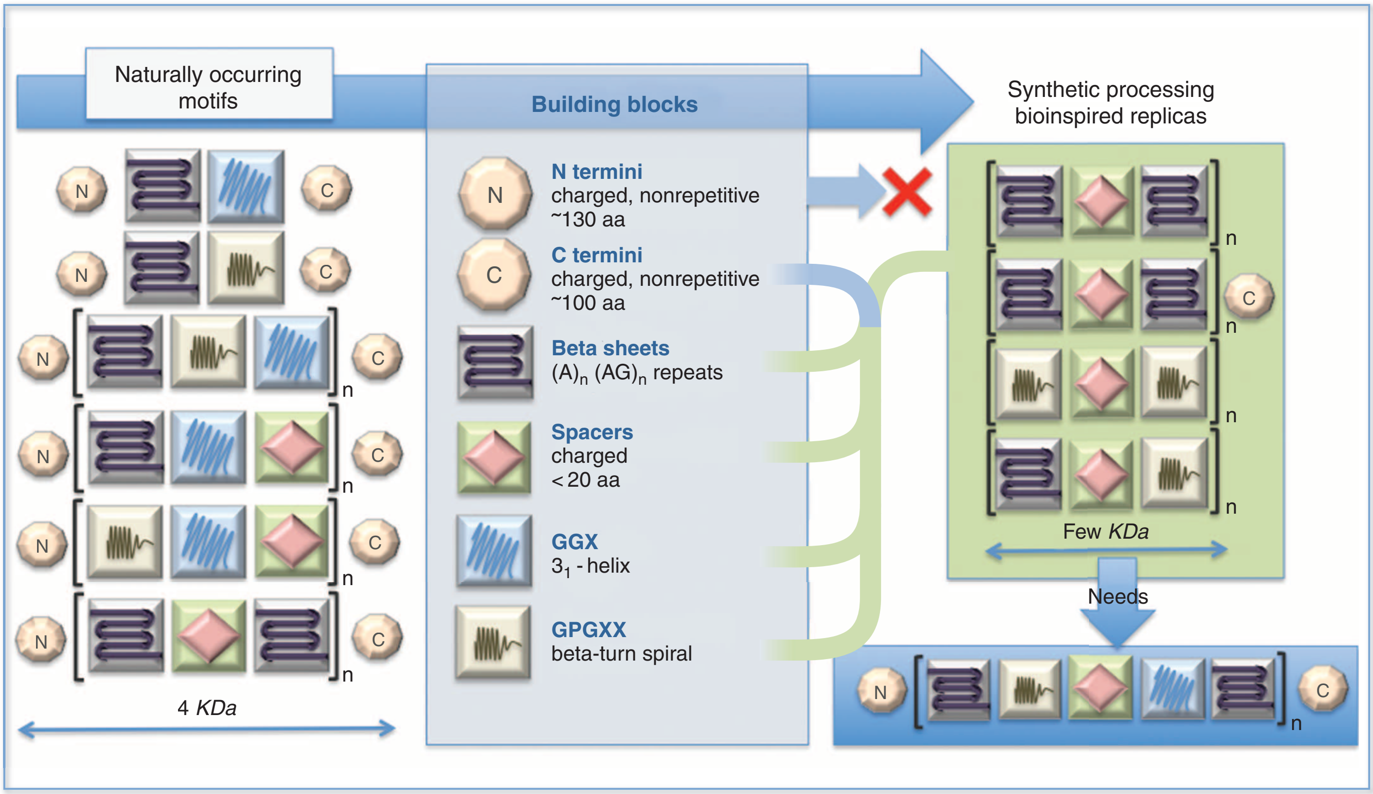

Fig. 2. Modular designs of silk proteins. Silks are fibrous proteins and are characterized by modular units linked together to form high molecular weight, highly repetitive proteins. These modular units or domains, each with specific amino acid sequences and chemistries, provide specific functions. In particular, sequence motifs such as polyalanine (polyA) and poly alanine-glycine (polyAG) (β sheet–forming), GXX (31-helix), GXG (stiffness), and GPGXX (β spiral) are key components in different silks whose relative positioning and arrangement are intimately tied with the end material properties. These domains are linked together to generate high molecular weights and also include characteristic and highly conserved N and C termini. Charged amino acids are strategically located at the chain ends and in spacers to optimize water interactions related to processing and assembly. Current modes of expression of silks in heterologous hosts are generally confined to a limited number of these modular units and lack the inclusion of both N- and C-terminal domains. The incorporation of all of these key domains, along with issues of size (number of modular units), will facilitate improved material properties from silks generated by recombinant DNA techniques.

are remarkable for their repetitive and modular nature, their size, and the highly evolved host cell requirements to meet the extreme demands of just a few amino acids (e.g., glycine and/or alanine in the case of silkworm silk) (*24*). Further, the level of silk protein generated in the silkworm during transition from the worm to the moth is remarkable, prompting research into the use of transgenic silkworms as production factories for cloned genes and the encoded proteins (*25*).

Whether transgenic animals or plants, transgenic silkworms themselves, *Escherichia coli*, or other hosts will become the most efficient system remains to be determined. Regardless, issues of secretion, stabilization of large modular gene structures, and determining metabolic demands during production still need to be resolved. These insights will not only drive improvements in silk expression but also provide important clues for the broader biotechnology community for protein expression needs. The role of processing, in combination with sequence chemistry, will play a critical role in silk material properties. Improved processing approaches for solutions and fibers, such as postspinning draw, water annealing, and the infusion of metals, can help to achieve outcomes that mimic native silks (*26*–*28*).

Future Directions

Down the road, efficient transgenic plants could be used to crop silks, much in the same way that cotton is harvested today. This would add to the all-green process involved in silk protein technologies and lay the foundation for continued propagation of the themes presented here. These approaches will need to be matched with scaled-up processing schemes to emulate or control material properties, from mechanical performance and degradation lifetimes to control of optical clarity. Further, with the above insights as a foundation, aside from pure silk proteins for materials, a new generation of silklike proteins can also be envisioned. Extending these design concepts to a broader range of chemistries, such as other types of protein block copolymers and other types of fusion or chimeric proteins, would all be more approachable with the advances outlined for pure silks. Although each of these systems would require answers to many of the above questions, each could find a place in the applications of polymeric materials in the future because of the compelling native functions of silks and the ability to conduct these processes in a green chemistry mode. This interest would be driven not only by the practical features of the products but also by the fascination with the process of silk spinning and the beauty and utility of silk materials.

Silk-based materials have been transformed in just the past decade from the commodity textile world to a growing web of applications in high-technology directions (Fig. 3) (*29*). Silk sutures have been used for thousands of years, along with other natural materials like animal gut, cotton, and linen. Most of these natural materials were replaced with nylon starting in the 1930s and later with degradable polymer systems from polyesters (e.g., polylactic acid and polylactic-co-glycolic acid). Today silk sutures are used primarily in eye and lip surgery, intraoral surgery, and for some skin wounds, mainly because of their excellent handling and tying capabilities. Silk sutures sold commercially today are defined by the U.S. Pharmacopeia (USP) as nonadsorbable, primarily because of wax coatings that negate proteolytic digestion in vivo. The

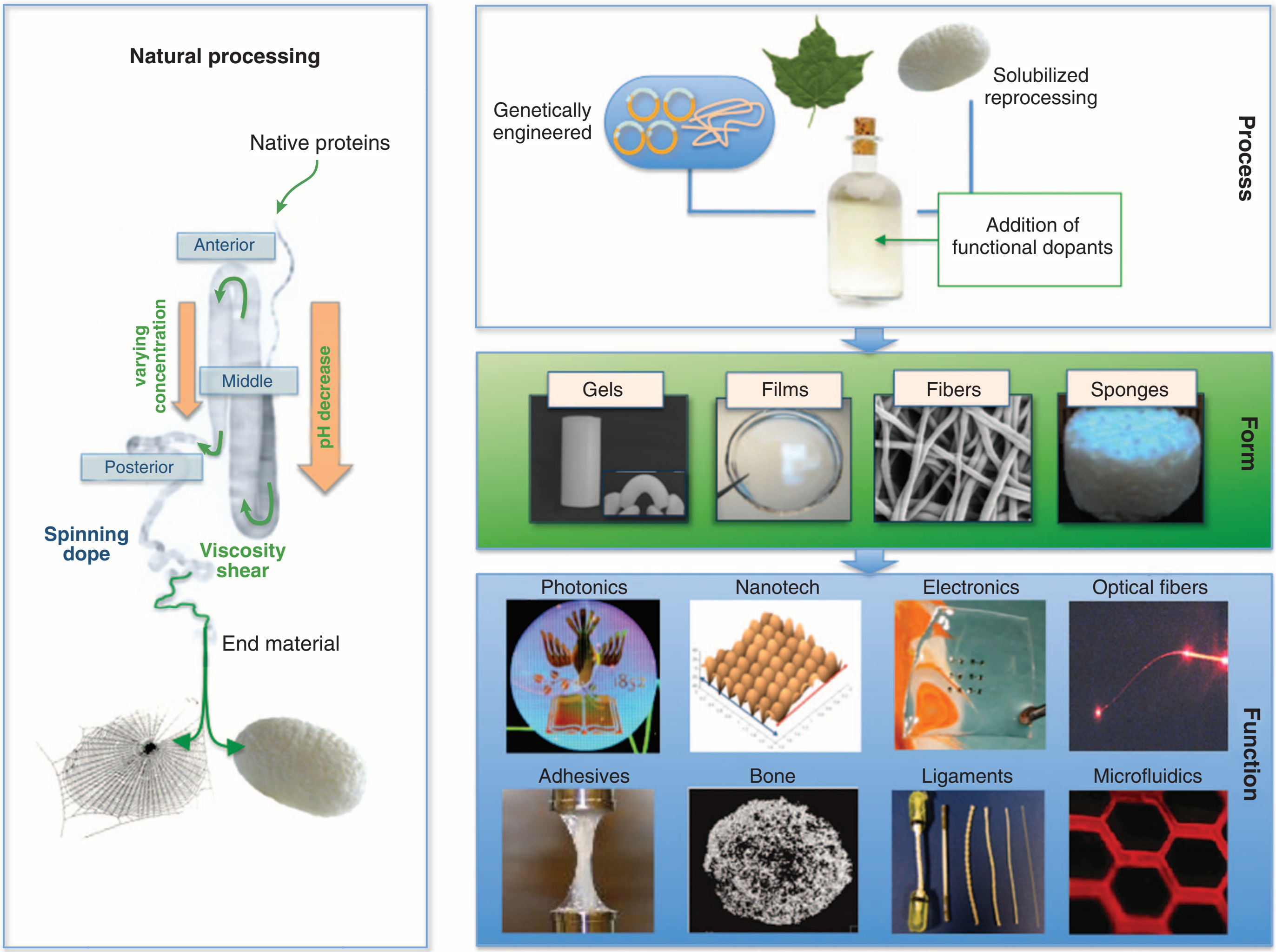

Fig. 3. Generating new materials from silks. Native silk processing on the left illustrates the transition from synthesis, storage, and spinning related to protein concentration, pH, salts, and physical phenomena. On the right, analogous processes with source materials from reconstituted native silk proteins or genetically engineered silks lead to new materials and technology platforms with control of mechanical, morphological, and structural features. A range of materials can be generated from silks through processing into hydrogels, fibers, sponges, films, and other forms. The properties of these systems can be modified (e.g., mechanical, degradation profile, and optical clarity) depending on the processing modes used and then generated into functional devices and technology platforms.

new generation of silks with controllable degradation rates based on processing, biomaterial scaffolds, and related systems for a range of medical needs is anticipated. In the next few years, silk sutures, drug delivery systems, and fiber-based tissue products that exploit the mechanical properties of silks can be envisioned for ligament, bone, and other tissue repairs. Follow-on applications for silks could include degradable and flexible electronic displays for improved physiological recording and function as well as environmentally compatible systems, and implantable optical systems for diagnosis and treatment (*30–32*). These systems would offer a new generation of devices with sensitivity and function unattainable with current materials. These silk-based medical devices would exploit controlled degradation lifetime, optical clarity, conformal contact with underlying substrates, and biocompatibility, all yielding novel functional materials from one system. Progress in these areas should also prompt polymer chemists to pursue synthetic mimics of silk as additional options to exploit the functional features and green chemistry and processing.

References and Notes

1. F. Vollrath, D. P. Knight, *Nature* **410**, 541 (2001).
2. H.-J. Jin, D. L. Kaplan, *Nature* **424**, 1057 (2003).
3. F. Vollrath, B. Madsen, Z. Shao, *Proc. Biol. Sci.* **268**, 2339 (2001).
4. J. M. Gosline, P. A. Guerette, C. S. Ortlepp, K. N. Savage, *J. Exp. Biol.* **202**, 3295 (1999).
5. Z. Shao, F. Vollrath, *Nature* **418**, 741 (2002).
6. G. R. Plaza *et al.*, *Macromolecules* **42**, 9877 (2009).
7. D. Porter, F. Vollrath, *Adv. Mater.* **21**, 487 (2009).
8. C. Holland, A. E. Terry, D. Porter, F. Vollrath, *Nat. Mater.* **5**, 870 (2006).
9. M. Xu, R. V. Lewis, *Proc. Natl. Acad. Sci. U.S.A.* **87**, 7120 (1990).
10. N. A. Ayoub *et al.*, *PLoS ONE* **2**, e514 (2007).
11. C. Vendrely, T. Scheibel, *Macromol. Biosci.* **7**, 401 (2007).
12. A. Rising, G. Hjälm, W. Engström, J. Johansson, *Biomacromolecules* **7**, 3120 (2006).
13. C. Wong *et al.*, *Appl. Phys. A* **82**, 223 (2006).
14. F. Hagn *et al.*, *Nature* **465**, 239 (2010).
15. G. Askarieh *et al.*, *Nature* **465**, 236 (2010).
16. M. B. Hinman, R. V. Lewis, *J. Biol. Chem.* **267**, 19320 (2001).
17. P. Calvert, *Nature* **393**, 309 (1998).
18. J. Cappello *et al.*, *Biotechnol. Prog.* **6**, 198 (1990).
19. J. T. Prince, K. P. McGrath, C. M. DiGirolamo, D. L. Kaplan, *Biochemistry* **34**, 10879 (1995).
20. S. R. Fahnestock, S. L. Irwin, *Appl. Microbiol. Biotechnol.* **47**, 23 (1997).
21. J. Scheller, K.-H. Gührs, F. Grosse, U. Conrad, *Nat. Biotechnol.* **19**, 573 (2001).
22. A. Lazaris *et al.*, *Science* **295**, 472 (2002).
23. C. Y. Hayashi, R. V. Lewis, *Science* **287**, 1477 (2000).
24. C. Z. Zhou *et al.*, *Nucleic Acids Res.* **28**, 2413 (2000).
25. M. Iizuka *et al.*, *FEBS J.* **276**, 5806 (2009).
26. Z. H. Zhu, K. Ohgo, T. Asakura, *eXPRESS Polymer Lett.* **2**, 885 (2008).
27. H.-J. Jin *et al.*, *Adv. Funct. Mater.* **15**, 1241 (2005).
28. S. M. Lee *et al.*, *Science* **324**, 488 (2009).
29. G. H. Altman *et al.*, *Biomaterials* **24**, 401 (2003).
30. F. G. Omenetto, D. L. Kaplan, *Nat. Photonics* **2**, 641 (2008).
31. D.-H. Kim *et al.*, *Nat. Mater.* **9**, 511 (2010).
32. D.-H. Kim *et al.*, *Appl. Phys. Lett.* **95**, 133701 (2009).

33. We thank the NIH, NSF, and Air Force Office of Science Research for support of the research on silk.

10.1126/science.1188936

Dopaminergic Network Differences in Human Impulsivity

Joshua W. Buckholtz,[1,2]*† Michael T. Treadway,[1]† Ronald L. Cowan,[3,4] Neil D. Woodward,[3,4] Rui Li,[5] M. Sib Ansari,[5] Ronald M. Baldwin,[5] Ashley N. Schwartzman,[1] Evan S. Shelby,[1] Clarence E. Smith,[3] Robert M. Kessler,[5] David H. Zald[1,3]

Individuals vary widely in their capacity to deliberate on the potential consequences of their choices before they act. Highly impulsive people frequently make rash, destructive decisions, and trait differences in impulsivity strongly predict risk for externalizing psychiatric disorders (*1*–*3*).

Dopamine (DA) has been theorized to play a key role in impulsivity (*4*, *5*), but the precise systems-level mechanisms linking variation in DA signaling to trait differences in impulsivity remain unclear, particularly in humans. Extrapolating from preclinical and human findings of impulsivity-linked alterations in DA functioning, we have developed a neurobiological model of individual differences in human impulsivity. According to this model, highly impulsive individuals are characterized by diminished midbrain autoreceptor availability, which leads to enhanced DA cell firing and potentiated DA release in terminal fields following exposure to novel, salient, or rewarding stimuli.

To test this model, we scanned 32 physically and psychiatrically healthy volunteers with positron emission tomography and [^{18}F]fallypride, a D2/D3-selective ligand that labels striatal and extrastriatal receptors, at placebo and after oral administration of 0.43 mg/kg d-amphetamine (AMPH) (*6*). Each participant completed the Barratt Impulsiveness Scale (BIS-11) (*3*). For each participant, we calculated voxelwise statistical parametric maps (SPMs) of D2/D3 receptor availability (binding potential, BP_{ND}) and AMPH-induced DA release (percent change in [^{18}F]fallypride binding from placebo; fig. S1) and correlated these SPMs with participants' BIS-11 total scores (*6*).

Trait impulsivity was inversely correlated with D2/D3 autoreceptor availability in the substantia nigra/ventral tegmental area (SN/VTA; Fig. 1A) and positively correlated with the magnitude of AMPH-induced DA release in the striatum (Fig. 1A). Consistent with an inhibitory influence of midbrain autoreceptors on DA release in terminal fields (*7*), SN/VTA D2/D3 BP_{ND} was inversely correlated with striatal DA release after AMPH administration (r = –0.42 and –0.35 for left and right striatum, respectively, each P < 0.05). We used path modeling (mediation analysis) to test our mechanistic hypothesis that lower SN/VTA autoreceptor availability leads to impulsivity by enhancing stimulated DA release in the striatum. This analysis confirmed that the ability of SN/VTA D2/D3 BP_{ND} to predict impulsiveness is at least in part mediated through the impact of SN/VTA autoreceptor availability on AMPH-induced striatal DA release (Fig. 1B).

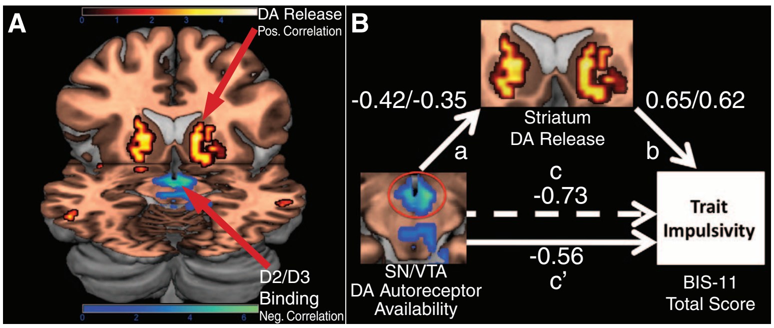

Fig. 1. (**A**) Rendering of two separate SPMs depicting negative correlations between BIS-11 scores and D2/D3 BP_{ND} (cool colors) and positive correlations between BIS-11 scores and AMPH-induced DA release (warm colors) ($P_{corrected}$ < 0.05; image thresholded at t > 3). For D2/D3 BP_{ND}, inverse associations emerged in the DA midbrain [anteriorly in the VTA, centered at 6, –3, –11 (x, y, z; Montreal Neurological Institute space)]. Peak coordinates for the striatal AMPH-induced DA release correlations are –16, 15, 5 (left) and 20, 23, –3 (right); cluster sizes are 167 voxels (left) and 216 voxels (right). Color bars represent z-statistic values. SPMs rendered on a T1-weighted magnetic resonance image template brain, with cuts at z = –11 and y = 16. (**B**) Path analysis demonstrating that the influence of midbrain D2/D3 availability on trait impulsivity is mediated through an impact on striatal AMPH-induced DA release. Path a shows coefficients for the effect of midbrain D2/D3 BP_{ND} (cluster outlined with red circle) on right and left striatal DA release. Path b shows the coefficients for the effect of striatal DA release on trait impulsivity. Paths c and c′ show coefficients for the total (dashed line) and direct (solid line) effects of midbrain D2/D3 BP_{ND} on trait impulsivity. All coefficients standardized. Sobel test for mediation: Z = –1.94, P = 0.05.

To explore the relevance of enhanced striatal release to risk for substance abuse, we examined the relationship between AMPH-induced striatal DA release and subjective responses to AMPH. Increased striatal DA release predicted stronger subjective desire for more drug after AMPH treatment (drug "wanting" ratings from the drug effects questionnaire; r = 0.48 and 0.47 for left and right striatum, respectively, each P < 0.01). Given that heightened subjective "wanting" responses to initial stimulant exposure is a risk factor for future drug dependence (*8*) and that BIS-11 scores predict drug craving in substance-dependent individuals (*9*), the present data suggest a neurobiological link between human impulsiveness and drug abuse vulnerability.

These results show that individual differences in midbrain autoreceptor availability are associated with the expression of impulsivity in humans, an effect that appears to be mediated, in part, through diminished inhibitory autoreceptor control over stimulated striatal DA release. Our findings suggest that dysregulation within ascending dopaminergic projection pathways subserving reward and motivation may produce deficits in impulse control, a critical feature of the psychopathological architecture underpinning substance abuse. Further, they provide a specific, plausible mechanism that links individual variability in DA network functioning to differences in human impulsivity.

References and Notes

1. L. Malloy-Diniz, D. Fuentes, W. B. Leite, H. Correa, A. Bechara, *J. Int. Neuropsychol. Soc.* **13**, 693 (2007).
2. A. Verdejo-Garcia, A. J. Lawrence, L. Clark, *Neurosci. Biobehav. Rev.* **32**, 777 (2008).
3. E. S. Barratt, M. S. Stanford, L. Dowdy, M. J. Liebman, T. A. Kent, *Psychiatry Res.* **86**, 163 (1999).
4. R. Cools, R. A. Barker, B. J. Sahakian, T. W. Robbins, *Neuropsychologia* **41**, 1431 (2003).
5. J. W. Dalley *et al.*, *Science* **315**, 1267 (2007).
6. Materials and methods are available as supporting material on *Science* Online.
7. M. Santiago, B. H. Westerink, *Eur. J. Pharmacol.* **204**, 79 (1991).
8. N. M. Lambert, M. McLeod, S. Schenk, *Addiction* **101**, 713 (2006).
9. M. L. Zilberman, H. Tavares, N. el-Guebaly, *BMC Psychiatry* **3**, 1 (2003).
10. This research was funded by the National Institute on Drug Abuse (R01DA019670-04).

Supporting Online Material

www.sciencemag.org/cgi/content/full/329/5991/532/DC1
Materials and Methods
SOM Text
Fig. S1
References

9 December 2009; accepted 23 April 2010
10.1126/science.1185778

[1]Department of Psychology, Vanderbilt University, Nashville, TN 37240, USA. [2]Neuroscience Graduate Program, Vanderbilt Brain Institute, Vanderbilt University, Nashville, TN 37240, USA. [3]Department of Psychiatry, Vanderbilt University, Nashville, TN 37240, USA. [4]Psychiatric Neuroimaging Program, Vanderbilt University, Nashville, TN 37240, USA. [5]Department of Radiology, Vanderbilt University, Nashville, TN 37240, USA.

*To whom correspondence should be addressed. E-mail: joshua.buckholtz@vanderbilt.edu
†These authors contributed equally to this work.

Quantifying *E. coli* Proteome and Transcriptome with Single-Molecule Sensitivity in Single Cells

Yuichi Taniguchi,[1]* Paul J. Choi,[1]* Gene-Wei Li,[1,2]* Huiyi Chen,[1,3]* Mohan Babu,[4] Jeremy Hearn,[1] Andrew Emili,[4,5] X. Sunney Xie[1]†

Protein and messenger RNA (mRNA) copy numbers vary from cell to cell in isogenic bacterial populations. However, these molecules often exist in low copy numbers and are difficult to detect in single cells. We carried out quantitative system-wide analyses of protein and mRNA expression in individual cells with single-molecule sensitivity using a newly constructed yellow fluorescent protein fusion library for *Escherichia coli*. We found that almost all protein number distributions can be described by the gamma distribution with two fitting parameters which, at low expression levels, have clear physical interpretations as the transcription rate and protein burst size. At high expression levels, the distributions are dominated by extrinsic noise. We found that a single cell's protein and mRNA copy numbers for any given gene are uncorrelated.

Gene expression is often stochastic, because gene regulation takes place at a single DNA locus within a cell. Such stochasticity is manifested in fluctuations of mRNA and protein copy numbers within a cell lineage over time and in variations of mRNA and protein copy numbers among a population of genetically identical cells at a particular time (*1*–*4*). Because both manifestations of stochasticity are connected, measurement of the latter allows the deduction of the gene expression dynamics in a cell (*5*). We aim to characterize such mRNA and protein distributions in single bacteria cells at a system-wide level.

Single-cell mRNA profiling has been carried out with cDNA microarray (*6*) and mRNA-sequencing (mRNA-seq) (*7*); nevertheless, these studies did not have single-molecule sensitivity and are not suitable for bacteria, which express mRNA at low copy numbers (*8*). A fluorescent protein reporter library of *Saccharomyces cerevisiae* (*9*) has proven to be extremely useful in protein profiling (*10*, *11*). However, the lack of sensitivity in existing flow cytometry or fluorescence microscopy techniques prevented the quantification of one-third of the labeled proteins because of their low copy numbers. In recent years, single-molecule fluorescence microscopy has been used to count mRNA (*12*–*16*) or protein (*8*, *17*) molecules in individual cells, especially in bacteria. Yet these methods have only been applied to a limited number of specific genes. Here we report single-cell global profiling of both mRNA and proteins with single-molecule sensitivity using a yellow fluorescent protein (YFP) fusion library for the model organism *Escherichia coli*.

[1]Department of Chemistry and Chemical Biology, Harvard University, Cambridge, MA 02138, USA. [2]Department of Physics, Harvard University, Cambridge, MA 02138, USA. [3]Department of Molecular and Cellular Biology, Harvard University, Cambridge, MA 02138, USA. [4]Banting and Best Department of Medical Research, Terrence Donnelly Centre for Cellular and Biomolecular Research, University of Toronto, Toronto M5S 3E1, Canada. [5]Department of Molecular Genetics, University of Toronto, Toronto M5S 1A8, Canada.

*These authors contributed equally to this work.
†To whom correspondence should be addressed. E-mail: xie@chemistry.harvard.edu

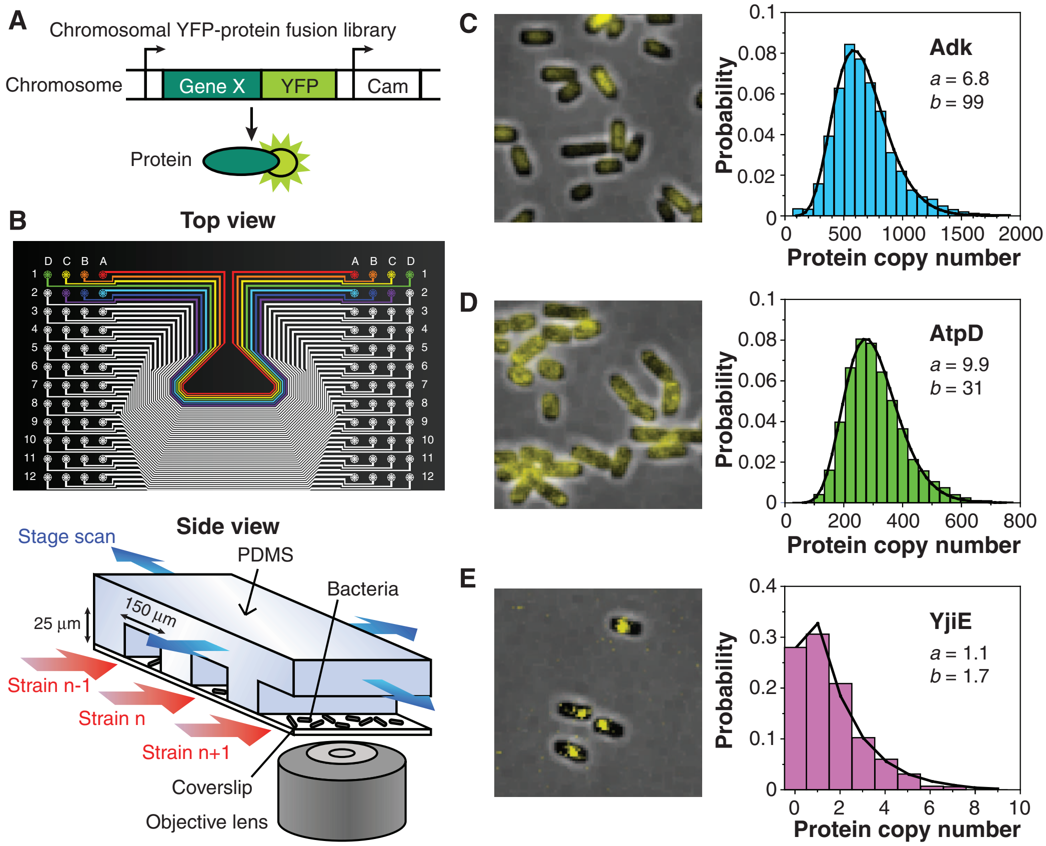

Fig. 1. Quantitative imaging of a YFP-fusion library. (**A**) Each library strain has a YFP translationally fused to the C terminus of a protein in its native chromosomal position. (**B**) A poly(dimethylsiloxane) (PDMS) microfluidic chip is used for imaging 96 library strains. *E. coli* cells of each strain are injected into separate lanes and immobilized on a polylysine-coated coverslip for automated fluorescence imaging with single-molecule sensitivity. (**C** to **E**) Representative fluorescence images overlaid on phase-contrast images of three library strains, with respective single-cell–protein level histograms that are fit to gamma distributions with parameters *a* and *b*. Protein levels are determined by deconvolution (*18*). The protein copy number per average cell volume, or the concentration, was determined as described in the main text and the SOM (*18*). (C) The cytoplasmic protein Adk uniformly distributed intracellularly. (D) The membrane protein AtpD distributed on the cell periphery. (E) The predicted DNA-binding protein YjiE with clear intercellular localization. Single YjiE-YFPs can be visualized because they are localized. Note that, unlike (C) and (D), the gamma distribution asymmetrically peaks near zero if *a* is close to or less than unity.

Single-molecule imaging of a YFP reporter library. We created a chromosomal YFP fusion library (Fig. 1A), in which each strain has a particular gene tagged with the YFP coding sequence. YFP can be detected with single-molecule sensitivity in live bacterial cells (*8*, *18*). We converted the C-terminal tags of an existing chromosomally affinity-tagged *E. coli* library (*19*, *20*) to *yfp* translational fusions using λ-RED recombination (*21*). Out of the 1400 strains attempted, 1018 strains were confirmed by sequencing and showed no significant growth defects. The list of strains is given in table S1 (*18*).

To facilitate high-throughput analyses of the YFP library strains, we implemented an automated imaging platform based on a microfluidic device (Fig. 1B) (*22*) that holds 96 independent library strains attached to a polylysine-coated coverslip. Each device was imaged with a single-molecule fluorescence microscope at a rate of ~4000 cells in 25 s per strain (Fig. 1C). Single-molecule sensitivity was confirmed by abrupt photobleaching of membrane-bound YFPs expressed at a low level (fig. S14) (*8*, *18*, *23*). Automated im-

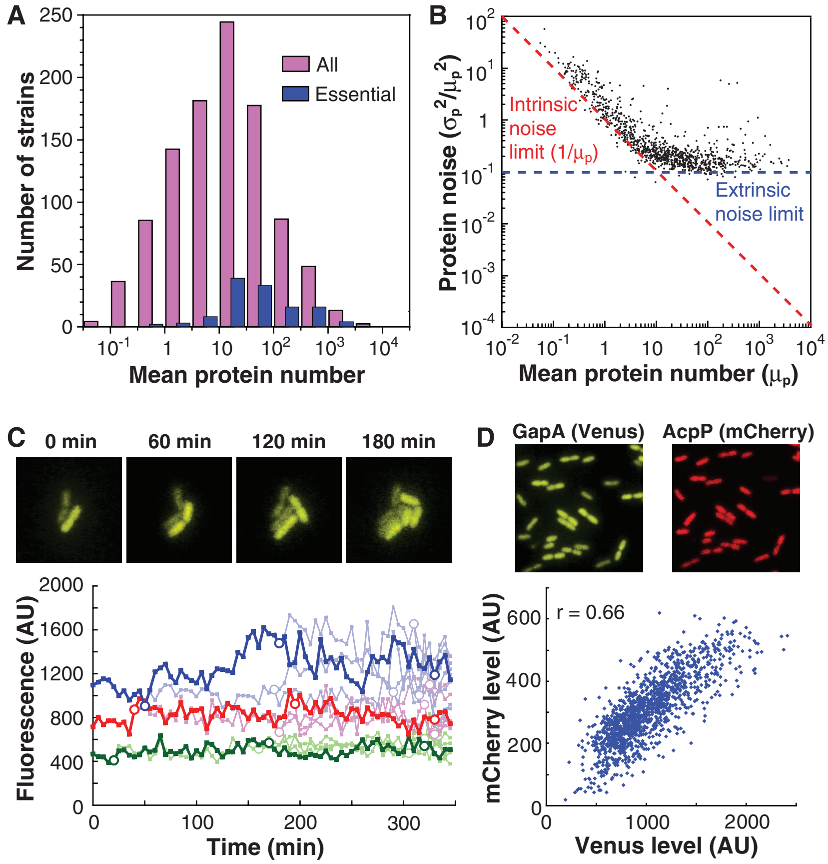

Fig. 2. Profiling of protein abundance and noise. (**A**) Average copy numbers of essential proteins (blue) and all proteins (pink) for 1018 library strains. Almost all essential proteins are expressed at more than an average of 10 copies per cell, although some nonessential proteins have lower abundances. (**B**) Protein expression noise (σ_p^2/μ_p^2) versus the mean copy number per cell (μ_p). When $\mu_p < 10$, protein expression noise is close to the intrinsic noise limit, which is inversely proportional to the mean (red dashed line). When $\mu_p > 10$, noise becomes independent of the mean and is above a plateau of ~0.1 (blue dashed lines), which is the extrinsic noise limit. (**C**) Real-time observation of the slow fluctuation of protein levels, at a time scale longer than a cell cycle, originating from extrinsic noise. Each time trace of fluorescence is normalized by cell size and represents a cell lineage of a strain expressing AcpP-YFP. The dark line follows a single lineage; the rest of the descendents have a lighter colored line. Each circle represents a cell division event. The variation among different cells arises primarily from slowly varying extrinsic noise, because the fluctuations within one cell over a cell cycle are comparatively small. (**D**) Two-color measurements of correlations of two different proteins in the same cell. Two highly expressed proteins, GapA and AcpP, are respectively labeled with Venus (YFP) and mCherry (RFP) in the same *E. coli* strain. The protein levels are correlated, with a correlation coefficient of 0.66, which supports the hypothesis that the dependence on global extrinsic factors like ribosomes, rather than gene-specific factors, dominates the extrinsic noise at high expression levels [see (*18*)].

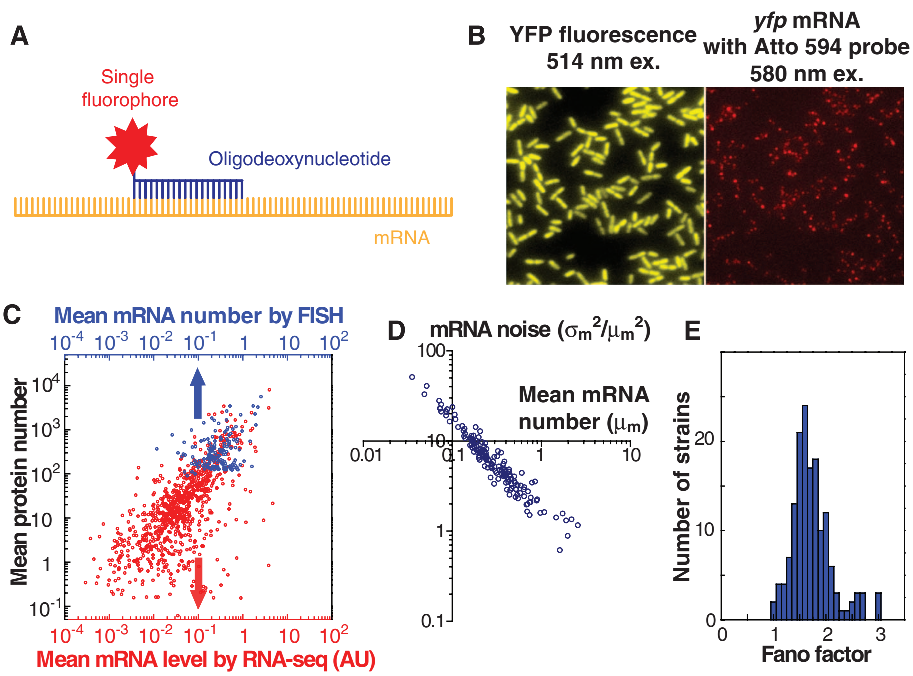

Fig. 3. mRNA profiling of the YFP-fusion library with single-molecule sensitivity in single cells. (**A**) The mRNA of a tagged gene can be detected by FISH against the *yfp* mRNA sequence by using a DNA oligomer probe that is labeled with a single Atto594 fluorophore. (**B**) (Left) Protein and (right) mRNA of the same gene are detected simultaneously in the same fixed cells. (**C**) Mean mRNA number, measured by RNA-seq (red) and by FISH (blue), and mean protein number are correlated. The respective Pearson correlation coefficients (*r*) are 0.54 and 0.77. Each dot is the average of a gene. The FISH data were taken for genes that express >100 copies of proteins per cell, whereas the RNA-seq data include all expressed mRNAs, which are not fused to the *yfp* tag. (**D**) mRNA noise (σ_m^2/μ_m^2) scales inversely with mRNA mean number (μ_m) and is higher than expected for Poisson distributions. (**E**) mRNA Fano factors for 137 highly expressed genes. The mRNA Fano factors (σ_m^2/μ_m) of the measured strains have similar values centered around 1.6, which indicate non-Poissonian mRNA production or degradation.

age analysis was performed to determine the distribution of single-cell protein abundance normalized by cell size (Fig. 1D) (*18*). Normalization by cell size is necessary to account for cell size and gene copy number variation due to the cell cycle. We removed the contribution of cellular autofluorescence by deconvolution (fig. S14) (*18*). The absolute protein level was obtained by calibration with single-molecule fluorescence intensities (fig. S1) (*18*) to determine the protein concentration (copy numbers per average cell volume). Independent reporter assays, based on the Miller assay, mass spectrometry, and Western blotting, confirmed that the resulting fluorescence accurately reports on native protein abundance (*18*) (figs. S4, S21, and S23).

The fluorescence images show the intracellular localization of protein (Fig. 1, C to E). Most cytoplasmic proteins were uniformly distributed intracellularly (Fig. 1C), whereas many membrane-bound or periplasmic proteins showed localization along the outer contours of the cell (Fig. 1D and table S3). Other proteins, including some DNA-bound proteins and low-copy membrane proteins, showed punctate localization (Fig. 1E).

Average protein abundances span five orders of magnitude, ranging from 10^{-1} to 10^4 molecules per cell (Fig. 2A). The average protein abundances of essential genes are higher than those for all genes. Of the 121 essential proteins in the library (*24*), 108 express at 10 or more molecules per cell (Fig. 2A), whereas about half of all the measured proteins are present at fewer than 10 molecules per cell (*18*). Of the low-expression genes, 60% have been annotated to date (*18*), and at least 25% were found to have a genetic interaction in a recent double-knockout study (*25*). The prevalence of proteins with very low copy number suggests that single-molecule experiments are necessary for bacteriology.

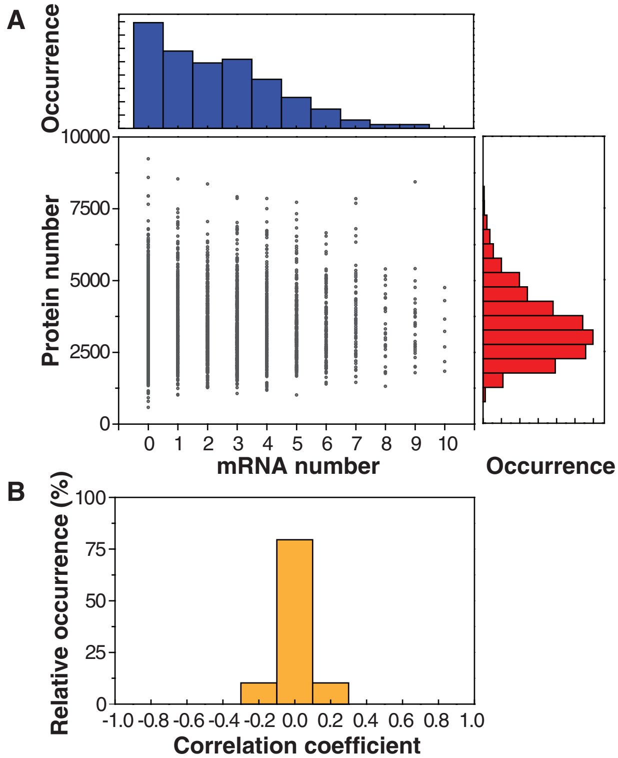

Fig. 4. No correlation between mRNA and protein levels in a single cell at a particular time. (**A**) (Top) mRNA and (right) protein levels. Protein versus mRNA copy number plot for the TufA-YFP strain, in which TufA is tagged with YFP. Each point represents a single cell of the strain. The correlation coefficient is $r = 0.01 \pm 0.03$ (mean ± SD, $n = 5447$). (**B**) Correlation coefficients from 129 strains with highly expressed labeled genes whose sampling error for the correlation coefficient is <0.1. The histogram indicates that the lack of correlation between mRNA and protein levels in a single cell is a general phenomenon.

Analysis of protein distributions. To obtain intrinsic properties of gene expression dynamics, we analyzed the protein expression distributions of different genes. We consider the kinetic scheme

$$\begin{array}{ccccc} \text{DNA} & \xrightarrow{k_1} & \text{mRNA} & \xrightarrow{k_2} & \text{Protein} \\ & & \gamma_1 \downarrow & & \gamma_2 \downarrow \\ & & \varnothing & & \varnothing \end{array} \qquad (1)$$

Here, k_1 and k_2 are the transcription and translation rates, respectively. γ_1 is the mRNA degradation rate, and γ_2 is the protein degradation rate. For stable proteins, including fluorescent protein fusions, γ_2 is dominated by the rate of dilution due to cell division and is insensitive to protein lifetime, which could be different for the fusion and native protein. The number of mRNAs produced per cell cycle is given by $a = k_1/\gamma_2$,

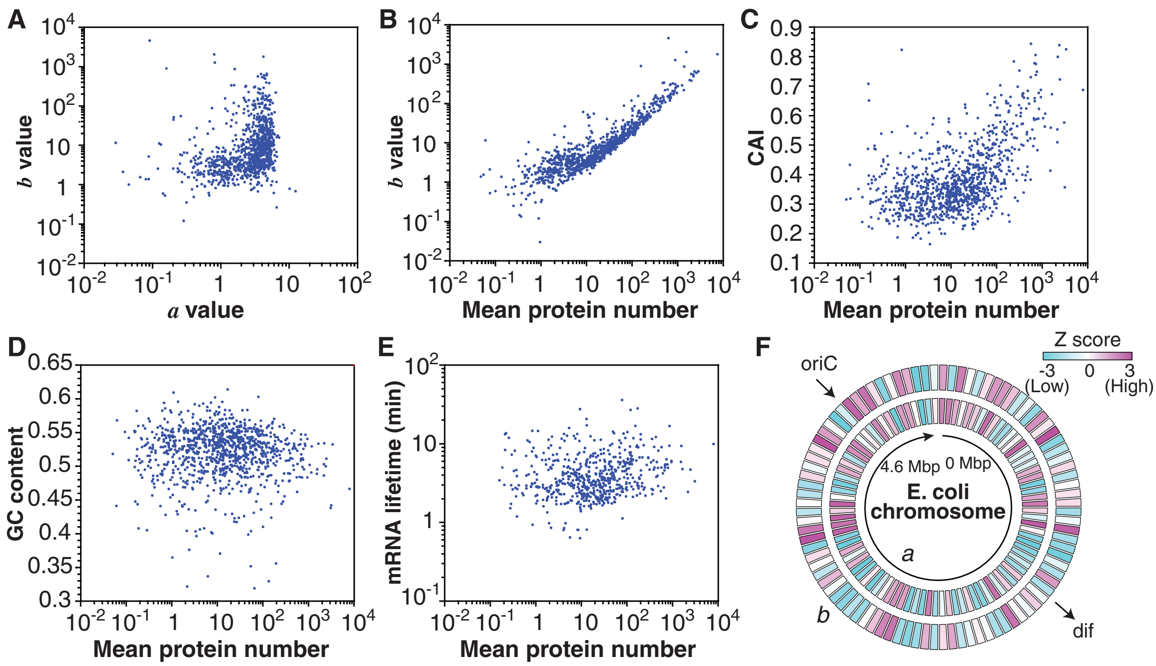

Fig. 5. Correlation between expression and gene characteristics. (**A**) Correlation plots of a and b ($r = 0.01$) and (**B**) mean protein expression versus b ($r = 0.72$). a and b values are calculated as $a = \mu_p^2/\sigma_p^2$ and $b = \sigma_p^2/\mu_p$, respectively, using the mean, μ_p, and standard deviation, σ_p, of the protein number histograms. Correlation plots of (**C**) mean protein expression versus CAI ($r = 0.40$), (**D**) GC content ($r = -0.06$), and (**E**) mRNA lifetime ($r = 0.08$). (**F**) Chromosomal dependence of a and b values. Z scores of more than 3 (indicated by red) represent a significantly larger value compared with the whole-genome distribution with >99.9% confidence; Z scores less than −3 (indicated by blue) represent a significantly smaller value. oriC is the origin of replication, and dif is the resolvase locus.

Table 1. Trends in expression levels and protein localization. Table of *Z* scores of subsets of gene classes characterized by protein and RNA mean, RNA lifetime, *a*, *b*, ratio of fluorescence detected on the edge compared with that on the inside of the cell (*E/I*), and the degree of punctate protein localization (*DP*). Leading strand corresponds to transcription in the same direction as the replication fork. PPI indicates protein-protein interactions. *Z* scores of more than 3 (indicated by red) represent a significantly larger value compared with the whole-genome distribution with >99.9% confidence; *Z* scores less than −3 (indicated by blue) represent a significantly smaller value.

		Protein					RNA	
Category	***n***	**Mean**	***a***	***b***	***E/I***	***DP***	**Mean**	**Lifetime**
All	1018	0.00	0.00	0.00	0.00	0.00	0.00	0.00
Essential gene	121	7.54	8.70	5.34	-2.19	-3.16	5.61	1.38
Nonessential gene	894	-2.74	-3.16	-2.02	0.74	1.30	-1.99	-0.32
Enzyme	410	3.98	4.28	1.85	-5.45	-3.04	3.30	3.15
Translation	17	4.04	3.36	3.30	-0.86	-3.52	3.30	-2.44
Turnover, degradation	13	3.05	3.60	2.08	-0.99	-1.76	2.37	2.14
Transcription factor	98	0.61	1.27	0.71	-2.95	4.29	-0.53	-2.53
Transporter	88	-0.84	0.45	-1.44	7.78	0.96	2.28	3.29
Lagging strand	425	-1.42	-1.95	-0.82	0.74	-0.07	-4.42	-3.63
Leading strand	593	1.12	1.62	0.61	-0.64	0.02	3.96	3.17
Gene length < 500 bp	193	4.06	1.09	3.34	-1.06	-2.98	2.67	-1.65
Gene length >= 500 bp	825	-1.92	-0.55	-1.72	0.57	1.45	-1.26	0.73
Known PPI	603	3.73	3.75	1.37	-3.69	-3.77	1.90	0.58
No known PPI	415	-4.68	-4.65	-1.73	4.28	4.43	-2.25	-0.61

and the protein molecules produced per mRNA is given by $b = k_2/\gamma_1$. It was shown theoretically (*5*, *26*) that, under the steady-state condition of Poissonian production of mRNA and an exponentially distributed protein burst size, as previously observed (*8*, *17*), Eq. 1 results in a gamma distribution of protein copy numbers, *x*, which is normalized by the average cell volume.

$$p(x) = \frac{x^{a-1}e^{-x/b}}{\Gamma(a)b^a} \qquad (2)$$

Here, Γ is a gamma function. The gamma distribution has the property that *a* is equal to the inverse of noise (σ_p^2/μ_p^2) and *b* is equal to the Fano factor (σ_p^2/μ_p), where σ_p^2 and μ_p are the variance and mean of the protein number distributions, respectively. Specific cases have provided experimental support for gamma distribution, but it has not been verified in a system-wide manner (*17*).

The distributions for 1009 out of the 1018 strains can be well fit by the gamma distribution, Eq. 2 (fig. S20) (*18*). Consistent with the gamma distribution, the observed distributions are skewed with the peak at zero for low-abundance proteins and have nonzero peaks for high-abundance proteins (Fig. 1, C to E). We note that the bimodal distribution of *lac* permease was observed in *E. coli* under certain inducer concentrations (*23*, *27*). We did not observe clear bimodal distributions among the 1018 strains under our growth conditions, which indicates that bimodal distributions are generally rare.

We note that an alternative mathematical solution to Eq. 1 gives a negative binomial distribution of protein copy numbers (*26*). However, the gamma distribution offers a more robust fit of experimental data at low expression levels, because the negative binomial fits are very sensitive to measurement error (*18*). The two distributions have similar fitting at high expression levels. Other functions, such as log-normal distributions, have been used phenomenologically to fit unimodal distributions (*10*, *18*). However, the gamma distribution fits better than the log-normal distribution for proteins with low expression levels (fig. S20) (*18*) and fits similarly well for proteins with high expression levels. Most important, the gamma distribution allows extraction of dynamic information from easy measurements of the steady-state distribution at low expression levels. The *a* and *b* values and the goodness of fits for the 1018 strains are given in table S6.

Global scaling of intrinsic and extrinsic protein noise. The protein noise ($\eta_p^2 \equiv \sigma_p^2/\mu_p^2$) exhibits two distinct scaling properties (Fig. 2B). Below 10 molecules per cell, η_p^2 is inversely proportional to protein abundance, indicative of intrinsic noise. In contrast, at higher expression levels (>10 molecules per cell), the noise reaches a plateau of ~0.1 and does not decrease further, which suggests that each protein has at least 30% variation in its expression level.

For proteins expressed at low levels, simple Poisson production and degradation of mRNA and protein, commonly termed intrinsic noise, are sufficient to account for the observed scaling of $\sigma_p^2/\mu_p^2 \propto 1/\mu_p$ (Fig. 2B) (*10*, *11*, *28*–*30*). This scaling property has also been observed for highly expressed yeast proteins (*10*, *11*). We verified Poisson kinetics by monitoring real-time protein production in single cells for several genes whose expression levels were low (table S4) (*18*); the result agrees with previous work on the repressed *lac* operon (*8*, *17*). The observed noise is always greater or equal to $1/\mu_p$, which suggests that specific regulatory methods do not decrease noise substantially below this limit.

For abundant proteins, the $1/\mu_p$ scaling no longer applies, and a large noise floor overwhelms the intrinsic noise contribution (Fig. 2B). This means that the interpretation of the two parameters $a = \mu_p^2/\sigma_p^2$ and $b = \sigma_p^2/\mu_p$ as the burst frequency (k_1/γ_2) and burst size (k_2/γ_1) applies well only at low expression levels, whereas the protein distributions at high expression levels are dominated by other factors extrinsic to the above model. We found that the noise floor does not result from cell size effects, nor did it arise from measurement noise (*18*).

We attribute the additional noise to extrinsic noise (*3*), that is, the slow variation of the values of *a* and *b*, which we confirm with real-time observation of protein levels for four randomly selected high-copy library strains. The high-expression noise fluctuates more slowly than the cell cycle (Fig. 2C) (*18*), so that the rate constants in Eq. 1 can be considered to be heterogeneous among cells.

If we assume that static or slowly varying heterogeneities of *a* and *b* exist with distributions *f* (*a*) and *g*(*b*), respectively, the protein distribution is

$$p(x) = \int_0^\infty \int_0^\infty \frac{x^{a-1}e^{-x/b}}{\Gamma(a)b^a} f(a)g(b)dadb \qquad (3)$$

Even if the normalized variances of *f* (*a*) and *g*(*b*), η_a^2 and η_b^2, are 0.1, Eq. 3 can still be approximated as a gamma distribution, which explains the generality of the gamma distribution fit of the data (*18*).

The noise plateau in Fig. 2B can be explained by calculating the expected noise from Eq. 3 (*18*, *26*, *31*)

$$\eta_p^2 = \frac{\langle b\rangle + \langle b\rangle\eta_b^2}{\mu_p} + \eta_a^2 + \eta_a^2\eta_b^2 + \eta_b^2 \qquad (4)$$

The extrinsic noise in the last three terms in Eq. 4 might originate from fluctuations in cellular components—such as metabolites, ribosomes, and polymerases (*30*, *32*)—and dominates the noise of high-copy proteins (μ_p >>1, Eq. 4).

We further demonstrate that the extrinsic noise is global to all high-expression genes by analyzing the correlations between expression levels of 13 pairs of randomly selected genes. Using YFP and red fluorescent protein (RFP) fusions as a pair of reporters (Fig. 2D), we observed statistically significant correlations between the expression levels of all gene pairs,

which confirmed the existence of a global noise factor. The observed correlation is quantitatively predicted by the observed noise floor (*18*).

Single-molecule RNA counting. To examine single-cell mRNA expression, we performed fluorescence in situ hybridization (FISH) with single-molecule sensitivity (*33*) (Fig. 3A), using a single universal Atto594-labeled 20-oligomer nucleotide probe targeting the *yfp* mRNA in our library. Because the same probe is used for all strains, the optimized hybridization efficiency is unbiased for every measured gene (*18*). We confirmed the validity of our transcript measurements with RNA-seq (table S6) (*18*).

We show that the YFP (yellow) and the mRNA (red) of the same gene can be simultaneously detected, and spectrally resolved, within a single fixed cell (Fig. 3B). Because of their low copy numbers, mRNA molecules are sparsely distributed within a cell, independent of YFP locations. By measuring the intensity of each fluorescent spot and counting the number of spots per cell, we determined mRNA copy numbers for individual cells. We used this single-molecule FISH method to quantify mRNA abundance and noise for 137 library strains with high protein expression (>100 proteins per cell).

At the ensemble level, the mean mRNA abundances among these 137 genes range from 0.05 to 5 per cell, and are moderately correlated with the corresponding mean protein expression level at the gene-by-gene basis (correlation coefficient r = 0.77) (Fig. 3C). The lack of complete correlation, as reported previously in other organisms, is often attributed to differences in posttranscriptional regulation. Here, with the ability to determine the absolute number of molecules per cell, we determined the ratio between the mean protein abundance and the mean mRNA abundance to range from 10^2 to 10^4.

At the single-cell level, the mRNA copy number distributions were broader than the Poisson distributions expected by the random generation and degradation of transcripts with constant rates (*18*). The mRNA noise scales in inverse proportion to the mean mRNA abundance (Fig. 3D), but mRNA Fano factor values (σ_m^2/μ_m), are close to ~1.6 (Fig. 3E), rather than unity, as expected for the Poissonian case. We excluded gene dosage effects by gating with the cell size to select the cells that have not yet gone through chromosome replication (*18*). The non-Poisson mRNA distributions indicate that the rate constant for mRNA generation or degradation fluctuates on a time scale similar to or longer than the typical mRNA degradation time, which has an average of ~5 to 10 min for our growth condition (*18*).

Simultaneous RNA and protein measurements in single cells. We now examine the extent to which the mRNA copy numbers and the protein levels are correlated in the same cells. We quantified single-cell mRNA and protein levels simultaneously (Fig. 3B). Figure 4A shows a two-dimensional scatter plot, in which each cell is plotted as a dot with its mRNA and protein levels on the x and y axes, respectively, for the translation elongation factor EF-Tu in the TufA-YFP strain. mRNA and protein copy numbers in a single cell are not correlated (r = 0.01 ± 0.03, SEM, n = 5447). In fact, among many different highly expressed strains surveyed, the correlation coefficients are all centered on zero (Fig. 4B), which indicates a general lack of mRNA-protein correlation of the same gene within a single cell.

The lack of mRNA-protein correlation can be explained by the difference in mRNA and protein lifetime. In *E. coli*, mRNA is typically degraded within minutes (table S6) (*18*), whereas most proteins, including fluorescent proteins, have a lifetime longer than the cell cycle (*18*, *34*). As a result, the mRNA copy number at any instant only reflects the recent history of transcription activity (a few minutes), whereas the protein level at the same instant represents the long history of accumulated expression (time scale of a cell cycle). However, additional factors such as extrinsic translational noise are necessary to explain fully the zero mRNA-protein correlation we observe (*18*). We note that the observed lack of correlation arises because the experiment only measured the copy numbers of protein and mRNA present at the moment of fixation of a single cell. This is not contradictory to the central dogma, which suggests that the mRNA level integrated over a long period of time should correlate with the protein level produced in the same cell, which is consistent with the notable correlation between the mRNA and protein levels averaged for many cells (Fig. 3C, *11*). However, our result offers a cautionary note for single-cell transcriptome analysis and argues for the necessity for single-cell proteome analysis.

Correlation of expression properties with biological factors. The correlation between the expression parameters and selected gene characteristics is shown in Fig. 5. Small a values correspond to a narrow range of b values, and large a values correspond to a wide range of b values (Fig. 5A). Highly expressed proteins (mean > 10) had high b values, whereas low-expression proteins had b values of about 1 (Fig. 5B). The protein expression levels had a weak correlation with the codon adaptation index (CAI, r = 0.42), but had little correlation with GC content (r = –0.06) and the mRNA lifetime (r = 0.08). The a and b values showed moderate dependence on the chromosome position (Fig. 5F). The correlation coefficients and Z scores between these two and additional parameters are summarized in table S2.

In addition, we characterized the statistical bias of the expression and localization parameters for functional gene categories, as measured by a Z score in Table 1 and table S3. Some functional categories are strongly correlated with parameters. For example, essential proteins have a strong correlation with high a (Z = 7.5) and high b (Z = 5.3). As expected, membrane transporters showed a high edge/inside ratio (Z = 7.3), and transcriptional repressors indicated high punctate localization (Z = 4.1). Proteins with no known protein-protein interactions have significantly reduced expression (Z = –4.7). We also found that shorter open reading frames may have higher protein expression levels (Z = 4.1). RNA expression tends to be higher for genes transcribed from the leading strand parallel to the movement of the replication fork (Z = 4.0). Thus, expression and localization properties can be significantly correlated with functional properties.

Comparison between *E. coli* and yeast. Protein abundance and noise have been investigated in yeast with flow cytometry for >2500 high-abundance proteins (*10*, *11*). The single-molecule sensitivity in single bacterial cells allowed us to characterize the full range of protein copy numbers in *E. coli*, which has not been realized in yeast. We found that *E. coli* proteins generally had larger noise and Fano factors than yeast proteins, even for those present at similar copy numbers (fig. S6) (*18*). A noise plateau due to extrinsic factors is present for both, but the extrinsic noise is larger in *E. coli*.

Conclusion. We have provided quantitative analyses of both abundance and noise in the proteome and transcriptome on a single-cell level for Gram-negative bacteria *E. coli*. Given that some proteins and most mRNAs of functional genes are present at low copy numbers in a bacterial cell, the single-molecule sensitivity afforded by our measurements is necessary for understanding stochastic gene expression and regulation. We discovered large fluctuations in low-abundance proteins, as well as a common extrinsic noise in high-abundance proteins. Furthermore, we found that, in a single cell, mRNA and protein levels for the same gene are completely uncorrelated. This result highlights the disconnect between proteome and transcriptome analyses of a single cell, as well as the need for single-cell proteome analysis. Taken together, a quantitative and integral account of a single-cell gene expression profile is emerging.

References and Notes

1. C. V. Rao, D. M. Wolf, A. P. Arkin, *Nature* **420**, 231 (2002).
2. J. M. Raser, E. K. O'Shea, *Science* **304**, 1811 (2004).
3. N. Rosenfeld, J. W. Young, U. Alon, P. S. Swain, M. B. Elowitz, *Science* **307**, 1962 (2005).
4. J. M. Pedraza, A. van Oudenaarden, *Science* **307**, 1965 (2005).
5. N. Friedman, L. Cai, X. S. Xie, *Phys. Rev. Lett.* **97**, 168302 (2006).
6. I. Tietjen *et al.*, *Neuron* **38**, 161 (2003).
7. F. Tang *et al.*, *Nat. Methods* **6**, 377 (2009).
8. J. Yu, J. Xiao, X. Ren, K. Lao, X. S. Xie, *Science* **311**, 1600 (2006).
9. W. K. Huh *et al.*, *Nature* **425**, 686 (2003).
10. A. Bar-Even *et al.*, *Nat. Genet.* **38**, 636 (2006).
11. J. R. Newman *et al.*, *Nature* **441**, 840 (2006).
12. J. M. Levsky, S. M. Shenoy, R. C. Pezo, R. H. Singer, *Science* **297**, 836 (2002).
13. A. Raj, C. S. Peskin, D. Tranchina, D. Y. Vargas, S. Tyagi, *PLoS Biol.* **4**, e309 (2006).
14. I. Golding, J. Paulsson, S. M. Zawilski, E. C. Cox, *Cell* **123**, 1025 (2005).
15. H. Maamar, A. Raj, D. Dubnau, *Science* **317**, 526 (2007).

16. D. Zenklusen, D. R. Larson, R. H. Singer, *Nat. Struct. Mol. Biol.* **15**, 1263 (2008).
17. L. Cai, N. Friedman, X. S. Xie, *Nature* **440**, 358 (2006).
18. Methods and discussion are available as supporting material on *Science* Online.
19. G. Butland *et al.*, *Nature* **433**, 531 (2005).
20. P. Hu *et al.*, *PLoS Biol.* **7**, e96 (2009).
21. D. Yu *et al.*, *Proc. Natl. Acad. Sci. U.S.A.* **97**, 5978 (2000).
22. J. C. McDonald *et al.*, *Electrophoresis* **21**, 27 (2000).
23. P. J. Choi, L. Cai, K. Frieda, X. S. Xie, *Science* **322**, 442 (2008).
24. T. Baba *et al.*, *Mol. Syst. Biol.* **2**, 2006.0008 (2006).
25. G. Butland *et al.*, *Nat. Methods* **5**, 789 (2008).
26. J. Paulsson, M. Ehrenberg, *Phys. Rev. Lett.* **84**, 5447 (2000).
27. A. Novick, M. Weiner, *Proc. Natl. Acad. Sci. U.S.A.* **43**, 553 (1957).
28. J. Paulsson, *Nature* **427**, 415 (2004).
29. M. Thattai, A. van Oudenaarden, *Proc. Natl. Acad. Sci. U.S.A.* **98**, 8614 (2001).
30. M. B. Elowitz, A. J. Levine, E. D. Siggia, P. S. Swain, *Science* **297**, 1183 (2002).
31. V. Shahrezaei, P. S. Swain, *Proc. Natl. Acad. Sci. U.S.A.* **105**, 17256 (2008).
32. P. S. Swain, M. B. Elowitz, E. D. Siggia, *Proc. Natl. Acad. Sci. U.S.A.* **99**, 12795 (2002).
33. A. M. Femino, F. S. Fay, K. Fogarty, R. H. Singer, *Science* **280**, 585 (1998).
34. A. L. Koch, H. R. Levy, *J. Biol. Chem.* **217**, 947 (1955).

35. We thank L. Xun, N. K. Lee, D. Court, C. Zong, R. Roy, and J. Agresti for experimental assistance; and E. Rubin, L. Cai, and J. Elf for helpful discussions. This work was supported by the Gates Foundation (X.S.X.), the NIH Pioneer Director's Award (X.S.X.), and the Canadian Institutes of Health Research (MOP-77639) (A.E.). Y.T. acknowledges additional support from the Japan Society for the Promotion of Science, the Uehara Memorial Foundation, and the Marubun Research Promotion Foundation, and P.J.C. from the John and Fannie Hertz Foundation.

Supporting Online Material
www.sciencemag.org/cgi/content/full/329/5991/533/DC1
Materials and Methods
SOM Text
Figs. S1 to S23
Tables S1 to S6
References

16 February 2010; accepted 4 June 2010
10.1126/science.1188308

Tissue-Engineered Lungs for in Vivo Implantation

Thomas H. Petersen,[1,2] Elizabeth A. Calle,[1] Liping Zhao,[3] Eun Jung Lee,[3] Liqiong Gui,[3] MichaSam B. Raredon,[1] Kseniya Gavrilov,[4] Tai Yi,[5] Zhen W. Zhuang,[6] Christopher Breuer,[5] Erica Herzog,[6] Laura E. Niklason[1,3]*

Because adult lung tissue has limited regeneration capacity, lung transplantation is the primary therapy for severely damaged lungs. To explore whether lung tissue can be regenerated in vitro, we treated lungs from adult rats using a procedure that removes cellular components but leaves behind a scaffold of extracellular matrix that retains the hierarchical branching structures of airways and vasculature. We then used a bioreactor to culture pulmonary epithelium and vascular endothelium on the acellular lung matrix. The seeded epithelium displayed remarkable hierarchical organization within the matrix, and the seeded endothelial cells efficiently repopulated the vascular compartment. In vitro, the mechanical characteristics of the engineered lungs were similar to those of native lung tissue, and when implanted into rats in vivo for short time intervals (45 to 120 minutes) the engineered lungs participated in gas exchange. Although representing only an initial step toward the ultimate goal of generating fully functional lungs in vitro, these results suggest that repopulation of lung matrix is a viable strategy for lung regeneration.

Lung diseases account for some 400,000 deaths annually in the United States (*1*). Human lungs do not generally repair or regenerate beyond the microscopic, cellular level. Currently, the only way to replace lung tissue is to perform lung transplantation, which is an expensive procedure that achieves only 10 to 20% survival at 10 years and one that is hampered by a severe shortage of donor organs (*2*). Recently, techniques have been developed to quantitatively decellularize complex organs such as heart, liver, and kidney (*3*–*5*). Acellular matrices can provide attractive scaffolds for repopulation with lung-specific cells for lung engineering because the extracellular matrix template should contain appropriate three-dimensional (3D) architecture and regional-specific cues for cellular adhesion. To be functional in vivo, an engineered lung should (i) contain lung-specific cells, (ii) display the branching geometry of the airways and contain a perfusing microvasculature, (iii) provide barrier function to separate blood from air, and (iv) have mechanical properties that allow ventilation at physiological pressures.

Here, we describe our progress toward the construction of a functional tissue-engineered lung, using rat as a model system. Our approach is summarized in Fig. 1. We first decellularized native lung tissue in order to remove all immunogenic cellular constituents (Fig. 1, A and B). We found that after careful decellularization, the tissue retained its alveolar micro-architecture, its ability to function as a barrier to particulates, and its tissue mechanics. Repopulation of the acellular lung matrix with mixed populations of neonatal lung epithelial cells resulted in regional-specific epithelial seeding in correct anatomic locations. To enhance the survival and differentiation of lung epithelium, we cultured the matrix in a bioreactor designed to mimic certain features of the fetal lung environment, including vascular perfusion and liquid ventilation (Fig. 1, C and D) (*6*). Lastly, we tested the functionality of the engineered lung tissue by implanting it for short time periods in a syngeneic rat model (Fig. 1E).

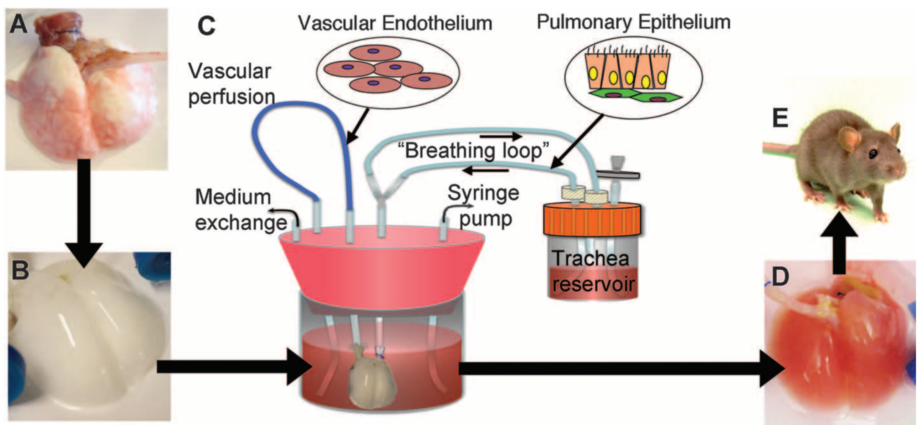

Fig. 1. Schema for lung tissue engineering. (**A**) Native adult rat lung is cannulated in the pulmonary artery and trachea for infusion of decellularization solutions. (**B**) Acellular lung matrix is devoid of cells after 2 to 3 hours of treatment. (**C**) Acellular matrix is mounted inside a biomimetic bioreactor that allows seeding of vascular endothelium into the pulmonary artery and pulmonary epithelium into the trachea. (**D**) After 4 to 8 days of culture, the engineered lung is removed from the bioreactor and is suitable for implantation into (**E**) the syngeneic rat recipient.

[1]Department of Biomedical Engineering, Yale University, New Haven, CT 06520, USA. [2]Department of Biomedical Engineering, Duke University, Durham, NC 27708, USA. [3]Department of Anesthesia, Yale University, New Haven, CT 06520, USA. [4]Department of Cellular and Molecular Physiology, Yale University, New Haven, CT 06520, USA. [5]Department of Surgery, Yale University, New Haven, CT 06520, USA. [6]Department of Internal Medicine, Yale University, New Haven, CT 06520, USA.

*To whom correspondence should be addressed. E-mail: laura.niklason@yale.edu

Preparation of a decellularized lung scaffold. We harvested lung tissue from adult Fischer 344 rats and treated the lungs in the vascular and airway compartments with detergent solutions (Fig. 1 and movie S1). The decellularization solution contains 3-[(3-cholamidopropyl)dimethylammonio]-1-propanesulfonate (CHAPS), a zwitterionic detergent, in a phosphate buffer at 1.0 M salt concentration (*7*). Vascular perfusion pressure was maintained below 20 mmHg, with total time of tissue exposure typically in the range of 2 to 3 hours. Analysis of the decellularized lung matrices by means of high-resolution micro-computed tomography (micro-CT) revealed intact lung architecture and an intact arterial tree and microvasculature (Fig. 2, A to C). The cells and nuclear material were removed with the decellularization process, but the alveolar septal architecture remained undisturbed (Fig. 2, E and F). Fluorometric DNA assay confirmed that approximately 99% of DNA was removed by the decellularization process (Fig. 2G), and immunoblotting for major histocompatibility complex I and II (MHC-I and MHC-II) as well as β-actin confirmed that decellularized lung matrices were depleted of these cellular markers (Fig. 2D). Scanning electron microscopy (SEM) confirmed that alveolar cells, red blood cells, and cellular proteins present in native lung were absent in the decellularized scaffold (Fig. 2, H and I, and fig. S3). Analysis of the matrix by means of transmission electron microscopy (TEM) revealed that the ultrastructure of the alveolar septae and the delicate microvessels surrounding the alveoli remained intact (Fig. 2J and fig. S3). Immunofluorescence and histochemical staining indicated that collagen, elastin, and laminin were preserved in decellularized matrices (figs. S4 and S5). Additionally, quantitative assays showed that extracellular matrix collagen was preserved, whereas elastin was partially depleted by the decellularization process (40% of elastin remains in acellular matrices), and sulfated glycosaminoglycans (GAGs) were >90% removed (Fig. 2G and fig. S4). Hence, the lung decellularization protocol produces an acellular matrix scaffold that retains the gross, microstructural, and ultrastructural properties of native lung, yet removal of antigenic cellular components is essentially complete.

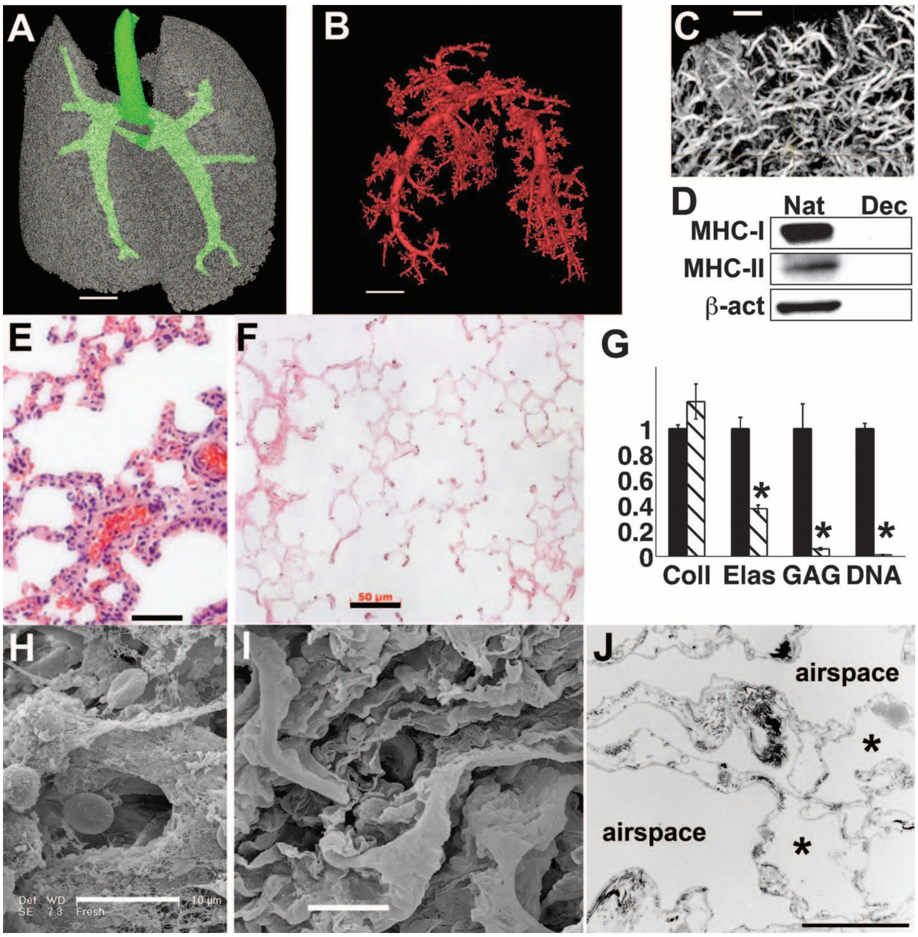

Fig. 2. Characterization of acellular lung matrix. (**A**) 3D micro-CT of the acellular matrix airway compartment. Large airways are in green. (**B**) Micro-CT angiography of vascular compartment, thresholded to visualize only large vessels. In (A) and (B), voxel size is 58 μm; scale bar, 4 mm. (**C**) Micro-CT angiography of smaller vessels in acellular lung. Voxel size, 6.5 μm; scale bar, 500 μm. (**D**) Immunoblot for MHC-1, MHC-II, and β-actin in native (Nat) and decellularized (Dec) lungs, showing removal of cellular proteins. (**E**) Hematoxylin and eosin (H&E) stain of native rat lung. (**F**) H&E stain of acellular lung matrix. Scale bar, 50 μm in (E) and (F). (**G**) Collagen (Coll), elastin (Elas), glycosaminoglycan (GAG), and DNA contents of native lung (black bars) and acellular matrices (hatched bars). Values are mean ± SD per lung ($n \geq 4$ lungs for all measures), scaled to 1 for native, with asterisk indicating $P < 0.05$ for difference between native and acellular matrices. (**H**) SEM of native rat lung. (**I**) SEM of acellular matrix. Scale bar, 10 μm in (H) and (I). (**J**) TEM of acellular lung matrix. Asterisk indicates capillaries in alveolar septa. Scale bar, 5 μm.

Properties of the lung bioreactor. The lung bioreactor contains a main reservoir in which the decellularized lung is mounted, using cannulae that are inserted into the trachea and pulmonary artery (fig. S1A). Culture medium is perfused into the pulmonary artery at physiological pressures (fig. S1B) (*7*). To provide negative-pressure ventilation of the engineered lung, a syringe pump withdraws a defined volume of air from the main bioreactor to create a negative pressure (Fig. 1C and figs. S1C and S2). Lung inflation under negative pressure is accompanied by inhalation of liquid medium from a trachea reservoir via a "breathing loop." For exhalation, the syringe pump returns air to the main reservoir, causing lung exhalation of liquid medium into the trachea reservoir.

To repopulate the decellularized matrix, we injected cells into the vascular or airway compartments, or both, and maintained the matrix in culture for up to 8 days (Fig. 1C). This produced an engineered lung tissue that could then be removed from the bioreactor for further analysis or that could be orthotopically transplanted into a rat recipient (Fig. 1, D and E).

Repopulation of acellular matrix to produce an engineered lung. Seeding of the decellularized matrix with mixed populations of neonatal rat lung epithelial cells (fig. S7) into the airway compartment generally resulted in good adherence of the cells to alveolar structures, as well as to small- and medium-sized airways (Fig. 3A). Microvascular lung endothelial cells, when injected into the pulmonary artery of acellular scaffolds, adhered throughout the scaffold vasculature (Fig. 3B). Seeded pulmonary epithelial cells replicated rapidly and rarely displayed markers of apoptotic cell death (Fig. 3, C and D), despite the difficulty in culturing such cells on standard tissue culture plastic in vitro (*8*). This observation suggests that substrate cues on the acellular lung matrix are important for pulmonary epithelial cell attachment and replication.

In the biomimetic bioreactor, vascular perfusion greatly enhanced endothelial adhesion and survival on the lung matrix (fig. S9, A and B). Negative pressure ventilation had multiple beneficial effects on cultured lung epithelium, including enhanced survival of epithelium in distal alveoli and clearance of epithelial secretions from the airway tree (fig. S9, C to F). Clearance of airway secretions through ventilation indicates that the developing epithelium is in communication with the airway tree and is not growing randomly within the matrix. In addition, ventilation

with air—as opposed to with culture medium—increased the numbers of type I alveolar epithelial cells, as well as the numbers of ciliated columnar epithelial cells (fig. S9, G to J). Engineered lungs also produce pro-surfactant proteins B and C (pro-SPB, pro-SPC), although we could not detect mature SPB (Fig. 3E). Surfactant proteins are critical for reducing alveolar surface tension and enabling lung inflation at physiologically normal pressures.

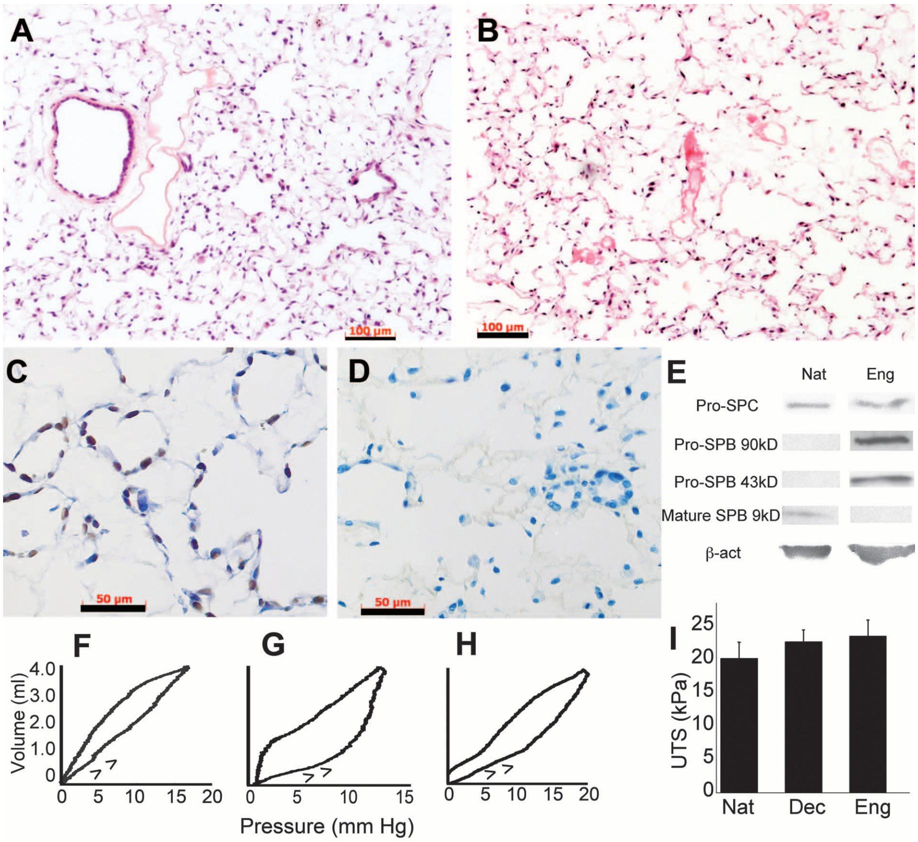

Fig. 3. Repopulation of the matrix with lung epithelial and endothelial cells and mechanical assessment of the engineered lungs. (**A**) H&E stain of mixed neonatal pulmonary epithelium seeded into acellular matrix and cultured for 8 days. (**B**) H&E stain of lung microvascular endothelium seeded into vascular compartment and cultured for 8 days. Scale bars, 100 μm in (A) and (B). (**C**) Proliferating cell nuclear antigen stain of epithelial culture after 8 days; brown nuclei are dividing. (**D**) Terminal deoxynucleotidyl transferase–mediated deoxyuridine triphosphate nick end labeling stain of epithelium after 4 days of culture detects no apoptotic cells (positive cells stain brown; green indicates nuclear counterstain). Scale bars, 50 μm in (C) and (D). (**E**) Immunoblots for pro-SPC indicates similar expression for native (Nat) and engineered (Eng) lung. Engineered lung expresses SPB precursor proteins at 43 and 90 kD, but no mature SPB. β-actin confirms similar protein loading. (**F** to **H**) Quasi-static compliance curves for (F) typical native, (G) acellular, and (H) engineered lungs; arrows indicate inflation arm of loop. (**I**) Mean ultimate tensile strengths (UTS) of native ($n = 4$), acellular ($n = 10$), and engineered ($n = 5$) lungs. Error bars are SD; there were no significant differences between any groups.

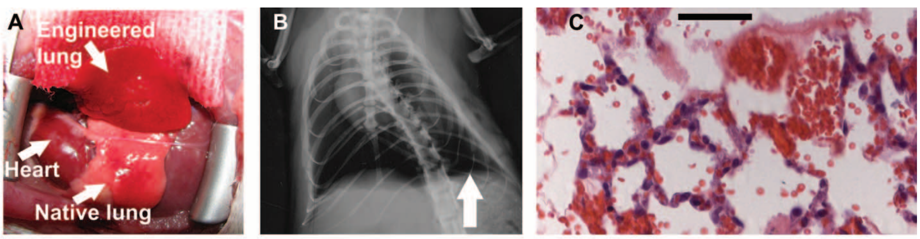

Fig. 4. Implantation of engineered lungs into rats. (**A**) Tissue-engineered left lung was implanted into adult Fischer 344 rat recipient and photographed ~30 min later. (**B**) X-ray image of rat showing the implanted engineered left lung (white arrow) and the right native lung. (**C**) H&E stain of explanted lung. Red blood cells perfusing septa are evident, and some red blood cells are present in airspaces. Scale bar, 50 μm.

We performed compliance testing on the engineered lungs under quasi-static conditions by injecting air into the lungs and monitoring resultant pressure changes. Typical compliance curves for native lung, acellular matrix, and repopulated engineered lungs are shown in Fig. 3, F to H. The compliance values were, respectively, 0.35 ± 0.08 ($n = 10$ measures), 0.09 ± 0.02 ($n = 4$ measures), and 0.14 ± 0.06 ($n = 5$ measures) mL/mmHg (mean ± SD, $P < 0.001$ for difference between native and both decellularized and engineered compliances). Compliance values were measured at initial filling of the lungs (arrowheads in Fig. 3, F to H), and thus lower compliances for decellularized matrix and engineered lung mean that these two tissues have higher "opening pressures," and less functional surfactant, than does native lung. Despite this difference, the overall stress-strain relationships and the ultimate tensile stresses were similar between the three groups (Fig. 3I and fig. S6). Thus, no substantial stiffening or weakening of the extracellular matrix occurs in the repopulated, engineered lungs as compared with native adult lungs.

To evaluate the distribution and phenotype of cells in the engineered lungs, we performed fluorescent immunohistochemical staining (fig. S8). Endothelial cells seeded into the vasculature were extensively distributed and expressed CD-31, as did comparable cells in native rat lung (fig. S8A). TEM analysis revealed the presence of tight junctions within the engineered endothelium, which is consistent with the development of some barrier function (fig. S10). With respect to the seeded lung epithelium, Clara cell secretory protein (CCSP)–positive cells, which in native lung are found in small airways, were found primarily in very small airway structures after 4 days and in larger structures after 8 days in engineered lungs (fig. S8B). Pro-SPC, a marker of type II alveolar epithelium, is normally present at the vertices of alveoli in native lung. In the engineered lungs, pro-SPC expression was diffuse in alveoli and in small airways after 4 days of culture, but at 8 days it showed a more native expression pattern at the vertices of alveoli (fig. S8C). In contrast, aquaporin-5—a specific marker for type I epithelium—was found diffusely throughout native alveoli and in engineered lungs after 4 days but was largely absent after 8 days (fig. S8D). This observation is consistent with previous work on neonatal rat development, which showed that type I cells do not fully differentiate until the post-natal period, when air breathing commences (*9*). Indeed, engineered lungs that were ventilated with air, as opposed to liquid culture medium, displayed more aquaporin-5 expression in alveoli after 8 days of culture (fig. S9, G and H) and also contained sparse ciliated epithelial cells (fig. S9, I and J). Additional cell types noted included mesenchymal cells and the airway epithelial progenitor basal cells (fig. S8, E and F). Hence, the engineered lungs contained many of the important cell types of native lung tissues. In addition, the spatial distribution of the various cell types was regional-specific, and with extended culture

Table 1. Gas exchange in engineered lungs implanted into rats. Shown are blood gas values and oxygen saturations for samples taken from rats implanted with an engineered lung. Values are mean ± SD; $n = 3$ samples for each sample type except for right pulmonary vein, in which $n = 2$ samples. Sat, saturation.

Sample location	pH	P_{O_2} (mmHg)	O_2 Sat (%)	P_{CO_2} (mmHg)
Pulmonary artery	7.30 ± 0.06	27 ± 7	44 ± 20	41 ± 13
Right pulmonary vein	7.53 ± 0.08	634 ± 69	100 ± 0	20 ± 1
Left (implant) pulmonary vein	7.68 ± 0.28	283 ± 48	100 ± 0	11 ± 5
Mixed pulmonary veins	7.58 ± 0.08	495 ± 174	100 ± 0	18 ± 3

periods in the bioreactor the overall pattern of cellular distribution and differentiation became more similar to that in native lung tissue.

To determine whether the decellularization and repopulation methodologies used in our studies of rat lungs were applicable to human tissues, we obtained human lung segments from a tissue bank and treated them with decellularization solutions for up to 6 hours (*7*). Histological staining showed that complete cellular removal was achieved, with preservation of alveolar architecture (fig. S11, A and B). We seeded the acellular matrices with A549 human epithelial carcinoma cells and endothelial cells derived from human cord-blood endothelial progenitor cells (*7*). The A549 cells adhered well to alveolar surfaces, and the endothelial cells adhered to the vasculature (fig. S11, C and D), supporting the notion that these approaches may also be applicable to human lung tissues.

Implantation of engineered lungs into rats. To determine whether engineered rodent lungs were implantable and functional for gas exchange, we performed orthotopic left lung transplantation in four animals (*7*). Acellular matrices were seeded with neonatal rat lung epithelium and lung microvascular endothelium and cultured for approximately 1 week in the bioreactor. For lung implantation, the native lungs were exposed via left thoracotomy, and the left lung was excised. After anticoagulation with heparin, the left mainstem bronchus, left pulmonary vein, and left pulmonary artery of the engineered lung were anastomosed to the recipient, the lung was ventilated with 100% oxygen, and blood flow was reestablished.

In all cases, the engineered lungs were easily suturable to the recipient and were ventilated with no visible air leak from the parenchyma (Fig. 4A and movie S2). All engineered lungs became perfused with blood over a period of seconds to minutes, with blood visibly turning from dark to bright red as the hemoglobin became oxygenated. Implantation times for engineered lungs ranged from 45 min to 2 hours. After perfusion and ventilation, blood gas samples were drawn from the pulmonary artery, left and right pulmonary veins (veins were clamped and samples drawn from each lung individually), and the unclamped pulmonary vein so as to document the extent of gas exchange occurring in the native and engineered lungs (Table 1).

Chest x-ray confirmed that the engineered lung was inflated with air, but the level of inflation was less than that of the native right lung (Fig. 4B). Histological evaluation of explanted engineered lungs revealed red blood cells in large blood vessels and septal microvessels, and some bleeding into airways, although this was modest (Fig. 4C). Blood gas analysis revealed that the tissue-engineered lungs were effective in exchanging oxygen and carbon dioxide (Table 1). Partial pressures of oxygen (P_{O_2}) increased from 27 ± 7 mmHg in the pulmonary artery to 283 ± 48 mmHg in the left pulmonary vein, indicating complete hemoglobin saturation and oxygenation. Hemoglobin saturation was 100% for both engineered left lung and native right lung venous samples. In addition, carbon dioxide removal was efficient, with CO_2 falling from 41 ± 13 mmHg in the pulmonary artery to 11 ± 5 mmHg in the left, engineered pulmonary vein. Although the P_{O_2} in the right pulmonary vein was higher than in the left (634 ± 69 versus 283 ± 48 mmHg), this difference may not be of substantial physiological consequence because hemoglobin saturation is complete above oxygen pressures of 100 mmHg (*10*).

Discussion. To date, cell therapy and tissue engineering have been applied less extensively to lung than to other tissues and organs (*11–13*). Many efforts in lung regeneration have involved synthetic scaffolds or simple in vitro culture systems. Such systems can regenerate certain microscopic features of alveolar architecture but have not yet produced tissue that can participate in gas exchange (*14*, *15*). Use of the decellularization paradigm for respiratory tissue was described in 2008, when Macchiarini and colleagues implanted a reseeded tracheal matrix into a patient with severe bronchomalacia (*16*).

In the current work, we have demonstrated the feasibility of producing an engineered lung that displays much of the microarchitecture of native lung and that can effect gas exchange for short periods of time when implanted into rats. Although these results are encouraging, multiple issues remain to be addressed before long-term engineered lung function can be realized. For example, alveolar barrier function must be improved so as to prevent any leakage of blood components into the airways. This can be accomplished through iterative improvement in the decellularization procedure in order to minimize alveolar septal damage (*17*). Production of surfactant should be increased (*18*), and differentiated columnar ciliated epithelium should be enhanced by more prolonged air breathing in culture (*19*). In addition, the efficiency of vascular endothelial coverage must be very high throughout the engineered lung vasculature. This is to prevent exposure of collagen-containing basement membrane to the circulation, with consequent thrombosis, because some clotting was noted at explant. Lastly, a decellularization strategy for lung regeneration will only become clinically useful when a suitable, autologous source of pulmonary epithelium can be identified, such as a resident lung stem cell or induced pluripotent stem cell (*20–24*).

References and Notes

1. American Lung Association, *Lung Disease Data 2008*, www.lungusa.org, accessed 4 March 2010.
2. J. B. Orens, E. R. Garrity Jr., *Proc. Am. Thorac. Soc.* **6**, 13 (2009).
3. H. C. Ott *et al.*, *Nat. Med.* **14**, 213 (2008).
4. T. W. Gilbert, T. L. Sellaro, S. F. Badylak, *Biomaterials* **27**, 3675 (2006).
5. P. M. Baptista *et al.*, *IEEE Eng. Med. Biol. Soc.* **31**, 6526 (2009).
6. M. R. Inanlou, M. Baguma-Nibasheka, B. Kablar, *Histol. Histopathol.* **20**, 1261 (2005).
7. Materials and methods are available as supporting material on *Science* Online.
8. J. L. Sporty, L. Horálková, C. Ehrhardt, *Expert Opin. Drug Metab. Toxicol.* **4**, 333 (2008).
9. D. Massaro, N. Teich, S. Maxwell, G. D. Massaro, P. Whitney, *J. Clin. Invest.* **76**, 1297 (1985).
10. N. C. Staub, in *Physiology*, R. M. Berne, M. N. Levy, Eds. (Mosby, St. Louis, ed. 4, 1998), chaps. 32 and 33.
11. C. F. Andrade, A. P. Wong, T. K. Waddell, S. Keshavjee, M. Liu, *Am. J. Physiol. Lung Cell. Mol. Physiol.* **292**, L510 (2007).
12. J. Cortiella *et al.*, *Tissue Eng.* **12**, 1213 (2006).
13. M. J. Mondrinos *et al.*, *Tissue Eng.* **12**, 717 (2006).
14. H. Sugihara, S. Toda, S. Miyabara, C. Fujiyama, N. Yonemitsu, *Am. J. Pathol.* **142**, 783 (1993).
15. Y. M. Lin, A. R. Boccaccini, J. M. Polak, A. E. Bishop, V. Maquet, *J. Biomater. Appl.* **21**, 109 (2006).
16. P. Macchiarini *et al.*, *Lancet* **372**, 2023 (2008).
17. D. O. DeFouw, *Am. Rev. Respir. Dis.* **127**, S9 (1983).
18. E. E. Bittar, in *Pulmonary Biology in Health and Disease* (Springer, New York, 2002).
19. T. E. Gray, K. Guzman, C. W. Davis, L. H. Abdullah, P. Nettesheim, *Am. J. Respir. Cell Mol. Biol.* **14**, 104 (1996).
20. D. Wang, J. E. Morales, D. G. Calame, J. L. Alcorn, R. A. Wetsel, *Mol. Ther.* **18**, 625 (2010).
21. J. Yu *et al.*, *Science* **318**, 1917 (2007).
22. C. F. Kim *et al.*, *Cell* **121**, 823 (2005).
23. H. J. Rippon *et al.*, *Proc. Am. Thorac. Soc.* **5**, 717 (2008).
24. B. Roszell *et al.*, *Tissue Eng. Part A* **15**, 3351 (2009).

25. We thank M. Colehour for help with bioreactor development and Western blotting, R. Homer for histologic assessment, and B. Stripp for the CCSP antibody. This work was funded by Yale University Department of Anesthesia and by NIH grant HL 098220 (to L.E.N.). T.H.P. is supported by NIH T32 GM007171. L.E.N. holds stock in Humacyte, a regenerative medicine company. The authors (L.E.N., T.H.P., and E.A.C.) and Yale University have filed a patent application related to tissue engineering of lungs.

Supporting Online Material

www.sciencemag.org/cgi/content/full/science.1189345/DC1
Materials and Methods
SOM Text
Figs. S1 to S11
Table S1
References

9 March 2010; accepted 14 June 2010
Published online 24 June 2010;
10.1126/science.1189345
Include this information when citing this paper.

Single-Shot Readout of a Single Nuclear Spin

Philipp Neumann,[1] Johannes Beck,[1] Matthias Steiner,[1] Florian Rempp,[1] Helmut Fedder,[1] Philip R. Hemmer,[2] Jörg Wrachtrup,[1]* Fedor Jelezko[1]*

Projective measurement of single electron and nuclear spins has evolved from a gedanken experiment to a problem relevant for applications in atomic-scale technologies like quantum computing. Although several approaches allow for detection of a spin of single atoms and molecules, multiple repetitions of the experiment that are usually required for achieving a detectable signal obscure the intrinsic quantum nature of the spin's behavior. We demonstrated single-shot, projective measurement of a single nuclear spin in diamond using a quantum nondemolition measurement scheme, which allows real-time observation of an individual nuclear spin's state in a room-temperature solid. Such an ideal measurement is crucial for realization of, for example, quantum error correction protocols in a quantum register.

Since the birth of quantum computing, researchers have sought scalable room-temperature systems that could be incorporated as quantum coprocessors. Much enthusiasm arose when room-temperature nuclear magnetic resonance (NMR) quantum computers were developed (*1*). However, these are essentially classical as they lack the ability to initialize and read out individual spins at room temperature (*2*). Recent efforts have focused on the development of ultracold quantum processors like trapped ions and superconducting qubits which operate at millikelvin temperatures (*3*). Electronic and nuclear spins associated with nitrogen-vacancy (NV) centers in diamond have been shown to be a room-temperature solid-state system with exceptionally long coherence times that fulfills most of the requirements needed to build a quantum computer (*4*–*7*). However, it lacked single-shot readout (*8*), and hence only the cryogenic version was considered to be applicable for most quantum information applications. For example, projective readout enables testing Bell-type inequalities and active feedback in quantum error correction protocols. Here, we experimentally showed single-shot readout of a single nuclear spin in diamond. Our technique is based on the repetitive readout of nuclear spins (*9*) and the essential decoupling of the nuclear from the electronic spin dynamics by means of a strong magnetic field (*10*).

The fluorescence time trace of a single NV center shown in Fig. 1B represents the real-time dynamics of a single nuclear spin and exhibits well-defined jumps attributed to abrupt, discontinuous evolution of the nuclear spin state (quantum jumps). The spin used in our experiments belongs to the nucleus of the nitrogen atom [^{14}N; nuclear spin $I = 1$ (*11*)] of a single NV defect in diamond (Fig. 1B). In essence, the measurement sequence consists of a correlation of the electron spin state of the NV color center with the nuclear spin state and a subsequent optical readout of the electron spin, which exhibits the nuclear spin state. Therefore, initially the electron spin is optically pumped into the electron spin sublevel $|0_e\rangle$ ($m_S = 0$) of its triplet ground state ($S = 1$) (*8*), leaving the nuclear spin in an incoherent mixture of its eigenstates ($|m_I = \rangle$)$|-1_n\rangle$, $|0_n\rangle$, and $|1_n\rangle$ (here and below states are defined according to electron and nuclear magnetic quantum numbers, m_S and m_I). The application of a narrowband, nuclear spin state–selective microwave (MW) π pulse flips the electron spin into the $|-1_e\rangle$ state conditional on the state of the nuclear spin. This operation is equivalent to a controlled not (CNOT) operation (Fig. 1A), in that it maps a specific nuclear spin state onto the electron spin (e.g., $|-1_n\rangle|0_e\rangle \rightarrow |-1_n\rangle|-1_e\rangle$, $|0_n\rangle|0_e\rangle \rightarrow |0_n\rangle|0_e\rangle$). This is possible because of the long coherence time of the NV center, providing a spectral linewidth of the electron spin transitions narrow enough to resolve the hyperfine structure. Because the fluorescence intensity differs by roughly a factor of 2 for electron spin states $|0_e\rangle$ and $|-1_e\rangle$ (*8*, *12*), these target states can be distinguished by shining a short laser pulse. This destroys the electron spin state but leaves the nuclear spin state population almost undisturbed under the experimental conditions. Thus, repeated application of this scheme allows nondestructive accumulation of fluorescence signal in order to determine the nuclear spin state optically.

The fidelity F to detect a given state in a single shot [reaching $F = 92 \pm 2\%$ in our experiments (*13*)] can be extracted from the photon-counting histograms (Fig. 2A), which show distinguishable peaks corresponding to different nuclear spin states. The fidelity is limited by the measurement time (bounded by relaxation time of the nuclear spin), fluorescence count rate, and magnetic resonance signal contrast. Further improvement in readout speed can be achieved by engineering of photon emission into photonic nanostructures (*14*). A consecutive measurement of the same spin state gives an identical result with a probability of (F^2) of ~82.5% (Fig. 2C). Such a correlation between consecutive measurements is the signature of so-called quantum nondemolition (QND) protocols (*15*). For the nitrogen nuclear spin qubit initially in a superposition of two states, the measurement affects its state by projection into one of the eigenstates, but does not demolish it (as happens with photons arriving at a photomultiplier tube or fluorescent atoms that are shelved in a dark state, which is not a qubit state). Hence, the same nuclear spin eigenstate can be redetected in consecutive measurements.

The difference between projective measurement and a practical QND has been analyzed in

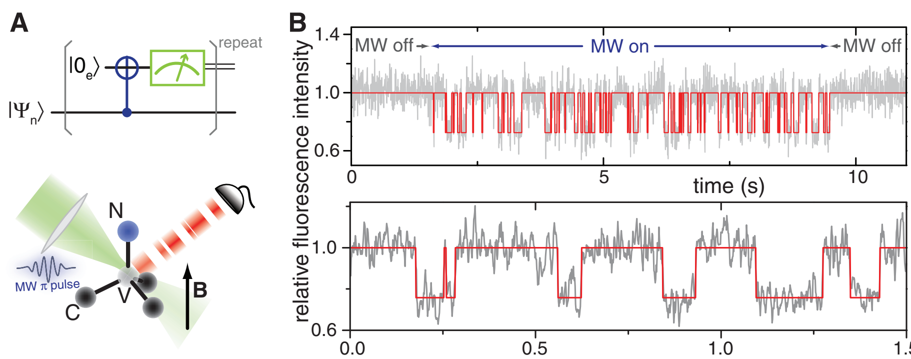

Fig. 1. Single-shot readout reveals quantum jumps of a single nuclear spin in real time. (**A**) Representation of the single-shot readout scheme. (**B**) Normalized fluorescence time traces (gray) showing quantum jumps of a single nuclear spin in real time. When MW pulses (controlled-NOT gates) are on, a telegraph-like signal appears, revealing the projective nature of this measurement. Low fluorescence intensity represents nuclear spin state $|-1_n\rangle$, and high fluorescence intensity indicates $|0_n\rangle$ or $|+1_n\rangle$. When MW pulses are off (upper trace), the fluorescence intensity remains high because it is not correlated with the nuclear spin state. Each data point was acquired by continuously repeating the readout scheme for 5 ms (2000 repetitions).

[1]3rd Physics Institute and Research Center SCoPE, University of Stuttgart, Pfaffenwaldring 57, Stuttgart 70550, Germany. [2]Department of Electrical and Computer Engineering, Texas A&M University, College Station, TX 77843, USA.

*To whom correspondence should be addressed. E-mail: f.jelezko@physik.uni-stuttgart.de (F.J.); wrachtrup@physik.uni-stuttgart.de (J.W.)

detail (*16*, *17*) and can be summarized as three conditions that must be simultaneously fulfilled in order to have a true QND measurement. Our system observable is the nuclear spin $\hat{I}_z$, our probe observable is the electron spin $\hat{S}_z$, and their Hamiltonians are H_n and H_e, respectively (*13*). The interaction Hamiltonian H_i for our case is separable $H_i = H_A + H_p$, where H_A describes the hyperfine interaction and H_p represents the MW field applied in the experiment.

The first condition for QND is simply that the probe observable $\hat{S}_z$ must be measurably influenced by the system observable $\hat{I}_z$ that we desire to measure. Therefore, the interaction Hamiltonian H_i has to depend on I_z and must not commute with the probe observable $\hat{S}_z$ ($[\hat{S}_z, H_i] \neq 0$) (*16*, *17*). These demands are met by the CNOT gate. The corresponding Hamiltonian $H_p = \Omega \exp(i\omega t)\ \hat{S}_x \otimes |-1_n\rangle\langle -1_n|$ acts for a time τ and flips the electron spin by an angle

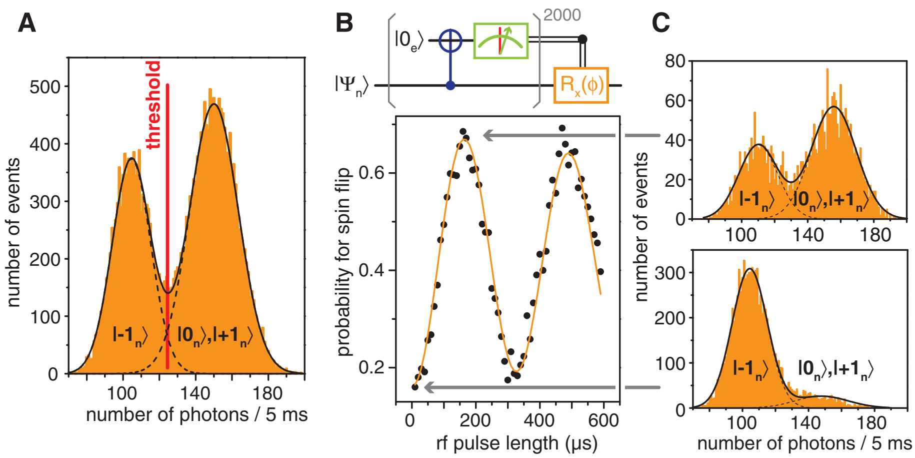

Fig. 2. Readout fidelity and conditional gates using single-shot readout. (**A**) Photon-counting histogram of a fluorescence time trace fitted by two Gaussian distributions (solid lines). Left and right peaks correspond to the dark ($|-1_n\rangle$) and bright ($|0_n\rangle$, $|+1_n\rangle$) states, respectively. By setting a threshold (red line), the nuclear spin state $|-1_n\rangle$ (fluorescence below threshold) can be distinguished from the other nuclear spin states (fluorescence above threshold). For the given lifetimes at 0.65 T and fluorescence levels, the fidelity to detect a given state correctly is 92 ± 2%. (**B**) Conditional nuclear spin Rabi oscillations and histograms. The wire diagram on top illustrates the conditional Rabi sequence. Only if the measurement outcome is $|-1_n\rangle$, a resonant radio-frequency (rf) pulse of certain length is applied on the nuclear spin transition $|-1_n\rangle \leftrightarrow |0_n\rangle$ and a subsequent measurement is performed. Otherwise the sequence is restarted immediately. (**C**) Conditional histograms. Two consecutive QND measurements have a high probability (≈82%) of giving the same outcome (lower histogram). If a rf π pulse is applied after detecting $|-1_n\rangle$, this probability drops to ≈33% (upper histogram). Possible reasons for the Rabi contrast of <1 are, for instance, the setup instability and imperfect initialization and readout of the electron spin.

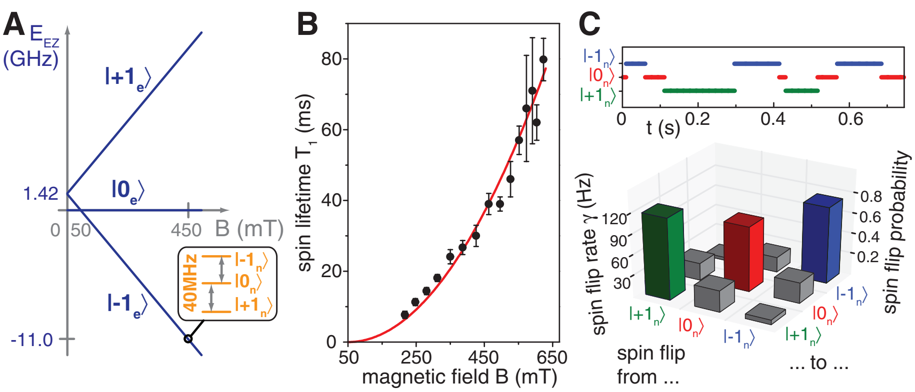

Fig. 3. Tuning nuclear spin dynamics. (**A**) Excited-state fine structure as a function of the magnetic field *B* (parallel to the NV axis). The inset shows the ^{14}N hyperfine structure (splitting of ~40 MHz). (**B**) Experimental results (black dots) confirm the predicted quadratic dependence of nuclear spin lifetime on the detuning from the level anticrossing [red line, $T_1 = 230\ \mu s \cdot mT^{-2}\ (B - 50\ mT)^2$]. (**C**) At every point in time, all three nuclear spin states were measured directly and a time trace was acquired. The upper graph shows a part of the corresponding quantum state trajectory (computer fit to the data as in Fig. 1C). The lower graph is the transition matrix calculated from analyzing ~10,000 quantum jumps. Off-diagonal elements represent spin-flip probabilities and diagonal elements represent the probability of remaining unchanged. The probabilities are proportional to spin flip rates under continuous application of the readout sequence. Error bars indicate the uncertainty in nuclear state lifetime measurements.

$\beta = \Omega\tau$ only for the nuclear spin $|-1_n\rangle$ subspace (Ω, Rabi frequency; ω, MW frequency). The strength of the QND measurement can by tuned by preparing the electron spin in a superposition state rather than in an eigenstate before the action of H_p (*18*).

The second QND condition requires that the system observable state I_z be stable with respect to back action of the measurement. This translates to the requirement that the system Hamiltonian must not be a function of the observable's conjugate ($\hat{I}_x$ or $\hat{I}_y$) in order to avoid back action of the measurement, which imposes a large uncertainty on the conjugates. In our case, this condition is fulfilled as long as the applied magnetic field is exactly parallel to the NV center symmetry axis (*13*).

The third condition is that the probe and system observables, $\hat{S}_z$ and $\hat{I}_z$ in our case, should not be mixed by any interactions that are neither intrinsic to the material nor created by the action of the MW or laser probes (i.e., that the nuclear spin is well isolated from the environment). In other words (*16*, *17*), the interaction Hamiltonian must commute with the observable ($[\hat{I}_z, H_i] = 0$). Fulfilling this condition perfectly is an impossible task for any experimental system, particularly in the solid state. However, defect center spins in diamond are very close to an ideal system for QND measurements. In the case of the NV center, the nuclear spin–selective MW pulse on the electron spin does not act on the nuclear spin subspace (hence $[\hat{I}_z, H_p] = 0$). However, the hyperfine coupling tensor $\underline{A}$ contains contributions parallel and perpendicular to the symmetry axis of the NV center ($A_\parallel$ and $A_\perp$), and the perpendicular component is responsible for an undesirable mixing. The first term of the hyperfine Hamiltonian $H_A = (\hat{S}_+\hat{I}_- + \hat{S}_-\hat{I}_+)A_\perp/2 + \hat{S}_z\hat{I}_z A_\parallel$ is noncommuting with $\hat{I}_z$ and therefore induces nuclear-electron spin flip-flop processes. This mixing is responsible for the quantum jumps in Fig. 1B. The key to succeeding at QND measurements is therefore to make this jump time longer than the measurement time.

To quantify the hyperfine induced flip-flop rate, assume an isotropic case ($A_\parallel \simeq A_\perp \simeq A$) and use the measured $A_\parallel$ = 40 MHz in the excited state (*19*, *20*). Electron-nuclear spin dynamics occur on a time scale of $2/A_\perp \sim 50$ ns in the vicinity of excited-state level anticrossing at magnetic field $B = 50$ mT (*19*, *21*) (Fig. 3A). Relaxation in the ground state is expected to be slower owing to a much weaker hyperfine coupling (*13*) and can be neglected here. The relaxation process slows down when the magnetic field along the NV symmetry axis is increased owing to the growing energy mismatch between electron and nuclear spin transitions due to increasing Zeeman shifts (Fig. 3A). A detailed analysis (*13*) and experimental data (Fig. 3B) show that the relaxation rate γ depends on the detuning δ from the level anticrossing (1.42 GHz) as $\gamma \sim (A_\perp^2/2)/[(A_\perp^2/2) + \delta^2]$ (i.e., like a Lorentzian lineshape). Hence, we expect a quadratic dependence of T_1 on the detuning from the excited-state level anticrossing

($T_1 = 1/\gamma \sim \delta^2$ for $\delta \gg A_\perp^2$). Experimental data confirm this behavior (Fig. 3B). This dependence also explains why quantum jumps were not observed in previous experiments with NV centers performed at low magnetic fields [similar magnetic field–enabled decoupling of nuclear spin was proposed recently for alkaline earth metal ions (*10*, *22*)]. The dominance of flip-flop processes is also visible in the quantum state trajectory of the nuclear spin shown in Fig. 3C (top). Here, jumps obey the selection rule $\Delta m_I = \pm 1$ imposed by the flip-flop term H_A. From analyzing the whole quantum state trajectory, a matrix showing the transition probabilities can be obtained (Fig. 3C, bottom).

Single-shot measurement of a single nuclear spin places diamond among leading quantum computer technologies. The high readout fidelity (92%) demonstrated in this work is already close to the threshold for enabling error correction (*23*), although the experiments were carried out in a moderate-strength magnetic field. Even though the optical excitation induces complex dynamics in the NV center (including passage into singlet electronic state), the nuclear spin relaxation rates are defined solely by electron-nuclear flip-flop processes induced by hyperfine interaction. Therefore, we expect improvement of T_1 by two orders of magnitude (reaching seconds under illumination) when a magnetic field of 5 T is used. This will potentially allow readout fidelities comparable with that achieved for single ions in traps (*24*). The present technique can be applied to multiqubit quantum registers (*5*, *6*, *25*), enabling tests of nonclassical correlations. Finally, single-shot measurements open new perspectives for solid-state sensing technologies. Spins in diamond are considered to be among the promising candidates for nanoscale magnetic field sensing (*26*, *27*). Currently their performance is limited by photon shot noise (*26*): "Digital" QND will provide improvement over conventional photon counting in the case of short acquisition time. This requires that the electron spin state used for magnetic field sensing can be mapped onto the nuclear spin with high accuracy, but this was already shown to be practical in NV diamond (*5*).

References and Notes

1. N. A. Gershenfeld, I. L. Chuang, *Science* **275**, 350 (1997).
2. W. S. Warren, *Science* **277**, 1688 (1997).
3. T. D. Ladd *et al.*, *Nature* **464**, 45 (2010).
4. L. Childress *et al.*, *Science* **314**, 281 (2006).
5. M. V. G. Dutt *et al.*, *Science* **316**, 1312 (2007).
6. P. Neumann *et al.*, *Science* **320**, 1326 (2008).
7. G. D. Fuchs, V. V. Dobrovitski, D. M. Toyli, F. J. Heremans, D. D. Awschalom, *Science* **326**, 1520 (2009).
8. F. Jelezko, T. Gaebel, I. Popa, A. Gruber, J. Wrachtrup, *Phys. Rev. Lett.* **92**, 076401 (2004).
9. L. Jiang *et al.*, *Science* **326**, 267 (2009).
10. A. V. Gorshkov *et al.*, *Phys. Rev. Lett.* **102**, 110503 (2009).
11. The presented single-shot readout works in the same way and shows a similar fidelity for the nuclear spin of the ^{15}N isotope.
12. A. Batalov *et al.*, *Phys. Rev. Lett.* **100**, 077401 (2008).
13. Supporting material is available on *Science* Online.
14. T. M. Babinec *et al.*, *Nat. Nanotechnol.* **5**, 195 (2010).
15. V. B. Braginsky, F. Y. Khalili, *Rev. Mod. Phys.* **68**, 1 (1996).
16. N. Imoto, H. A. Haus, Y. Yamamoto, *Phys. Rev. A* **32**, 2287 (1985).
17. C. M. Caves, K. S. Thorne, R. W. P. Drever, V. D. Sandberg, M. Zimmermann, *Rev. Mod. Phys.* **52**, 341 (1980).
18. T. C. Ralph, S. D. Bartlett, J. L. O'Brien, G. J. Pryde, H. M. Wiseman, *Phys. Rev. A* **73**, 012113 (2006).
19. G. D. Fuchs *et al.*, *Phys. Rev. Lett.* **101**, 117601 (2008).
20. M. Steiner, P. Neumann, J. Beck, F. Jelezko, J. Wrachtrup, *Phys. Rev. B* **81**, 035205 (2010).
21. V. Jacques *et al.*, *Phys. Rev. Lett.* **102**, 057403 (2009).
22. I. Reichenbach, I. H. Deutsch, *Phys. Rev. Lett.* **99**, 123001 (2007).
23. E. Knill, *Nature* **434**, 39 (2005).
24. A. H. Myerson *et al.*, *Phys. Rev. Lett.* **100**, 200502 (2008).
25. L. Jiang, J. M. Taylor, A. S. Sorensen, M. D. Lukin, *Phys. Rev. A* **76**, 062323 (2007).
26. J. R. Maze *et al.*, *Nature* **455**, 644 (2008).
27. G. Balasubramanian *et al.*, *Nature* **455**, 648 (2008).

28. We thank F. Dolde for fabrication of microwave structures; N. Zarrabi for assistance with data analysis; J. Mayer and P. Bertet for helpful information on QND measurements in superconducting qubits; and M. D. Lukin, J. Twamley, F. Y. Khalili, and J. O'Brien for comments and discussions. We thank G. Denninger for the loan of a X-band microwave synthesizer. This work was supported by the European Union, Deutsche Forschungsgemeinschaft (SFB/TR21 and FOR1482), Bundesministerium für Bildung und Forschung, and Landesstiftung BW.

Supporting Online Material

www.sciencemag.org/cgi/content/full/science.1189075/DC1
Methods
SOM Text
Figs. S1 to S6
References

3 March 2010; accepted 21 June 2010
Published online 1 July 2010;
10.1126/science.1189075
Include this information when citing this paper.

Strain-Induced Pseudo–Magnetic Fields Greater Than 300 Tesla in Graphene Nanobubbles

N. Levy,[1,2]*† S. A. Burke,[1]*‡ K. L. Meaker,[1] M. Panlasigui,[1] A. Zettl,[1,2] F. Guinea,[3] A. H. Castro Neto,[4] M. F. Crommie[1,2]§

Recent theoretical proposals suggest that strain can be used to engineer graphene electronic states through the creation of a pseudo–magnetic field. This effect is unique to graphene because of its massless Dirac fermion-like band structure and particular lattice symmetry (C_{3v}). Here, we present experimental spectroscopic measurements by scanning tunneling microscopy of highly strained nanobubbles that form when graphene is grown on a platinum (111) surface. The nanobubbles exhibit Landau levels that form in the presence of strain-induced pseudo–magnetic fields greater than 300 tesla. This demonstration of enormous pseudo–magnetic fields opens the door to both the study of charge carriers in previously inaccessible high magnetic field regimes and deliberate mechanical control over electronic structure in graphene or so-called "strain engineering."

Graphene, a single atomic layer of carbon, displays remarkable electronic and mechanical properties (*1*, *2*). Many of graphene's distinctive properties arise from a linear band dispersion at low carrier energies (*3*) that leads to Dirac-like behavior within the two-dimensional (2D) honeycomb lattice—charge carriers travel as if their effective mass is zero (*1*). An intriguing recent prediction is that a distortion of the graphene lattice should create large, nearly uniform pseudo–magnetic fields and give rise to a pseudo–quantum Hall effect (*4*). Whereas an elastic strain can be expected to induce a shift in the Dirac point energy from local changes in electron density, it is also predicted to induce an effective vector potential that arises from changes in the electron-hopping amplitude between carbon atoms (*5*). This strain-induced gauge field can give rise to large pseudo–magnetic fields (B_s) for appropriately selected geometries of the applied strain (*1*, *6*). In such situations, the charge carriers in graphene are expected to circulate as if under the influence of an applied out-of-plane magnetic field (*7*–*10*). It has recently been proposed that a modest strain field with triangular symmetry will give approximately uniform, quantizing B_s upward of tens of tesla (*4*).

Here, we report the measurement of Landau levels (LLs) arising from giant strain-induced pseudo–magnetic fields in highly strained graphene nanobubbles grown on the Pt(111) surface. Lan-

[1]Department of Physics, University of California Berkeley, Berkeley, CA 94720, USA. [2]Materials Science Division, Lawrence Berkeley National Laboratory, Berkeley, CA 94720, USA. [3]Instituto de Ciencia de Materiales de Madrid (CSIC), Madrid 28049, Spain. [4]Department of Physics, Boston University, Boston, MA 02215, USA.

*These authors contributed equally to this work.
†Present address: Center for Nanoscale Science and Technology, National Institute of Standards and Technology, Gaithersburg, MD 20899, USA.
‡Present address: Department of Physics and Astronomy and Department of Chemistry, University of British Columbia, Vancouver, BC V6T 121, Canada.
§To whom correspondence should be addressed. E-mail: crommie@berkeley.edu

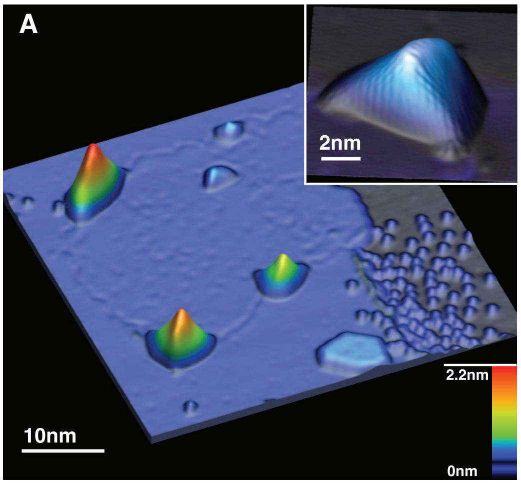

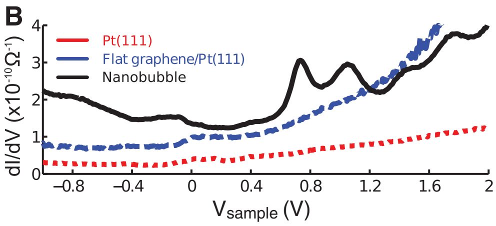

Fig. 1. STM images and STS spectra taken at 7.5 K. (**A**) Graphene monolayer patch on Pt(111) with four nanobubbles at the graphene-Pt border and one in the patch interior. Unreacted ethylene molecules and a small hexagonal graphene patch can be seen in the lower right ($I_{tunneling}$ = 50 pA, V_{sample} = 350 mV, 3D *z*-scale enhanced 4.6×). (Inset) High-resolution image of a graphene nanobubble showing distorted honeycomb lattice resulting from strain in the bubble ($I_{tunneling}$ = 50 pA, V_{sample} = 200 mV, max *z* = 1.6 nm, 3D *z*-scale enhanced 2×). (**B**) STS spectra of bare Pt(111), flat graphene on Pt(111) (shifted upward by 3×10^{-11} ohm^{-1}), and the center of a graphene bubble (shifted upward by 9×10^{-11} ohm^{-1}). V_{mod} = 20 mV.

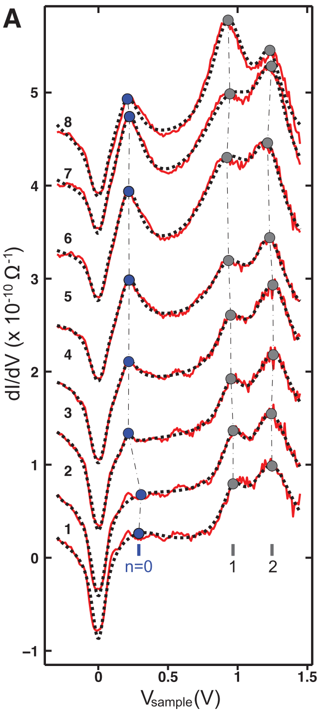

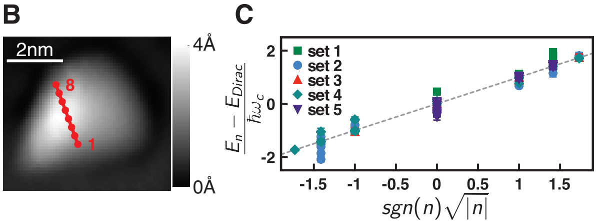

Fig. 2. (**A**) Sequence of eight *dI/dV* spectra (*T* ~ 7.5 K, V_{mod} = 20 mV) taken in a line across a graphene nanobubble shown in the image in (**B**). Red lines are data with quartic background subtracted; black dotted lines are Lorentzian peak fits (center of peaks indicated by dots, with blue dots indicating *n* = 0). Vertical dash-dot lines follow the energy progression of each peak order. (**C**) Normalized peak energy versus $sgn(n)\sqrt{|n|}$ for peaks observed on five different nanobubbles follow expected scaling behavior from Eq. 1 (dashed line).

dau quantization of the electronic spectrum was observed by scanning tunneling microscopy (STM), which revealed pseudo–magnetic fields in excess of 300 T. Such enormous strain-induced pseudo–magnetic fields may allow the electronic properties of graphene to be controlled through various schemes for applying strain (*11*), as well as the exploration of new high-field physical regimes.

Strained graphene nanobubbles were created by in situ growth of sub-monolayer graphene films in ultrahigh vacuum on a clean Pt(111) surface (*12*) in order to avoid external contamination and trapped gases. The epitaxial graphene was grown by exposure of Pt(111) to ethylene followed by annealing (*13*, *14*). Graphene grown on Pt is expected to be minimally coupled to the substrate, compared to graphene grown on other catalytic metals (*15*, *16*). A Dirac-like band structure is preserved for graphene on Pt(111), as verified by a recent photoemission study (*17*). An STM topograph of the graphene/Pt(111) surface prepared in this manner (Fig. 1A) reveals a flat graphene patch (partially surrounded by Pt) that encompasses five graphene nanobubbles. Graphene nanobubbles frequently appear near the edges of a graphene patch, but are also sometimes observed in the center of flat patches or near the boundaries between patches and are presumably pinned near these locations (Fig. 1A). These nanobubbles are likely related to the larger-scale "wrinkle" structures observed by low energy electron microscopy that form upon cooling as a result of the differing thermal expansion coefficients of graphene and the platinum surface (*17*).

Individual nanobubbles often have a triangular shape (Fig. 1A, inset), reflecting the lattice symmetry of the graphene and the underlying Pt surface, and are typically 4 to 10 nm across and 0.3 to 2.0 nm tall. Atomic-resolution imaging of the nanobubbles confirms the honeycomb structure of graphene here (Fig. 1A, inset), although the lattice is distorted because of the large strain occurring in these structures. The expected strain-induced pseudo–magnetic field in a graphene nanobubble can be estimated by using the relation $\Phi = (\beta h^2/la)\Phi_0$ for the flux per ripple in a distorted graphene sheet (*6*), where *h* is the height, *l* is the width, *a* is on the order of the C-C bond length, and Φ_0 is the quantum of flux. The parameter $\beta = \partial \log(t)/\partial \log(a)$ relates the change in the hopping amplitude between nearest neighbor carbon atoms (*t*) to bond length and has a typical magnitude of $2 < \beta < 3$ for graphene. For a nanobubble of $l = 4$ nm and $h = 0.5$ nm, this yields a B_s of order 100 T. The large curvature and correspondingly high strain incorporated into the triangular nanoscale bubbles observed here make them ideal candidates for the observation of pseudo-LL because of large strain-induced pseudo–magnetic fields.

The local electronic structure of strained graphene nanobubbles and surrounding graphene films was characterized by scanning tunneling spectroscopy (STS) performed at ~ 7.5 K by using standard lock-in techniques to obtain differential conductance (*dI*/*dV*). The measurement of *dI*/*dV* reflects features in the local density of states (LDOS) of the surface at the position of the STM tip (*18*). STS measurement of the bare Pt surface was used to calibrate the LDOS of the tip upon approach and between sequences of spectra. STS spectra measured over the bare Pt regions (Fig. 1B) are relatively featureless and show the expected Pt(111) surface state (*19*). Spectra recorded over the flat graphene patches show a subtly modified structure compared with the clean Pt(111) surface, and no clear signatures of the graphene Dirac point were observed in these regions (Fig. 1B). Spectra measured at the boundary between the flat graphene and the nanobubbles (fig. S2) exhibit features consistent with a Dirac point located ~300 mV above the Fermi energy, as recently observed by photoemission (*17*), as well as a gaplike feature with a full width at half maximum (FWHM) of 127 ± 9 mV centered at the Fermi energy (V_{sample} = 0) recently

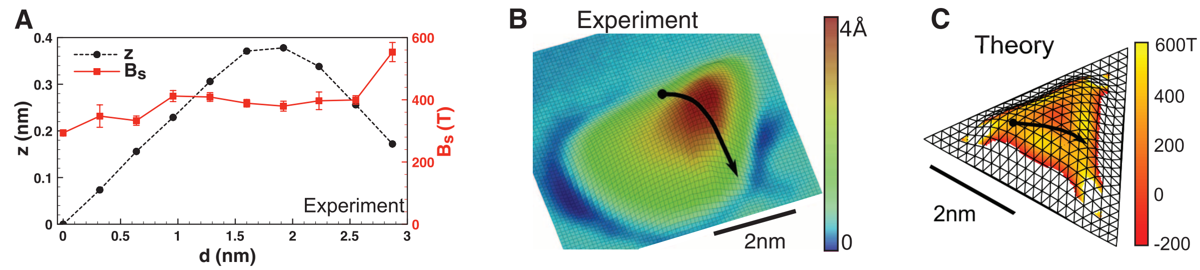

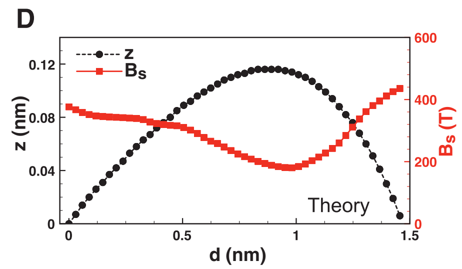

Fig. 3. (**A**) Experimental topographic line scan and experimentally determined B_s profile over the tip trajectory shown by black line in (B). (**B**) STM topography of graphene nanobubble. (**C**) Topography of theoretically simulated graphene nanobubble with calculated B_s color map. (**D**) Simulated topographic line scan and B_s profiles extracted from line shown in (C).

associated with phonon-assisted inelastic tunneling (*20*).

STS measurements made directly over the nanobubble regions exhibit a succession of relatively strong peaks, spaced by more than 100 meV, which do not appear in the spectra on other regions of the sample (Fig. 1B). The peaks are typically weaker at negative bias, which may be attributed to the expected shorter vertical extension of wavefunctions at lower energies. These peaks in the LDOS of the graphene nanobubble are unlike features seen previously in STS performed on graphene in the absence of a magnetic field on SiC (*21*, *22*) and SiO_2 (*20*, *23*) substrates and often overwhelm the usual graphene features. Figure 2A shows a series of spectra taken at different positions across a single nanobubble (topography shown in Fig. 2B). These spectra display the typical nanobubble peak structure as well as the inelastic feature at the Fermi energy described above [a broader bias range is shown in (fig. S3)]. Similar peak structure was observed on 10 different nanobubbles with four different STM tips, with some variation in peak spacing and amplitude that we presume was caused by variations in strain-induced electronic structure arising from different nanobubble geometries.

These peaks observed in the nanobubble LDOS can be attributed to LLs originating from a strain-induced pseudo–magnetic field. Other possible origins that we rule out as unlikely include confinement effects and defect creation. Confinement of Dirac fermions in graphene is difficult because of Klein tunnelling and the suppression of backscattering (*1*). If confinement somehow occurred at the nanobubble edges, the peaks observed would be expected to follow a different progression, most notably missing the n = 0 peak observed in spectra taken at the center of most nanobubbles (*24*). Confinement would also result in strong nodal patterns in LDOS (*24*), which were not observed. The production of defect states by strain is also unlikely because of the high energetic barrier toward defect creation. It is possible that some nanobubbles were formed at defect sites in the as-grown graphene, but the nanobubbles that we measured did not show signatures of defect physics in spectroscopy, such as tip height dependence of peak positions associated with the charging of defect states.

The most likely explanation for the nanobubble peaks is that they arise from a large, relatively uniform strain-induced pseudo–magnetic field. This pseudo–magnetic field is expected to mimic the influence of a real magnetic field applied perpendicular to the graphene sheet and give rise to LLs (*4*). These appear as a series of peaks in STS as they do for the case of a real magnetic field (*25*, *26*). Specifically, the 2D massless Dirac nature of charge carriers near the Fermi energy causes the progression of peaks in the LDOS to follow the expression (*7*, *8*):

$$E_n = \mathrm{sgn}(n)\hbar\omega_c\sqrt{|n|} + E_{\mathrm{Dirac}},$$

$$\omega_c = \sqrt{2e\hbar v_F^2 B_s} \tag{1}$$

where E_n is the position in energy of the nth LL with respect to the Fermi level, ω_c is the cyclotron resonance frequency arising from B_s, and v_F is the Fermi velocity. Both positive and negative n will appear symmetrically about the Dirac point, corresponding to electron and hole states, respectively, as well as an $n = 0$ state coincident with the Dirac point (*1*, *7*, *8*).

The energy progression expected for LLs in graphene can be compared to STS data taken on a nanobubble by fitting the spectra with a sequence of Lorentzian peaks following Eq. 1 with a simple polynomial background (Fig. 2A). The observed peak structure follows the expected progression well, and a value of B_s for position "1" in Fig. 2A was determined to be 350 ± 40 T (energies of the n = 0, 1, and 2 states from the fit are shown below the spectrum for this position). Additional peaks that largely follow the expected $\mathrm{sgn}(n)\sqrt{|n|}$ progression were also observed over a wider bias range. Small deviations from this progression occur for higher energy peaks, because the graphene dispersion is not strictly linear in this range. A plot of normalized energy $(E_n - E_{\mathrm{Dirac}})/\hbar\omega_c$ versus $\mathrm{sgn}(n)\sqrt{|n|}$, shown in Fig. 2C, compiled from spectra on five different nanobubbles, demonstrates the expected scaling behavior for LLs in graphene.

The offset and spacing of the peak progression changes over different positions on individual nanobubbles, indicating a spatial variation of B_s and E_{Dirac}. The B_s profile across a strained nanobubble was extracted from the spectral peak spacing at different positions across a nanobubble, shown in Fig. 3B. As seen in Fig. 3A, the B_s profile is reasonably flat across the center of the bubble, indicating a relatively uniform pseudo–magnetic field of 300 to 400 T for this particular geometry. E_{Dirac}, coincident with the n = 0 LL, ranges from 0.2 to 0.3 eV across this region of the nanobubble. This variation in E_{Dirac} indicates scalar potential variations across the nanobubble, as expected for an elastic deformation that does not constitute a pure shear strain (*1*, *5*).

To compare the experimental spatial dependence of the strain-induced pseudo–magnetic field to theoretical predictions, we simulated a triangular nanobubble with similar geometry to that shown in Figs. 2A and 3B by using continuum elasticity theory (*27*) [see supporting information for details (*12*)]. In this calculation, the edges of a triangular graphene patch were brought in toward the center to simulate the strain arising from the different coefficients of thermal expansion of graphene and the underlying Pt(111) substrate during experimental sample preparation. The predicted pseudo–magnetic field arising from this strain field was also calculated following (*4*). A 3D plot of the simulated nanobubble shape with the pseudo–magnetic field strength shown as a color map is displayed in Fig. 3C (the corresponding experimental nanobubble is shown in Fig. 3B). The simulated and experimental topographic profiles agree well, as seen by the com-

parison between Fig. 3, A and D. The simulated B_s profile (Fig. 3D) also agrees reasonably well with the experimentally extracted B_s (Fig. 3A) given that there are some differences in shape and uncertainty in the exact boundary conditions. The main discrepancy is that the experimental B_s profile appears much more uniform than the simulated one, which may be attributed to spatial averaging of the LDOS over the magnetic length scale of ~1.5 nm. The simulated and experimental nanobubbles both exhibit a relatively uniform strain-induced pseudo–magnetic field of 200 to 400 T across the central region with increasing field at the edges.

The exceptional flexibility and strength of graphene membranes (*28*, *29*) coupled with the large strain-induced fields observed suggest that strain engineering of nanoscale energy levels (*11*, *30*) may be a viable means of controlling the electronic structure of graphene, even at room temperature. The experimental demonstration of these enormous pseudo–magnetic fields also provides a new basis for the study of extreme high magnetic field regimes in a condensed-matter environment.

References and Notes

1. A. H. Castro Neto, F. Guinea, N. M. R. Peres, K. S. Novoselov, A. K. Geim, *Rev. Mod. Phys.* **81**, 109 (2009).
2. A. K. Geim, K. S. Novoselov, *Nat. Mater.* **6**, 183 (2007).
3. P. R. Wallace, *Phys. Rev.* **71**, 622 (1947).
4. F. Guinea, M. I. Katsnelson, A. K. Geim, *Nat. Phys.* **6**, 30 (2010).
5. F. Guinea, A. K. Geim, M. I. Katsnelson, K. S. Novoselov, *Phys. Rev. B* **81**, 035408 (2010).
6. F. Guinea, M. I. Katsnelson, M. A. H. Vozmediano, *Phys. Rev. B* **77**, 075422 (2008).
7. Y. B. Zhang, Y. W. Tan, H. L. Stormer, P. Kim, *Nature* **438**, 201 (2005).
8. K. S. Novoselov *et al.*, *Nature* **438**, 197 (2005).
9. K. I. Bolotin, F. Ghahari, M. D. Shulman, H. L. Stormer, P. Kim, *Nature* **462**, 196 (2009).
10. X. Du, I. Skachko, F. Duerr, A. Luican, E. Y. Andrei, *Nature* **462**, 192 (2009).
11. V. M. Pereira, A. H. Castro Neto, *Phys. Rev. Lett.* **103**, 046801 (2009).
12. Materials and methods are available as supporting material on *Science* Online.
13. T. A. Land, T. Michely, R. J. Behm, J. C. Hemminger, G. Comsa, *Surf. Sci.* **264**, 261 (1992).
14. M. Enachescu, D. Schleef, D. F. Ogletree, M. Salmeron, *Phys. Rev. B* **60**, 16913 (1999).
15. A. B. Preobrajenski, M. L. Ng, A. S. Vinogradov, N. Martensson, *Phys. Rev. B* **78**, 073401 (2008).
16. M. Gao *et al.*, *Appl. Phys. Lett.* **96**, 053109 (2010).
17. P. Sutter, J. T. Sadowski, E. Sutter, *Phys. Rev. B* **80**, 245411 (2009).
18. J. A. Stroscio, W. J. Kaiser, *Scanning Tunneling Microscopy* (Academic Press, San Diego, CA, 1993).
19. J. Wiebe *et al.*, *Phys. Rev. B* **72**, 193406 (2005).
20. Y. B. Zhang *et al.*, *Nat. Phys.* **4**, 627 (2008).
21. V. W. Brar *et al.*, *Appl. Phys. Lett.* **91**, 122102 (2007).
22. G. M. Rutter *et al.*, *Science* **317**, 219 (2007).
23. V. W. Brar *et al.*, *Phys. Rev. Lett.* **104**, 036805 (2010).
24. J. Akola, H. P. Heiskanen, M. Manninen, *Phys. Rev. B* **77**, 193410 (2008).
25. D. L. Miller *et al.*, *Science* **324**, 924 (2009).
26. G. Li, E. Y. Andrei, *Nat. Phys.* **3**, 623 (2007).
27. H. S. Seung, D. R. Nelson, *Phys. Rev. A* **38**, 1005 (1988).
28. C. Lee, X. D. Wei, J. W. Kysar, J. Hone, *Science* **321**, 385 (2008).
29. J. S. Bunch *et al.*, *Nano Lett.* **8**, 2458 (2008).
30. W. Z. Bao *et al.*, *Nat. Nanotechnol.* **4**, 562 (2009).

31. Research supported by the Director, Office of Science, Office of Basic Energy Sciences, Materials Sciences and Engineering Division, of the U.S. Department of Energy (DOE) under contract no. DE-AC02-05CH11231 (instrumentation development and materials synthesis) and DOE contract no. DE-FG02-08ER46512 (experimental data analysis), by the Office of Naval Research Multidisciplinary University Research Initiative (MURI) award no. N00014-09-1-1066 (experimental STM measurements) and MURI award no. N00014-09-1-1063 (electronic structure calculations), and by Ministerio de Ciencia e Innovación (MICINN) (Spain), award nos. FIS2008-00124/CSD2007-00010 (continuum elasticity simulations). A.H.C.N. acknowledges the support of the Miller Institute for Basic Research. S.A.B. and K.L.M. acknowledge fellowship support from Natural Sciences and Engineering Research Council (Canada) and NSF, respectively. The authors declare no competing financial interests. Requests for materials should be addressed to M.F.C.

Supporting Online Material

www.sciencemag.org/cgi/content/full/329/5991/544/DC1
Materials and Methods
SOM Text
Figs. S1 to S7
References

30 April 2010; accepted 29 June 2010
10.1126/science.1191700

Probing the Superfluid–to–Mott Insulator Transition at the Single-Atom Level

W. S. Bakr,[1] A. Peng,[1] M. E. Tai,[1] R. Ma,[1] J. Simon,[1] J. I. Gillen,[1] S. Fölling,[1,2] L. Pollet,[1] M. Greiner[1]*

Quantum gases in optical lattices offer an opportunity to experimentally realize and explore condensed matter models in a clean, tunable system. We used single atom–single lattice site imaging to investigate the Bose-Hubbard model on a microscopic level. Our technique enables space- and time-resolved characterization of the number statistics across the superfluid–Mott insulator quantum phase transition. Site-resolved probing of fluctuations provides us with a sensitive local thermometer, allows us to identify microscopic heterostructures of low-entropy Mott domains, and enables us to measure local quantum dynamics, revealing surprisingly fast transition time scales. Our results may serve as a benchmark for theoretical studies of quantum dynamics, and may guide the engineering of low-entropy phases in a lattice.

Microscopic measurements can reveal properties of complex systems that are not accessible through statistical ensemble measurements. For example, scanning tunneling microscopy has allowed physicists to identify the importance of nanoscale spatial inhomogeneities in high-temperature superconductivity (*1*), and single-molecule microscopy (*2*) has enabled studies of local dynamics in chemical reactions, revealing the importance of multiple reaction pathways (*3*). Whereas previous ultracold quantum gas experiments focused primarily on statistical ensemble measurements, the recently introduced single atom–single lattice site imaging technique in a quantum gas microscope (*4*) opens the door for probing and controlling quantum gases on a microscopic level. Here, we present a microscopic study of an atom-lattice system that realizes the bosonic Hubbard model and exhibits a quantum phase transition from a superfluid to a Mott insulator (*5*–*7*).

In the weakly interacting superfluid regime, the many-body wave function factorizes into a product of states with well-defined phase on each lattice site, known as coherent states, with Poissonian number fluctuations. As the strength of the interaction increases, the number distribution is narrowed, resulting in a fixed atom number state on each site deep in the Mott insulator regime. We study this change in the number statistics across the transition; these microscopic studies are complementary to previous experiments that have focused on measuring ensemble properties such as long-range phase coherence, excitation spectra, or compressibility (*7*–*9*). Local properties such as on-site number statistics (*10*) had been accessible only indirectly (*8*, *11*, *12*) and were averaged over several shells of superfluid and Mott insulating domains in the inhomogeneous system, complicating quantitative interpretation. More recently, the shell structure was imaged through tomographic (*13*), spectroscopic (*14*), and in situ imaging techniques, coarse-grained over several lattice sites (*15*).

We started with a two-dimensional (2D) ^{87}Rb Bose-Einstein condensate of a few thousand atoms confined in a single well of a standing wave, with a harmonic oscillator length of 130 nm (*16*). The condensate resided 9 μm from an in-vacuum lens that was part of an imaging system with a resolution of ~600 nm. This high-resolution system

[1]Department of Physics, Harvard University, Cambridge, MA 02138, USA. [2]Institut für Physik, Ludwig-Maximilians-Universität, 80799 München, Germany.

*To whom correspondence should be addressed. E-mail: greiner@physics.harvard.edu

was used to project a square lattice potential onto the pancake cloud with a periodicity of a = 680 nm, as described in (4). The lattice depth was ramped exponentially with a time constant of 81 ms up to a maximum depth of $16E_r$, where E_r is the recoil energy of the effective lattice wavelength given by $h^2/8ma^2$ (where m is the mass of ^{87}Rb and h is Planck's constant). In a homogeneous system in two dimensions, the transition to a Mott insulator with one atom per site occurs at a ratio of interaction energy to tunneling rate of $U/J = 16.7$ (17–19), corresponding to a lattice depth of $12.2E_r$. During this ramp, the initial transverse confinement of 9.5 Hz was increased such that the cloud size remained approximately constant. After preparing the many-body state, we imaged the atoms by increasing the lattice depth by a factor of several hundred, and then illuminated the atoms with laser cooling light that served to localize the atoms while fluorescence photons were collected by high-resolution optics. As a result of the imaging process, the many-body wave function was projected onto number states on each lattice site. In addition, light-assisted collisions immediately ejected atoms in pairs from each lattice site, leaving behind an atom on a site only if its initial occupation was odd (20). The remaining atoms scattered several thousand photons during the exposure time and could be detected with high fidelity. By preparing the sample repeatedly under the same conditions, we deduced the probability p_{odd} of having an odd number of atoms on a site before the measurement.

For a coherent state on a lattice site with mean atom number λ, p_{odd} is given by ½[1 – exp(−2λ)] < ½. In a Mott-insulating region in the zero temperature and zero tunneling limit, $p_{odd} = 1$ for shells with an odd atom number per site, and $p_{odd} = 0$ for shells with an even atom number per site. Figure 1, A to D, shows fluorescence images in a region of the cloud as the final depth of the lattice is increased. The initial superfluid density was chosen to obtain an insulator with two shells on the Mott side of the transition; the region shown is in the outer shell containing one atom per site. For high filling fractions, the lattice sites in the images were barely resolved, but the known geometry of the lattice and imaging system point-spread function obtained from images at sparser fillings allowed reliable extraction of site occupations (16).

We used 24 images at each final lattice depth to determine p_{odd} for each site. The transverse confining potential varied slowly relative to the lattice spacing, and the system was, to a good approximation, locally homogeneous. We made use of this to improve the error in our determination of p_{odd} by averaging over a group of lattice sites—in this case, 51 sites for regions in the first shell and 30 sites for regions in the second shell (Fig. 1E). In the $n = 1$ shell, we detected an atom on a site with probability 94.9 ± 0.7% at a lattice depth of $16E_r$. We measured the lifetime of the gas in the imaging lattice and determined that 1.75 ± 0.02% of the occupied sites were detected as unoccupied, as a result of atoms lost during the imaging exposure time (1 s) because of background gas collisions. The average occupation numbers and error bars shown in Fig. 1E include corrections for this effect.

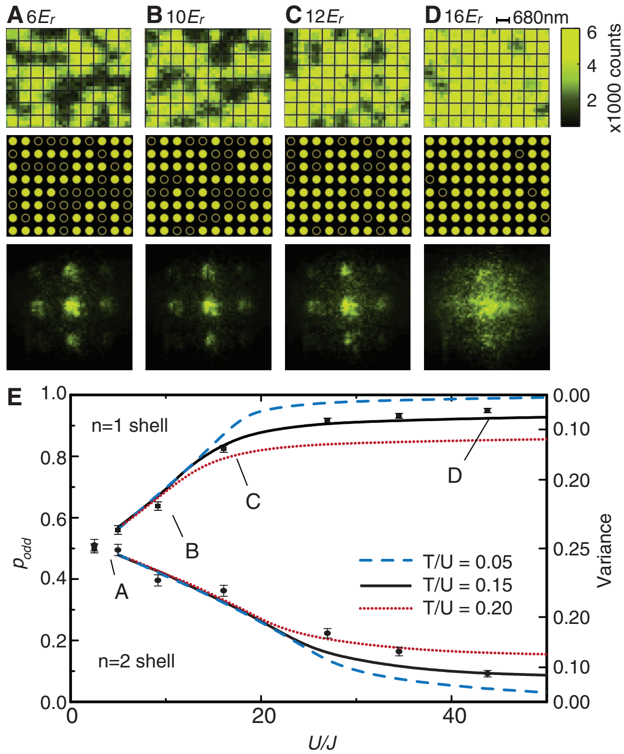

Fig. 1. Single-site imaging of atom number fluctuations across the superfluid–Mott insulator transition. (**A** to **D**) Images within each column are taken at the same final 2D lattice depth of $6E_r$ (A), $10E_r$ (B), $12E_r$ (C), and $16E_r$ (D). Top row: In situ fluorescence images from a region of 10 × 8 lattice sites within the $n = 1$ Mott shell that forms in a deep lattice. In the superfluid regime [(A) and (B)], sites can be occupied with odd or even atom numbers, which appear as full or empty sites, respectively, in the images. In the Mott insulator, occupancies other than 1 are highly suppressed (D). Middle row: results of the atom detection algorithm (16) for images in the top row. Solid and open circles indicate the presence and absence, respectively, of an atom on a site. Bottom row: Time-of-flight fluorescence images after 8-ms expansion of the cloud in the 2D plane as a result of nonadiabatically turning off the lattice and the transverse confinement (averaged over five shots and binned over 5 × 5 lattice sites). (**E**) Measured value of p_{odd} versus the interaction-to-tunneling ratio U/J. Data sets, with 1σ error bars, are shown for regions that form part of the $n = 1$ (squares) and $n = 2$ (circles) Mott shells in a deep lattice. The lines are based on finite-temperature Monte Carlo simulations in a homogeneous system at constant temperature-to-interaction ratio (T/U) of 0.20 (dotted red line), 0.15 (solid black line), and 0.05 (dashed blue line). The axis on the right is the corresponding odd-even variance given by $p_{odd}(1 - p_{odd})$.

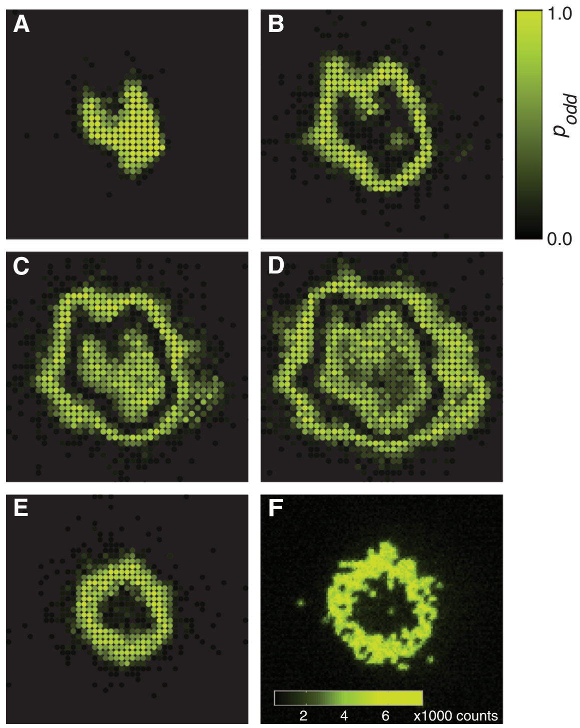

Fig. 2. Single-site imaging of the shell structure in a Mott insulator. (**A** to **D**) The images show p_{odd} on each site determined by averaging 20 analyzed fluorescence images. The lattice depth is $22E_r$ and the transverse confinement is 45 Hz. As the atom number is increased, the number of shells in the insulator increases from one to four. The value of p_{odd} for odd-numbered shells is close to 1; for even-numbered shells, it is close to 0. The atom numbers, determined by in situ imaging of clouds expanded in the plane, are 120 ± 10 (A), 460 ± 20 (B), 870 ± 40 (C), and 1350 ± 70 (D). (**E** and **F**) Long-wavelength disorder can be corrected by projecting an appropriate compensation light pattern onto the atoms, resulting in nearly circular shells. (E) p_{odd} (average of 20 analyzed images); (F) a single-shot raw image (arbitrary units).

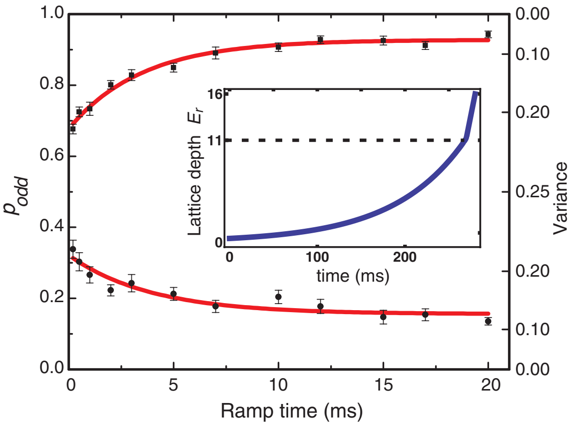

Fig. 3. Dynamics of on-site number statistics for a fast ramp from the superfluid regime to the Mott regime. p_{odd} at the end of the ramp versus ramp time is shown in the $n = 1$ (squares) and $n = 2$ (circles) shells, averaged over 19 data sets with 1σ error bars. Red lines are exponential fits. Inset shows the two-part ramp used in this experiment. The first part is a fixed adiabatic exponential ramp (t = 81 ms) and the second is a linear ramp starting at $11E_r$ and ending at $16E_r$. The duration of the second ramp is varied in the experiment.

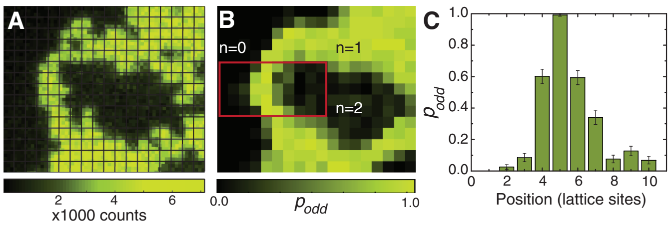

Fig. 4. Low-entropy Mott domains observed in a steep potential gradient. (**A**) Single-shot in situ image of a Mott insulator in a $16E_r$ deep lattice with 25-Hz transverse confinement. The ring is an n = 1 insulator enclosing an n = 2 region. (**B**) Average p_{odd} over 24 images. Each pixel corresponds to a single lattice site. The red rectangle encloses a region containing a Mott insulator with n = 1, a few lattice sites wide. (**C**) Column average of p_{odd} over the sites within the red rectangle in (B), with 1σ error bars.

Measuring the defect density in the Mott insulator provides sensitive local thermometry deep in the Mott regime. Thermometry in the Mott state has been a long-standing experimental challenge (*21*, *22*) and has acquired greater importance as experiments approach the regime of quantum magnetism (*23*–*25*), where the temperature scale should be on the order of the superexchange interaction energy. Our method directly images the excitations of the n = 1 Mott insulator, holes and doublons, because they both appear as missing atoms in the images. Similarly, for Mott insulators with higher fillings n, sites with excitations (n + 1, n − 1) can be detected through their opposite-parity signal. For a finite tunneling rate J much smaller than the interaction energy U, the admixture fraction of coherent hole-doublon pair excitations is $\sim(J/U)^2$, whereas any other excitations are due to incoherent thermal fluctuations and are suppressed by a Boltzmann factor, exp($-U/T$).

The theory curves presented in Fig. 1E are the predicted p_{odd} in the two shells for different values of T/U. The curves were obtained using a quantum Monte Carlo "worm" algorithm (*26*, *27*), and the average temperature extracted using the data points at the three highest U/J ratios was $T/U \approx 0.16 \pm 0.03$. At the transition point for n = 1, this corresponds to a temperature of 1.8 nK. Assuming this value of T/U to be the overall temperature, the thin layer between the Mott shells should be superfluid, and the transition to a normal gas is expected around a critical temperature of zJ = 2.8 nK, where z is the number of nearest neighbors in the lattice (*28*).

Next, we studied the global structure of the Mott insulator. The high-resolution images provide an atom-by-atom picture of the concentric shell structure, including the transition layers between the insulating shells. In Fig. 2, A to D, the formation of the various shells, up to the fourth, is shown as the atom number in the trap is increased. Slowly varying optical potential disorder causes deviation from circular symmetry in the shells. The contour lines of the potential are directly seen in the images in Fig. 2. In Fig. 2, E and F, we compensated for this disorder by projecting a light pattern, generated using a digital micromirror device, through the objective (*16*), resulting in a nearly circular shell structure.

In a second series of experiments, we used on-site number statistics to probe the adiabaticity time scale for the transition, focusing on the local dynamics responsible for narrowing the number distribution. We started by increasing the lattice depth adiabatically to $11E_r$, still in the superfluid regime, using the same ramp described previously. Next, the depth was ramped linearly to $16E_r$, where, for an adiabatic ramp, a Mott insulator should form. The ramp time was varied from 0.2 to 20 ms, and p_{odd} was measured in the first and second shells as before (Fig. 3). We found that the data fit well to exponential curves that asymptotically approach the value of p_{odd} obtained in the adiabatic case. The fitted time constant in the first shell is 3.5 ± 0.5 ms; in the second shell, the constant is 3.9 ± 1.3 ms.

Relative to the critical value of the tunneling time h/J_c = 68 ms for the first shell, the observed dynamics were counterintuitively fast. This can be understood by using a simple picture of two atoms in a double well. In this system, as the tunneling is varied, the minimal gap between the ground state and the first excited state is U, which sets the adiabaticity time scale. It is an open question whether this argument can be generalized to a lattice. In an infinite system, the appearance of Goldstone modes in the superfluid regime leads to a vanishing gap at the transition point, but the density of states is low for energies much less than U (*29*). In fact, the 1/e time scale observed experimentally is comparable to h/U_c = 4.1 ms, where U_c is the critical interaction energy for an n = 1 insulator.

Although the local number statistics change on a fast time scale of h/U, entropy redistribution in the inhomogeneous potential should occur on a much slower time scale of h/J. Because superfluid and normal domains have a larger specific heat capacity than Mott domains, in an inhomogeneous system, entropy is expelled from the Mott domains and accumulates in the transition regions after crossing the phase transition if the system is in thermal equilibrium (*30*). However, in bulk Mott regions, the insulating behavior makes entropy transport difficult, and global thermalization is slow on experimental time scales (*31*). In our system, optical potential corrugations produce sizable potential gradients in some regions, leading to a heterostructure of almost 1D Mott domains, about one to two lattice sites thick, surrounded by transition layers (Fig. 4). We found remarkably low defect densities and sharp transitions between superfluid and Mott states in these regions. The measured defect probability per site in the domain shown is 0.8 ± 0.8%. In these microscopic domains, each site of a Mott domain is in contact with a superfluid region. Such a configuration is likely to lead to fast thermalization, which would explain the low defect density we observed. This suggests that the lowest entropies in a Mott insulator might be obtained under conditions where the chemical potential is engineered so as to obtain alternating stripes (2D) or layers (3D) of insulating and superfluid regions (*32*, *19*).

In addition to the number statistics studied in this work, single-site imaging could be applied to study spatial correlations in strongly correlated quantum gases (*33*), and to directly measure entanglement in a quantum information context. The low-defect Mott states we detect would provide an ideal starting point for quantum magnetism experiments; if the low entropy in the Mott domains can be carried over to spin models, it should be possible to realize magnetically ordered states such as antiferromagnets, which could be directly detected with single-site imaging.

References and Notes

1. K. M. Lang *et al.*, *Nature* **415**, 412 (2002).
2. T. Basché, W. E. Moerner, M. Orrit, U. P. Wild, *Single-Molecule Optical Detection, Imaging and Spectroscopy* (Wiley-VCH, Cambridge, 1997).
3. X. Zhuang *et al.*, *Science* **288**, 2048 (2000).

4. W. S. Bakr, J. I. Gillen, A. Peng, S. Fölling, M. Greiner, *Nature* **462**, 74 (2009).
5. M. P. A. Fisher, P. B. Weichman, G. Grinstein, D. S. Fisher, *Phys. Rev. B* **40**, 546 (1989).
6. D. Jaksch, C. Bruder, J. I. Cirac, C. W. Gardiner, P. Zoller, *Phys. Rev. Lett.* **81**, 3108 (1998).
7. M. Greiner, O. Mandel, T. Esslinger, T. W. Hänsch, I. Bloch, *Nature* **415**, 39 (2002).
8. R. Jördens, N. Strohmaier, K. Günter, H. Moritz, T. Esslinger, *Nature* **455**, 204 (2008).
9. U. Schneider *et al.*, *Science* **322**, 1520 (2008).
10. B. Capogrosso-Sansone, E. Kozik, N. Prokof'ev, B. Svistunov, *Phys. Rev. A* **75**, 013619 (2007).
11. M. Greiner, O. Mandel, T. W. Hänsch, I. Bloch, *Nature* **419**, 51 (2002).
12. F. Gerbier, S. Fölling, A. Widera, O. Mandel, I. Bloch, *Phys. Rev. Lett.* **96**, 090401 (2006).
13. S. Fölling, A. Widera, T. Müller, F. Gerbier, I. Bloch, *Phys. Rev. Lett.* **97**, 060403 (2006).
14. G. K. Campbell *et al.*, *Science* **313**, 649 (2006).
15. N. Gemelke, X. Zhang, C. L. Hung, C. Chin, *Nature* **460**, 995 (2009).
16. See supporting material on *Science* Online.
17. M. Köhl, H. Moritz, T. Stöferle, C. Schori, T. Esslinger, *J. Low Temp. Phys.* **138**, 635 (2005).
18. I. B. Spielman, W. D. Phillips, J. V. Porto, *Phys. Rev. Lett.* **98**, 080404 (2007).
19. B. Capogrosso-Sansone, Ş. Söyler, N. Prokof'ev, B. Svistunov, *Phys. Rev. A* **77**, 015602 (2008).
20. M. T. DePue, C. McCormick, S. L. Winoto, S. Oliver, D. S. Weiss, *Phys. Rev. Lett.* **82**, 2262 (1999).
21. D. M. Weld *et al.*, *Phys. Rev. Lett.* **103**, 245301 (2009).
22. S. Trotzky *et al.*, http://arxiv.org/abs/0905.4882 (2009).
23. L. M. Duan, E. Demler, M. D. Lukin, *Phys. Rev. Lett.* **91**, 090402 (2003).
24. E. Altman, W. Hofstetter, E. Demler, M. D. Lukin, *N. J. Phys.* **5**, 113 (2003).
25. S. Trotzky *et al.*, *Science* **319**, 295 (2008).
26. N. V. Prokof'ev, B. V. Svistunov, I. S. Tupitsyn, *Phys. Lett. A* **238**, 253 (1998).
27. L. Pollet, K. V. Houcke, S. M. Rombouts, *J. Comput. Phys.* **225**, 2249 (2007).
28. F. Gerbier, *Phys. Rev. Lett.* **99**, 120405 (2007).
29. M. Knap, E. Arrigoni, W. von der Linden, *Phys. Rev. B* **81**, 024301 (2010).
30. L. Pollet, C. Kollath, K. Van Houcke, M. Troyer, *N. J. Phys.* **10**, 065001 (2008).
31. C. L. Hung, X. Zhang, N. Gemelke, C. Chin, *Phys. Rev. Lett.* **104**, 160403 (2010).
32. M. Popp, J. Garcia-Ripoll, K. G. Vollbrecht, J. I. Cirac, *Phys. Rev. A* **74**, 013622 (2006).
33. E. Kapit, E. Mueller, http://arxiv.org/abs/1004.4903 (2010).
34. We thank G. Jotzu, E. Demler, D. Pekker, B. Wunsch, T. Kitagawa, E. Manousakis, W. Ketterle, and M. D. Lukin for stimulating discussions. Supported by a grant from the Army Research Office with funding from the Defense Advanced Research Projects Agency Optical Lattice Emulator program, and grants from Air Force Office of Scientific Research Multidisciplinary University Research Initiative, NSF, an Alfred P. Sloan Fellowship (M.G.), and the Swiss National Science Foundation. The simulations were run on the Brutus cluster at ETH Zürich.

Supporting Online Material
www.sciencemag.org/cgi/content/full/science.1192368/DC1
Materials and Methods
References

17 May 2010; accepted 8 June 2010
Published online 17 June 2010;
10.1126/science.1192368
Include this information when citing this paper.

Ultrathin PbS Sheets by Two-Dimensional Oriented Attachment

Constanze Schliehe,[1] Beatriz H. Juarez,[2] Marie Pelletier,[1] Sebastian Jander,[1] Denis Greshnykh,[1] Mona Nagel,[1] Andreas Meyer,[1] Stephan Foerster,[1] Andreas Kornowski,[1] Christian Klinke,[1] Horst Weller[1]*

Controlling anisotropy is a key concept in the generation of complex functionality in advanced materials. For this concept, oriented attachment of nanocrystal building blocks, a self-assembly of particles into larger single-crystalline objects, is one of the most promising approaches in nanotechnology. We report here the two-dimensional oriented attachment of lead sulfide (PbS) nanocrystals into ultrathin single-crystal sheets with dimensions on the micrometer scale. We found that this process is initiated by cosolvents, which alter nucleation and growth rates during the primary nanocrystal formation, and is finally driven by dense packing of oleic acid ligands on {100} facets of PbS. The obtained nanosheets can be readily integrated in a photodetector device without further treatment.

Controlled assembly leading to anisotropic nanostructures poses a conceptual challenge in the field of materials research. Penn and Banfield *et al.* (*1*, *2*) described crystal growth, in which oxide nanoparticles coalesce in well-defined crystalline orientations. Their method of oriented attachment of nanocrystals is now one of the most favorable techniques to grow linear or zig-zag–type one-dimensional (1D) nanostructures. In addition to strong size-quantization effects occurring in these structures, their big advantage is solution processability, which makes them attractive candidates for optoelectronic and thermoelectric applications in low-cost integrated systems. 1D assemblies of oriented attachment have been reported, and, in most cases, the anisotropy during self-assembly is caused by crystal planes with preferred reactivity and dipole moments in the crystallites. However, systems with cubic-crystal symmetry (such as PbS and PbSe), in which beautiful 1D oriented attachment occurs, are somewhat more difficult to explain. Oriented attachment, in this case, should result in 3D networks rather than 1D structures. The common explanation assumes that, despite the strict monodispersity of the samples, inhomogeneities in the chemical composition of surface planes exist and result in dipole moments within the nanocrystals. On the other hand, organic ligand molecules play a crucial role in such processes by capping nanoparticle surfaces selectively and may hinder, modify, or trigger an oriented attachment (*3*). In this work, we show that the formation of ordered and densely packed ligand surface layers of oleic acid on {100} PbS surfaces can drive the normally isotropic crystal growths into a 2D oriented attachment of nanocrystals. In addition, the presence of chlorine-containing cosolvents during the initial nucleation and growth process of the nanocrystals plays a prominent role.

[1]Institute of Physical Chemistry, University of Hamburg, 20146 Hamburg, Germany. [2]IMDEA Nanoscience, Ciudad Universitaria de Cantoblanco 28049, Madrid, Spain.

*To whom correspondence should be addressed. E-mail: weller@chemie.uni-hamburg.de

Syntheses of lead chalcogenide nanoparticles (*4*–*7*) can lead to a large variety of particle shapes through slight changes of the reaction conditions. The mechanism of how small traces of organophosphine compounds may alter the course of the reactions has been reported, which underlines their complexity (*8*). For other systems, like CdS nanoparticles, shape control has been reported by the addition of small amounts of HCl (*9*) or chlorine-containing solvents such as 1,2-dichloroethane (DCE); for example, in the case of CdSe nanorods attached to carbon nanotubes (*10*). Reported strategies to generate 2D nanostructures are based on the use of lamellar-like templates (*11*) or thin superstructures by assembly (*12*–*14*).

Our approach is based on a standard synthetic procedure to generate nearly spherical PbS nanoparticles (*15*). After 3 min, the resulting dotlike particles have a mean diameter of ~5 nm. In contrast, ultrathin PbS nanosheets, as depicted in Fig. 1, are formed in the presence of chlorine-containing compounds such as DCE or similar linear chloroalkanes (fig. S1). The nanosheets have lateral dimensions of several hundred nanometers and stack showing Moiré patterns caused by the interference between the crystalline lattices of the individual sheets (see fig. S2 for Moiré patterns and corresponding simulations).

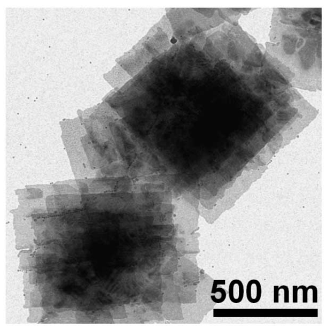

Fig. 1. TEM image of stacked PbS nanosheets using 1,1,2-trichloroethane.

The formation of the sheets occurs within the first 1 to 3 min of the reaction. To investigate the mechanism of formation, we followed the temporal evolution of the sheets by optical spectroscopy and high-resolution transmission electron microscopy (HRTEM). For practical reasons, we slowed down the sheet formation by reducing the reaction temperature to 70°C immediately after the thioacetamide injection [see the supporting online material (SOM)]. Figure 2A shows the absorption and emission spectra at various stages of the reaction. Within the first 50 s, the solution turned reddish brown, and clearly structured spectra evolved with an absorption maximum at 675 nm and a narrow emission band at 790 nm. These features indicate small, isolated quantum dots of 2.8 ± 0.5 nm, which can clearly be identified by TEM (fig. S3). As the reaction evolved, the fluorescence band of the quantum dots decreased, and an unstructured absorption of sheets arose, partially due to the occurrence of turbidity. However, the spectral position of the original bands, and, thus, the size of the particles, do not change during this process, proving that sheets are formed directly from the nanoparticles by oriented attachment. The growth of either ultrathin sheets or larger particles (in the absence of chlorine-containing compounds) is determined by the behavior of the PbS nanocrystals that originally formed.

Nanocrystals as small as 2.8 nm could not be isolated if DCE (or a similar chlorine-containing compound) was not added to the reaction mixture. A TEM sample taken during the rapid process of oriented attachment shows various stages of sheet formation. The original particles (Fig. 2B) can be recognized together with fused aggregates (Fig. 2C), as well as porous structures similar to the one shown in Fig. 2D. In Fig. 2B, in which an individual particle in a slightly tilted [100] orientation is depicted, an angle of 135° at the crystalline edges can be identified. This is taken as an indication of the presence of {110} surface planes. A reasonable model for such a small crystallite is shown in the inset of this figure. A close inspection of Fig. 2C identifies this structure as an aggregate of three nanocrystals fused in two dimensions. Even in the porous framework structure of Fig. 2D, the size and shape of the original particles, as well as their crystalline orientation, is visible (figs. S4 to S6). Uniform nanosheets, however, can be obtained several minutes after the sulfur precursor injection (Fig. 2E; see SOM for synthetic details).

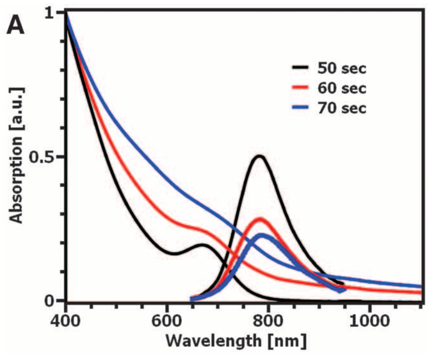

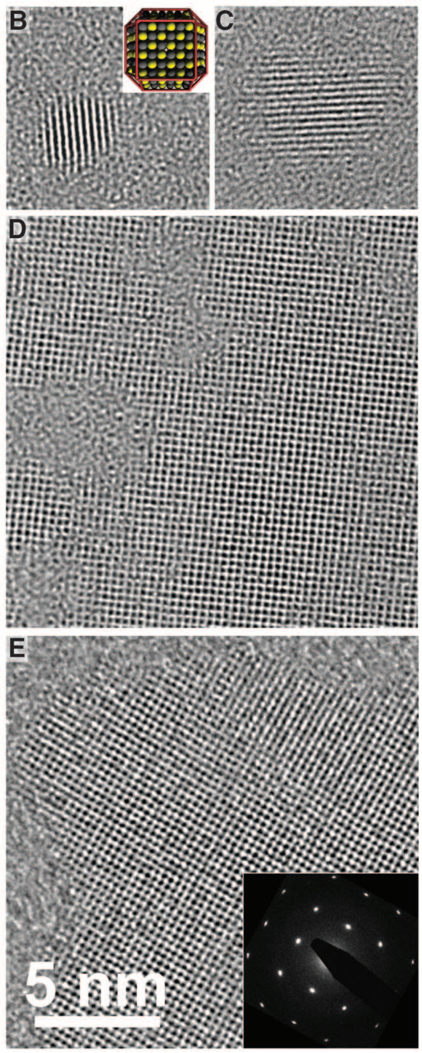

Fig. 2. (**A**) Absorption and emission spectra of the nanoparticles with reaction time. The absorption spectra were normalized to the absorption at 400 nm, and the emission spectra to the maximum of each curve. a.u., arbitrary units. (**B**) TEM image of an ultrasmall PbS nanoparticle at early stages of the reaction. (Inset) Model structure of a truncated cuboctahedron. (**C**) First step of attachment. (**D**) Later, the structures merge with some holes due to nonideal attachment. (**E**) At the end of the synthesis, quasi-continuous sheets are formed. (Inset) Electron diffraction pattern of the PbS sheets.

The HRTEM image of a sheet region depicted in Fig. 2E shows a single-crystalline structure with crossed (200) lattice planes displaying an angle of 45° relative to the sheet edges. This indicates a sheet growth parallel to the <110> axes. Although most of their edges in <110> directions are atomically flat over large distances, some regions clearly show a zig-zag pattern with exposed {100} facets with dimensions corresponding to those of the original quantum dots. Selected-area electron diffraction pattern of individual sheets confirms this observation, showing a monocrystalline galena structure in [100] orientation with pronounced (200) and (220) reflexes. The x-ray diffraction pattern shows that the HRTEM characterization of individual sheets is representative of the entire sample (fig. S8).

In the crystalline-equivalent PbSe and PbTe systems, Murray *et al.* discovered that truncated cubes with sizes of ~10 nm evolve from ~5-nm cuboctahedrons with six {100} and eight {111} facets. They explained this result by a faster growth-rate perpendicular to the {111} facets (*16*, *17*). Their findings also suggest that {110} facets are highly reactive and, therefore, are preferentially consumed during the nanoparticle growth. The structure of PbS nanocrystals that merge into PbS sheets is shown in Fig. 3. The shape is that of a truncated cuboctahedron with 6 {100}, 8 {111}, and 12 {110} facets. Upon crystal growth, the particles try to minimize the most energetically unfavorable surface facets by fast growth perpendicular to the respective facet. In the case of PbS particles larger than 10 nm (*18*), this results in truncated cubes with mainly {100} surface planes (path A in Fig. 3). We do not observe the formation of PbS sheets in the absence of DCE (or a similar chloride compound), whereas in the presence of chloride compounds, which are known to act as lead complexing agents (*19*), the kinetics of nucleation and growth are altered, leading to ~3-nm particles (as shown in Fig. 2B), which should still exhibit the reactive {110} surfaces. Because

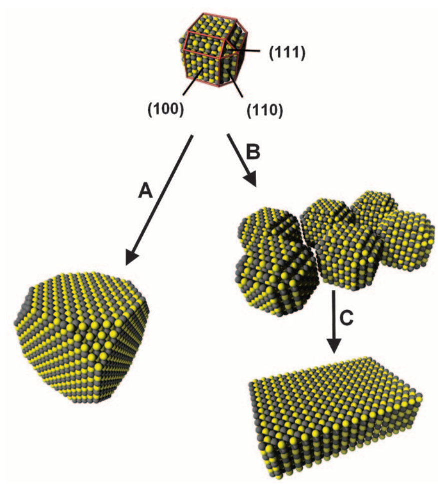

Fig. 3. Schematic illustration of large-particle (**A**) and sheet formation (**B** and **C**) from small PbS quantum dots.

Ostwald ripening plays only a negligible role during PbS nanoparticle formation, these small crystallites stabilize by oriented attachment via the {110} facets (path B in Fig. 3). The expected egg tray–like structure is unlikely to be stable and will undergo a surface reconstruction (path C in Fig. 3), resulting in a flat sheet (Fig. 2E). The ensuing sheet should be thinner than the original building blocks by up to 30%. This reconstruction, understood as the diffusion and accommodation of the atoms under favorable thermodynamic conditions (100°C), also contributes to a decrease in the porosity of the sheets. We performed small-angle x-ray scattering (SAXS) of the stacked PbS layers (Fig. 4). The sample was positioned in a coplanar configuration with the SAXS beam to obtain information about the sheet thickness and orientational distribution. A highly anisotropic dumbbell-type scattering pattern characteristic for sheets oriented nearly parallel to the q_x direction can be seen in the upper-left inset of Fig. 4. The best simulation fit was calculated assuming a regular stacking of disks with a long period of 5.8 nm and PbS sheet thickness of 2.2 nm. The resultant distance between the sheets of 3.6 nm is attributed to an oleic acid bilayer. This behavior strongly supports the notion of an interplanar crystalline oleic acid bilayer, which is not interpretable by randomly coiled and interpenetrating chains. The formation of the stacked layers occurs most probably by an attachment of quantum dots or small-sheet structures on top of already formed nanosheets, which then act as a nucleus for further 2D attachment. The stacked structure can also be observed by atomic force microscopy (fig. S9).

One question remains, however, as to why oriented attachment leads to 2D structures rather than 3D structures. Our results strongly support the idea that the assembly of oleic acid in a highly ordered monolayer on the {100} surfaces plays a key role in the formation and further stacking of PbS sheets. Oleic acid is well known to assemble vertically on various substrates and to form bilayer structures (*20–22*). The thickness of a monolayer was determined from single-crystal data and ranges from 1.7 to 2.4 nm in the reported crystal structures. The latter mainly varies by the conformation next to the double bond and the relative orientation of the oleic acids within one monolayer. These reported values fit well with the observed interplanar distance of 3.6 nm in stacked sheets. The formation of a dense and highly ordered oleic acid layer covering the PbS nanosheets also allows the system to bind a maximum number of oleic acid molecules. The resulting release of adsorption enthalpy, combined with the stabilization by interalkyl van der Waals forces, obviously overcompensates for the decrease in entropy and results in a net release of Gibbs energy. The 2D oriented attachment and the reconstruction from the egg-tray structure to flat sheets would, from this point of view, not only be driven by minimizing high-energy surfaces, but also by structural changes caused by the oleic acid molecules. Whereas one expects the ligands to exist in a randomly coiled state on the highly curved surface of small particles, they instead appear in a highly ordered phase on the flat {100} planes. In general, we believe that similar effects may hold in shape control, self-assembly, and templated growth of nanocrystals. For example, ligand-driven self-assembly of nanocrystals into aggregated wires (1D) and vesicles (curved 2D) was recently observed for amphiphilic CdSe quantum dots (*23*).

The thin-film structure of the sheets should decisively affect the quantum confinement of photogenerated carriers. In accordance with the reported dimensions, no confinement is expected in the lateral direction, whereas the structures should be strongly confined vertically. Differences in layer thickness and confinement in one dimension may strongly influence the optical features. Correlated confocal microscopy and TEM inspections (fig. S10) confirm this assumption by showing an emission signal coming from two different individual stacks of PbS sheets at a wavelength of ~720 nm.

Nanoparticle arrays are currently in the spotlight for low-cost device fabrication, like photodetectors (*24–29*). Typical 2D assemblies require physical or chemical treatments to remove the insulating organic shell capping. The lack of ligands in the in-plane dimensions of raw PbS 2D sheets produces intrinsically outstanding photoconductive properties, as shown in Fig. 5. PbS sheets bridging two gold electrodes on a SiO_2 substrate exhibit low, dark conductance between ±0.1 V without substantial hysteresis. Upon illumination with a 532-nm laser, however, the conductance increases by more than two orders of magnitude at an illumination intensity of 2.0 mW/cm^2. This yields an efficiency value (actual photocurrent divided by the theoretical maximum current due to photon impact) of ~1.1 at 0.1 V (which corresponds to a responsivity of 0.472 A/W). Taking into account that the number of absorbed photons is only a small fraction of the incident, this value shows that the increase in current cannot be due to harvesting of photogenerated charge carriers only. The filling of trap states is most probably responsible for the current gain. In contrast to currently investigated devices made from ligand-stabilized PbS nanocrystals, the ready-made, nontreated nanosheets reported here are remarkably conductive due to missing in-plane ligands and continuous connection through the monocrystal.

We have shown that chlorine-containing cosolvents can direct the colloidal synthesis of PbS nanoparticles into 2D nanosheets by oriented attachment. We believe that this is a consequence of the size of the nanoparticles and, hence, the

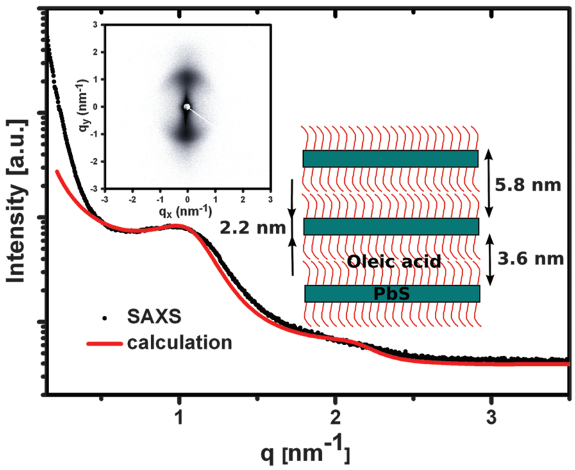

Fig. 4. Cross section of the scattering intensity along the q_y axis (black points) and simulated diffraction curve (red). The scattering image is depicted in the upper-left inset. The highly anisotropic dumbbell-type scattering pattern is characteristic for sheets oriented nearly parallel to the q_x direction. The result could be modeled with assumed disks of 2.2-nm thickness and a spacing ligand of 3.6 nm, as depicted in the lower-right diagram.

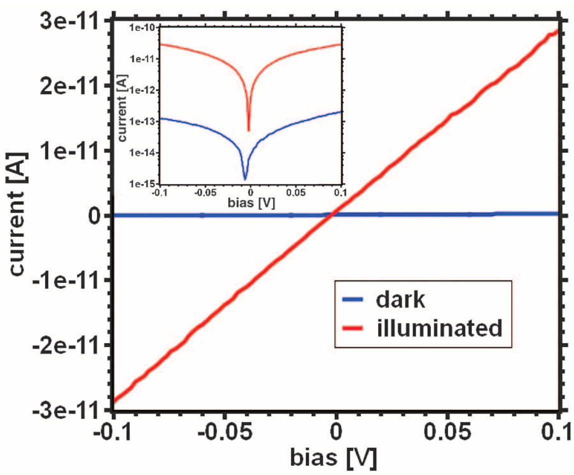

Fig. 5. Current-voltage curves of PbS sheets with (red) and without (blue) illumination with a green laser. The thin film of stacks of PbS sheets covers a detection area of 0.5 by 6 μm between two gold electrodes. (**Inset**) Current-voltage curves on logarithmic scale.

presence of {110} reactive facets, which disappear as the nanoparticles grow. The presence of DCE or similar chlorine-containing compounds yields small nanoparticles of ~3 nm in diameter, exposing the highly reactive {110} facets so as to trigger an oriented-attachment process. Both the oriented attachment and the strong crystalline correlation between the nanosheets in stacked aggregates are most likely driven by the formation of a highly ordered oleic acid bilayer between the PbS nanosheets. The absence of ligands in the in-plane direction of the ultrathin sheets yields a prominent photoconductivity response in the pristine dried nanomaterial.

References and Notes

1. R. L. Penn, J. F. Banfield, *Science* **281**, 969 (1998).
2. J. F. Banfield, S. A. Welch, H. Zhang, T. T. Ebert, R. L. Penn, *Science* **289**, 751 (2000).
3. J. Polleux, N. Pinna, M. Antonietti, M. Niederberger, *Adv. Mater.* **16**, 436 (2004).
4. Y. W. Jun, J. S. Choi, J. Cheon, *Angew. Chem. Int. Ed.* **21**, 3414 (2006).
5. A. J. Houtepen *et al.*, *J. Am. Chem. Soc.* **128**, 6792 (2006).
6. E. Lifshitz *et al.*, *Nano Lett.* **3**, 857 (2003).
7. T. L. Mokari, M. J. Zhang, P. D. Yang, *J. Am. Chem. Soc.* **129**, 9864 (2007).
8. J. S. Steckel, B. K. H. Yen, D. C. Oertel, M. G. Bawendi, *J. Am. Chem. Soc.* **128**, 13032 (2006).
9. K. T. Yong, Y. Sahoo, M. T. Swihart, P. N. Prasad, *J. Phys. Chem. C* **111**, 2447 (2007).
10. B. H. Juárez *et al.*, *J. Am. Chem. Soc.* **130**, 15282 (2008).
11. J. S. Son *et al.*, *Angew. Chem. Int. Ed.* **48**, 6861 (2009).
12. Z. Y. Tang, Z. Zhang, Y. Wang, S. C. Glotzer, N. A. Kotov, *Science* **314**, 274 (2006).
13. H. G. Yang, H. C. Zeng, *Angew. Chem. Int. Ed.* **43**, 5930 (2004).
14. Z. Huo *et al.*, *Nano Lett.* **9**, 1260 (2009).
15. M. Nagel, G. S. Hickey, A. Frömsdorf, A. Kornowski, H. Weller, *Z. Phys. Chem.* **221**, 427 (2007).
16. K. S. Cho, D. V. Talapin, W. Gaschler, C. B. Murray, *J. Am. Chem. Soc.* **127**, 7140 (2005).
17. J. J. Urban, D. V. Talapin, E. V. Shevchenko, C. B. Murray, *J. Am. Chem. Soc.* **128**, 3248 (2006).
18. T. Duan, W. Lou, X. Wang, Q. Xue, *Colloids Surf. A Physicochem. Eng. Asp.* **310**, 86 (2007).
19. E. Capek, K. E. Schwarzhans, *Monatsh. Chem.* **118**, 419 (1987).
20. F. Kaneko *et al.*, *J. Phys. Chem. B* **101**, 1803 (1997).
21. S. R. Craig *et al.*, *J. Cryst. Growth* **128**, 1263 (1993).
22. S. Abrahamsson, I. Ryderstedt-Nahringbauer, *Acta Crystallogr.* **15**, 1261 (1962).
23. M. S. Nikolic *et al.*, *Angew. Chem. Int. Ed.* **48**, 2752 (2009).
24. D. V. Talapin, C. B. Murray, *Science* **310**, 86 (2005).
25. J. M. Luther *et al.*, *ACS Nano* **2**, 271 (2008).
26. M. V. Kovalenko, M. Scheele, D. V. Talapin, *Science* **324**, 1417 (2009).
27. K. Szendrei *et al.*, *Adv. Mater.* **21**, 683 (2009).
28. T. S. Mentzel *et al.*, *Phys. Rev. B* **77**, 075316 (2008).
29. G. Konstantanos *et al.*, *Nature* **442**, 180 (2005).

30. B.H.J. thanks the European Commission for grant ERG FP7-PEOPLE-ERG-2008 and the Spanish Ministry of Science and Innovation for grant RYC-2007-01709.

Supporting Online Material
www.sciencemag.org/cgi/content/full/329/5991/550/DC1
Materials and Methods
Figs. S1 to S11
References

8 February 2010; accepted 30 June 2010
10.1126/science.1188035

Steric Effects in the Chemisorption of Vibrationally Excited Methane on Ni(100)

Bruce L. Yoder, Régis Bisson, Rainer D. Beck*

Newly available, powerful infrared laser sources enable the preparation of intense molecular beams of quantum-state prepared and aligned molecules for gas/surface reaction dynamics experiments. We present a stereodynamics study of the chemisorption of vibrationally excited methane on the (100) surface of nickel. Using linearly polarized infrared excitation of the C-H stretch modes of two methane isotopologues [$CH_4(\nu_3)$ and $CD_3H(\nu_1)$], we aligned methane's angular momentum and vibrational transition dipole moment in the laboratory frame. An increase in methane reactivity of as much as 60% is observed when the laser polarization is parallel rather than normal to the surface. The dependence of the alignment effect on the rotational branch used for excitation indicates that alignment of the vibrational transition dipole moment of methane is responsible for the steric effect. Potential explanations for the steric effect in terms of an alignment-dependent reaction barrier height or electronically nonadiabatic effects are discussed.

The need to understand the dynamics of gas/surface reactions is driven by the critical role that these reactions play in many industrial processes, such as heterogeneous catalysis for molecular synthesis and chemical vapor deposition of thin films. Highly detailed state-resolved measurements are required to reveal the underlying microscopic dynamics and reaction mechanisms. Quantum-state–resolved data also enable stringent tests of theoretical models of gas/surface reactivity. The choice of methane chemisorption on a Ni surface as a model system is pragmatic, because C-H bond activation of this system is the rate-limiting step in steam reforming of CH_4 to produce industrial hydrogen and syngas, the starting material for the synthesis of many commercial compounds.

In the late 1970s, the use of molecular beams for reactivity measurements on single-crystal surfaces enabled the preparation of reactant molecules with well-defined translational energy and incident angle. Molecular beam studies clearly demonstrated that the translational energy of the incident CH_4 activates its chemisorption (*1*). Laser excitation of methane isotopologues to specific rovibrational quantum states (*2*–*4*) further refined the measurements, providing unequivocal evidence that the chemisorption is also activated by vibrational excitation of the incident methane molecule in a mode- (*5*) and bond-specific (*6*) manner that statistical models (*7*) fail to capture.

In the experiments described here, we move a step beyond quantum-state resolution, by exerting steric control over this gas/surface reaction. Excitation by linearly polarized infrared radiation prepares CH_4 in a single rovibrationally excited state with aligned angular momentum $\vec{J}$ and vibrational transition dipole moment $\vec{\mu}_{if}$ in the laboratory frame (*8*). The resulting aligned, state-prepared reactants are used to detect and

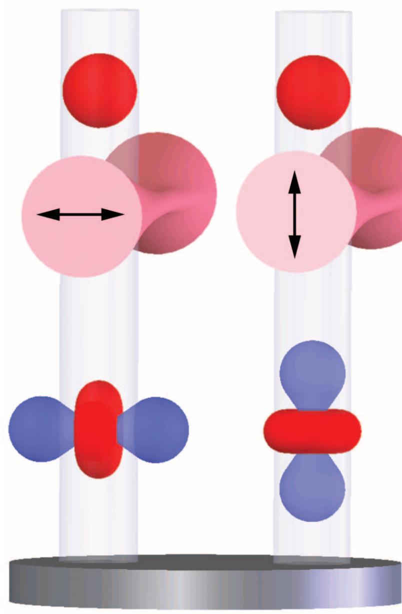

Fig. 1. Schematic of the state-prepared and laser-aligned molecular beam deposition experiment. A molecular beam of CH_4 with initially isotropic spatial distribution of angular momentum $\vec{J}$ (indicated by the red spheres at top) impinges on a Ni(100) surface at normal incidence. Before surface impact, the molecules traverse a continuous, linearly polarized laser beam focused in the direction of the molecular beam. Incident CH_4 is prepared in a specific rovibrationally excited state by rapid adiabatic passage (*16*) through the resonant laser beam. The resulting probability distributions for $\vec{J}$ (red) and vibrational transition dipole moment $\vec{\mu}_{if}$ (blue) are depicted for the case of R(0) excitation and two orthogonal polarization directions indicated by the double-headed arrows.

Laboratoire de Chimie Physique Moléculaire, Ecole Polytechnique Fédérale de Lausanne, Lausanne, Switzerland.

*To whom correspondence should be addressed. E-mail: rainer.beck@epfl.ch

quantify steric effects in the reaction of vibrationally excited methane isotopologues with a Ni(100) surface. Here, alignment refers to an anisotropic spatial distribution of $\vec{J}$ and $\vec{\mu}_{if}$ vectors, which is either preferentially parallel or perpendicular to a laboratory fixed axis such as the electric field vector $\vec{E}$ of the excitation laser. In contrast, orientation describes a preference in vectorial direction of $\vec{J}$ and $\vec{\mu}_{if}$ (i.e., parallel or antiparallel) relative to $\vec{E}$.

Polanyi highlighted the opportunity to study stereodynamics in surface reactions, given that a single-crystal surface represents a perfectly oriented reaction partner (*9*). What is needed to completely define the collision geometry in a gas/surface reaction is a method to orient or align incident molecules relative to the surface plane. Several techniques have been used to study alignment and orientation effects in gas/surface reactions, such as hexapole state-selection followed by reactant orientation in a static electric field (*10*, *11*), reactant alignment by resonance-enhanced multiphoton ionization (REMPI) by linearly polarized light (*12*), and collisional rotational alignment in supersonic jet expansions (*13*). Another method to obtain information about gas/surface stereodynamics is linearly polarized REMPI of molecules desorbing from a surface, coupled with analysis using the principle of detailed balance (*14*, *15*). Unfortunately, none of these techniques is applicable to CH_4.

In contrast to previous stereodynamical studies of gas/surface reactions, our experiments align molecules without permanent dipole moments and probe specifically the alignment-dependent reactivity of vibrationally excited neutral reactant molecules. We explore whether the reactivity of vibrationally excited CH_4 depends on the alignment of $\vec{J}$ and/or $\vec{\mu}_{if}$ relative to the surface plane, with the aim of elucidating the mechanism of the vibrationally mode-specific reactivity (*5*), which is not fully understood.

We performed the experiments in a surface science–molecular beam apparatus (*4*, *16*). First, we exposed the Ni(100) surface in two different locations to an identical dose of vibrationally excited $CH_4(\nu_3)$, prepared with one quantum of the antisymmetric C-H stretch vibration ν_3, via the R(0) transition at 3028.75 cm^{-1} but with different laser polarization directions (Fig. 1). Then, quantum-state–resolved reaction probabilities were measured using Auger electron spectroscopy detection of surface-bound C. Comparison of the detected amount of surface carbon (C) resulting from the two depositions indicated that the CH_4 reactivity is up to 60% higher for ν_3-R(0) excitation (Fig. 2, top) with the laser polarization parallel to the plane of the surface than for perpendicular polarization. The observed alignment effect was quantified by calculating the alignment contrast Δ_p

$$\Delta_p = \frac{S_0^{\parallel} - S_0^{\perp}}{S_0^{\parallel} + S_0^{\perp}} \qquad (1)$$

where $S_0^{\parallel}$ and $S_0^{\perp}$ are state-resolved initial reaction probabilities for the excited state of CH_4 prepared with laser polarization parallel and perpendicular to the surface plane, respectively. Based on nine repeated measurements, $\Delta_p = 0.216 \pm 0.016$ for excitation of the ν_3-R(0) transition of CH_4, with error limits of $\pm 2\sigma$ from the standard deviation of replicate measurements.

In order to ascertain whether the observed reactivity difference is due solely to alignment effects of the vibrationally excited CH_4, we performed the corresponding pair of depositions using excitation via the ν_3-P(1) transition, which produces no alignment of the excited molecules (*8*). In agreement with our interpretation, we observed no significant difference between the $CH_4(\nu_3)$ reactivity for parallel and perpendicular laser polarizations ($\Delta_p = 0.016 \pm 0.029$, four measurements) for excitation via the ν_3-P(1) transition (Fig. 2, middle). We verified that the detected C is formed exclusively by chemisorption of ν_3-excited CH_4 by repeating the deposition experiment with the excitation laser slightly detuned from the ν_3 resonance. With the laser off-resonance, no C signal was detectable on the surface where the molecular beam had impinged (Fig. 2, bottom). Corresponding measurements for ν_1-excited trideuteromethane, CD_3H, yielded $\Delta_p = 0.178 \pm 0.028$ for the ν_1-R(0) transition and $\Delta_p = 0.009 \pm 0.015$ for the ν_1-P(1) transition, where ν_1 is the C-H stretch normal mode of CD_3H with a band origin at 2993 cm^{-1}.

In our experimental setup, the homogeneous linewidths of the rovibrational transitions are dominated by transit time broadening to more than 1 MHz. Because the hyperfine splittings for CH_4 and CD_3H are in the range of 50 to 200 kHz, the laser coherently excites all hyperfine levels when the methane molecules pass through the excitation laser beam. After excitation at time $t = 0$, the interaction between methane's nuclear spin and $\vec{J}$ leads to a dephasing of the hyperfine components, which scrambles alignment created at $t = 0$ on a time scale of the inverse of methane's hyperfine splitting. By measuring Δ_p for excitation of the R(0) transition at distances between 1 and 30 mm from the target surface, we extracted a time scale for the $CH_4(\nu_3)$ hyperfine dephasing of ≈15 μs (fig. S2). Hyperfine depolarization was observed to be faster for CD_3H (≈5 μs) than for CH_4, which is in agreement with the larger splitting of CD_3H hyperfine levels (*8*). Extrapolation of the measured hyperfine decay of Δ_p toward $t = 0$ predicts an insignificant reduction for excitation at 1 mm from the surface, compared to a hypothetical preparation directly on the surface.

To explore the origin of the alignment dependence of the $CH_4(\nu_3)$ and $CD_3H(\nu_1)$ surface reactivity, we determined the alignment contrast Δ_p for excitation via R-, Q-, and P-branch transitions (fig. S3) and compared the experimental results to calculated alignment coefficients for angular momentum $A_0^{(2)}$ and vibrational transition dipole moment β_{axis}, using expressions given by Zare and others (*17*–*19*). Inspection of Fig. 3A shows a sign change for $A_0^{(2)}$ when switching from R- to Q-branch excitation, whereas the β_{axis} coefficients remain positive (Fig. 3B). The fact that

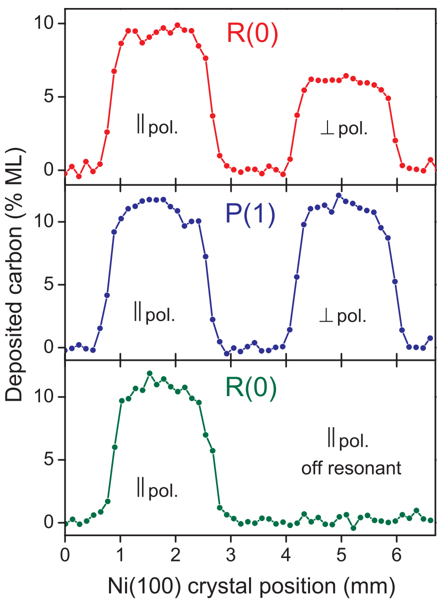

Fig. 2. Auger-detected C signal resulting from exposure of a clean Ni(100) surface to $CH_4(\nu_3)$ with translational energy of 34 kJ/mol, rovibrationally excited 1 mm upstream of the surface, irradiated with laser polarization parallel (II pol.) or perpendicular (⊥ pol.) to the surface plane. (**Top**) $CH_4(\nu_3)$ excited via R(0). (**Middle**) $CH_4(\nu_3)$ excited via P(1). (**Bottom**) $CH_4(\nu_3)$ excited via R(0) (left) and CH_4 irradiated by laser output detuned from resonance (right). Surface temperature is 473 K in all cases.

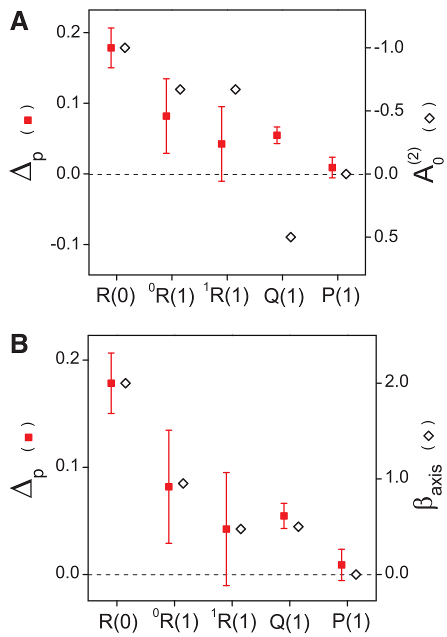

Fig. 3. Comparison of the observed alignment contrast Δ_p for $CD_3H(\nu_1 = 1)$ with (**A**) the angular momentum alignment coefficient $A_0^{(2)}$ and (**B**) the vibrational alignment coefficient β_{axis}. The vertical axes of the graphs are scaled so that their origins and the values associated with R(0) excitation coincide for Δ_p and $A_0^{(2)}$ in (A) and Δ_p and β_{axis} in (B). Error bars are $\pm 2\sigma$ from replicate measurements.

alignment contrasts Δ_p for $CD_3H(\nu_1)$ (Fig. 3) and $CH_4(\nu_3)$ (fig. S10) are positive for both R- and Q-branch transitions and scale with β_{axis} leads us to conclude that the observed reactivity enhancement is due to an alignment of the vibrational transition dipole moment $\vec{\mu}_{if}$ rather than the angular momentum $\vec{\mathbf{J}}$, which is similar to the findings of Simpson *et al*. for the reaction of vibrationally excited CH_4 and CD_3H with gas-phase Cl atoms (*8*).

To map out the polarization angle dependence of the alignment effect, we measured the reactivity for $CH_4(\nu_3)$ and $CD_3H(\nu_1)$ for R(0) excitation at several intermediate polarization angles, in addition to 0° (∥ pol) and 90° (⊥ pol). The results (figs. S11 and S12) show a continuous decrease in reactivity from the highest reactivity for parallel polarization to the lowest reactivity for perpendicular polarization for both $CH_4(\nu_3)$ and $CD_3H(\nu_1)$.

In dynamical stereochemistry, the preferred reactant bond alignment reflects the minimum energy path from reactants to products on the multidimensional potential energy surface (PES) via the reaction's transition state. For example, the state-resolved experiments of Hou *et al*. (*14*) imply a much higher reactivity for broadside than for end-on collisions of D_2 with Cu(111) at low collision energy, indicating an alignment-dependent barrier height for this reaction, with a minimum barrier occurring for a D-D bond alignment parallel to the surface. However, for CH_4 dissociation on transition metals, calculations of the transition state structure for the dissociation of CH_4 on Ni(100) (*20*–*22*) predict the dissociating C-H bond to be elongated and oriented toward the surface at nearly 45° from the surface normal and barrier heights ranging from 60 to 90 kJ/mol.

Excitation of the infrared-active C-H stretch fundamentals $CH_4(\nu_3)$ and $CD_3H(\nu_1)$ by linearly polarized light aligns the vibrational transition dipole moment; i.e., the net C-H stretch, preferentially along the laser polarization axis. For $CD_3H(\nu_1)$, where $\vec{\mu}_{if}$ is along the C-H bond axis, the excitation also aligns the C-H bond. Recent state-resolved experiments proved this reaction to be bond-specific by demonstrating that the excited C-H bond dissociates selectively in the chemisorption of $CD_3H(\nu_1)$ on Ni(111) (*6*).

In comparing the polarization direction leading to the highest reactivity of $CD_3H(\nu_1)$ on Ni(100) with the calculated transition state structure (*20*–*22*), one must consider that the laser excitation defines alignment and not orientation of the C-H bond in CD_3H. Excitation with ∥ polarization aligns the excited C-H bond preferentially parallel to the surface plane, whereas ⊥ polarization produces $CD_3H(\nu_1)$ with the C-H bond along the surface normal, but pointing either toward the surface or away from it. Our measurements therefore probe the average reactivity between the two orientations compatible with a given alignment direction. Such averaging could shift the maximum in the angle dependence away from the transition state angle and toward the parallel polarization direction if C-H orientations pointing away from the surface are nearly nonreactive and the variation in reactivity for C-H bond orientations toward the surface is small.

However, the observation of very similar polarization angle dependences for the reactivity of aligned $CD_3H(\nu_1)$ and $CH_4(\nu_3)$ with larger Δ_p values for $CH_4(\nu_3)$ is inconsistent with the idea that the polarization angle dependence reflects the transition state geometry of the reaction. $CH_4(\nu_3)$ has four identical C-H bonds with tetrahedral geometry that share the antisymmetric stretch excitation of the ν_3 normal mode. The reactivity of $CH_4(\nu_3)$ on Ni(100) should show a different polarization angle dependence and smaller Δ_p values than what is observed for $CD_3H(\nu_1)$ if the orientation of the vibrating C-H bond relative to the transition state geometry were to determine the enhancement. In fact, R(0) excitation by linearly polarized light prepares $CH_4(\nu_3)$ in a state with $J = 1$, $l = 1$, and $N = 0$ (*8*), where J, l, and N designate the total, vibrational, and rotational angular momentum, respectively. This state of $CH_4(\nu_3)$ is rotationless ($N = 0$); i.e., it is characterized by a spatially isotropic rotational wave function for which any orientation of the H atoms is equally probable. Classically, CH_4 in this state can be visualized as an ellipsoid vibrating along a principal axis, with the H atoms located on the ellipsoidal surface with unknown orientation (*8*). The direction of the laser polarization controls the alignment of the principal axis of the vibrating ellipsoid without specifying the C-H bond alignment of CH_4. The fact that we observed the highest alignment effect ($\Delta_p = 0.216 \pm 0.016$) for this rotationless state of $CH_4(\nu_3)$ is a strong indication that the observed steric effects are due to the net C-H stretch alignment rather than C-H bond alignment.

The underlying mechanism for the alignment-dependent reactivity of vibrationally excited methane on Ni(100) is not obvious. The higher dissociation probability of methane with the net C-H stretch aligned parallel to the surface could be due to either an alignment dependence of the dissociation probability of the vibrationally excited molecule or to an alignment dependence of the rate of vibrational energy transfer to the surface.

A canonical interpretation explains our results in terms of an alignment-dependent barrier height on a multidimensional reactive PES for the methane/surface system. Dynamical calculations of methane dissociation on a realistic PES with up to 15 degrees of freedom may be needed to understand which degrees of freedom play a decisive role in the observed steric effects. Such a high-dimensional PES [based on the Born-Oppenheimer (BO) approximation] and corresponding dynamics simulations are being developed (*23*) to arrive at a predictive understanding of this important reaction. Our state-resolved, alignment-dependent data can guide such calculations.

Alternatively, the alignment dependence could be due to steric effects in vibrational relaxation rate between the vibrationally excited, incident methane and electron-hole (e-h) pair excitations in the Ni surface (*24*). An early model for vibrational energy transfer between a vibrating molecule and a metal surface (*25*) consists of an oscillating dipole interacting with its electric image dipole induced in the conducting surface. A classical calculation (*26*), treating vibrational relaxation as ohmic dissipation of the induced image current, predicts a maximum dissipation rate for dipole alignment perpendicular to the surface plane, which is twice the minimum rate calculated for parallel dipole alignment. The higher predicted dissipation rate for the perpendicular dipole is consistent with the lower reactivity for this alignment direction if vibrational energy transfer to e-h pairs were significant during the approach of a vibrating methane molecule toward the metal surface.

The image dipole model could also explain the mode-specific reactivity previously observed in comparing the isoenergetic symmetric and antisymmetric C-H stretch normal modes ν_3 and ν_1 of CH_4 (*2*, *27*). In contrast to the infrared-active ν_3 mode, the ν_1-normal mode of CH_4 is only Raman-active and carries no vibrational transition dipole moment from the ground state. Therefore, $CH_4(\nu_1)$ cannot induce an image dipole in the metal surface, which excludes this potential pathway for vibrational energy transfer for ν_1. A $CH_4(\nu_1)$ reactivity observed to be up to 10-fold higher (*27*) than for $CH_4(\nu_3)$ (*2*) is consistent with this model. However, there is currently no direct experimental evidence that e-h pair excitation occurs on the subpicosecond time scale of the reactive collisions of vibrationally excited CH_4 with a metal surface. Theoretical modeling beyond the BO approximation, including the participation of electronically nonadiabatic channels (*28*), should be pursued to shed light on the important question of whether e-h pair excitation plays a significant role in CH_4 chemisorption.

Irrespective of the mechanism, observation that the methane reactivity depends on the initial vibrational alignment, prepared far from the surface, implies the absence of significant steering effects under our experimental conditions. In other words, anisotropic molecule/surface interactions are unable to orient or steer the incident molecule into its lowest-energy reaction path on the subpicosecond time scale of the reactive collision in our experiments.

Furthermore, the observation of an alignment-dependent reactivity of methane on Ni(100) constitutes further evidence for a nonstatistical mechanism of methane chemisorption, beyond the previously reported mode specificity (*5*) and bond selectivity (*6*). Our results show that methane's reaction probability is not simply controlled by the available (vibrational) energy but is state-specific and sensitive to C-H stretch alignment. These observations are incompatible with statistical rate theory, which assumes complete randomization of

initial conditions in the collision complex and predicts reaction rates solely on the basis of energetics (*7*).

References and Notes

1. S. T. Ceyer, D. J. Gladstone, M. McGonigal, M. T. Schulberg, in *Investigations of Surfaces and Interfaces: Part A* (Wiley, New York, 1993).
2. L. B. F. Juurlink, P. R. McCabe, R. R. Smith, C. L. DiCologero, A. L. Utz, *Phys. Rev. Lett.* **83**, 868 (1999).
3. J. Higgins, A. Conjusteau, G. Scoles, S. L. Bernasek, *J. Chem. Phys.* **114**, 5277 (2001).
4. M. P. Schmid, P. Maroni, R. D. Beck, T. R. Rizzo, *Rev. Sci. Instrum.* **74**, 4110 (2003).
5. R. D. Beck *et al.*, *Science* **302**, 98 (2003).
6. D. R. Killelea, V. L. Campbell, N. S. Shuman, A. L. Utz, *Science* **319**, 790 (2008).
7. H. L. Abbott, A. Bukoski, I. Harrison, *J. Chem. Phys.* **121**, 3792 (2004).
8. W. R. Simpson, T. P. Rakitzis, S. A. Kandel, A. J. Orr-Ewing, R. N. Zare, *J. Chem. Phys.* **103**, 7313 (1995).
9. J. C. Polanyi, R. J. Williams, *J. Chem. Phys.* **88**, 3363 (1988).
10. E. W. Kuipers, M. G. Tenner, A. W. Kleyn, S. Stolte, *Phys. Rev. Lett.* **62**, 2152 (1989).
11. M. Brandt, T. Greber, N. Bowering, U. Heinzmann, *Phys. Rev. Lett.* **81**, 2376 (1998).
12. J. N. Greeley, J. S. Martin, J. R. Morris, D. C. Jacobs, *J. Chem. Phys.* **102**, 4996 (1995).
13. L. Vattuone *et al.*, *Angew. Chem. Int. Ed.* **43**, 5200 (2004).
14. H. Hou, S. J. Gulding, C. T. Rettner, A. M. Wodtke, D. J. Auerbach, *Science* **277**, 80 (1997).
15. W. A. Diño, H. Kasai, O. Ayao, *Phys. Rev. Lett.* **78**, 286 (1997).
16. Materials and methods are available as supporting material on *Science* Online.
17. C. H. Greene, R. N. Zare, *Phys. Rev. A* **25**, 2031 (1982).
18. R. N. Zare, *Angular Momentum: Understanding Spatial Aspects in Chemistry and Physics* (Wiley, New York, 1988).
19. E. H. Van Kleef, I. Powis, *Mol. Phys.* **96**, 757 (1999).
20. O. Swang, K. Faegri, O. Gropen, U. Wahlgren, P. Siegbahn, *Chem. Phys.* **156**, 379 (1991).
21. Y. A. Zhu, Y. C. Dai, D. Chen, W. K. Yuan, *J. Mol. Catal. Chem.* **264**, 299 (2007).
22. A. K. Tiwari, S. Nave, B. Jackson, *J. Chem. Phys.* **132**, 134702 (2010).
23. S. Nave, B. Jackson, *Phys. Rev. B* **81**, 233408 (2010).
24. A. M. Wodtke, D. Matsiev, D. J. Auerbach, *Prog. Surf. Sci.* **83**, 167 (2008).
25. B. N. J. Persson, M. Persson, *Solid State Commun.* **36**, 175 (1980).
26. B. N. J. Persson, S. Andersson, *Phys. Rev. B* **29**, 4382 (1984).
27. P. Maroni *et al.*, *Phys. Rev. Lett.* **94**, 246104 (2005).
28. N. Shenvi, S. Roy, J. C. Tully, *Science* **326**, 829 (2009).

29. We thank A. C. Luntz for helpful discussions. Financial support was provided by the Swiss National Science Foundation (grant no. 124666) and the École Polytechnique Fédérale de Lausanne.

Supporting Online Material
www.sciencemag.org/cgi/content/full/329/5991/553/DC1
Materials and Methods
Figs. S1 to S12
References

3 May 2010; accepted 2 July 2010
10.1126/science.1191751

Decrease in the CO_2 Uptake Capacity in an Ice-Free Arctic Ocean Basin

Wei-Jun Cai,[1]* Liqi Chen,[2] Baoshan Chen,[1] Zhongyong Gao,[2] Sang H. Lee,[3] Jianfang Chen,[4] Denis Pierrot,[5,6] Kevin Sullivan,[5,6] Yongchen Wang,[1] Xinping Hu,[1] Wei-Jen Huang,[1] Yuanhui Zhang,[2] Suqing Xu,[2] Akihiko Murata,[7] Jacqueline M. Grebmeier,[8] E. Peter Jones,[9] Haisheng Zhang[4]

It has been predicted that the Arctic Ocean will sequester much greater amounts of carbon dioxide (CO_2) from the atmosphere as a result of sea ice melt and increasing primary productivity. However, this prediction was made on the basis of observations from either highly productive ocean margins or ice-covered basins before the recent major ice retreat. We report here a high-resolution survey of sea-surface CO_2 concentration across the Canada Basin, showing a great increase relative to earlier observations. Rapid CO_2 invasion from the atmosphere and low biological CO_2 drawdown are the main causes for the higher CO_2, which also acts as a barrier to further CO_2 invasion. Contrary to the current view, we predict that the Arctic Ocean basin will not become a large atmospheric CO_2 sink under ice-free conditions.

The CO_2 concentration in the atmosphere has increased greatly since the industrial revolution, and ~30% of the CO_2 released has been taken up by the ocean. This process slows the increase of this greenhouse gas in the atmosphere and thus global warming (*1*), but will likely affect ocean ecosystems via acidification (*2*, *3*). The Arctic Ocean has great potential for taking up atmospheric CO_2 owing to high biological production in the large ocean margin areas and low temperature (*4*, *5*). A recent synthesis suggested that the Arctic Ocean, though constituting only 3% of the world's ocean surface area and mostly ice-covered, accounts for 5 to 14% of the total ocean CO_2 uptake (*6*). This value is highly uncertain, however, owing to relatively few observations and rapid climate changes. The Arctic is widely viewed as the area on Earth most sensitive to climate changes (*1*), with acidification more pronounced than that of any other ocean (*2*). Sea ice melt in the Arctic Ocean has increased steadily over recent decades, proceeding faster in the past three summers (2007 to 2009) than any model prediction (Fig. 1) (*7*–*9*). It has been postulated that an ice-free condition in the Arctic Ocean basins would allow for uptake of a substantial amount of additional CO_2 from the atmosphere (*6*). How CO_2 concentrations in the Arctic surface water may change in response to sea ice melt is, therefore, an important issue for the scientific community and general public.

[1]Department of Marine Sciences, University of Georgia, Athens, GA 30602, USA. [2]Key Lab of Global Change and Marine Atmospheric Chemistry, Third Institute of Oceanography, SOA, Xiamen 361005, China. [3]Korea Polar Research Institute, Incheon 406-840, Republic of Korea. [4]Laboratory of Marine Ecosystem and Biogeochemistry, Second Institute of Oceanography, SOA, Hangzhou 310012, China. [5]Ocean Chemistry Division, National Oceanic and Atmospheric Administration–Atlantic Oceanographic and Meteorological Laboratory, Miami, FL 33149, USA. [6]Cooperative Institute of Marine and Atmospheric Sciences, University of Miami, Miami, FL 33149, USA. [7]Research Institute for Global Change, Japan Agency for Marine-Earth Science and Technology, Yokosuka, Kanagawa 237-0061, Japan. [8]Chesapeake Biological Laboratory, University of Maryland Center for Environmental Science, Solomons, MD 20688, USA. [9]Department of Fisheries and Oceans, Ocean Sciences Division, Bedford Institute of Oceanography, Dartmouth, Nova Scotia, Canada B2Y 4A2.

*To whom correspondence should be addressed. E-mail: wcai@uga.edu

In the summer of 2008, we conducted a high-resolution underway survey of partial pressure of CO_2 (p_{CO_2}) across the Canada Basin in the western Arctic Ocean where substantial melting of ice had occurred (Fig. 1 and fig. S1). Surface-water temperature was as high as 0° to 5°C in the central Canada Basin (Fig. 2A). Extensive ice melt in this region resulted in salinity values as low as 24 parts per thousand (‰) (Fig. 2B) and ice concentration less than 15% (Fig. 1). Compared to an earlier underway survey in summer 1999, temperatures had increased by 3°C and salinities decreased by ~2‰ (Fig. 2, D and E). During the Arctic Ocean Section (AOS) study in summer 1994, all areas north of 72°N were under ice cover (Fig. 1) with surface seawater temperatures below −1.5°C and salinities above 30‰ (Fig. 2, D and E).

During the summer of 2008, surface-water p_{CO_2} was below the atmospheric level (~375 μatm) in the entire survey area (Fig. 2C). The lowest p_{CO_2} (120 to 250 μatm) occurred in marginal sea areas, in agreement with earlier observations (*4*, *10*–*13*). In the ice-free region of the Canada Basin to the northeast, however, there was a large area of relatively high p_{CO_2} (320 to 365 μatm) that had not been observed before. It contrasted sharply with p_{CO_2} values of 260 to 300 μatm in the summer of 1999 and the very low p_{CO_2} (<260 μatm) from the summer of 1994 (Fig. 2F). Further north (≥77°N), where melting of ice in 2008 was less extensive, p_{CO_2} dropped quickly to below 280 μatm (Fig. 2C). Surface p_{CO_2} also decreased from the central Canada Basin to areas west of 170°W, where ice cover was relatively heavy, temperature was lower, and salinity was higher.

In ocean margin areas where p_{CO_2} was very low, dissolved inorganic carbon (DIC) was greatly depleted relative to alkalinity (TA), a quasi-conservative tracer (Fig. 3). Such a DIC decrease indicates net ecosystem production of organic carbon or removal of CO_2 in the surface mixed layer (*5*). In the ice-free region of the Canada Basin, however, both DIC and TA followed the theoretical mixing line of seawater and ice meltwater, indicating no appreciable net biolog-

ical removal. In the partially ice-covered basin areas, moderate DIC depletion or CO_2 removal against TA was observed (Fig. 3).

Surface-water $p\text{CO}_2$ in the Arctic Ocean is affected by several processes, including mixing of various source waters (i.e., seawater, river water, and meltwater), temperature change, air-sea gas exchange, biological CO_2 fixation, and microbial recycling of organic carbon (Fig. 4) (*4*–*6*). Assisted by prolonged daylight, nutrient-rich Pacific source water results in high biological CO_2 assimilation ("B" in Fig. 4) in the western Arctic marginal seas (*5*, *14*) [net primary production rate (NPP) was measured as 114 ± 132 mmol m^{-2} day^{-1} during summer 2008, table S1]. This water is diluted by river water and ice meltwater as it flows through the ocean margins and basins. However, the mixing of river-seawater ("R" in Fig. 4) does not change the $p\text{CO}_2$ level substantially at S > 15‰. Melting of sea ice ("I" in Fig. 4), by contrast, will greatly reduce $p\text{CO}_2$ because of a very low $p\text{CO}_2$ level in the meltwater (*15*).

Our observations of high $p\text{CO}_2$ values in the Canada Basin in summer 2008 reveal a dynamic feature of how surface $p\text{CO}_2$ in the Arctic Ocean may respond to ice melt. Warming ("W" in Fig. 4) in the basin would partly explain the $p\text{CO}_2$ increase (*5*, *10*). However, when all $p\text{CO}_2$ values are normalized (or scaled) to the same temperature, the 2008 values are still much higher than those of 1994 and 1999 except in heavily ice-covered areas (fig. S2), indicating the importance of other processes. We offer the following explanation for this behavior. On the basis of the linear DIC-TA relation (Fig. 3) and very low nutrient supplies (*14*), we assume near-zero net biological CO_2 fixation in the Canada Basin. Moreover, we assume that before the ice melts in early spring,

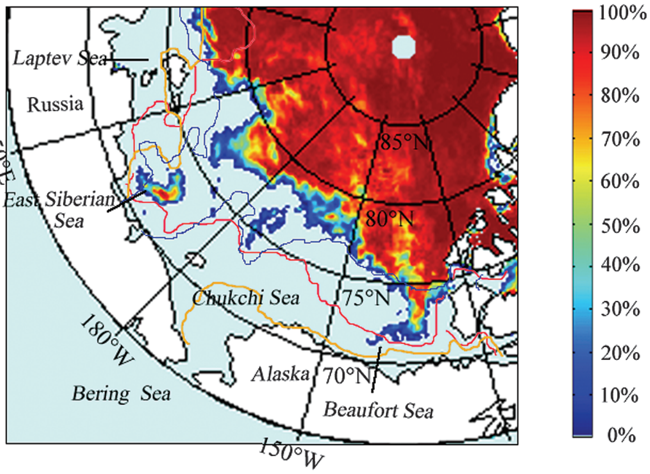

Fig. 1. Arctic ice concentrations from the Advanced Microwave Scanning Radiometer for Earth-Observing System (AMSR-E) for the first week of September 2008. The blue color contour line indicates the ice edge on 12 August when the survey vessel first reached 75°N. Ice edge is defined as 15% of ice concentration. The gold and red lines represent the ice edge in the first week of September 1994 and 1999, respectively. Data are from http://nsidc.org/data/docs/daac/ae_si12_12km_tb_sea_ ice_and_snow.gd.html.

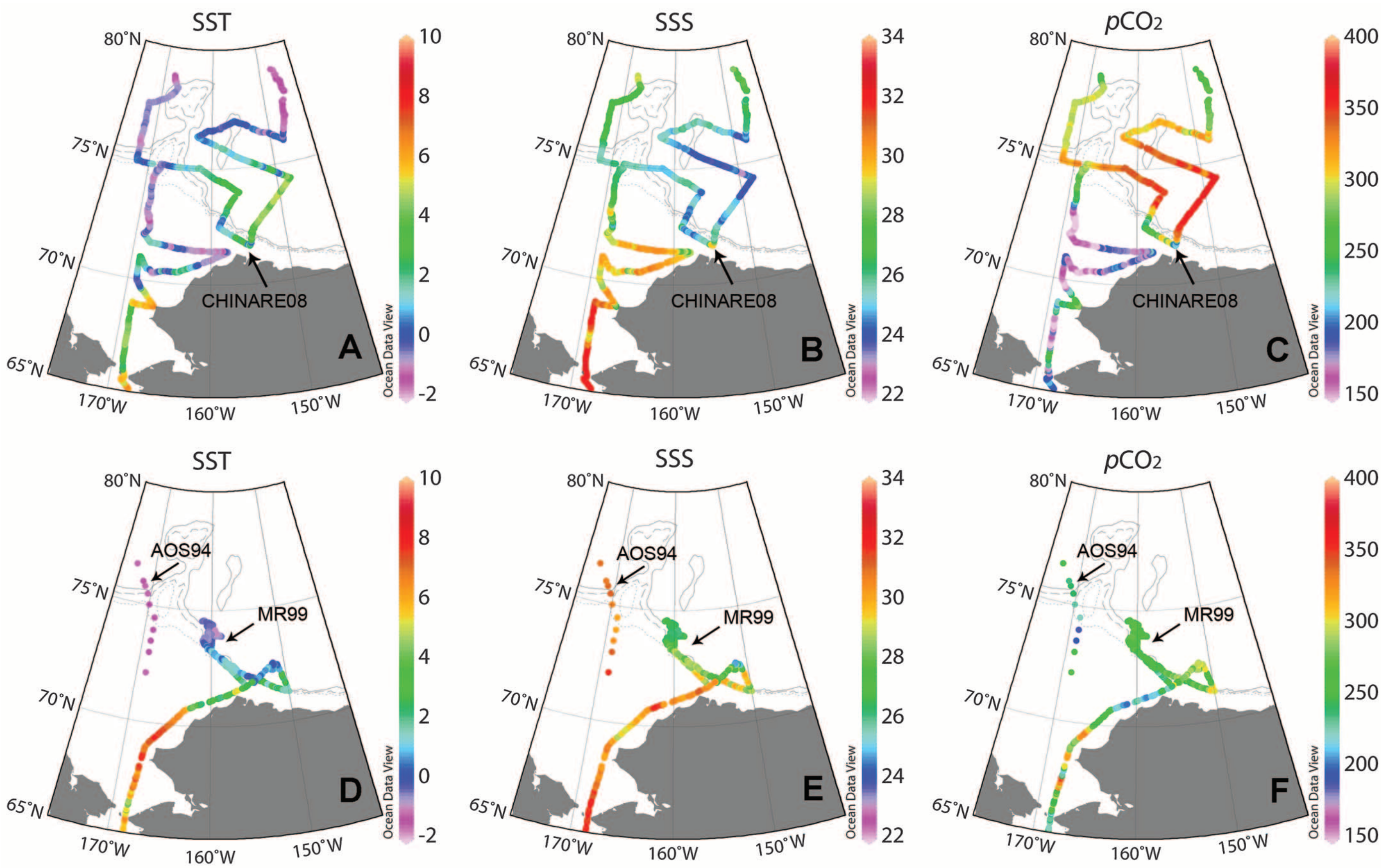

Fig. 2. Distribution of sea surface temperature (SST) in °C (**A**), salinity (SSS) in ‰ (**B**), and $p\text{CO}_2$ in μatm or 10^{-6} atm (**C**) during summer 2008 as well as temperature (**D**), salinity (**E**), and $p\text{CO}_2$ (**F**) in summer 1999 and 1994. CHINARE08, China National Arctic Research Expedition 2008. MR99 underway survey data were obtained in summer 1999. AOS94, Arctic Ocean Section 1994. During CHINARE08, the survey vessel arrived at 66°N on 1 August, 75°N, 168°W on 6 August, 75°N, 155°W on 12 August, and 85°N on 28 August, and it returned to 75°N, 172°W on 6 September. The atmospheric $p\text{CO}_2$ was 375 and 360 μatm, respectively, in the summer of 2008 and 1999. Ocean Data View (http://odv.awi.de) was used for the plots. From the shore to the central basin, the three lines (dotted, dashed, and solid) indicate 250-, 500-, and 1000-m water depth, respectively.

pCO$_2$ in the basin was similar to the value under ice-covered conditions measured during the summer of 1994 at 225 µatm (Fig. 2F). Then, the mixing of seawater with low-CO$_2$ meltwater would reduce pCO$_2$ by 50 to 60 µatm (Fig. 4). An increase in temperature of 4° to 6°C in summer 2008 would increase pCO$_2$ by about 50 µatm (i.e., ~4.2%/°C) (*5*, *10*). Thus, CO$_2$ increase due to warming would roughly cancel out CO$_2$ reduction due to mixing with meltwater in the ice-free region.

The main factor increasing the surface-water pCO$_2$ is CO$_2$ uptake from the atmosphere. For a 1.5- to 2-month ice-free period (by the end of August), CO$_2$ replenishment from the atmosphere would raise the surface-seawater pCO$_2$ to about 340 µatm at a temperature of 4°C in this area (Fig. 4), which is similar to our observations [see text in supporting online material (SOM) for the model simulation]. This conclusion would be strengthened if pCO$_2$ in the early spring was higher than we have assumed as a result of accumulation from the previous summer. The same is true if the mixed layer depth is shallower or the wind speed is stronger than we used for simulations. Similarly, for a 1-month ice-free period, CO$_2$ uptake would increase the surface pCO$_2$ to 280 µatm in the summer of 1999 (Fig. 4).

This atmospheric CO$_2$ control mechanism operates because of a shallow mixed-layer depth of less than 20 m in the Canada Basin during summertime (fig. S3). This shallow depth and strong stratification allow a relatively quick re-equilibration with the atmosphere. The rapid increase in surface pCO$_2$, then, slows further CO$_2$ uptake by decreasing air-sea pCO$_2$ gradient (ΔpCO$_2$), the driving force for the gas exchange. ΔpCO$_2$ was as high as 60 to 80 µatm in the southern Canada Basin in September 1999. It dropped sharply to only 10 to 55 µatm in August 2008. When this reduction in driving force is included, the CO$_2$ invasion for a 100-day ice-free period is 0.64 mol m^{-2} (or 6.4 mmol m^{-2} day^{-1}) in 2008 (see SOM text). This flux is 85% less than the previous estimate of 46 mmol m^{-2} day^{-1} based on an open-water condition measured during summer 2002 to 2004 at the southern margin of the Canada Basin (*5*). If we apply this asymptotic reduction of driving force to the newly ice-free basin area of 0.6×10^{12} m^2, we estimate an extra CO$_2$ invasion flux of only 4.6×10^{12} g C year^{-1}, compared to a much higher estimate of 33×10^{12} g C year^{-1} under constant ΔpCO$_2$ (*6*).

Light-limited biological primary production rate will increase when sea ice is thinning and melting and with increased open-water area and longer ice-free period (*7*, *14*, *16*). Indeed, we observed increased biological CO$_2$ removal in the partially ice-covered basin areas (Figs. 2 and 3). Once the region was ice-free, however, the linear mixing behavior of DIC relative to TA in 2008 indicates a negligible net ecosystem production rate in the central basin areas (Fig. 3). Measured NPP rates (1.9 ± 1.0 mmol m^{-2} day^{-1}, table S1) in the ice-free region in summer 2008 indicate no increase or even possibly a decrease in biological production compared to the ice-covered conditions in summer 1994 (2.5 ± 1.1 mmol m^{-2} day^{-1}) (*17*). Our conclusion is consistent with the observation of no increase in satellite-derived chlorophyll concentrations between 2003 and 2008 in the basin area (*18*). Low net biological CO$_2$ fixation in the Canada Basin is likely due to a poor supply of nitrate to the surface mixed layer as a result of strong stratification from greatly increased meltwater input (fig. S3) (*7*, *16*, *19*). Nutrient availability to surface water would limit not only water column productivity (*14*, *16*) but also ice-algal productivity (*20*). High stratification and limited nutrient supply to the surface water may have already caused a shift in ecosystem toward

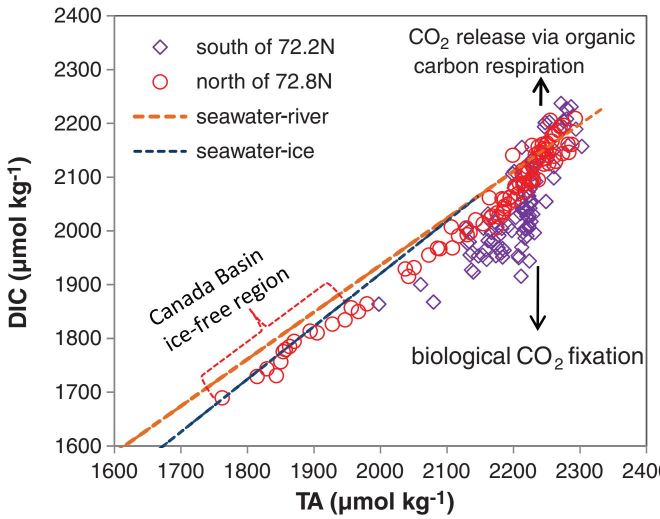

Fig. 3. Dissolved inorganic carbon (DIC) versus total alkalinity (TA) plot. Data are from 0 to 125 m and are divided into south of 72.2°N (all marginal seas) and between 72.8°N and 78.0°N (mostly basin areas). For the latter, the low-TA and low-salinity data are from surface waters from the Canada Basin ice-free region and are marked; the rest are either from western and northern edges of the basin where ice-cover was heavy or from subsurface waters. The brown dashed line is the theoretical mixing line of the seawater and the river water. The blue dashed line is the mixing line of seawater (diluted by river water to S = 30‰) with the ice meltwater. The end-member DIC and TA values of the three source waters were decided independently from the literature (see SOM text). Data from 100- to 125-m depths, located on or above the mixing line, reflect recycling of organic carbon.

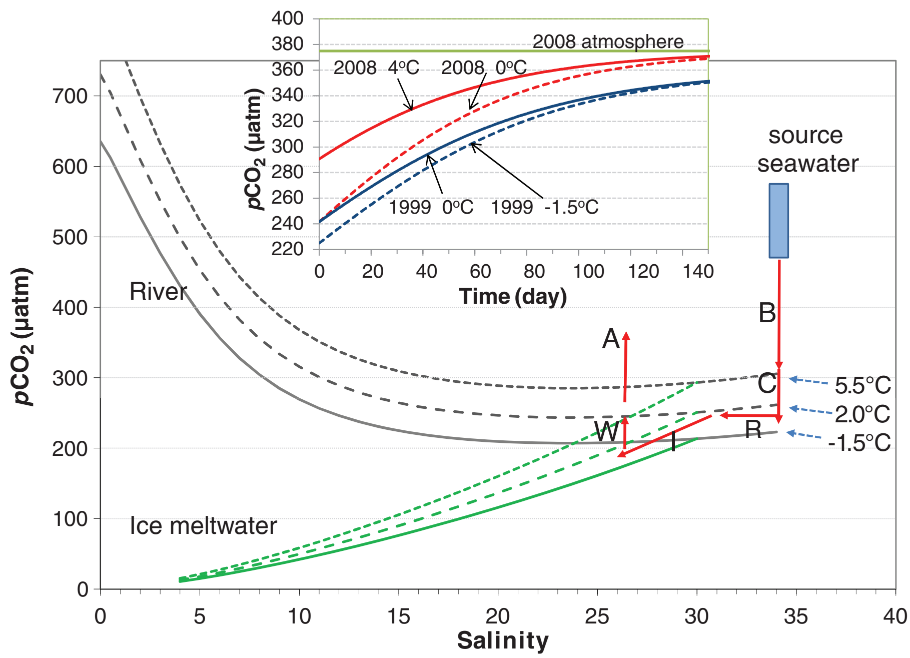

Fig. 4. Model simulations of factors influencing surface-water pCO$_2$ in the Arctic Ocean. The red arrows represent processes denoted by B (biology), C (cooling), R (river input), I (ice melt), W (warming), and A (atmospheric CO$_2$ invasion). The three black curves represent pCO$_2$ variation during the mixing between seawater and river water at three temperatures, whereas the three green curves represent mixing between seawater and meltwater at these temperatures. The source water, Bering Sea slope water at 200 m upwelled to the sea surface, has a pCO$_2$ of 420 to 572 µatm, which is reduced to 223 to 306 µatm by a biological CO$_2$ fixation of 95 µmol kg^{-1}. This water is diluted by river water to S = 30‰, and then by ice meltwater. The time course of CO$_2$ invasion into the surface water is simulated in the inserted graph (see SOM for details).

smallest algae in the Canada Basin, potentially favoring carbon retention and CO_2 release (*19*). However, it is difficult to predict the net role of increased stratification versus sustained wind mixing in these newly ice free regions. Wind-driven upwelling and mixing of nutrient and CO_2 rich subsurface water is expected or already has been shown to have a major impact on carbon dynamics and ecosystem in the Arctic (*21*) or Antarctic (*22*) marginal areas. Such an impact is likely small in the central Canada Basin where increased stratification is a dominant feature (fig. S3).

In addition, warmer temperatures likely would enhance microbial respiration of organic carbon, potentially reducing net community production (*23*). Moreover, increased warming also would promote permafrost thawing and coastal erosion in the Arctic continents, increasing riverine inputs of organic carbon (*24*, *25*) that is subsequently metabolized to CO_2, thus further contributing to the elevated p_{CO_2}. Finally, in future years, when sea surface temperature further increases after all ice is melted during summertime, as is predicted to occur within 30 years (*9*), the Arctic Ocean basin CO_2 uptake capacity would reduce further because of the warming effect on surface-water p_{CO_2}.

The observed summer 2008 p_{CO_2} distribution suggests that, as ice continues to melt in the near future, the air-sea CO_2 flux will be enhanced in the Arctic Ocean owing to the increased area of open water and longer period of ice-free time. The increase in surface-water p_{CO_2} due to this CO_2 uptake would accelerate the negative impact of ocean acidification on pelagic and benthic ecosystems. However, the CO_2 uptake would quickly weaken because surface-water p_{CO_2} will equilibrate with the atmosphere within a short time owing to a shallow mixed-layer depth, strong surface-water stratification, surface warming, and low biological CO_2 fixation.

References and Notes

1. S. Solomon *et al.*, *Climate Change 2007: The Physical Science Basis: Contribution of Working Group I to the Fourth Assessment Report of the Intergovernmental Panel on Climate Change* (Cambridge Univ. Press, Cambridge, 2007).
2. M. Steinacher, F. Joos, T. L. Frölicher, G.-K. Plattner, S. C. Doney, *Biogeosciences* **6**, 515 (2009).
3. M. Yamamoto-Kawai, F. A. McLaughlin, E. C. Carmack, S. Nishino, K. Shimada, *Science* **326**, 1098 (2009).
4. L. G. Anderson, K. Olsson, M. Chierici, *Global Biogeochem. Cycles* **12**, 455 (1998).
5. N. R. Bates, *J. Geophys. Res.* **111**, C10013 (2006).
6. N. R. Bates, J. T. Mathis, *Biogeosciences* **6**, 2433 (2009).
7. K. R. Arrigo, G. L. van Dijken, S. Pabi, *Geophys. Res. Lett.* **35**, L19603 (2008).
8. J. C. Comiso, C. L. Parkinson, R. Gersten, L. Stock, *Geophys. Res. Lett.* **35**, L01703 (2008).
9. M. Wang, J. E. Overland, *Geophys. Res. Lett.* **36**, L07502 (2009).
10. A. Murata, T. Takizawa, *Cont. Shelf Res.* **23**, 753 (2003).
11. S. Kaltin, L. G. Anderson, *Mar. Chem.* **94**, 67 (2005).
12. A. Fransson, M. Chierici, Y. Nojiri, *Cont. Shelf Res.* **29**, 1317 (2009).
13. L. Chen, Z. Gao, *Deep Sea Res. Part II Top. Stud. Oceanogr.* **54**, 2619 (2007).
14. L. A. Codispoti, C. N. Flagg, J. H. Swift, *Deep Sea Res. Part II Top. Stud. Oceanogr.* **56**, 1144 (2009).
15. S. Rysgaard, R. N. Glud, M. K. Sejr, J. Bendtsen, P. B. Christensen, *J. Geophys. Res.* **112**, C03016 (2007).
16. S. Pabi, G. L. van Dijken, K. R. Arrigo, *J. Geophys. Res.* **113**, C08005 (2008).
17. M. Gosselin, M. Levasseur, P. A. Wheeler, R. A. Horner, B. C. Booth, *Deep Sea Res. Part II Top. Stud. Oceanogr.* **44**, 1623 (1997).
18. J. M. Grebmeier, S. E. Moore, J. E. Overland, K. E. Frey, R. Gradinger, *EOS* **91**, 161 (2010).
19. W. K. W. Li, F. A. McLaughlin, C. Lovejoy, E. C. Carmack, *Science* **326**, 539 (2009).
20. R. Gradinger, *Deep Sea Res. Part II Top. Stud. Oceanogr.* **56**, 1201 (2009).
21. E. Carmack, D. C. Chapman, *Geophys. Res. Lett.* **30**, 1778 (2003).
22. M. Montes-Hugo *et al.*, *Science* **323**, 1470 (2009).
23. P. L. Yager, J. W. Deming, *Limnol. Oceanogr.* **44**, 1882 (1999).
24. L. Guo, R. W. MacDonald, *Global Biogeochem. Cycles* **20**, GB2011 (2006).
25. D. A. Hansell, D. Kadko, N. R. Bates, *Science* **304**, 858 (2004).

26. We thank R. Wanninkhof, P. Yager, and N. Bates for discussions; J. Zhao for the salinity and temperature data; and H. Li and S. Gao for sample collection. Funding for the CHINARE CO_2 survey and subsequent synthesis was provided by the Ministry of Science and Technology of China (2009DFA22920), the Natural Science Foundation of China (40531007), and the U.S. National Oceanic and Atmospheric Administration (NA05OAR4311161 and NA09OAR4310078) and NSF (ARC-0909330). The measurements for primary production of phytoplankton were funded by a Korean Arctic Research project (PM09020). We also thank the Chinese Arctic and Antarctic Administration and the Polar Research Institute of China for their support. We are grateful to the captain and crew of icebreaker *Xuelong*.

Supporting Online Material

www.sciencemag.org/cgi/content/full/science.1189338/DC1
Materials and Methods
SOM Text
Figs. S1 to S3
Tables S1 and S2
References

9 March 2010; accepted 28 June 2010
Published online 22 July 2010;
10.1126/science.1189338
Include this information when citing this paper.

Microbial Biosynthesis of Alkanes

Andreas Schirmer,* Mathew A. Rude, Xuezhi Li, Emanuela Popova, Stephen B. del Cardayre

Alkanes, the major constituents of gasoline, diesel, and jet fuel, are naturally produced by diverse species; however, the genetics and biochemistry behind this biology have remained elusive. Here we describe the discovery of an alkane biosynthesis pathway from cyanobacteria. The pathway consists of an acyl–acyl carrier protein reductase and an aldehyde decarbonylase, which together convert intermediates of fatty acid metabolism to alkanes and alkenes. The aldehyde decarbonylase is related to the broadly functional nonheme diiron enzymes. Heterologous expression of the alkane operon in *Escherichia coli* leads to the production and secretion of C13 to C17 mixtures of alkanes and alkenes. These genes and enzymes can now be leveraged for the simple and direct conversion of renewable raw materials to fungible hydrocarbon fuels.

Efforts to transition from fossil fuels to renewable alternatives have focused on the conversion of renewable biomass to "drop-in" compatible fuels and chemicals (*1*–*3*). Routes to renewable hydrocarbons are emerging, but to date, these require expensive chemical hydrogenation. Alkanes, observed throughout nature, are produced directly from fatty acid metabolites—for example, as plant cuticular waxes (*4*), as insect pheromones (*5*), and with unknown functions in numerous organisms (*6*–*9*). Biochemical studies of alkane biosynthesis have focused on eukaryotic systems, with most evidence supporting a decarbonylation of fatty aldehydes as the primary mechanism (*10*, *11*). Although *cer1* from *Arabidopsis thaliana* has been proposed as a candidate gene encoding this activity (*12*), no studies conclusively associate any gene with these biochemical activities.

Alkanes have been reported in a diversity of microorganisms, but some results remain controversial (*13*, *14*). From our assessment, the most consistent reports are from the cyanobacteria (*9*, *15*, *16*) and natural habitats dominated by cyanobacteria (*17*). Heptadecane is the most abundant alkane reported in these photoautotrophic bacteria, an observation consistent with the "$n - 1$" rule for alkanes, resulting from decarbonylation of typically even-numbered fatty aldehydes. Because cyanobacteria are phylogenetically homogeneous, with more than 50 sequenced genomes publicly available, our search began with comparative biochemistry and genomics. Eleven cyanobacterial strains of known sequence were photoautotrophically grown, and their culture extracts were evaluated for hydrocarbon production (Table 1). Ten of these strains produced alkanes, mainly heptadecane and pentadecane, along with alkenes, presumably derived from unsaturated fatty aldehydes. However, one strain, *Synechococcus* sp. PCC7002, did not produce alkanes. On the assumption that an alkane biosynthesis pathway was not present in *Synechococcus* sp. PCC7002, we undertook a subtractive genome analysis. The 10 genomes of the alkane-producing cyanobacteria were intersected, and the PCC7002 genome was subtracted by using a 40% sequence identity cut-off to select orthologs. Seventeen genes common to the 10 producing strains remained, and 10 of these already had assigned

LS9, Inc., 600 Gateway Boulevard, South San Francisco, CA 94080, USA.

*To whom correspondence should be addressed. E-mail: aschirmer@ls9.com

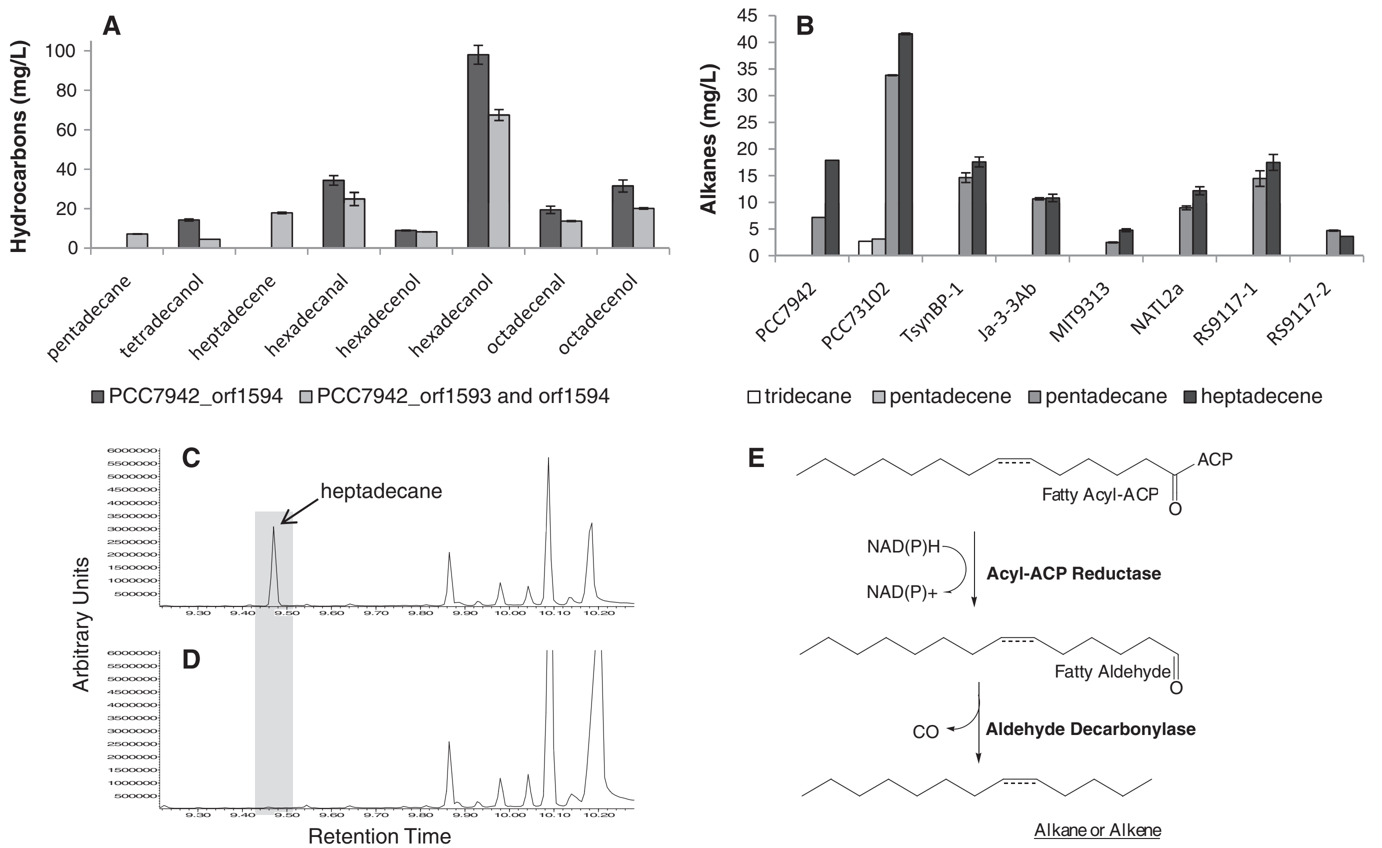

Fig. 1. Demonstration that a two-gene pathway widespread in cyanobacteria is responsible for alkane biosynthesis. (**A**) *E. coli* MG1655 does not produce hydrocarbons. When *S. elongatus* PCC7942_orf1594 was expressed, *E. coli* produced fatty aldehydes and fatty alcohols. The coexpression of *S. elongatus* PCC7942_orf1593 and orf1594 led to alkane, alkene, fatty aldehyde, and fatty alcohol production. (**B**) For comparison, selected PCC7942_orf1593 orthologs from other cyanobacteria were coexpressed with PCC7942_orf1594 in *E. coli*, and all produced similar compounds [only alkanes and alkenes are shown; fig. S1 shows an example of a detailed gas chromatography–mass spectrometry (GC-MS) trace of a recombinant hydrocarbons mixture]. (**C**) *Synechocystis* sp. PCC6803 has the ability to synthesize the alkane heptadecane. (**D**) Deletion of the two adjacent *Synechocystis* sp. PCC6803 orfs sll0208 and sll0209, *S. elongatus* PCC7942_orf1593 and 1594 orthologs, abolished heptadecane biosynthesis. GC-MS traces are shown. (**E**) Model of the alkane biosynthesis pathway in cyanobacteria consisting of a fatty aldehyde–generating acyl-ACP reductase (e.g., PCC7942_orf1594 or sll0209) and a fatty aldehyde decarbonylase (e.g., PCC7942_orf1593 or sll0208). The PCC7942_orf1593 orthologs in (B) are from the following strains: *N. punctiforme* PCC73102, *Thermosynechococcus elongatus* BP-1, *Synechococcus* sp. Ja-3-3Ab, *P. marinus* MIT9313, *P. marinus* NATL2A, and *Synechococcus* sp. RS9117, which has two paralogs (RS9117-1 and -2).

functions (table S2). Two of the remaining hypothetical proteins stood out as likely candidates for alkane biosynthesis. Representative of these were open reading frames orf1593 and orf1594 from *S. elongatus* PCC7942. PCC7942_orf1594 belongs to the short-chain dehydrogenase or reductase family, whereas PCC7942_orf1593 shared similarity to the ferritin-like or ribonucleotide reductase–like family. Because alkane biosynthesis was predicted to proceed via the decarbonylation of fatty aldehydes, it was possible that PCC7942_orf1594 catalyzed the reduction of a fatty acid intermediate, such as an acyl carrier protein (ACP) or coenzyme A (CoA) acyl-thioester, to form a fatty aldehyde (*18*, *19*), and that PCC7942_orf1593, which is similar to enzymes that catalyze radical-based chemical reactions such as ribonucleotide reductase R2 (*20*), was the decarbonylase. PCC7942_orf1593 and orf1594 orthologs appear to occur only in cyanobacteria and likely form a conserved operon, because they are found adjacent to each other in a majority of cyanobacterial genomes (table S3). *Cyanothece* sp. PCC7424 was the only additional strain identified that lacked orthologs to these sequences.

Table 1. Occurrence of alkanes in selected cyanobacteria with fully sequenced genomes (*21*).

Cyanobacterium	Genome size (Mb)	Hydrocarbons previously reported	Alkanes observed in this study
Synechococcus elongatus PCC7942	2.7	Yes*	Heptadecane, pentadecane
S. elongatus PCC6301	2.7	Yes*	Heptadecane, pentadecane
Synechocystis sp. PCC6803	3.5	Not reported	Heptadecane
Prochlorococcus marinus CCMP1986	1.7	Not reported	Pentadecane
Anabaena variabilis ATCC29413	6.4	Yes†	Heptadecane, methyl-heptadecane
Nostoc punctiforme PCC73102	9.0	Not reported	Heptadecane
Gloeobacter violaceus PCC7421	4.6	Not reported	Heptadecane
Nostoc sp. PCC7120	6.2	Not reported	Heptadecane, methyl-heptadecane
Cyanothece sp. PCC7425	5.7	Not reported	Heptadecane
Cyanothece sp. ATCC51142	4.9	Not reported	Pentadecane
Synechococcus sp. PCC7002	3.0	Yes*	No alkanes observed

*From (*9*), in which *S. elongatus* and *Synechococcus* sp. PCC7002 are listed under their former names *Anacystis nidulans* and *Agmenellum quadruplicatum*, respectively. †From (*26*).

To test the hypothesis that the *S. elongatus* PCC7942_orf1593 and orf1594 family proteins were necessary and sufficient for alkane biosynthesis, a genetic "knock in" and "knock out" strategy was taken. PCC7942_orf1593 and orf1594 were expressed both separately and together in *Escherichia coli*, and extracts of these cells were evaluated for the production of hydrocarbons.

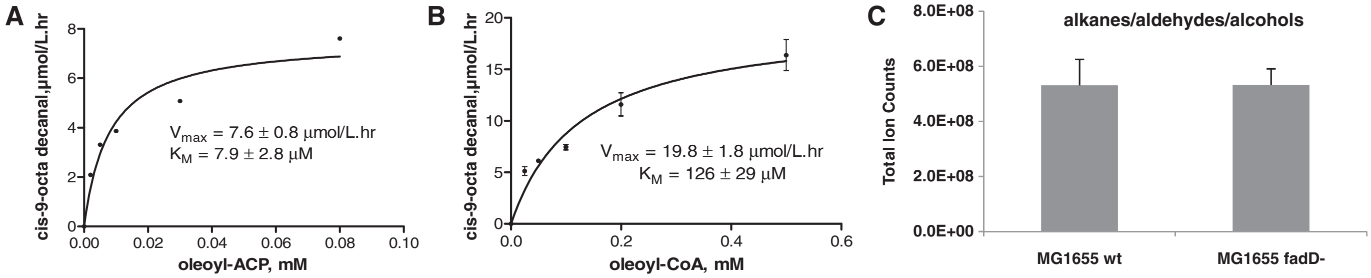

Fig. 2. Demonstration that *S. elongatus* PCC7942_orf1594 encodes an acyl-ACP reductase. (**A** and **B**) Michaelis-Menten plots for PCC7942_orf1594 protein with oleoyl-ACP and oleoyl-CoA as substrates. NADPH concentration was 2 mM. (**C**) Comparison of hydrocarbon production of *E. coli* wild-type and an *E. coli fadD* deletion strain. Both strains express *S. elongatus* PCC7942_orf1593 and orf1594. *fadD* encodes the major acyl-CoA synthetase of *E. coli*. As this strain lacks the ability to synthesize acyl-CoAs, hydrocarbons are derived directly from acyl-ACP.

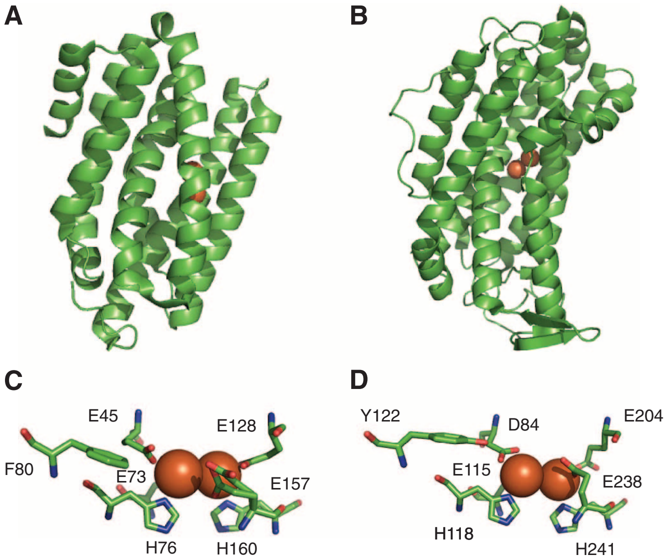

Fig. 3. Comparison of the similar three-dimensional structures of a cyanobacterial aldehyde decarbonylase and ribonucleotide reductase R2 from *E. coli*. (**A**) Aldehyde decarbonylase from *P. marinus* MIT9313 from PDB file 2OC5. (**B**) Ribonucleotide reductase R2 from *E. coli* from PDB file 1RIB. (**C**) Active site of the *P. marinus* MIT9313 aldehyde decarbonylase. (**D**) Active site of the *E. coli* ribonucleotide reductase R2. Amino acid residues that coordinate the metal centers are shown. The active site of *E. coli* ribonucleotide reductase R2 also shows a tyrosine, which is part of the diiron(III)–tyrosyl radical cofactor and which is replaced with a phenylalanine in the aldehyde decarbonylase structure. The structure of *P. marinus* MIT9313 aldehyde decarbonylase shows two iron atoms bound, but it cannot be excluded that the active enzyme is a manganese/iron protein (see text). Structures were viewed in PyMOL.

Although *E. coli* produced no detectable hydrocarbons, extracts of PCC7942_orf1594-expressing cells contained substantial quantities of even-chain fatty aldehydes and fatty alcohols (Fig. 1A), whereas coexpression of both PCC7942_orf1593 and orf1594 resulted in the production of odd-chain alkanes and alkenes, as well as even-chain fatty aldehydes and fatty alcohols (Fig. 1A). Thus, PCC7942_orf1593 and orf1594 are sufficient for in vivo alkane biosynthesis, and fatty aldehydes are likely the biosynthetic intermediates. Expression of PCC7942_orf1593 alone was indistinguishable from the *E. coli* negative control, which was expected, because *E. coli* does not naturally produce fatty aldehydes. The production of fatty alcohols upon PCC7942_orf1594 expression can be attributed to intrinsic activities in *E. coli* that reduce fatty aldehydes to fatty alcohols, as is observed upon expression of fatty acyl-CoA reductases (*19*). Although it is possible that fatty alcohols may be biosynthetic intermediates, for mechanistic reasons it seems unlikely, and in vitro experiments support this hypothesis (see below). Fifteen additional PCC7942_orf1593 orthologs from various cyanobacteria were evaluated (table S3), and all conferred alkane production when expressed in *E. coli* together with PCC7942_orf1594. Alkane profiles of selected strains in Fig. 1B show that the "recombinant hydrocarbon" mixtures are primarily made up of pentadecane and heptadecene. Strains with the highest titers, e.g., coexpressing the orf1593 orthologs from *Nostoc punctiforme* PCC73102, produced a mixture of tridecane, pentadecene, pentadecane, and heptadecene, typically at a ratio of 10:10:40:40. Alkane titers were over 300 mg/liter when a modified mineral medium was used (*21*), and more than 80% of the hydrocarbons were found outside the cells (fig. S2).

In *S. elongatus* PCC7942, orf1593 and orf1594 appear to be part of a larger operon that contains a gene encoding a subunit of the acetyl-CoA carboxylase (*accA*), which is essential for growth. To avoid any polar effects of deleting the genes, we replaced the PC7942_orf1593 and 1594 orthologs in *Synechocystis* sp. PCC6803 (where the orthologous genes apparently form only a bicistronic operon) with a kanamycin-resistance cassette. This replacement abolished the presence of alkanes (Fig. 1, C and D) in the extracts of photoautoptrophically grown cells. Thus, these genes are both necessary for alkane biosynthesis in cyanobacteria and sufficient to confer alkane biosynthesis in a heterologous host, such as *E. coli*. Our findings further support the model of odd-chain alkane biosynthesis through the decarbonylation of even-chain fatty aldehydes.

The proposed pathway for alkane biosynthesis is depicted in Fig. 1E. To evaluate this model, we undertook a preliminary in vitro characterization of the purified recombinant enzymes (*21*). Acyl-acyl carrier protein (acyl-ACP) and acyl-coenzyme A (acyl-CoA), the major activated forms of fatty acids in bacteria, were evaluated as substrates for PCC7942_orf1594. When incubated with acyl-ACP or acyl-CoA (e.g., oleoyl-ACP and oleoyl-CoA), PCC7942_orf1594 catalyzed the reduced nicotinamide adenine dinucleotide phosphate ($NADP^+$) (NADPH)–dependent reduction to the corresponding fatty aldehyde (e.g., *cis*-9-octadecenal) and required divalent cations, such as magnesium for catalysis. Fatty alcohols were not observed in the in vitro reaction. Although both fatty acyl thioesters were substrates, the Michaelis constant (K_M) for acyl-ACP was 8 ± 2 μM, and that for acyl-CoA was 130 ± 30 μM (Fig. 2, A and B). Accordingly, we named this enzyme acyl-ACP reductase (AAR), because it appears that acyl ACP is kinetically preferred and is likely the in vivo substrate. This hypothesis is supported by our finding that PCC7942_orf 1593 and orf1594 coexpression in an *E. coli* strain devoid of acyl-CoAs (the major acyl-CoA synthetase gene *fadD* was deleted) led to very similar levels of hydrocarbon production, comparable to those in an *E. coli* wild-type strain (Fig. 2C). This substrate selectivity distinguishes AAR from fatty acyl-CoA reductases (FAR) that specifically reduce acyl-CoAs but not acyl-ACPs to fatty aldehydes (*19*).

Comparison of PCC7942_orf1593 to the sequence database suggested that the cyanobacterial aldehyde decarbonylases are members of the ferritin-like or ribonucleotide reductase–like family of nonheme diiron enzymes (*20*). This was confirmed by a crystal structure of the

PCC7942_orf1593 ortholog from *Prochlorococcus marinus* MIT9313, PMT1231, solved by the Joint Center of Structural Genomics (protein database entry PDB|2OC5|A) but without assigning an enzymatic function. We confirmed that PMT1231, like PCC7942_orf1593, is an active aldehyde decarbonylase, because it conferred alkane biosynthesis to *E. coli* when coexpressed with PCC7942_orf1594 (Fig. 1B). The three-dimensional structure shows similarities to the 8 α-helical bundle of the second subunit of *E. coli* ribonucleotide reductase (R2) (*22*) (Fig. 3, A and B). In the solved structures, both proteins have two irons coordinated to histidine and aspartate or glutamate residues (Fig. 3, C and D). In R2, the diiron is part of a diiron(III)–tyrosyl radical cofactor that is essential to the ribonucleotide reduction process as a radical-chain initiator (*20*). The radical is then transduced to the catalytic R1 subunit. Homology modeling revealed that this tyrosine residue in R2 (Tyr^{122}) was replaced by phenylalanine residues in the aldehyde decarbonylases (e.g., Phe^{80} in PMT1231) (Fig. 3, C and D), which suggested that decarbonylation does not include a diiron(III)–tyrosyl radical cofactor. To examine the possibility that another conserved tyrosine might form such a cofactor in the aldehyde decarbonylases, we replaced a tyrosine, which was conserved in all cyanobacterial decarbonylases and appeared to be within 6 Å of the diiron (e.g., Tyr^{135} in PMT1231), with phenylalanine. This mutation had no detectable effect on alkane biosynthesis activity in vivo (fig. S3), which suggested that decarbonylation proceeds through a mechanism different from ribonucleotide reductase R2. A different class of R2s, exemplified by the R2 from *Chlamydia trachomatis*, is a manganese/iron and not a diiron protein, and it does not use a diiron(III)-tyrosyl but a stable manganese(IV)/iron(III) cofactor for radical initiation (*23*). At present, we cannot exclude that active aldehyde decarbonylases are manganese/iron proteins—heterologous expression in *E. coli* might result in mismetallation. Aldehyde decarbonylases are also considerably smaller than ribonucleotide reductase R2s (220 to 250 versus 300 to 400 amino acids) and lack the C-terminal region that, in R2, interacts with the R1 subunit.

To evaluate in vitro decarbonylation, we tested the purified aldehyde decarbonylase from *Nostoc punctiforme* PCC73102, NpunR1711, which had shown the highest in vivo activity (Fig. 1B), with octadecanal as substrate in the presence or absence of different cofactors. As a number of nonheme diiron enzymes require ferredoxin, ferredoxin reductase, and reducing equivalents for activity (*24*, *25*), we tested commercially available spinach ferredoxin and ferredoxin reductase and NADPH. Indeed, in vitro decarbonylation of octadecanal to heptadecane was only observed in the presence of ferredoxin, ferredoxin reductase, and NADPH, and omitting any one of these cofactors completely abolished in vitro activity of the decarbonylase (fig. S4). As coexpression of a cyanobacterial acyl-ACP reductase and aldehyde decarbonylase is sufficient for in vivo alkane biosynthesis in *E. coli* (see above), ferredoxin and ferredoxin reductase components essential for decarbonylation must be provided at least to some extent by endogenous *E. coli* proteins.

The genes and enzymes described here provide a foundation for the deeper understanding and further development of this pathway. The ability to biologically convert renewable carbohydrate selectively to fuel-grade alkanes without hydrogenation is an important step toward the goal of low-cost renewable transportation fuels.

References and Notes

1. J. L. Fortman *et al.*, *Trends Biotechnol.* **26**, 375 (2008).
2. J. R. Regalbuto, *Science* **325**, 822 (2009).
3. M. A. Rude, A. Schirmer, *Curr. Opin. Microbiol.* **12**, 274 (2009).
4. L. Samuels, L. Kunst, R. Jetter, *Annu. Rev. Plant Biol.* **59**, 683 (2008).
5. J. A. Tillman, S. J. Seybold, R. A. Jurenka, G. J. Blomquist, *Insect Biochem. Mol. Biol.* **29**, 481 (1999).
6. N. Ladygina, E. G. Dedyukhina, M. B. Vainshtein, *Process Biochem.* **41**, 1001 (2006).
7. P. Metzger, C. Largeau, *Appl. Microbiol. Biotechnol.* **66**, 486 (2005).
8. G. A. Strobel *et al.*, *Microbiology* **154**, 3319 (2008).
9. K. Winters, P. L. Parker, C. Van Baalen, *Science* **163**, 467 (1969).
10. T. M. Cheesbrough, P. E. Kolattukudy, *Proc. Natl. Acad. Sci. U.S.A.* **81**, 6613 (1984).
11. M. Dennis, P. E. Kolattukudy, *Proc. Natl. Acad. Sci. U.S.A.* **89**, 5306 (1992).
12. M. G. Aarts, C. J. Keijzer, W. J. Stiekema, A. Pereira, *Plant Cell* **7**, 2115 (1995).
13. T. G. Tornabene, *Experientia* **38**, 43 (1982).
14. L. P. Wackett, J. A. Frias, J. L. Seffernick, D. J. Sukovich, S. M. Cameron, *Appl. Environ. Microbiol.* **73**, 7192 (2007).
15. A. G. McInnes, J. A. Walter, J. L. C. Wright, *Lipids* **15**, 609 (1980).
16. V. M. Dembitsky, M. Srebnik, *Biochemistry (Mosc.)* **67**, 1276 (2002).
17. J. Shiea, S. C. Brassell, D. M. Ward, *Org. Geochem.* **15**, 223 (1990).
18. T. T. P. Doan *et al.*, *J. Plant Physiol.* **166**, 787 (2009).
19. S. Reiser, C. Somerville, *J. Bacteriol.* **179**, 2969 (1997).
20. J. Stubbe, P. Riggs-Gelasco, *Trends Biochem. Sci.* **23**, 438 (1998).
21. Materials and methods are available as supporting material on *Science* Online.
22. P. Nordlund, B. M. Sjöberg, H. Eklund, *Nature* **345**, 593 (1990).
23. W. Jiang *et al.*, *Science* **316**, 1188 (2007).
24. J. Müller, A. A. Lugovskoy, G. Wagner, S. J. Lippard, *Biochemistry* **41**, 42 (2002).
25. C. H. Wu, W. Jiang, C. Krebs, J. Stubbe, *Biochemistry* **46**, 11577 (2007).
26. S. W. Fehler, R. J. Light, *Biochemistry* **9**, 418 (1970).

27. We thank M. Alibhai for homology modeling, S. Brubaker for bioinformatics work, T. Baron for technical assistance, and C. Chang for help with preparing Fig. 3. The patent applications WO 2009/140695 and WO 2009/140696 are relevant to this paper. All authors have a financial interest in LS9, Inc. We would like to dedicate this paper to the memory of C. Richard Hutchinson, who died on 5 January 2010. "Hutch" was an important mentor for A.S. and S.B.d.C. He will be missed.

Supporting Online Material
www.sciencemag.org/cgi/content/full/329/5991/559/DC1
Materials and Methods
Figs. S1 to S4
Tables S1 to S3
References

4 February 2010; accepted 16 June 2010
10.1126/science.1187936

Btbd7 Regulates Epithelial Cell Dynamics and Branching Morphogenesis

Tomohiro Onodera,[1]* Takayoshi Sakai,[1,2]*† Jeff Chi-feng Hsu,[1]* Kazue Matsumoto,[1] John A. Chiorini,[3] Kenneth M. Yamada[1]†

During embryonic development, many organs form by extensive branching of epithelia through the formation of clefts and buds. In cleft formation, buds are delineated by the conversion of epithelial cell-cell adhesions to cell-matrix adhesions, but the mechanisms of cleft formation are not clear. We have identified Btbd7 as a dynamic regulator of branching morphogenesis. Btbd7 provides a mechanistic link between the extracellular matrix and cleft propagation through its highly focal expression leading to local regulation of Snail2 (Slug), E-cadherin, and epithelial cell motility. Inhibition experiments show that Btbd7 is required for branching of embryonic mammalian salivary glands and lungs. Hence, *Btbd7* is a regulatory gene that promotes epithelial tissue remodeling and formation of branched organs.

Branching morphogenesis is a fundamental developmental process generating the branched epithelia of many organs, including lungs, kidneys, and the mammary and salivary glands (*1*–*8*). Branches are generated by local outgrowths or by formation of clefts that subdivide epithelia into buds. Bud or tubule extension is promoted by various growth factors (*9*–*11*), but the mechanism of cleft formation is poorly understood. One model for cleft formation involves the local loss of epithelial cell-cell adhesions and replacement by interactions with extracellular matrix accumulating within clefts (*9*, *12*, *13*).

The matrix protein fibronectin is required for salivary, kidney, and lung branching (*13*–*15*).

[1]Laboratory of Cell and Developmental Biology, National Institute of Dental and Craniofacial Research, National Institutes of Health, Bethesda, MD 20892–4370, USA. [2]Department of Oral-Facial Disorders, Osaka University Graduate School of Dentistry, Yamadaoka, Suita, Osaka 565-0871, Japan. [3]Molecular Physiology and Therapeutics Branch, National Institute of Dental and Craniofacial Research, National Institutes of Health, Bethesda, MD 20892–4370, USA.

*These authors contributed equally to this work.
†To whom correspondence should be addressed. E-mail: sakai@dent.osaka-u.ac.jp (T.S.); kyamada@mail.nih.gov (K.M.Y.)

Wedges of fibronectin translocate inward as clefts form between randomly motile epithelial cells, accompanied by loss of the cell-cell adhesion molecule E-cadherin in cells adjacent to the fibronectin (*13*, *16*). How a matrix molecule can drive cleft formation and branching is unknown. We have identified the activity of a regulatory gene termed *Btbd7* at cleft-forming sites and provide mechanistic insight for dynamic cleft propagation in branching morphogenesis.

We focused initially on the mouse submandibular salivary gland, a classical model for analyzing mechanisms of branching morphogenesis (*12*, *17*, *18*). During branching, we observed local loss of the relatively columnar organization of cells in the outer layer of salivary epithelia (*19*) near the bottom of advancing clefts (Fig. 1, A to C, and fig. S1). Time-lapse confocal microscopy of glands from enhanced green fluorescent protein (EGFP)–expressing transgenic mice suggested that transient intercellular gaps form at this site as clefts advance, which we confirmed directly using fluorescent dextran to document dynamic gap formation as clefts deepen (Fig. 1D and fig. S2).

To search for a regulatory gene that might be involved in this process, we compared genes expressed in laser-microdissected epithelial cells from cleft regions versus end bud epithelial cells using T7 amplification and serial analysis of gene expression (SAGE) (Fig. 1E). As expected (*13*), fibronectin was strongly differentially expressed in cleft epithelial cells compared with buds (124/20,053 tags versus 4/22,244 tags; $P < 0.001$). Tags corresponding to Btbd7 [BTB (POZ) domain containing 7] were identified in cleft but not bud cells: 7/20,053 versus 0/22,244 tags, respectively ($P < 0.01$). This preliminary finding was confirmed by quantitative polymerase chain reaction (qPCR) with reverse transcription.

The deduced Btbd7 protein contains 1130 amino acids with two putative BTB/POZ domains (fig. S3). Regulatory proteins containing BTB domains are evolutionarily conserved from *Drosophila* to mammals (*20*, *21*). Btbd7 mRNA expression in developing salivary glands was highest at embryonic day 13 (E13), a stage of particularly active salivary gland branching (Fig. 1, F and G). Btbd7 expression by in situ hybridization showed striking concentration around the bottom and lower sides of forming clefts, whereas other salivary epithelial regions showed little or no expression (Fig. 2, A to D, and fig. S4). The Btbd7-expressing cells surround sites of high fibronectin concentration at the base of forming clefts (*13*, *16*), suggesting that Btbd7 might be induced by fibronectin or other matrix proteins. Because Btbd7 is also expressed in mesenchyme containing high levels of fibronectin (fig. S4), we used mesenchyme-free explants of intact embryonic salivary gland epithelia. Fibronectin induced Btbd7 expression ($P < 0.001$), whereas collagen I and IV had no effect (Fig. 2E). Thus, *Btbd7* is a fibronectin-induced gene. This Btbd7 induction was accompanied by morphological conversion of the outer layer of columnar epithelial cells to a less organized pattern within 2 hours (Fig. 2G), which mimicked the cell shape changes in vivo during cleft formation (e.g., Fig. 1, A to C). This fibronectin-induced epithelial disorganization could be rescued by small interfering RNA (siRNA) knockdown of Btbd7 (Fig. 2H and fig. S5).

To identify mechanisms of Btbd7 function, we turned to the well-characterized Madin-Darby canine kidney (MDCK) cell model for epithelial cell interactions (*22*). Transient Btbd7 transfection of MDCK cells or tetracycline-regulated expression in stably transfected cells (*23*) induced labile cell-cell adhesions and scattering of MDCK epithelial cell colonies to dispersing cell clusters in both two-dimensional (2D) cultures and 3D collagen gels (figs. S6 and S7). This cell dispersal was associated with loss of E-cadherin from cell boundaries according to immunolocalization (Fig. 3, A to F) and 77.1 ± 2.5% decreased E-cadherin protein levels by immunoblotting (Fig. 3G). Btbd7 expression stimulated the velocity of cell movement in 2D cell culture by a factor of 2, with increased random migration (fig. S6). It induced outward cell dispersal from aggregates in 3D collagen gels (fig. S7). Therefore, Btbd7 can induce loss of E-cadherin and increased cell dispersal in 2D and 3D, suggesting that the previously observed loss of E-cadherin in salivary gland cells adjacent to forming clefts in vivo (*13*) was due to the local induction of Btbd7.

Epithelial cell dispersal is often regulated by transcription factors such as Snail, Snail2 (Slug), and Twist1. Btbd7 expression induced Snail2 mRNA in MDCK cells with little effect on the expression of Snail and Twist1 (Fig. 3H). Immunostaining confirmed that Btbd7 expression induces Snail2 expression and accumulation of this transcription factor in the nucleus (fig. S8). This induction of Snail2 was not required for Btbd7-induced loss of E-cadherin (fig. S9), analogous to the inde-

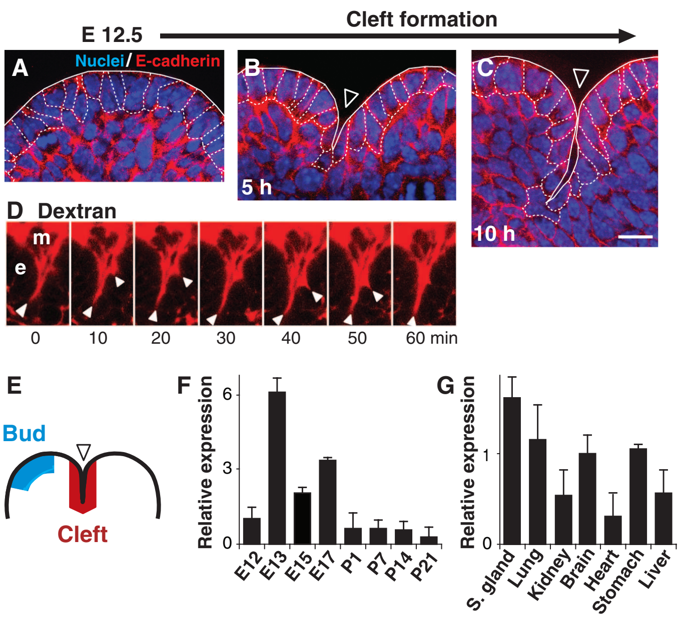

Fig. 1. Cleft formation and Btbd7. (**A** to **C**) Formation of clefts in a submandibular gland at E12.5 (A) or in glands cultured for 5 hours (B) or 10 hours (C). Fixed samples were stained with antibody to E-cadherin (red) and 4′,6′-diamidino-2-phenylindole (DAPI) (blue). Clefts (open triangles), basement membrane (white line), and E-cadherin (white dashed line) at cell boundaries of outer epithelial cells. (**D**) Cleft progression by transient gap formation as visualized by tetramethylrhodamine-labeled dextran. e, epithelium; m, mesenchyme. (**E**) Diagram of laser-microdissected developing salivary gland (red, cleft; blue, bud region). (**F** and **G**) Btbd7 mRNA expression by qPCR in developing embryonic and postnatal salivary glands (F) and in other organs (G). Scale bar, 10 μm.

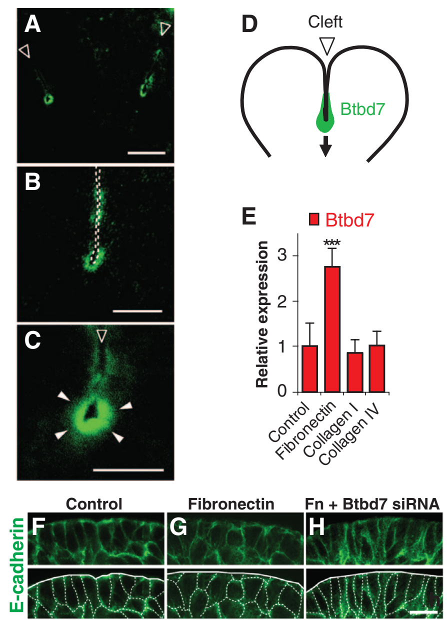

Fig. 2. Btbd7 expression and regulation by fibronectin. (**A** to **C**) In situ hybridization of Btbd7 around the lower sides and bottom of clefts at various stages and magnifications. Open triangles and dotted lines show locations of clefts. Filled triangles highlight Btbd7 expression at the base of a cleft. (**D**) Diagram of Btbd7 transcript pattern. (**E**) Btbd7 mRNA expression in salivary epithelial cells is induced by fibronectin as quantified by qPCR. (**F** to **H**) Exogenous fibronectin (Fn) reduces the organization of the outer layer of columnar epithelial cells; its effects are blocked by Btbd7 siRNA. Epithelia were stained for E-cadherin; traces below each image show basement membrane (white line) and E-cadherin (dashed line). Scale bars, (A to C) 50 μm; (F to H) 10 μm. ***$P < 0.001$. Error bars, SEM.

pendent regulation of Snail2 and E-cadherin in hepatocyte growth factor–treated MDCK cells (*24*).

After identifying this putative Btbd7 regulatory pathway in a model epithelial system, we searched for it in intact embryonic mouse tissues. Besides major increases of fibronectin and Btbd7 mRNA in cells adjacent to salivary clefts compared with bud epithelial cells of the same glands, Snail2 mRNA level was also elevated by a factor of 3.4 in cells near clefts ($P < 0.02$) (Fig. 4A). Incubating isolated salivary gland epithelia with purified fibronectin induced Btbd7 rapidly within 20 min, followed by the induction of Snail2 at 60 min (Fig. 4B). These kinetics in intact salivary epithelia are consistent with the induction of Snail2 by Btbd7 observed in MDCK cells in vitro. To investigate this relationship more directly, we performed siRNA knockdowns of Btbd7 versus Snail2 in salivary epithelial cultures. Btbd7 knockdown inhibited fibronectin-induced Snail2 expression, whereas Snail2 knockdown did not affect Btbd7 expression, indicating that Btbd7 is upstream of Snail2 (Fig. 4C).

To determine whether Btbd7 is necessary for branching morphogenesis, we suppressed Btbd7 expression in organ cultures of intact salivary glands using siRNA. Treatment with each of four different Btbd7 siRNA sequences produced substantial, morphologically similar suppression of cleft formation at 48 to 72 hours (Fig. 4, D and E, and fig. S10). Fewer (64% less) buds formed, but the buds were larger with the total volume of buds remaining about the same even though branching was inhibited (Fig. 4F). Cleft propagation speeds measured from time-lapse video movies (movie S1) decreased from 6.2 ± 1.1 μm/hour in controls to 3.7 ± 1.0 μm/hour in Btbd7 knockdown glands, confirming Btbd7's role in cleft propagation. We also tested whether Snail2 expression is required for branching morphogenesis using siRNA knockdown. Branching was inhibited ~67% by inhibition of Snail2 (fig. S11), confirming its functional role in branching morphogenesis.

Although Btbd7 is normally expressed only focally in embryonic epithelia, we investigated whether global overexpression by viral gene transfer to developing salivary epithelia could promote function. Ex vivo fragments of salivary epithelium transduced with adenoviral Btbd7 showed substantially enhanced tissue spreading (fig. S12), consistent with the in vitro stimulation of MDCK cell dispersal by Btbd7. Virus microinjection and expression of GFP-Btbd7 versus GFP in intact embryonic salivary glands produced a small but statistically significant increase in branching morphogenesis (fig. S13). Larger effects might be found if it were technically feasible to mimic the dynamic translocation of focal Btbd7 expression during cleft formation.

Branching morphogenesis of other organs, such as lungs and kidneys, can differ in the relative contributions to branching of bud outgrowth versus cleft formation. Nevertheless, fibronectin contributes to branching morphogenesis in these organs, especially lung (*14*, *15*, *25*), suggesting mechanistic commonalities. Although clefts in lung are broad curves rather than slits, Btbd7 is also expressed in lung at sites of epithelial curvature (fig. S14). Branching morphogenesis of embryonic lungs was similarly inhibited by Btbd7 siRNA but not by control siRNA (Fig. 4, G and H). We conclude that Btbd7 is needed for both mammalian salivary gland and lung branching morphogenesis.

Our data establish a mechanism for cleft propagation involving Btbd7 as a mediator of epithelial dynamics and organ branching. A schematic model of this stepwise mechanism is shown in fig. S15. The local accumulation of fibronectin in forming clefts rapidly induces the regulator Btbd7, which in turn induces local expression of the cell-scattering gene *Snail2* and suppresses E-cadherin levels, thereby altering cell morphology and reducing cell-cell adhesion. This stimulates cell separation at the base of forming clefts by local, dynamic intercellular gap formation and promotes cleft progression. Inhibiting any of these regulatory steps (i.e., fibronectin accumulation or function, Btbd7 expression, or Snail2 expression) inhibits branching morphogenesis. This hierarchy of steps provides a mechanistic pathway for cleft formation in epithelial branching.

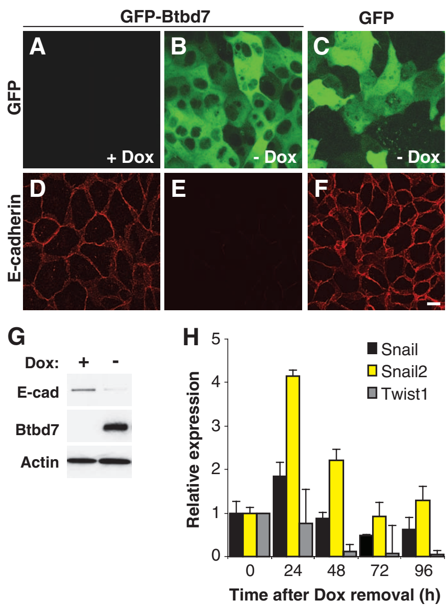

Fig. 3. Btbd7 suppresses E-cadherin and induces Snail2. (**A** to **C**) Pooled, stably transfected MDCK cells were established for Tet-off regulation of expression of GFP-Btbd7 (A, B) or GFP alone (C) by doxycycline (Dox) removal to induce Btbd7. (**D** to **F**) The same cells were immunostained for E-cadherin. (**G**) Decrease of total E-cadherin protein by Western blot analysis after Btbd7 expression. (**H**) Btbd7 expression induces Snail2 expression by qPCR. Scale bar, 20 μm.

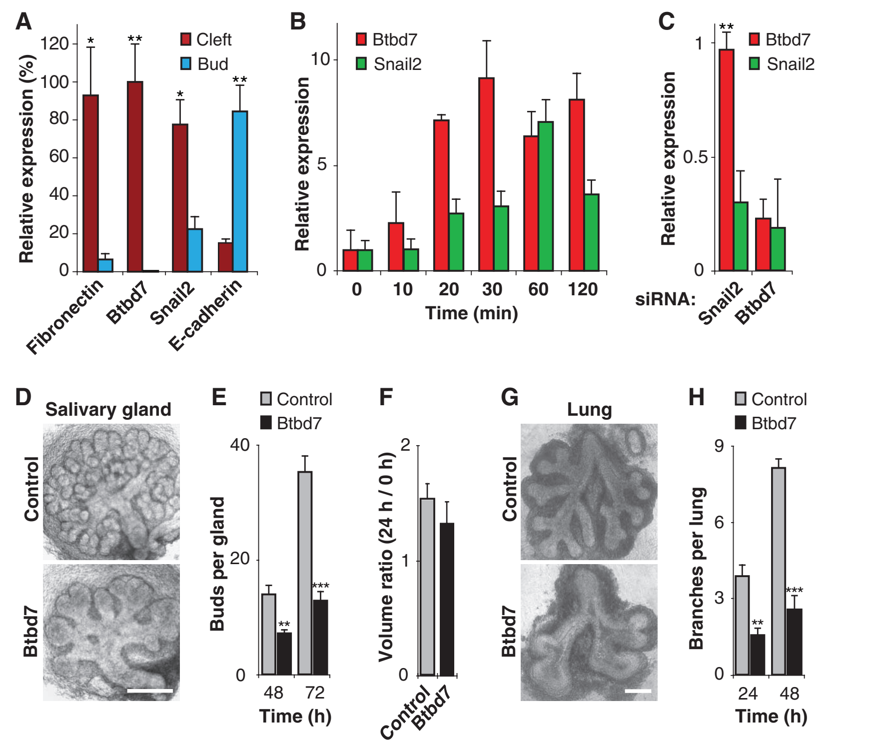

Fig. 4. Btbd7 expression induced by fibronectin regulates Snail2 expression and is required for branching morphogenesis. (**A**) mRNA expression of fibronectin, Btbd7, Snail2, and E-cadherin in cleft versus bud epithelia by qPCR. (**B**) Induction of Btbd7 and Snail2 expression after fibronectin addition to isolated salivary epithelium by qPCR. (**C**) Effects on epithelial expression of Btbd7 and Snail2 by siRNA knockdown of each gene. (**D** and **E**) Effect of Btbd7 siRNA knockdown in salivary gland organ culture (D) and quantification of numbers of buds per gland (E) ($n = 8$). (**F**) Total bud volume after siRNA transfection. (**G** and **H**) Effect of Btbd7 siRNA knockdown in embryonic lung (G) with quantification of branches (H) ($n = 15$). Scale bar, 100 μm. *$P < 0.05$; **$P < 0.01$; ***$P < 0.001$. Error bars, SEM.

References and Notes

1. J. A. Davies, *Bioessays* **24**, 937 (2002).
2. R. J. Metzger, M. A. Krasnow, *Science* **284**, 1635 (1999).
3. B. L. Hogan, P. A. Kolodziej, *Nat. Rev. Genet.* **3**, 513 (2002).
4. M. M. Zegers, L. E. O'Brien, W. Yu, A. Datta, K. E. Mostov, *Trends Cell Biol.* **13**, 169 (2003).
5. J. Que, M. Choi, J. W. Ziel, J. Klingensmith, B. L. Hogan, *Differentiation* **74**, 422 (2006).
6. J. E. Fata, Z. Werb, M. J. Bissell, *Breast Cancer Res.* **6**, 1 (2004).
7. R. B. Widelitz, J. M. Veltmaat, J. A. Mayer, J. Foley, C. M. Chuong, *Semin. Cell Dev. Biol.* **18**, 255 (2007).
8. M. M. Shah, R. V. Sampogna, H. Sakurai, K. T. Bush, S. K. Nigam, *Development* **131**, 1449 (2004).
9. V. N. Patel, I. T. Rebustini, M. P. Hoffman, *Differentiation* **74**, 349 (2006).
10. G. R. Dressler, *Annu. Rev. Cell Dev. Biol.* **22**, 509 (2006).
11. W. V. Cardoso, J. Lü, *Development* **133**, 1611 (2006).
12. B. S. Spooner, H. A. Thompson-Pletscher, B. Stokes, K. E. Bassett, *Dev. Biol.* **3**, 225 (1986).
13. T. Sakai, M. Larsen, K. M. Yamada, *Nature* **423**, 876 (2003).
14. S. E. Gill, M. C. Pape, K. J. Leco, *Dev. Biol.* **298**, 540 (2006).
15. S. P. De Langhe *et al.*, *Dev. Biol.* **277**, 316 (2005).
16. M. Larsen, C. Wei, K. M. Yamada, *J. Cell Sci.* **119**, 3376 (2006).
17. C. Grobstein, *Nature* **172**, 869 (1953).
18. W. P. Daley, K. M. Gulfo, S. J. Sequeira, M. Larsen, *Dev. Biol.* **336**, 169 (2009).
19. J. L. Walker *et al.*, *Dev. Dyn.* **237**, 3128 (2008).
20. S. Zollman, D. Godt, G. G. Privé, J. L. Couderc, F. A. Laski, *Proc. Natl. Acad. Sci. U.S.A.* **91**, 10717 (1994).
21. R. Perez-Torrado, D. Yamada, P. A. Defossez, *Bioessays* **28**, 1194 (2006).
22. F. Martin-Belmonte, K. Mostov, *Curr. Opin. Cell Biol.* **20**, 227 (2008).
23. M. Gossen, H. Bujard, *Proc. Natl. Acad. Sci. U.S.A.* **89**, 5547 (1992).
24. P. Leroy, K. E. Mostov, *Mol. Biol. Cell* **18**, 1943 (2007).
25. J. Roman, *Exp. Lung Res.* **23**, 147 (1997).
26. We thank M. Hoffman, M. Larsen, and K. Musselmann for advice. T.O. was supported by a fellowship from the Japan Society for the Promotion of Science (JSPS). This work was supported in part by the Intramural Research Program of the NIH, NIDCR, and by Grants-in-Aid for Scientific Research (B) (21390534) from the JSPS to T.S. The SAGE data sets are available at the Gene Expression Omnibus (GEO) database under accession number GSE22374.

Supporting Online Material

www.sciencemag.org/cgi/content/full/329/5991/562/DC1
Materials and Methods
Figs. S1 to S15
References
Movie S1

10.1126/science.1191880

Early Chordate Origins of the Vertebrate Second Heart Field

Alberto Stolfi,[1] T. Blair Gainous,[1] John J. Young,[1] Alessandro Mori,[1]* Michael Levine,[1]† Lionel Christiaen[1,2]†

The vertebrate heart is formed from diverse embryonic territories, including the first and second heart fields. The second heart field (SHF) gives rise to the right ventricle and outflow tract, yet its evolutionary origins are unclear. We found that heart progenitor cells of the simple chordate *Ciona intestinalis* also generate precursors of the atrial siphon muscles (ASMs). These precursors express *Islet* and *Tbx1/10*, evocative of the splanchnic mesoderm that produces the lower jaw muscles and SHF of vertebrates. Evidence is presented that the transcription factor COE is a critical determinant of ASM fate. We propose that the last common ancestor of tunicates and vertebrates possessed multipotent cardiopharyngeal muscle precursors, and that their reallocation might have contributed to the emergence of the SHF.

The vertebrate heart initially forms as a tube from a population of precursor cells termed the first heart field (FHF). Cells from the adjacent second heart field (SHF) are then progressively added to the developing heart (*1*, *2*). In avian and mammalian hearts, the FHF contributes mainly to the left ventricle, whereas the SHF gives rise to the outflow tract and large portions of the right ventricle and atria. Both fields arise from common mesodermal progenitors, although the detailed lineage relationships between FHF and SHF remain uncertain (*1*, *3*). SHF-like territories have been identified in frog (*4*, *5*), zebrafish (*6*), and lamprey (*7*), yet evidence for a deeper evolutionary origin remains obscured by the absence of a clear SHF in invertebrates (*8*).

Tunicates are the sister group to the vertebrates (*9*). Studies on a model tunicate, the ascidian *Ciona intestinalis*, have revealed conserved regulatory mechanisms underlying chordate heart development (*10*). The *Ciona* heart arises from a pair of blastomeres (named the B7.5 cells, by Conklin's nomenclature) in gastrulating embryos (*11*). Localized expression of *MesP* in B7.5 cells determines their competence to form the heart (Fig. 1A) (*12*, *13*). Subsequently, fibroblast growth factor signaling induces expression of *FoxF* and the heart determinants *NK4* (*tinman/Nkx2.5*), *GATAa*, and *Hand-like/NoTrlc* in the anterior B7.5 granddaughter cells [the trunk ventral cells (TVCs)] (Fig. 1B) (*13*, *14*). FoxF activates downstream target genes that control the migration of the TVCs to the ventral trunk region (Fig. 1C) (*14*, *15*).

After metamorphosis, descendants of the B7.5 lineage give rise to the heart (Fig. 1D). B7.5 descendants also generate the atrial siphon muscles (ASMs) that surround the excurrent openings of the peribranchial atrium (Fig. 1D), as well as longitudinal muscles (LoMs) arising from the ASMs during metamorphosis (fig. S7). The contribution of the B7.5 lineage to ASMs is consistent with conventional lineage tracing performed in the distantly related ascidian *Halocynthia roretzi* (*16*). Cardiomyocytes and ASMs are distinguished by expression of the myosin heavy chain (MHC) genes *MHC2* and *MHC3* (*17*), respectively (fig. S3). Thus, they constitute distinct muscle types arising from common progenitor cells.

Live imaging of the B7.5 lineage cells allowed the characterization of events leading to the separation of heart and ASMs (Fig. 1E). After their migration to the ventral trunk region, each TVC undergoes two successive asymmetric divisions along the mediolateral axis to produce six cells on either side of the ventral midline (Fig. 1, E and F, time points 0 to 2; movie S1). The larger daughter cells (lateral TVCs) are positioned lateral to the smaller medial TVCs. Subsequent symmetric cell divisions result in an array of ~24 cells: eight lateral TVCs (four on either side) bracketing 16 medial TVCs (Fig. 1, E and F, time points 3 to 5; movie S2) (*18*).

A second migration occurs several hours after hatching. Each group of lateral TVCs detaches from the medial TVCs and migrates dorsally as a polarized cluster of cells on either side of the trunk. They eventually form a ring of cells underneath the atrial siphon primordia (Fig. 1, G and H, and movie S3). Targeted inhibition of TVC specification blocked the formation of ASMs (fig. S4). These observations demonstrate that the lateral TVCs correspond to the precursors of the ASMs.

The ASMs are evocative of vertebrate jaw muscles arising from lateral/splanchnic mesoderm (SpM): *Ciona* TVCs and vertebrate anterior SpM both express orthologs of *Nkx2.5* and *FoxF* and derive from progenitors that expressed *MesP* during gastrulation (*5*, *19*, *20*). In chick and mouse embryos, much of the anterior SpM gives rise to the SHF, but some precursors migrate into the first branchial arch and form intermandibular muscles (*21*, *22*). A key marker of the anterior SpM and SHF is the LIM-homeodomain transcription factor Islet1 (Isl1) (*4*–*6*, *21*). The single *Ciona Islet* (*23*) gene is expressed in several tissues including the ASM precursors, which maintain *Islet* expression during their migration away from the medial TVCs (fig. S1). The latter possibly show weak and transient *Islet* expression, which is reminiscent of that reported in the FHF of vertebrates (*19*).

Islet expression was further characterized using defined enhancers (fig. S2). Reporter transgenes containing ~3.2 kb of the *Islet* 5′ flanking region exhibited localized expression in the lateral TVCs, and in ASMs in juveniles (Fig. 2, A to C). In contrast, *MesP* reporter transgenes labeled the entire B7.5 lineage, including both ASMs and heart (e.g., Fig. 1, C and D, and fig. S5). The

[1]Center for Integrative Genomics, Division of Genetics, Genomics and Development, Department of Molecular and Cell Biology, University of California, Berkeley, CA 94720, USA. [2]Center for Developmental Genetics, Department of Biology, New York University, 1009 Silver Center, 100 Washington Square East, New York, NY 10003, USA.

*Present address: Forest Laboratories Inc., 909 Third Avenue, New York, NY 10022, USA.

†To whom correspondence should be addressed. E-mail: mlevine@berkeley.edu (M.L.); lc121@nyu.edu (L.C.)

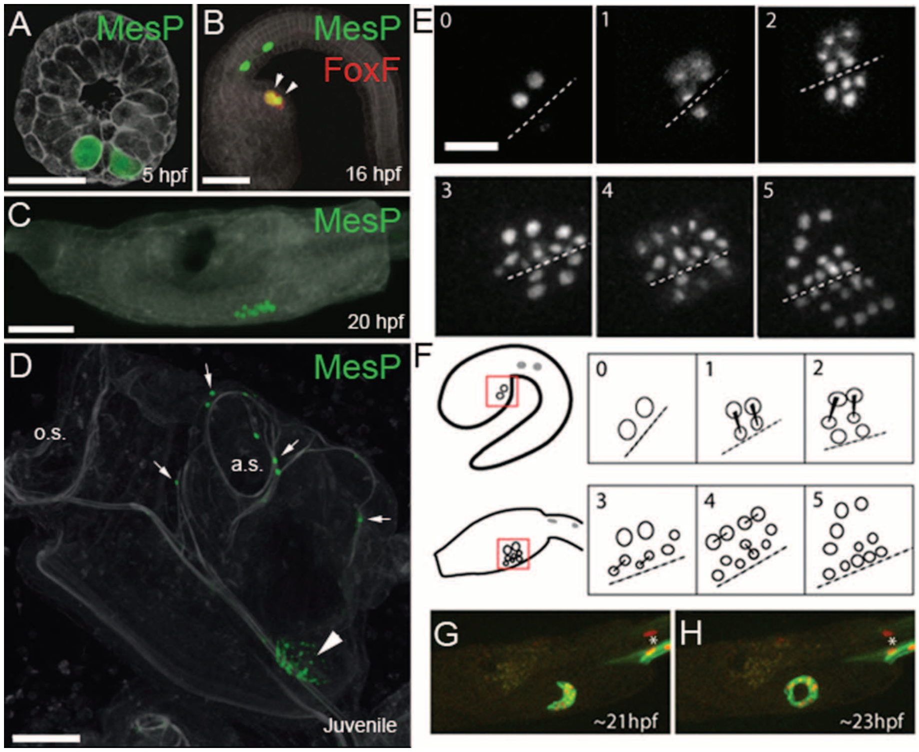

Fig. 1. Contribution of trunk ventral cells (TVCs) to heart and atrial siphon muscles (ASMs). (**A**) Immunodetection of β-gal expression (green) in B7.5 cells in a gastrulating embryo transfected with *MesP>lacZ* transgene. (**B**) Visualization of *MesP>lacZ* (green) and *FoxF[TVC enhancer]>mCherry* (red) expression in B7.5 descendants in a tailbud-stage embryo. (**C**) Expression of a *MesP>Histone2B(H2B)::GFP* fusion protein (green) in a tadpole. (**D**) Visualization of *MesP>H2B::CFP* (green) in a stage 38 juvenile [~100 hours post-fertilization (hpf)]. Expression is visible in the heart (arrowhead), ASMs, and longitudinal muscles (LoMs) (arrows). *MesP* is activated only in the B7.5 pair of cells at the gastrula stage. a.s., atrial siphon; o.s., oral siphon. (**E**) Frames from movie S1 (time points 0 to 2) and S2 (time points 3 to 5). Dashed line indicates ventral midline. Right-side cells are partially visible at time points 1 and 2. Stereotyped cell divisions (see text) result in four lateral TVCs on either side of the embryo flanking ~16 medial TVCs. The four lateral TVCs on either side detach and migrate to form ASMs. Medial cells form the heart. Cells were visualized as two independent time-lapse sequences of embryos transfected with *MesP>H2B::GFP/CFP*. (**F**) Cartoon representing the events in (E). (**G** and **H**) Frames from movie S3 showing left-side ASM precursors expressing *MesP>H2B::mCherry* (red) and *MesP>PH::GFP* (green). ASM precursors encircle the siphon primordium, between 21 hpf (G) and 23 hpf (H). Scale bars, 50 μm [(A) to (D)], 20 μm (E). Asterisks identify anterior tail muscles (ATMs).

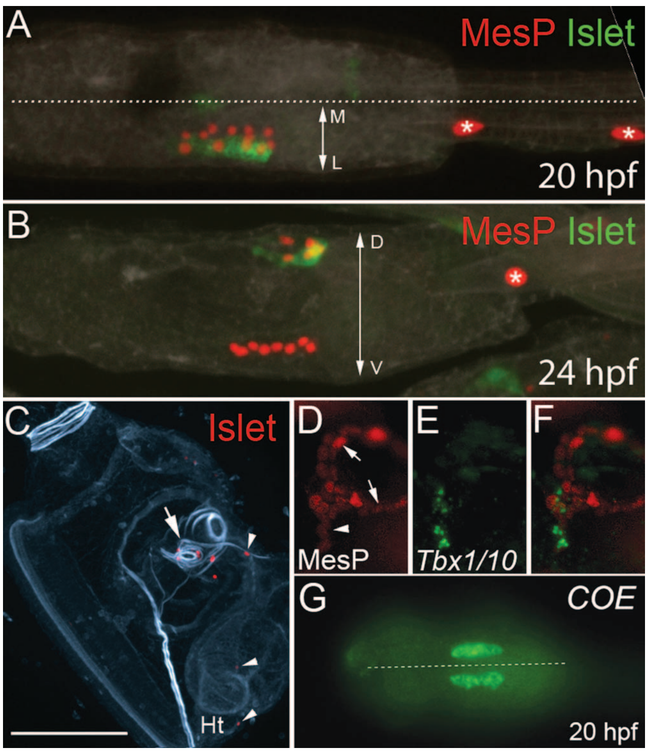

Fig. 2. ASM-specific gene expression. (**A**) Dorsal view of electroporated larva exhibiting mosaic incorporation (left side) of *Islet>GFP* (green) and *MesP>H2B::mCherry* (red) transgenes at 20 hpf, before the migration of the lateral TVCs. *Islet>GFP* expression is restricted to lateral TVCs. Dotted line indicates midline; M and L indicate medial and lateral, respectively. (**B**) Lateral view of larva expressing same transgenes as in (A) at 24 hours, after migration of *Islet>GFP*-positive lateral TVC descendants around the atrial siphon primordium. D, dorsal; V, ventral. (**C**) Juvenile (~100 hpf) raised from embryo transfected with *Islet>H2B::mCherry* (red), with transgene expression visible around atrial siphons (arrow) and longitudinal muscles (arrowheads), but not heart (Ht). F-actin is stained by phallacidin (blue-green). Scale bar, 100 μm. (**D**) Magnified view (see fig. S7) of LoMs (arrowhead) segregating from ASMs (arrows) during metamorphosis, visualized by *MesP>lacZ* expression (red). Panel width is ~100 μm. (**E**) In situ hybridization of *Tbx1/10* (green). (**F**) Merged view of (D) and (E), showing activation of *Tbx1/10* in LoMs. (**G**) *COE* expression in lateral TVCs at 20 hpf revealed by in situ hybridization. Dotted line indicates ventral midline.

heart primordium is situated ventrally and medially to the *Islet*+ ASM progenitors (Fig. 2A). This is reminiscent of the positioning of the FHF relative to *Isl1*+ SHF/pharyngeal mesoderm in basal vertebrates (*4*, *5*, *7*). Furthermore, LoM precursors segregating from the ASMs express the *Ciona* ortholog of *Tbx1* (*24*), an important regulator of SHF and pharyngeal mesoderm development in vertebrates (*25*) (Fig. 2, D to F, and fig. S7). Taken together, these results suggest homology between the ASM/LoM precursors of tunicates and the progenitors of lower jaw muscles and SHF of vertebrates.

Preliminary functional assays suggest that Islet is not instructive for the specification of ASMs (fig. S10). In the course of these studies, we found that the transcription factor *Collier/Olf1/EBF* (*COE*) is expressed early in the ASM precursors (Fig. 2G and fig. S11). To determine whether this localized expression is instructive for ASM specification, we used the *FoxF* TVC enhancer to misexpress COE in all TVCs (*13*). In 96% of transfected embryos, all TVC descendants migrated toward the atrial siphon placodes and expressed *Islet>GFP* (Fig. 3, A and B, fig. S6, and movie S4). More than half (56%) of the transfected embryos grew into juveniles that lacked a heart but still had ASMs (Fig. 3, D, E, and G to J, and fig. S6), which suggests that COE is sufficient to specify a lateral TVC identity and subsequent ASM fate.

Similar misexpression of a repressor form of COE (COE::WRPW) resulted in the reciprocal phenotype: All TVC descendants remained in the ventral trunk, and *Islet>GFP* expression was abolished (Fig. 3, A and C, and fig. S6). Upon metamorphosis, TVC descendants differentiated into enlarged hearts (Fig. 3, D, F to H, K, and L, and fig. S8). Inhibition of COE function thus transforms the entire TVC lineage into heart tissue, in-

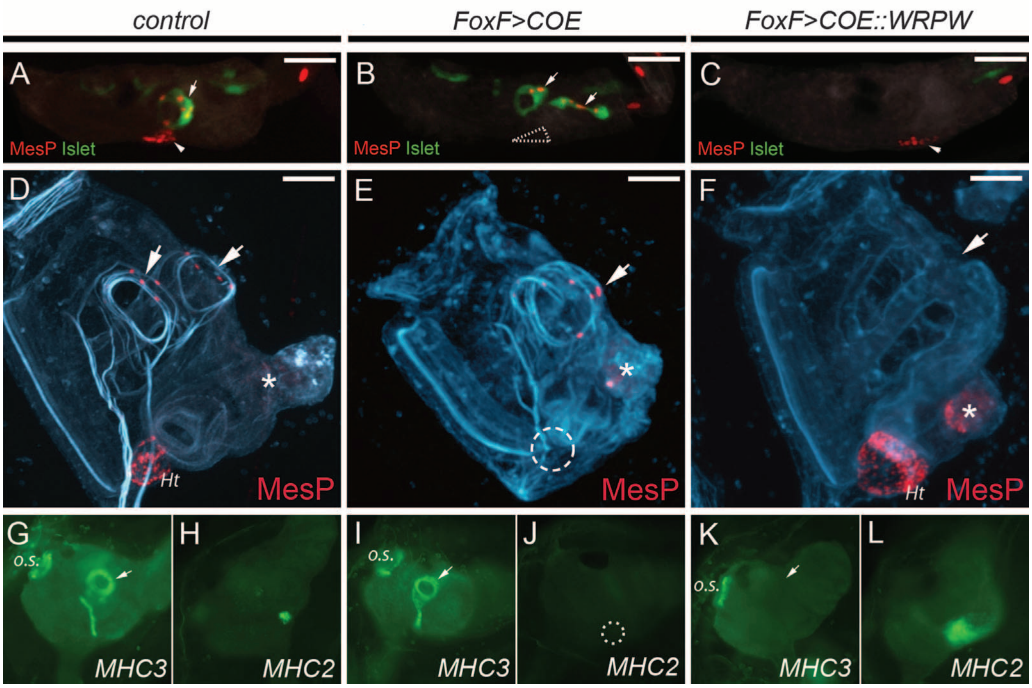

Fig. 3. COE controls ASM specification. (**A** to **C**) Larvae cotransfected with *MesP>H2B::mCherry* (red), *Islet>GFP* (green), and (A) *FoxF>lacZ*, (B) *FoxF>COE*, or (C) *FoxF>COE::WRPW*. (B) All TVCs are transformed into ASM precursors (arrows). No heart primordium is formed (dashed triangle). (C) All TVC descendants form a heart (arrowhead) with no *Islet>GFP* expression. (**D**) Juveniles raised from embryos transfected with *MesP>H2B::mCherry* (red), counterstained with phallacidin (blue-green). H2B::mCherry$^+$ B7.5 descendants populate the heart (Ht) and ASMs (arrows) (residual larval muscle staining indicated by asterisk). (**E**) Cotransfection with the *FoxF>COE* transgene, resulting in no heart (usual location indicated by dashed circle) but normal ASMs (arrow). (**F**) Coexpression of the *FoxF>COE:WRPW* transgene. TVCs form an expanded heart and there are no ASMs (arrow). (**G** and **H**) In situ hybridization on wild-type juveniles, showing *MHC3* and *MHC2* expression in ASMs (arrow) and heart, respectively. (**I** and **J**) *FoxF>COE* results in loss of *MHC2* expression (dashed circle), but not *MHC3* expression (arrow). (**K** and **L**) *FoxF>COE::WRPW* abolishes *MHC3* expression (arrow) and leads to expanded *MHC2* expression. Scale bars, 50 μm; o.s., oral siphons.

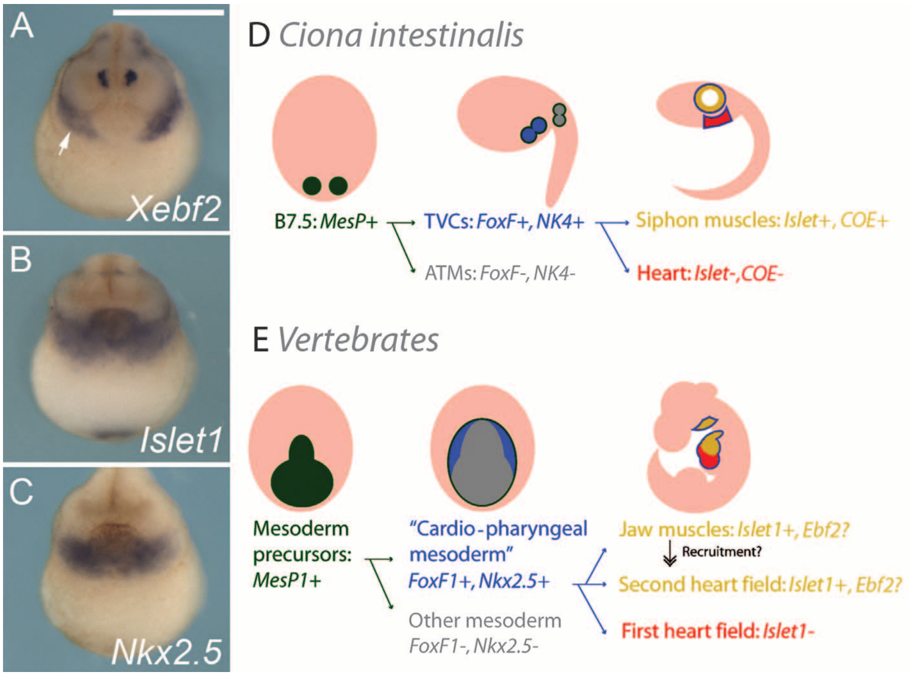

Fig. 4. Comparison to vertebrate pharyngeal mesoderm. (**A** to **C**) Expression of the *COE* ortholog *Xebf2* and anterior lateral mesoderm/SHF markers *Nkx2.5* and *Islet1* in *X. tropicalis* embryos at NF stage 20. (A) Expression of *Xebf2* (white arrow) partially overlaps that of *Islet1* (B) and *Nkx2.5* (C) in pharyngeal mesoderm lateral to the heart primordium. Scale bar, 500 μm. (**D** and **E**) The cardiopharyngeal lineages of *Ciona* (D) and vertebrates (E). (D) Summary of differential expression of selected regulatory genes in the B7.5 lineage. (E) Expression of orthologous genes in mouse development. Evolutionary reallocation of *Islet1*$^+$ cardiopharyngeal precursors toward the heart might have given rise to the SHF.

dicating that COE activity is required for ASM specification.

The COE homolog Collier/Knot is involved in muscle type specification in *Drosophila* (*26*), but a role for COE in vertebrate SHF or jaw muscle development has not been reported. As a first step toward determining whether COE factors might play a conserved role in vertebrates, we performed in situ hybridization of the *COE* orthologs *Xebf2* and *Xebf3* in *Xenopus tropicalis* embryos (Fig. 4, A to C, and fig. S9). *Xebf2* expression was seen in *Nkx2.5*$^+$/*Isl1*$^+$ anterior lateral mesoderm, where *Tbx1* is also expressed (*5*).

The preceding results suggest that the last common ancestor of tunicates and vertebrates had a population of cardiopharyngeal mesoderm, which (i) arose from *MesP*-expressing early mesoderm, (ii) expressed orthologs of *FoxF* and *Nkx2.5*, and (iii) had the potential to give rise to both heart tissue and pharyngeal muscles, which (iv) correlated with differential maintenance of *Islet* expression. Moreover, *COE* might be a conserved determinant of chordate pharyngeal mesoderm development.

We propose that the reallocation of *Islet*$^+$ cardiopharyngeal progenitors among the heart and cranial myogenic fields supported the emergence of the SHF (Fig. 4, D and E). In *Ciona*, *Islet*$^+$ cells do not contribute to the heart, but targeted expression of COE::WRPW was sufficient to convert them into cardiomyocytes. It is conceivable that the reallocation of *Islet*$^+$ pharyngeal muscle progenitors toward SHF depended on the interca-

lation of cardiac regulatory network components (e.g., *GATA4*, *Mef2c*) downstream of *Islet* (*27*).

An ancient connection between heart and craniofacial muscles has been proposed on the basis of the role of an *Nkx2.5* ortholog in the pharynx of the nematode *Caenorhabditis elegans*, which lacks a heart (*28*). *Haikouella lanceolata*, a fossil chordate from the Lower Cambrian, shows a putative heart adjacent to a muscularized pharyngeal atrium (*29*). The shared lineage of cardiomyocytes and pharyngeal muscles in tunicates hints that a pool of common precursors could have formed both heart and pharyngeal atrium muscles in a *Haikouella*-like ancestor. Northcutt and Gans (*30*) proposed that muscular ventilation of the pharyngeal arches was a key transition in the evolution of the vertebrates. Therefore, the cardiopharyngeal mesoderm could have been instrumental in the coevolution of circulatory, respiratory, and feeding functions in tunicates and vertebrates.

References and Notes

1. M. Buckingham, S. Meilhac, S. Zaffran, *Nat. Rev. Genet.* **6**, 826 (2005).
2. R. Abu-Issa, M. L. Kirby, *Annu. Rev. Cell Dev. Biol.* **23**, 45 (2007).
3. S. M. Meilhac, M. Esner, R. G. Kelly, J. F. Nicolas, M. E. Buckingham, *Dev. Cell* **6**, 685 (2004).
4. T. Brade, S. Gessert, M. Kühl, P. Pandur, *Dev. Biol.* **311**, 297 (2007).
5. S. Gessert, M. Kuhl, *Dev. Biol.* **334**, 395 (2009).
6. E. de Pater *et al.*, *Development* **136**, 1633 (2009).
7. N. Kokubo *et al.*, *Evol. Dev.* **12**, 34 (2010).
8. J. M. Perez-Pomares, J. M. Gonzalez-Rosa, R. Munoz-Chapuli, *Int. J. Dev. Biol.* **53**, 1427 (2009).
9. F. Delsuc, H. Brinkmann, D. Chourrout, H. Philippe, *Nature* **439**, 965 (2006).
10. B. Davidson, *Semin. Cell Dev. Biol.* **18**, 16 (2007).
11. Y. Satou, K. S. Imai, N. Satoh, *Development* **131**, 2533 (2004).
12. L. Christiaen, A. Stolfi, B. Davidson, M. Levine, *Dev. Biol.* **328**, 552 (2009).
13. B. Davidson, W. Shi, J. Beh, L. Christiaen, M. Levine, *Genes Dev.* **20**, 2728 (2006).
14. J. Beh, W. Shi, M. Levine, B. Davidson, L. Christiaen, *Development* **134**, 3297 (2007).
15. L. Christiaen *et al.*, *Science* **320**, 1349 (2008).
16. T. Hirano, H. Nishida, *Dev. Biol.* **192**, 199 (1997).
17. M. Ogasawara *et al.*, *Dev. Genes Evol.* **212**, 173 (2002).
18. B. Davidson, W. Shi, M. Levine, *Development* **132**, 4811 (2005).
19. O. W. Prall *et al.*, *Cell* **128**, 947 (2007).
20. J. Kang, E. Nathan, S. M. Xu, E. Tzahor, B. L. Black, *Dev. Biol.* **334**, 513 (2009).
21. E. Nathan *et al.*, *Development* **135**, 647 (2008).
22. E. Tzahor, *Dev. Biol.* **327**, 273 (2009).
23. P. Giuliano, R. Marino, M. R. Pinto, R. De Santis, *Mech. Dev.* **78**, 199 (1998).
24. N. Takatori *et al.*, *Dev. Dyn.* **230**, 743 (2004).
25. Z. Zhang, T. Huynh, A. Baldini, *Development* **133**, 3587 (2006).
26. M. Crozatier, A. Vincent, *Development* **126**, 1495 (1999).
27. E. N. Olson, *Science* **313**, 1922 (2006).
28. P. G. Okkema, E. Ha, C. Haun, W. Chen, A. Fire, *Development* **124**, 3965 (1997).
29. J. Y. Chen, D. Y. Huang, C. W. Li, *Nature* **402**, 518 (1999).
30. C. Gans, R. G. Northcutt, *Science* **220**, 268 (1983).
31. We thank D. Hendrix for computational analysis, A. Cooc for technical assistance, and R. Harland, I. Philipp, and T. J. Park for advice. Supported by NSF grant IOB 0445470 (M.L.), NIH training grant 0745322 (T.B.G.), and a New York University Faculty of Arts and Science start-up package (L.C.).

Supporting Online Material
www.sciencemag.org/cgi/content/full/329/5991/565/DC1
Materials and Methods
Figs. S1 to S11
Movies S1 to S4

29 March 2010; accepted 17 June 2010
10.1126/science.1190181

Identification of a Cell of Origin for Human Prostate Cancer

Andrew S. Goldstein,[1] Jiaoti Huang,[2,3,6] Changyong Guo,[2,4] Isla P. Garraway,[2,4] Owen N. Witte[1,5,6]*

Luminal cells are believed to be the cells of origin for human prostate cancer, because the disease is characterized by luminal cell expansion and the absence of basal cells. Yet functional studies addressing the origin of human prostate cancer have not previously been reported because of a lack of relevant in vivo human models. Here we show that basal cells from primary benign human prostate tissue can initiate prostate cancer in immunodeficient mice. The cooperative effects of AKT, ERG, and androgen receptor in basal cells recapitulated the histological and molecular features of human prostate cancer, with loss of basal cells and expansion of luminal cells expressing prostate-specific antigen and alpha-methylacyl-CoA racemase. Our results demonstrate that histological characterization of cancers does not necessarily correlate with the cellular origins of the disease.

Prostate cancer research has been hindered by an absence of model systems in which the disease is initiated from primary human prostate epithelial cells, precluding investigation of transforming alterations and cells of origin. Commonly used human prostate cancer cell lines and xenografts are derived from metastatic lesions. Murine prostate cancer models prohibit testing of species-specific therapies such as monoclonal antibodies against human proteins (*1*). An ideal model system would be human cell–derived and present as a multifocal disease, to accurately represent the heterogeneity of prostate malignancy (*2*). The system should allow one to investigate the role that specific genetic alterations and paracrine signals play in disease initiation and progression. Finally, the model system should be highly malleable, allowing for comparisons of lesions derived from different cell populations or driven by different genetic alterations. We created such a system by directly transforming naïve adult human prostate epithelium with genetic alterations that are commonly found in human prostate cancer. Activation of the PI 3-kinase pathway, typically via loss of PTEN (*3*), and increased expression of the ETS-family transcription factor ERG through chromosomal translocation (*4*) occur frequently together in human prostate cancer and cooperate to promote disease progression in mice (*5*–*7*). Androgen receptor (AR) is commonly up-regulated in human prostate cancer, and the androgen signaling axis is implicated in late-stage disease (*8*).

Luminal cells are generally accepted as the cells of origin for human prostate cancer (*9*, *10*), because pathologists diagnose the disease based on the absence of basal cell markers (*11*). Evidence from the mouse implicates both luminal cells (*12*–*14*) and basal cells (*15*–*17*) in prostate cancer initiation. Although murine cancer cell-of-origin studies typically involve transgenic mice with oncogene expression or Cre-mediated deletion of tumor suppressors driven by cell type–specific promoters (*18*), parallel studies in the human system require both a method to reliably separate subpopulations of primary cells and an in vivo transformation model.

In addition to rare neuroendocrine cells and reported intermediate phenotypes, the three main epithelial cell populations described in the human prostate are K5 (keratin 5)$^+$ K14$^+$ K8/18^{lo} basal cells, K5$^+$ K14$^-$ K8/18^{lo} basal cells, and K5$^-$ K14$^-$ K8/18^{hi} luminal cells (*19*). No commonly accepted strategy exists to isolate such populations from dissociated human prostate tissue. We have previously demonstrated expression of CD49f (integrin alpha 6) and Trop2 (TACSTD2) in human prostate tissue by immunohistochemical staining and flow cytometry, where these two antigens distinguish four separate populations (*20*, *21*). To determine the cellular identities of each population, we performed intracellular flow cytometry for basal (K14) and luminal (K18) keratins on primary human prostate cells, in addition to Western blot and quan-

[1]Molecular Biology Institute, University of California, Los Angeles (UCLA), Los Angeles, CA 90095, USA. [2]Jonsson Comprehensive Cancer Center, UCLA, Los Angeles, CA 90095, USA. [3]Department of Pathology and Laboratory Medicine, UCLA, Los Angeles, CA 90095, USA. [4]Department of Urology, UCLA, Los Angeles, CA 90095, USA. [5]Department of Microbiology, Immunology and Molecular Genetics; Department of Molecular and Medical Pharmacology; Howard Hughes Medical Institute, David Geffen School of Medicine, UCLA, Los Angeles, CA 90095, USA. [6]Eli and Edythe Broad Center of Regenerative Medicine and Stem Cell Research, UCLA, Los Angeles, CA 90095, USA.

*To whom correspondence should be addressed at Howard Hughes Medical Institute, UCLA, Los Angeles, 675 Charles E. Young Drive South, 5-748 MRL, Los Angeles, CA 90095–1662, USA. E-mail: owenwitte@mednet.ucla.edu

titative reverse transcription polymerase chain reaction (qRT-PCR) analyses on fractions isolated by fluorescence-activated cell sorting (FACS). The CD49f^{lo}Trop2^{hi} fraction expresses high levels of the luminal keratins K8 and K18, low or negative levels of basal keratins K5 and K14, and high expression of AR and of several androgen-regulated genes such as *prostate-specific antigen* (*PSA*), *Nkx3-1*, and *TMPRSS2* (Fig. 1, A to C, and fig. S1). The CD49f^{hi}Trop2^{hi} fraction expresses high levels of K5 and the basal transcription factor p63, and shows two discrete peaks for K14 by intracellular flow cytometry, presumably containing both K14^{+} and K14^{-} basal cells (Fig. 1, A to C, and fig. S1). CD49f^{hi}Trop2^{hi} cells express intermediate levels of the luminal-type keratins (Fig. 1A), confirming previous reports that basal cells express low but detectable levels of K8/18 (*19*). CD117 (Kit) expression is not enriched in either epithelial fraction (fig. S1). The results from three different approaches confirm that we can reproducibly enrich for the isolation of basal and luminal epithelial cells from primary human prostate tissue. The remaining cells are negative for both epithelial keratins, and gene expression analysis indicates enrichment in CD31^{+} von Willebrand factor (VWF)$^{+}$ endothelial cells (CD49f^{hi}Trop2^{-}) and CD90^{+} Vimentin^{+} stromal cells (CD49f^{lo} Trop2^{-}) (Fig. 1, A to C, and fig. S1).

Classic human epithelial transformation studies involve an initial selection process via immortalization through manipulation with genetic influences, such as the SV40 T-antigen and/or the catalytic subunit of telomerase, in addition to the selected oncogenes (*22*). We wanted to avoid culture selection by directly transforming primary cells before transplantation, so we looked to a recent report by Morrison and colleagues to gain insight into in vivo conditions. Quintana *et al.* reported that the number of primary human melanoma cells capable of tumor formation could be vastly improved by transplanting primary cells subcutaneously with Matrigel into NOD-SCID-IL-2Rγ^{null} (NSG) mice (*23*). Adapting this strategy, we transduced primary human prostate cells with lentivirus, combined these cells with murine urogenital sinus mesenchyme (UGSM) cells in Matrigel, and injected the combination subcutaneously into NSG mice. Starting materials were obtained from patients undergoing radical prostatectomy surgeries, and benign tissues were carefully separated from cancer tissues by an experienced urologic pathologist. Benign starting materials were negative for expression of human prostate malignancy markers and displayed no features of histologic transformation (fig. S2). Transplantation of cells without genetic modification never resulted in prostatic intraepithelial neoplasia (PIN) or cancer, demonstrating an absence of malignant cells in starting materials.

We transduced 10^{5} primary human prostate basal or luminal cells with a control lentivirus carrying the fluorescent marker red fluorescent protein (RFP) and found that both cell types were capable of lentiviral transduction (fig. S3). We next combined freshly sorted cells with UGSM in Matrigel and transplanted them into NSG mice. Although we were concerned that one cell type might preferentially undergo apoptosis in response to sorting, injection, or residence in the subcutaneous space, we found that both cell types survived at relatively equal rates (fig. S4). When grafts were harvested after 8 to 16 weeks in vivo, outgrowths were observed only from basal cells (Fig. 1D). Luminal-derived grafts lacked epithelial structures and mimicked transplantation of UGSM cells alone (Fig. 1D). Basal-derived prostatic tubules exhibited a remarkable similarity to the native architecture of the gland, demonstrated by an outer K5^{+} p63^{+} basal cell layer and one or multiple K8^{+} AR^{+} luminal layers (Fig. 1E). As few as 5000 basal cells were sufficient to generate ducts with distinct basal and luminal layers (table S1). Dissociated cells from grafts recapitulated the original four populations by flow cytometry, discerned by expression of Trop2 and CD49f (Fig. 1F). Staining for a human-specific Trop2 antibody confirmed the

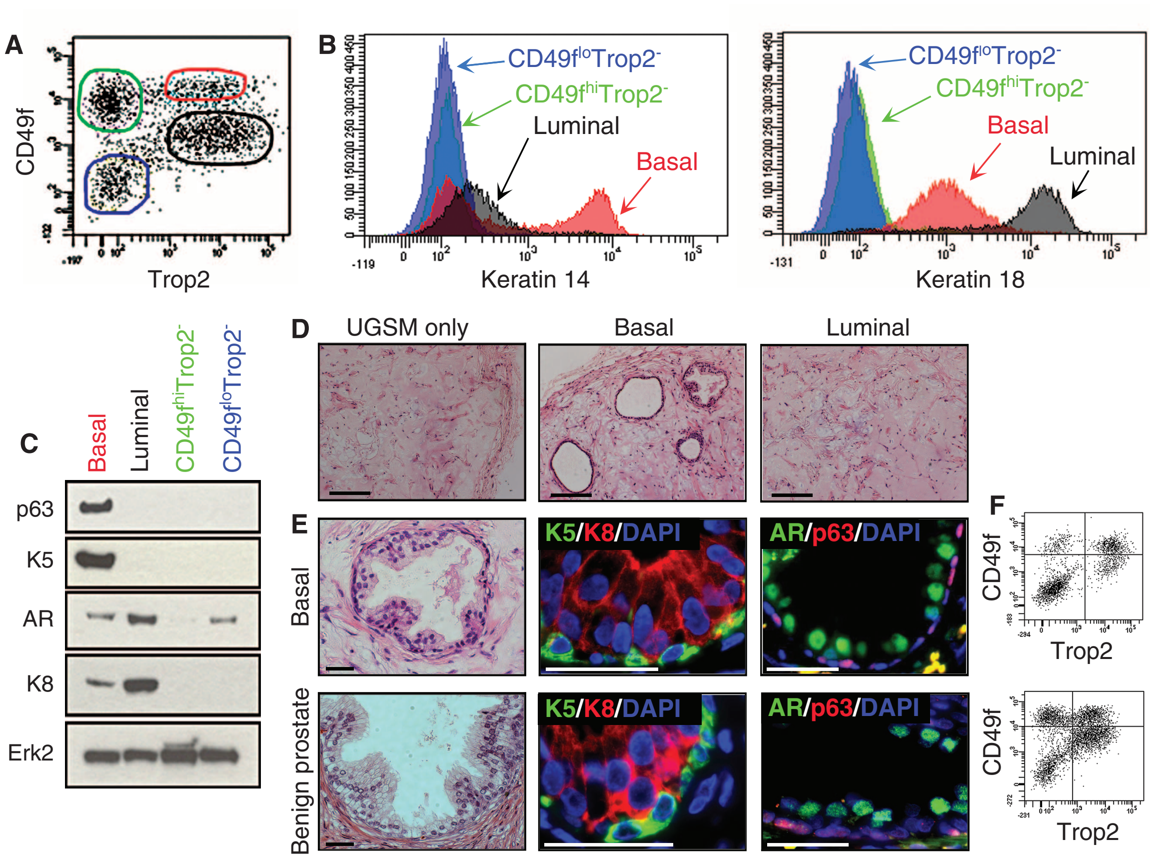

Fig. 1. Purification of epithelial cell fractions from primary prostate tissue. (**A**) FACS plots show the distribution of dissociated primary prostate cells, based on expression of CD49f and Trop2 and gates drawn to distinguish four populations. (**B**) Expression of K14 and K18 for each of the four populations indicated in (A). (**C**) Immunoblots of lysates from each subpopulation, analyzed for expression of basal proteins K5 and p63 and luminal proteins K8 and AR. Erk2 is included as a loading control. (**D**) H&E-stained sections of outgrowths generated from dissociated cells transplanted subcutaneously into NSG mice. Scale bars, 200 μm. (**E**) Tissue generated from human prostate basal cells (top row) resembles benign human prostate tissue (bottom row). H&E staining shows tubule structure. High-power images of immunostained prostatic tubules demonstrate the presence of distinct basal and luminal layers. Yellow spots are negative for DAPI and indicate autofluorescent spots rather than nuclei. Scale bars, 40 μm. (**F**) FACS plots show the presence of four populations with regard to CD49f and Trop2 staining on dissociated cells from basal-derived outgrowths or benign human prostate tissue.

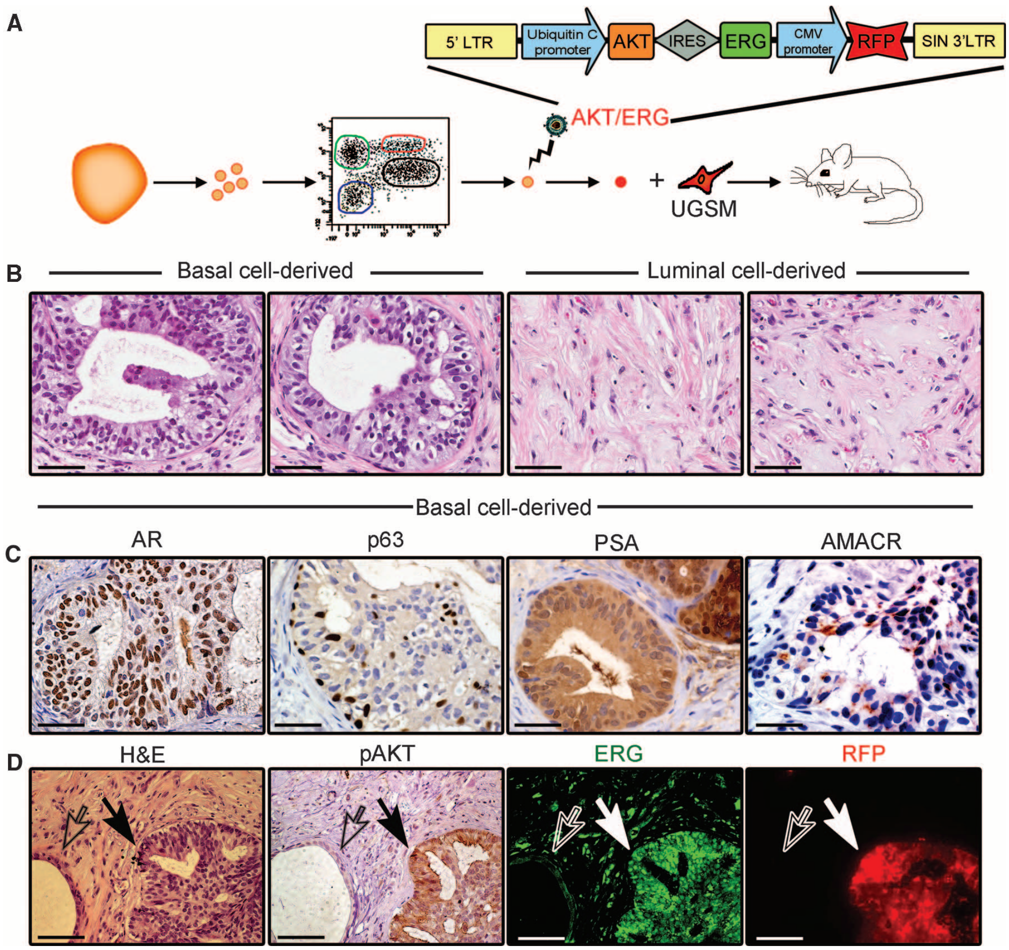

Fig. 2. A model of PIN initiated in primary basal cells. (**A**) Schematic of cell sorting, lentiviral infection (with bicistronic vector encoding activated/myristoylated AKT, ERG, and the fluorescent marker RFP), and transplantation to induce initiation of PIN. LTR, long terminal repeat; IRES, internal ribosome entry site; CMV, cytomegalovirus. (**B**) Images of H&E-stained sections of grafts derived from transduced basal and luminal cells. Scale bars, 50 μm. (**C**) Immunohistochemistry of basal cell–derived lesions demonstrates prominent nuclear expression of AR, with retention of p63^{+} cells, and cytoplasmic staining for PSA and AMACR within PIN lesions. Scale bars, 50 μm. (**D**) Serial sections of basal cell–derived PIN (solid arrow) next to a benign tubule (open arrow) that was not infected with lentivirus. High levels of expression of RFP (red), membrane-bound phospho-AKT (brown), and nuclear ERG (green) in PIN (solid arrow) but not in the neighboring uninfected benign tubule (open arrow) are shown. Scale bars, 100 μm.

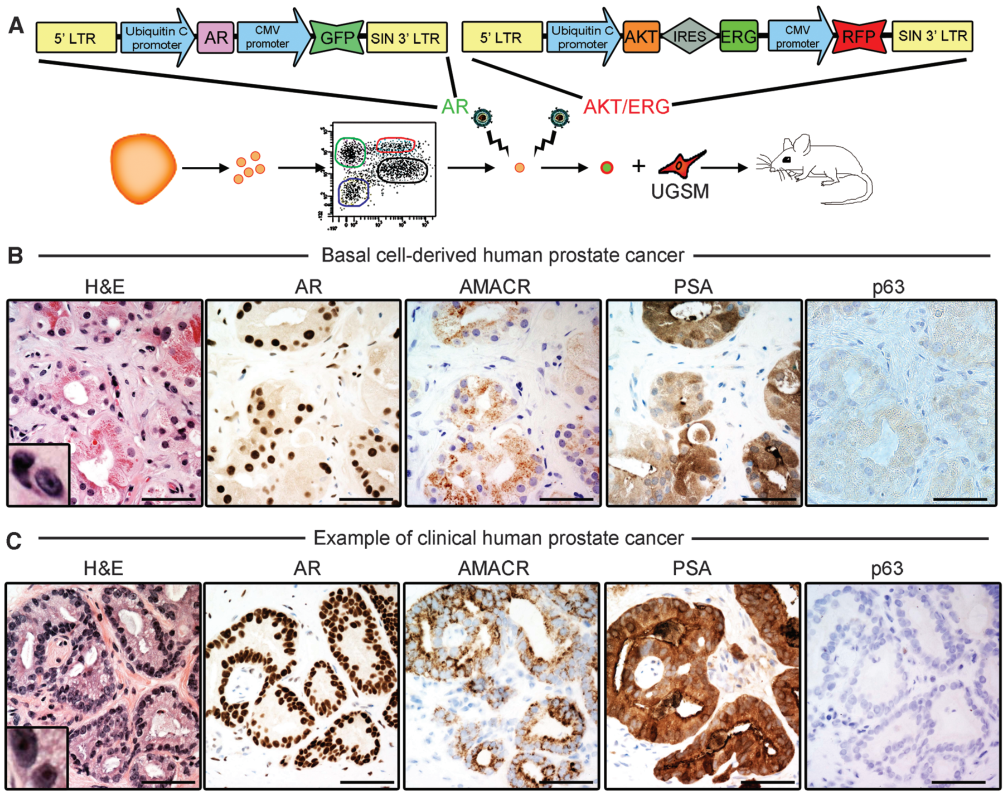

Fig. 3. A model of prostate cancer initiated in primary basal cells. (**A**) Schematic of cell sorting, double lentiviral infection (with GFP-encoding AR vector and bicistronic AKT/ERG vector), and transplantation to induce initiation of prostate cancer. (**B** and **C**) High-power images show similar staining patterns between basal cell–derived human prostate cancer (B) and clinical human prostate cancer (C). H&E insets demonstrate hyperchromatic nuclei with visible nucleoli at high magnification. Cancer lesions are positive for AR, AMACR, and PSA and do not express the basal cell marker p63. Scale bars, 50 μm. Low-power images provided in fig. S6 demonstrate the heterogeneity of disease grade in both clinical human prostate cancer and basal cell–derived human prostate cancer, with coexistence of benign, PIN, and cancer structures.

development of human prostatic tissue (fig. S5). Results were reproducible for four independent patient samples and showed little variation between replicate grafts.

We next introduced a lentivirus carrying both activated (myristoylated) AKT and ERG (*7*) into primary basal and luminal cells (Fig. 2A). After 8 to 16 weeks in vivo, we observed the development of abnormal structures expressing AKT, nuclear ERG, and the fluorescently linked marker RFP (Fig. 2, B and D) from primary basal cells but not luminal cells (Fig. 2B). Structures lacking RFP expression, indicating an absence of lentiviral infection, were benign, demonstrating the requirement for expression of oncogenes to initiate a malignant phenotype. We observed an expansion of AR^+ luminal-like cells with retention of the $p63^+$ basal layer in basal cell–derived lesions (Fig. 2C). In many areas, cells were positive for both PSA and AMACR (Fig. 2C), a marker of both high-grade PIN and prostate cancer (*24*). Based on the presence of morphologically malignant AR^+/PSA^+ luminal cells surrounded by $p63^+$ basal cells, basal cell–derived lesions fulfill the histological criteria for the diagnosis of high-grade PIN, the precursor lesion to invasive prostate cancer (*25*).

We evaluated whether additional genetic alterations could be used to recapitulate human prostate cancer. Primary cells were transduced with the RFP-marked lentivirus carrying AKT and ERG and a green fluorescent protein (GFP)–marked lentivirus carrying AR (*26*) (Fig. 3A). Combination of AKT, ERG, and AR resulted in the development of adenocarcinoma from basal cells (Fig. 3B) but not luminal cells. Although some basal cell–derived structures retained expression of p63 and resembled PIN (fig. S6), many glands had lost the basal layer (Fig. 3B and fig. S6), a defining histological feature used by pathologists for the diagnosis of human prostate cancer (*11*). Cancerous glands expressed PSA (Fig. 3B and fig. S7), AR, and AMACR (Fig. 3B) in patterns indistinguishable from those in patient samples of clinical prostate cancer (Fig. 3C). At high power, cells from cancer lesions exhibited hyperchromatic nuclei with visible nucleoli [Fig. 3, B and C, hematoxylin and eosin (H&E) insets]. Clinical prostate cancer presents as a multifocal disease with considerable heterogeneity of disease grade (*2*). Within the same grafts, we observed lesions that correspond to benign structures ($AR^+/PSA^+/p63^+/AMACR^-$), PIN ($AR^+/PSA^+/p63^+/AMACR^+$), and cancer ($AR^+/PSA^+/p63^-/AMACR^+$), recapitulating the mixed histology found in cancer patients (fig. S6).

Cells within the basal fraction can regenerate benign prostate tissue in immunodeficient mice. Introduction of oncogenic alterations in the target cells can induce a disease that mimics human prostate cancer, establishing basal cells as one cell of origin for prostate cancer. Our results support studies in the mouse demonstrating that histological characterization of cancers in the absence of functional studies can be misleading for determining cells of origin (*27–30*). As the human prostate epithelial hierarchy is further delineated, additional cell types may be identified with cancer-initiating properties.

Even though basal cells express low levels of AR, they share the property of androgen-independence (*31*) with late-stage castration-resistant prostate cancer cells (*8*), suggesting that pathways involved in basal cell function and self-renewal may play a role in tumor cell survival and disease recurrence after androgen withdrawal. Therefore, further investigation of target cells may provide insight into treatments for castration-resistant prostate cancer.

References and Notes

1. K. J. Pienta *et al.*, *Prostate* **68**, 629 (2008).
2. E. T. Ruijter, C. A. van de Kaa, J. A. Schalken, F. M. Debruyne, D. J. Ruiter, *J. Pathol.* **180**, 295 (1996).
3. M. Yoshimoto *et al.*, *Cancer Genet. Cytogenet.* **169**, 128 (2006).
4. S. A. Tomlins *et al.*, *Science* **310**, 644 (2005).
5. B. S. Carver *et al.*, *Nat. Genet.* **41**, 619 (2009).
6. J. C. King *et al.*, *Nat. Genet.* **41**, 524 (2009).
7. Y. Zong *et al.*, *Proc. Natl. Acad. Sci. U.S.A.* **106**, 12465 (2009).
8. C. D. Chen *et al.*, *Nat. Med.* **10**, 33 (2004).
9. H. Okada *et al.*, *Virchows Arch. A Pathol. Anat. Histopathol.* **421**, 157 (1992).
10. J. K. Parsons, W. R. Gage, W. G. Nelson, A. M. De Marzo, *Urology* **58**, 619 (2001).
11. K. J. Wojno, J. I. Epstein, *Am. J. Surg. Pathol.* **19**, 251 (1995).
12. X. Ma *et al.*, *Cancer Res.* **65**, 5730 (2005).
13. X. Wang *et al.*, *Nature* **461**, 495 (2009).
14. T. Iwata *et al.*, *PLoS ONE* **5**, e9427 (2010).
15. D. A. Lawson *et al.*, *Proc. Natl. Acad. Sci. U.S.A.* **107**, 2610 (2010).
16. D. J. Mulholland *et al.*, *Cancer Res.* **69**, 8555 (2009).
17. S. Wang *et al.*, *Proc. Natl. Acad. Sci. U.S.A.* **103**, 1480 (2006).
18. N. Barker *et al.*, *Nature* **457**, 608 (2009).
19. A. P. Verhagen *et al.*, *Cancer Res.* **52**, 6182 (1992).
20. A. S. Goldstein *et al.*, *Proc. Natl. Acad. Sci. U.S.A.* **105**, 20882 (2008).
21. I. P. Garraway *et al.*, *Prostate* **70**, 491 (2010).
22. W. C. Hahn *et al.*, *Nature* **400**, 464 (1999).
23. E. Quintana *et al.*, *Nature* **456**, 593 (2008).
24. C. L. Wu *et al.*, *Hum. Pathol.* **35**, 1008 (2004).
25. J. E. McNeal, D. G. Bostwick, *Hum. Pathol.* **17**, 64 (1986).
26. L. Xin *et al.*, *Proc. Natl. Acad. Sci. U.S.A.* **103**, 7789 (2006).
27. K. K. Youssef *et al.*, *Nat. Cell Biol.* **12**, 299 (2010).
28. E. Passegué, E. F. Wagner, I. L. Weissman, *Cell* **119**, 431 (2004).
29. C. W. So *et al.*, *Cancer Cell* **3**, 161 (2003).
30. A. Cozzio *et al.*, *Genes Dev.* **17**, 3029 (2003).
31. H. F. English, R. J. Santen, J. T. Isaacs, *Prostate* **11**, 229 (1987).

32. We thank B. Anderson for manuscript preparation; D. Cheng for cell sorting; Y. Zong for vectors; H. Zhang for tissue preparation; and A. Chhabra, B. Van Handel, D. Mulholland, C. Soroudi, and T. Stoyanova for discussion and technical help. A.S.G. is supported by an institutional Ruth L. Kirschstein National Research Service Award (GM07185). J.H. is supported by the American Cancer Society, the Department of Defense (DOD) Prostate Cancer Research Program, and the UCLA SPORE in Prostate Cancer (principal investigator, R. Reiter). I.P.G is supported by the DOD and the Jean Perkins Foundation. O.N.W. is an Investigator of the Howard Hughes Medical Institute. J.H., I.P.G., and O.N.W. are supported by a Challenge Award from the Prostate Cancer Foundation.

Supporting Online Material
www.sciencemag.org/cgi/content/full/329/5991/568/DC1
Materials and Methods
Figs. S1 to S7
Table S1
References

23 March 2010; accepted 24 June 2010
10.1126/science.1189992

Astrocytes Control Breathing Through pH-Dependent Release of ATP

Alexander V. Gourine,[1]* Vitaliy Kasymov,[1] Nephtali Marina,[1] Feige Tang,[2] Melina F. Figueiredo,[2] Samantha Lane,[2] Anja G. Teschemacher,[2] K. Michael Spyer,[1] Karl Deisseroth,[3] Sergey Kasparov[2]*

Astrocytes provide structural and metabolic support for neuronal networks, but direct evidence demonstrating their active role in complex behaviors is limited. Central respiratory chemosensitivity is an essential mechanism that, via regulation of breathing, maintains constant levels of blood and brain pH and partial pressure of CO_2. We found that astrocytes of the brainstem chemoreceptor areas are highly chemosensitive. They responded to physiological decreases in pH with vigorous elevations in intracellular Ca^{2+} and release of adenosine triphosphate (ATP). ATP propagated astrocytic Ca^{2+} excitation, activated chemoreceptor neurons, and induced adaptive increases in breathing. Mimicking pH-evoked Ca^{2+} responses by means of optogenetic stimulation of astrocytes expressing channelrhodopsin-2 activated chemoreceptor neurons via an ATP-dependent mechanism and triggered robust respiratory responses in vivo. This demonstrates a potentially crucial role for brain glial cells in mediating a fundamental physiological reflex.

The role of astrocytes in the brain is by no means limited to just providing structural and metabolic support to neurons. Astrocytes are closely associated with cerebral blood vessels and are thought to regulate cerebrovascular tone, adjusting blood supply to match

local metabolic demands (*1*–*6*). A single astrocyte may enwrap several neuronal somata (*7*) and make contact with thousands of synapses (*8*), potentially regulating synaptic strength and information processing (*4*, *9*–*14*). However, direct evidence demonstrating the functional role of astrocytes in complex behaviors is only now starting to emerge (*15*).

Astrocytes provide a vascular-neuronal interface and are in a position to quickly relay blood-borne stimuli to the activities of neuronal networks. Does this have a functional role in the detection of the relevant stimuli by brain chemosensors that monitor key homeostatic parameters, including glucose concentration, pH, and partial pressure of CO_2 (P_{CO_2})? Here, we tested the hypothesis that astrocytes residing within the respiratory chemoreceptor areas of the brainstem are functional respiratory pH sensors [supporting online material (SOM) text 2.1 and 2.2].

Because astrocytes are electrically nonexcitable but display Ca^{2+} excitability (reactive increases in cytosolic $[Ca^{2+}]_i$ concentration), we studied their behavior using genetically encoded Ca^{2+} indicator *Case12* (SOM text 1.3) (*16*, *17*). *Case12* was expressed in astrocytes residing at and near the classical chemosensitive area (*18*) of the ventral surface of the medulla oblongata (VS) of rats by using an adenoviral vector with enhanced shortened glial fibrillatory acidic protein (GFAP) promoter (figs. S1 and S2 and SOM text 1.3) (*19*).

In vivo, a 0.2 pH unit decrease on the VS of anesthetized and artificially ventilated rats (n = 7 rats) evoked an immediate increase in $[Ca^{2+}]_i$ across the field of astrocytes transduced with *Case12* (Fig. 1A and movie S1). Intracellular acidification reduces *Case12* fluorescence and may therefore mask the late phases of the response (SOM text 1.3 and 2.5). Prolonged and sustained astrocytic $[Ca^{2+}]_i$ responses were observed more laterally, at the level of the chemosensitive retrotrapezoid nucleus (RTN) (Fig. 1A). Subsequent histological examination of the chemoresponsive areas confirmed contacts of transduced astrocytes with pia mater and penetrating arterioles (fig. S3).

Propagating Ca^{2+} excitation of ventral medullary astrocytes in response to acidification was also observed in different in vitro preparations such as acute horizontal brainstem slices of adult rats (n = 56 slices) (Fig. 1, B and C, and movie S2), organotypic brainstem slice cultures (n = 114 slices) (Fig. 1E, fig. S4, and movie S3), and dissociated VS cell cultures (n = 19 cultures) (fig. S5). In brainstem slices of adult rats, in which blood vessels were visualized with lectin, many pH-sensitive astrocytes were found to be located adjacent to the VS vasculature (Fig. 1F).

Acidification-induced Ca^{2+} excitation of VS astrocytes is unlikely to be secondary to increased activity of local neurons. To minimize neuronal influences, tetrodotoxin (blocker of voltage-activated sodium channels) and muscimol (potent γ-aminobutyric acid type A receptor agonist) were applied. Both drugs were found to silence RTN neurons (the only known type of pH-responsive neurons in this area), but neither drug affected pH-induced $[Ca^{2+}]_i$ responses monitored using *Case12* or Rhod-2 fluorescence (Fig. 1D and fig. S6). Furthermore, activation of RTN chemoreceptor neurons (n = 11 neurons) by current injection failed to trigger $[Ca^{2+}]_i$ elevations even in the immediately adjacent astrocytes (fig. S7).

High pH-sensitivity is a distinctive feature of astrocytes residing near the VS. Astrocytes from the cerebral cortex or dorsal brainstem generated no $[Ca^{2+}]_i$ signals in response to acidification (fig. S8). Moreover, low-magnification Rhod-2 imaging throughout the whole brainstem cross-section revealed that chemosensory stimulation evokes Ca^{2+} responses originating

[1]Neuroscience, Physiology, and Pharmacology, University College London, London WC1E 6BT, UK. [2]Department of Physiology and Pharmacology, University of Bristol, Bristol BS8 1TD, UK. [3]Department of Bioengineering, Stanford University, Stanford, CA 94305, USA.

*To whom correspondence should be addressed. E-mail: a.gourine@ucl.ac.uk (A.V.G.); sergey.kasparov@bristol.ac.uk (S.K.)

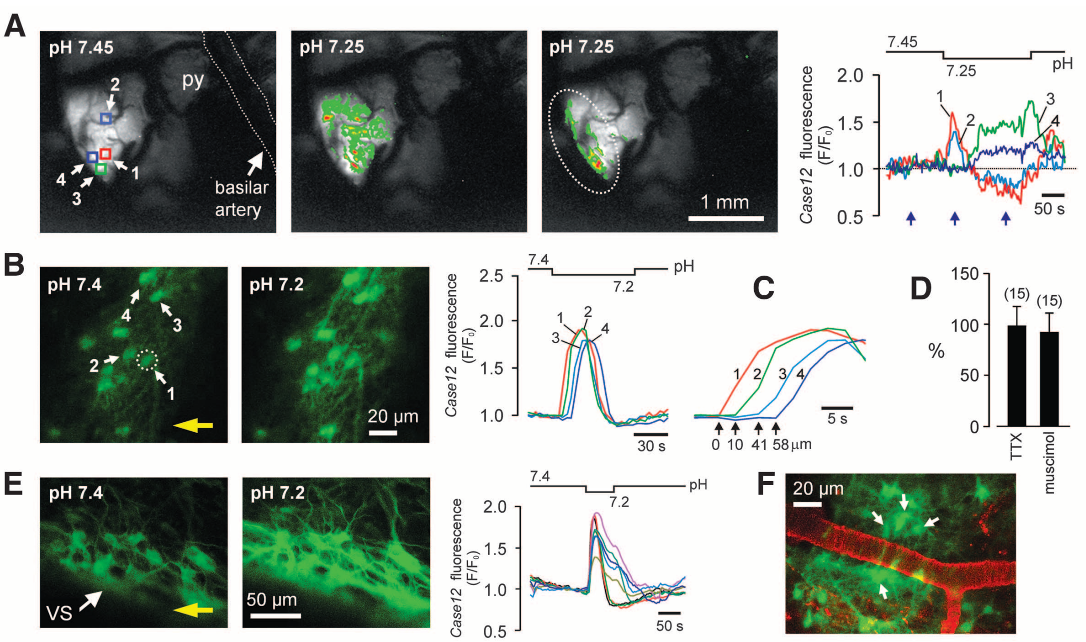

Fig. 1. Astrocytes residing near the VS are exquisitely pH-sensitive. (**A**) In vivo imaging of pH-evoked astrocytic $[Ca^{2+}]_i$ responses in the ventrolateral area of the brainstem surface transduced with AVV-sGFAP-*Case12* in an anesthetized adult rat. (Far right) Changes in VS astrocytic $[Ca^{2+}]_i$ in response to a decrease in pH. (Left) Pseudocolored images were taken at times indicated by arrows. Squares indicate regions of interest. Here and elsewhere, the pH bar shows when the solution with lower pH is reaching and starts leaving the preparation. The dashed line outlines the approximate boundary of the RTN. py, pyramidal tract. (**B**) VS astrocytes identified by means of *Case12* fluorescence in a horizontal slice from an adult rat in which the ventral medulla was transduced with AVV-sGFAP-*Case12*. Acidification induces rapid increases in $[Ca^{2+}]_i$ as determined by changes in *Case12* fluorescence. The two fluorescent images were obtained (left) before and (right) at the peak of $[Ca^{2+}]_i$ response. The circle indicates an astrocyte responding first to pH change in the field of view. The yellow arrow shows the direction of the flow in the chamber. (**C**) Zoomed-in Ca^{2+} transients in order to emphasize the latency differences between responses of individual astrocytes shown in (B). (**D**) No effect of TTX or muscimol on acidification-induced $[Ca^{2+}]_i$ responses in VS astrocytes expressed as percentage of the peak initial response. Numbers of individual astrocytes sampled from three to five separate experiments are given in brackets. (**E**) Acidification-evoked $[Ca^{2+}]_i$ responses in VS astrocytes of organotypic brainstem slice transduced with AVV-sGFAP-*Case12*. The yellow arrow shows the direction of the flow in the chamber. (**F**) VS vasculature visualized with lectin in a horizontal slice prepared from an AVV-sGFAP-*Case12*–transduced rat. Arrows point at pH-responsive astrocytes.

and propagating only near the VS (n = 8 slice preparations) (fig. S9 and movie S4).

Propagation of pH-evoked Ca^{2+} excitation among ventral medullary astrocytes is largely mediated by the actions of adenosine triphosphate (ATP) (SOM text 2.3). A decrease in pH from 7.4 to 7.2 (at constant [HCO_3^-] and nominal P_{CO_2}) triggers sustained ATP release from the VS (peak increase 1.0 ± 0.3 μM, n = 8 horizontal brainstem slice preparations of young adult rats) (Fig. 2A), confirming our previous findings (*20*). Blockade of ATP signaling dramatically diminishes pH-evoked astrocytic responses: In cultured and acute brainstem slices, pH-evoked astrocytic Ca^{2+} responses were abolished in the presence of ATP-hydrolyzing enzyme apyrase (25 U ml^{-1}) (Fig. 2, B and E). Furthermore, ATP receptor antagonists MRS2179 (3 μM), pyridoxalphosphate-6-azophenyl-2',4'-disulfonic acid (PPADS) (5 μM), or 2′,3′-O-(2,4,6-trinitrophenyl) (TNP)–ATP (20 nM) reduced acidification-induced astrocytic $[Ca^{2+}]_i$ signals by 82% (P = 0.005) (Fig. 2C), 80% (P = 0.005), and 83% (P = 0.048), respectively (Fig. 2E). In line with the absence of acidification-induced $[Ca^{2+}]_i$ responses in Ca^{2+}-free medium (Fig. 2E and fig. S10), this pharmacological profile suggests the involvement of ionotropic ATP receptors (SOM text 2.4).

In response to a decrease in pH, the VS astrocytes spread Ca^{2+} excitation partially via gap junctions and predominantly through exocytotic release of ATP (SOM text 2.3). Gap junction blocker carbenoxolone at high concentration (100 μM) was only partially effective in reducing astrocytic $[Ca^{2+}]_i$ responses (by 43%; P = 0.001) (Fig. 2E and fig. S11). In contrast, brefeldine A (vesicular trafficking inhibitor; 50 μM) or bafilomycin A (vesicular H^+-ATPase inhibitor; 2 μM) both effectively abolished acidification-induced Ca^{2+} excitation of VS astrocytes (Fig. 2, D and E). Neither brefeldine A nor bafilomycin A prevented responses of VS astrocytes to applied ATP (Fig. 2D), indicating that astrocytic reactivity to ATP was not affected by these compounds.

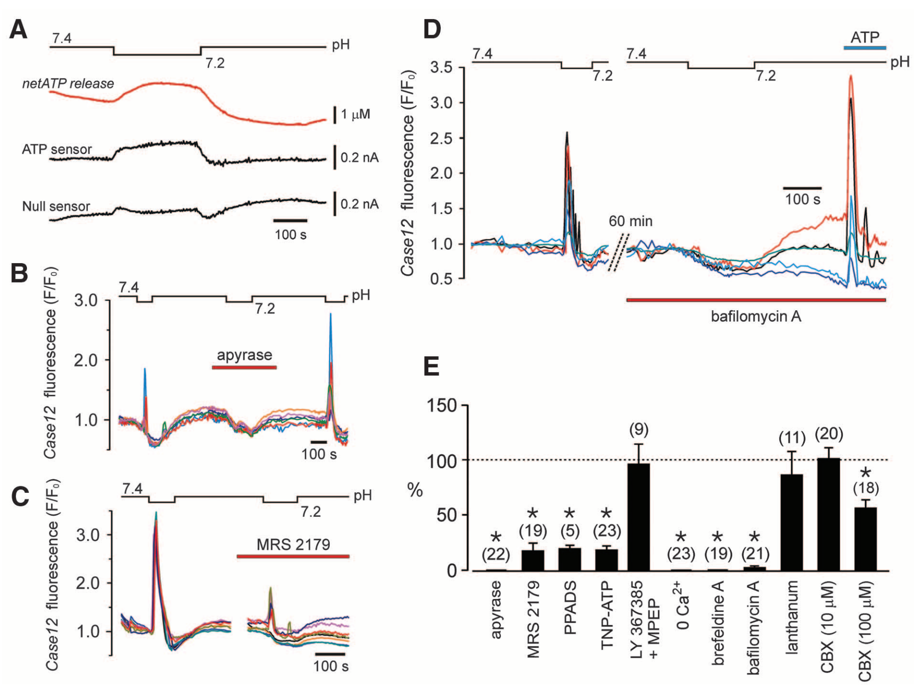

Fig. 2. Exocytotic release of ATP propagates pH-induced Ca^{2+} excitation among VS astrocytes. (**A**) A 0.2-unit decrease in pH induces sustained ATP release from the VS as detected with biosensors placed on the pia mater in horizontal slices prepared from adult rats. "netATP" trace represents the difference in signal between ATP and null (control) sensor currents. (**B**) Apyrase abolishes pH-evoked $[Ca^{2+}]_i$ responses in VS astrocytes. Traces illustrate the effects of apyrase on pH-induced changes in *Case12* fluorescence of six individual astrocytes (adult rat slice preparation). The decrease in signal is due to acidification-induced quenching of *Case12* fluorescence. (**C**) The effect of MRS2179 on acidification-induced $[Ca^{2+}]_i$ responses of eight individual VS astrocytes (organotypic brainstem slice). (**D**) Bafilomycin A abolishes pH-evoked Ca^{2+} excitation of VS astrocytes (five individual astrocytes in slice preparation of an adult rat). (**E**) The effects of apyrase, ATP receptor antagonists, $mGlu_{1a}$ and $mGlu_5$ receptor antagonists (LY367385 and MPEP, 100 μM each), blockers of pannexin/connexin hemichannels and gap junctions lanthanum (100 μM) and carbenoxolone (CBX), or inhibitors of exocytotic mechanisms on acidification-induced $[Ca^{2+}]_i$ responses in VS astrocytes expressed as the percentage of the initial response. Numbers of individual astrocytes sampled from three to five separate experiments are given in brackets (*P < 0.05).

Released ATP also links astrocytic excitation to the increased activity of medullary chemoreceptor neurons. The RTN, which is adjacent to the VS, has been advocated to play a key role in central respiratory chemosensitivity (*21*) (SOM text 2.7). RTN neurons respond to changes in pH, reside within the marginal VS glial layer or have extensive dendritic projections to it, project to the respiratory network, and stimulate breathing upon activation (*21*, *22*).

RTN neurons characteristically express transcription factor Phox2b and were fluorescently labeled with enhanced green fluorescent protein (EGFP) in organotypic slices by using an adenoviral vector with PRSx8 promoter [Phox2b-activated promoter (*23*)] (Fig. 3A). A decrease in pH led to a reversible depolarization of all recorded RTN neurons (n = 8 neurons) (Fig. 3, A and B). Caudally located catecholaminergic C1 neurons were insensitive to pH (fig. S12). MRS2179 (10 μM; n = 8 neurons) (Fig. 3, A and B) or apyrase (25 U ml^{-1}; n = 3 neurons) (fig. S13) had no effect on resting membrane potential but markedly reduced pH-evoked depolarizations of RTN neurons (P = 0.014 and P = 0.04, respectively). In a separate experiment, $[Ca^{2+}]_i$ responses of RTN neurons were visualized by using a genetically encoded Ca^{2+} sensor TN-XXL (*24*) expressed under PRSx8 promoter control (Fig. 3C). Again, acidification-induced $[Ca^{2+}]_i$ elevations in RTN neurons were suppressed by MRS2179 (3 μM, n = 9 neurons, P = 0.008) (Fig. 3, C and D), confirming that their pH-sensitivity is largely mediated by prior release of ATP (SOM text 2.7).

In order to mimic Ca^{2+} excitation of astrocytes, we generated an adenoviral vector in which a mutant of the light-sensitive channelrhodopsin-2 [ChR2-H134R (*25*, *26*)] is fused to a far red-shifted fluorescent protein Katushka1.3 (*27*) and expressed by using enhanced GFAP promoter (Fig. 3E and fig. S14) (*19*). In primary cultures and in brainstem slices of adult rats, astrocytes transduced with this construct displayed robust increases in $[Ca^{2+}]_i$ in response to 470 nm light (Fig. 3F and figs. S15 to S17).

Optogenetic activation of VS astrocytes transduced with AVV-sGFAP-ChR2(H134R)-Katushka1.3 in organotypic brainstem slices triggered immediate ATP release (fig. S18) and evoked long-lasting (28 ± 9 min) depolarizations of all recorded DsRed-labeled RTN neurons (n = 13 neurons) (Fig. 3, G to I). These depolarizations were reversibly prevented in the presence of MRS2179 (10 μM) (P = 0.002) (Fig. 3, H and I).

To determine the functional importance of Ca^{2+} excitation of VS astrocytes, we conducted experiments in anesthetized, vagotomized, and artificially ventilated rats transduced with AVV-sGFAP-ChR2(H134R)-Katushka1.3 in the ventral areas of the brainstem. The VS was exposed, and phrenic nerve activity was recorded so as to monitor central respiratory drive. Unilateral illumination (445 nm) of the transduced side of the

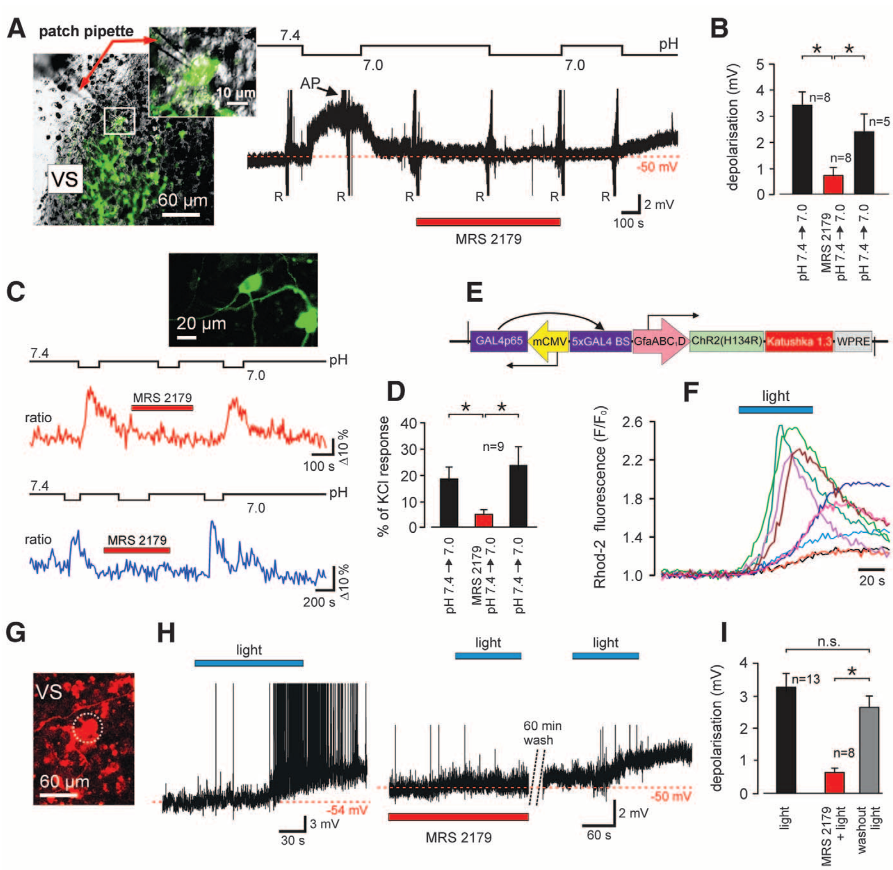

Fig. 3. ATP mediates responses of chemoreceptor neurons to decreases in pH or evoked by selective light-induced Ca^{2+} excitation of adjacent astrocytes. (**A**) (Left) Image of the ventral aspect of an organotypic brainstem slice showing EGFP-labeled Phox2b-expressing RTN neurons, one of which is patch clamped. (Right) Time-condensed record of the membrane potential of an RTN neuron responding to acidification in the absence and presence of MRS2179. AP, action potentials (truncated); R, resistance tests using current pulses. (**B**) Summary of MRS2179 effect on pH-evoked depolarizations in RTN neurons. (**C**) Effect of MRS2179 on acidification-induced $[Ca^{2+}]_i$ responses of RTN neurons from two different experiments (ratiometric imaging using TN-XXL). (Inset) RTN neurons expressing TN-XXL. (**D**) Summary data showing significant effect of MRS2179 on pH-evoked $[Ca^{2+}]_i$ responses of RTN neurons. (**E**) Layout of AVV-sGFAP-ChR2(H134R)-Katushka1.3. (**F**) Primary astrocytes displaying increases in $[Ca^{2+}]_i$ in response to 470 nm light. (**G**) Ventral aspect of the organotypic slice showing a recorded DsRed2-labeled RTN neuron surrounded by ChR2(H134R)-Katushka1.3–expressing astrocytes. (**H**) Membrane potential of two different RTN neurons illustrating their responses to light activation of adjacent ChR2(H134R)-expressing astrocytes in the (left) absence, (middle) presence, or (right) after washout of MRS2179. (**I**) Effects of MRS2179 on depolarizations of RTN neurons evoked by optogenetic activation of neighboring astrocytes (*$P < 0.05$).

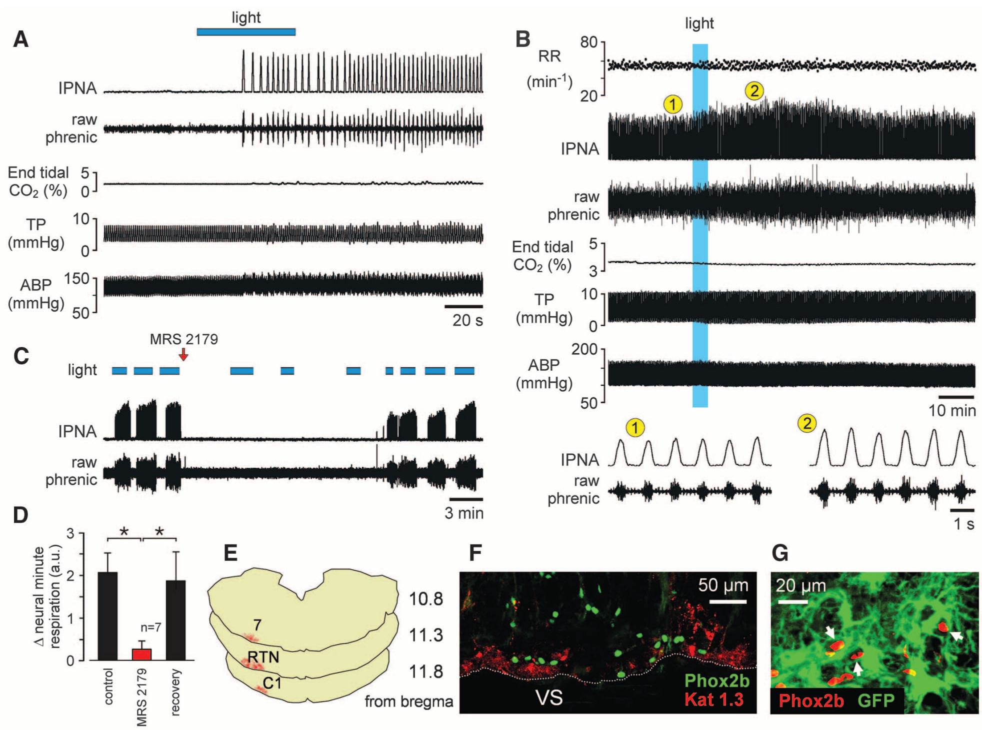

Fig. 4. Optogenetic activation of VS astrocytes stimulates breathing in vivo. (**A**) Unilateral photostimulation of VS astrocytes expressing ChR2(H134R)-Katushka1.3 is sufficient to trigger respiratory activity from hypocapnic apnea in an anesthetized rat. Hypocapnic apnea was induced by means of mechanical hyperventilation to reduce arterial levels of $P_{CO_2}/[H^+]$ below the apneic threshold. IPNA, integrated phrenic nerve activity; TP, tracheal pressure; ABP, arterial blood pressure. (**B**) Lasting effect of light activation of VS astrocytes in an animal breathing normally. RR, respiratory rate. (1) and (2) indicate expanded traces of phrenic nerve activity before and after photostimulation of VS astrocytes. (**C**) Time-condensed record illustrating effects of repeated stimulations of VS astrocytes on phrenic nerve activity before and after a single application of MRS2179 (100 µM, 20 µl) on the VS. Spontaneous recovery of the response over time can be seen. (**D**) Summary data of MRS2179 effect on the increases in neural minute respiration (the product of phrenic frequency and amplitude) evoked by light activation of VS astrocytes (*$P < 0.05$). (**E**) Rostrocaudal distribution of astrocytes expressing ChR2(H134R)-Katushka1.3 in the brainstem of the rat from the experiment shown in (A). 7, facial nucleus; RTN, retrotrapezoid nucleus; C1, catecholaminergic cell group. (**F**) ChR2(H134R)-Katushka1.3 (Kat 1.3) expression in astrocytes is identified by red fluorescence distributed near the VS in close association with Phox2b-immunoreactive neurons (green nuclei). Shown is the coronal brainstem section. (**G**) Phox2b-expressing chemoreceptor RTN neurons (red nuclei) embedded in the astrocytic network (astrocytes were transduced with *Case12* in this example so as to reveal their morphology).

VS triggered robust respiratory activity from hypocapnic apnea in all eight animals tested (Fig. 4A and movie S5). An increase in phrenic nerve amplitude was also observed after optogenetic activation of VS astrocytes in six animals breathing normally ($P < 0.01$) (Fig. 4B). MRS2179 prevented the respiratory effects of optogenetic stimulation of astrocytes ($n = 7$ rats, $P = 0.006$) (Fig. 4, C and D). No responses were induced after illumination of the brainstem side not expressing the transgene. Histological analysis of the areas that stimulation of which evoked increases in breathing (Fig. 4E) revealed close association of transduced astrocytes with the VS and Phox2b-expressing neurons (Fig. 4F).

Although previous reports suggested that astrocytes could potentially be important for chemoreception (*28*, *29*), it was generally believed that central respiratory chemosensory function is a property of one or several highly specialized neuronal populations located in the medulla oblongata and pons. Although our data do not exclude the existence of such neurons, we demonstrate that astrocytes may as well fulfill an equivalent role. Indeed, astrocytes are intimately associated with blood vessels supplying the lower brainstem: Surface pial arteries rest on glia limitans, whereas penetrating arterioles and capillaries are enwrapped by astrocytic end-feet (fig. S3). Therefore, astrocytes anatomically are ideally positioned to monitor the composition of the arterial blood entering the brain and integrate this information with $P_{CO_2}/[H^+]$ levels of brain parenchyma. They have the ability to sense physiological changes in $P_{CO_2}/[H^+]$ and then impart these changes to the respiratory neuronal network to modify breathing patterns and adjust lung ventilation accordingly [although the initial chemosensory event linking a decrease in pH with VS astrocytic $[Ca^{2+}]_i$ response as yet remains unknown (SOM text 2.6)]. This identifies astroglia as an important component of one of the most fundamental mammalian homeostatic reflexes and provides direct evidence for an active role of astrocytes in functionally relevant information processing in the central nervous system.

References and Notes

1. R. D. Fields, B. Stevens-Graham, *Science* **298**, 556 (2002).
2. M. Zonta *et al.*, *Nat. Neurosci.* **6**, 43 (2003).
3. T. Takano *et al.*, *Nat. Neurosci.* **9**, 260 (2006).
4. P. G. Haydon, G. Carmignoto, *Physiol. Rev.* **86**, 1009 (2006).
5. C. Iadecola, M. Nedergaard, *Nat. Neurosci.* **10**, 1369 (2007).
6. G. R. Gordon, H. B. Choi, R. L. Rungta, G. C. Ellis-Davies, B. A. MacVicar, *Nature* **456**, 745 (2008).
7. M. M. Halassa, T. Fellin, H. Takano, J. H. Dong, P. G. Haydon, *J. Neurosci.* **27**, 6473 (2007).
8. E. A. Bushong, M. E. Martone, Y. Z. Jones, M. H. Ellisman, *J. Neurosci.* **22**, 183 (2002).
9. J. Kang, L. Jiang, S. A. Goldman, M. Nedergaard, *Nat. Neurosci.* **1**, 683 (1998).
10. O. Pascual *et al.*, *Science* **310**, 113 (2005).
11. X. Wang *et al.*, *Nat. Neurosci.* **9**, 816 (2006).
12. P. Jourdain *et al.*, *Nat. Neurosci.* **10**, 331 (2007).
13. J. Schummers, H. Yu, M. Sur, *Science* **320**, 1638 (2008).
14. C. Henneberger, T. Papouin, S. H. Oliet, D. A. Rusakov, *Nature* **463**, 232 (2010).
15. M. M. Halassa *et al.*, *Neuron* **61**, 213 (2009).
16. E. A. Souslova *et al.*, *BMC Biotechnol.* **7**, 37 (2007).
17. Materials and methods are available as supporting material on *Science* Online.
18. H. H. Loeschcke, *J. Physiol.* **332**, 1 (1982).
19. B. Liu, J. F. Paton, S. Kasparov, *BMC Biotechnol.* **8**, 49 (2008).
20. A. V. Gourine, E. Llaudet, N. Dale, K. M. Spyer, *Nature* **436**, 108 (2005).
21. D. K. Mulkey *et al.*, *Nat. Neurosci.* **7**, 1360 (2004).
22. S. B. Abbott *et al.*, *J. Neurosci.* **29**, 5806 (2009).
23. D. Y. Hwang, W. A. Carlezon Jr., O. Isacson, K. S. Kim, *Hum. Gene Ther.* **12**, 1731 (2001).
24. M. Mank *et al.*, *Nat. Methods* **5**, 805 (2008).
25. V. Gradinaru *et al.*, *J. Neurosci.* **27**, 14231 (2007).
26. In the mutants, amino acids were substituted at certain locations; for example, H134R indicates that histidine (H) at position 134 was replaced by arginine (R).
27. D. Shcherbo *et al.*, *Biochem. J.* **418**, 567 (2009).
28. Y. Fukuda, Y. Honda, M. E. Schläfke, H. H. Loeschcke, *Pflugers Arch.* **376**, 229 (1978).
29. N. A. Ritucci, J. S. Erlichman, J. C. Leiter, R. W. Putnam, *Am. J. Physiol.* **289**, R851 (2005).

30. We are grateful to The Wellcome Trust (grant 079040) and British Heart Foundation for financial support. A.V.G. is a Wellcome Trust Senior Research Fellow.

Supporting Online Material

www.sciencemag.org/cgi/content/full/329/5991/571/DC1
Materials and Methods
SOM Text
Figs. S1 to S26
Table S1
References
Movies S1 to S5

9 April 2010; accepted 25 June 2010
10.1126/science.1190721

NEW PRODUCTS

MOBILITY INSTRUMENT

The Mobius mobility instrument incorporates several patent-pending innovations to realize fast and reliable measurement of macromolecular electrophoretic mobilities. In addition to measuring mobilities of large particles such as liposomes and virus-like particles, this laser-based instrument achieves reproducible measurements of traditionally challenging protein samples, including antibody formulations, bovine serum albumin, and lysozyme. It is designed to measure protein mobilities rather than particulates. In colloidal suspensions, the amount of charge and screening developed at the interfaces between particles and media are important in determining the formulation stability. For many biomolecules such as proteins, electrostatic interactions also exercise a profound influence on the conformations and functions. Because direct measurement of the interfacial potential is rarely feasible, the electrophoretic mobility has become the most widely accepted proxy for molecular charge.

Wyatt Technology

For info: 805-681-9009 | www.wyatt.com

OLIGONUCLEOTIDE ANALYSIS

The Clarity Oligo-MS columns are for rapid and efficient liquid chromatography–mass spectroscopy (LC-MS) characterization and quality control of synthetic RNA and DNA. Based on the manufacturer's core-shell particle technology, the new C18 columns deliver significantly shorter run times than traditional media, along with increased resolution and sensitivity. With the high resolving power of Clarity Oligo-MS, impurities in complex synthetic mixtures can be separated from the peak of interest in less than 10 minutes. These new columns are packed with either 2.6 μm or 1.7 μm particles, enabling high efficiency on any high-performance LC or ultrahigh-performance LC (UHPLC) platform. The 2.6 μm columns operate at reduced backpressures compared with other oligonucleotide-specific columns, delivering UHPLC performance on any LC instrument, and methods are easily transferable. The 1.7 μm columns boost the performance of existing sub-2 μm methods on high-pressure systems.

Phenomenex

For info: 310-212-0555 | www.phenomenex.com

DENSITY AND REFRACTIVE INDEX METERS

The LiquiPhysics Excellence density meters and refractometers are simple to operate, sophisticated, and secure, making them suitable tools for compliance with the many regulatory demands of the pharmaceutical industry. The One Click user interface allows quick, simple, and direct access to all routine tasks and provides clear user information with easy shortcut buttons to start routine tasks immediately. The modular design facilitates the combined measurements of density with refractive index, color, and/or pH and conductivity. Powerful sampling and automation units can entirely automate measurements, thoroughly clean the instrument, and use certified combined liquid reference materials. Its software offers smooth and seamless integration with a laboratory information management system by organizing comprehensive sample lists containing all relevant data in order to automate quality control processes.

Mettler Toledo

For info: 800-638-8537 | www.mt.com/LiquiPhysics

PROCESS-CONTROL SENSORS

ARC sensors, designed for pH, dissolved oxygen, and conductivity measurements, feature a built-in microprocessor that can communicate with standard analog (4-20A) and digital ModBus interfaces and are safe to sterilize with autoclave, CIP, and SIP. The ARC View Handheld provides a local display configured with ARC Wi wireless communication, allowing users mobility while monitoring data from multiple sensors. Three ARC package options are offered: ARC Vital allows customers to communicate simply via analog or digital communication and without the use of a transmitter; the enhanced ARC Versa system combines the reliability of ARC Vital with the convenience of wireless communication; and the top-of-the-line ARC Vision system incorporates digital technology that enables creation of wired or wireless sensor networks.

Hamilton Company

For info: 800-648-5950 | www.hamiltoncompany.com

NUCLEIC ACID ANALYSIS

The MassArray Analyzer 4 mass spectrometry system is a high-performance nucleic acid analysis platform designed to meet the demand for a benchtop instrument with flexibility across multiple applications, improved reliability, and faster performance. With the capability for quantitative gene expression analysis and epigenetic nucleic acid methylation analysis, as well as high throughput genotyping and single nucleotide polymorphism fine mapping applications, the analyzer is designed to empower the basic and translational research community to advance findings from basic genetic and biomarker studies toward clinical utility in diagnosis, prognosis, and monitoring of disease. The system is configured to provide increased throughput, faster time-to-results, and the ability to cost-effectively run from tens to thousands of samples daily, making it suitable for use in basic and translational research.

Sequenom

For info: 877-443-6663 | www.sequenom.com

Electronically submit your new product description or product literature information! Go to **www.sciencemag.org/products/newproducts.dtl** for more information.

Newly offered instrumentation, apparatus, and laboratory materials of interest to researchers in all disciplines in academic, industrial, and governmental organizations are featured in this space. Emphasis is given to purpose, chief characteristics, and availability of products and materials. Endorsement by *Science* or AAAS of any products or materials mentioned is not implied. Additional information may be obtained from the manufacturer or supplier.

POSITIONS OPEN

POSTDOCTORAL FELLOWSHIP in Bioinformatics and Statistics

The Center for Bioinformatics of the U.S. FDA's National Center for Toxicological Research (NCTR) seeks qualified postdoctoral candidates in the field of bioinformatics with emphasis on study of drug-induced liver injury. The position is open immediately. The position requires a diverse range of expertise in data mining, machine learning, statistics, and biology. The successful candidates need to have a Ph.D. degree in either bioinformatics/computational biology or toxicology with experience in bioinformatics. The candidate must possess experience in analyzing data for microarray gene expression and next generation sequencing. Knowledge in toxicology, in general, and hepatotoxicity in particular will be highly beneficial. The starting salary is $57,000. *U.S. citizenship or permanent resident alien status (not H-1 visa holder) is preferred.* However, other applicants with Optional Practical Training (OPT) or H-1 holder willing to convert to J-1 status are also considered. The foreign applicants can enroll in the program with J-1 visa.

To express your interest in this position, electronically send or mail your curriculum vitae, the names and contact information of two references, and a statement of research interests (maximum two pages) to:

Weida Tong, Ph.D.
Director, Center for Bioinformatics
FDA/NCTR, 3900 NCTR Road, HFT-130,
Jefferson, AR 72079
E-mail: weida.tong@fda.hhs.gov
Telephone: 870-543-7142

NCTR, located 35 miles south of Little Rock, Arkansas, is a research center of the FDA, U.S. Department of Health and Human Services. The mission of NCTR is to conduct peer-reviewed scientific research that supports and anticipates FDA's current and future regulatory needs. *NCTR is an Equal Opportunity/Affirmative Employer.*

POSTDOCTORAL RESEARCH POSITIONS San Diego State University Heart Institute–SDSU Research Foundation

The San Diego State University Heart Institute is recruiting **POSTDOCTORAL FELLOWS** to work in a dynamic, state-of-the-art cardiovascular cell and molecular biology research setting in the laboratory of the Institute Director **Dr. Chris Glembotski,** studying roles for heart-derived secreted cytokines (cardiomyokines) on cardiac protection and repair. Applicants should have a Ph.D. in a relevant field, demonstrated expertise in basic cell and molecular biology, including methods to examine gain- and loss-of-gene-function in culture and animal models of heart disease, excellent communication skills, a record of peer-reviewed journal publications, and the desire and ability to write and submit competitive research grant applications. Salary is commensurate with experience; excellent benefits. Applicants should submit a cover letter, curriculum vitae, and a description of research experience and professional goals with the application for **Job #100120** at **website: https://jobsfoundation.sdsu.edu** or call **telephone: 619-594-5703.** *Equal Employment Opportunity/Affirmative Action/Title IX Employer.*

POSTDOCTORAL AND STAFF POSITIONS The RNA Institute University at Albany

Several Postdoctoral Associate and Laboratory Manager positions are open in the Agris and Fabris Laboratories within the recently established RNA Institute of the University at Albany (State University of New York). Applicants are sought with expertise in any of the following areas: (a) molecular biology/biochemistry with experience in RNA and protein expression; (b) modern high-field nuclear magnetic resonance instrumentation; (c) mass spectrometry and hyphenated separation techniques; or (d) structural biology with experience in restrained molecular dynamics calculations. See complete ads at **website: http://www.albany.edu/rna/employment.shtml.**

The University at Albany is an Equal Employment Opportunity/Affirmative Action/IRCA/ADA employer.

POSITIONS OPEN

PASTEUR FOUNDATION

POSTDOCTORAL FELLOWSHIPS Institut Pasteur, Paris, France

Come work in Paris at the Institut Pasteur, the world-renowned, private, biomedical research organization. We invite applications from outstanding Fellowship candidates to any of 130 laboratories within our 10 departments. Areas include: developmental and cell biology, epidemiology, immunology, genomics, genetics, microbiology, neuroscience, structural biology, parasitology, mycology and virology. Next deadline: September 17, 2010. Annual package is $70,000 for three years. *U.S. citizenship required.*

E-mail: pasteurus@aol.com. Website: http://www.pasteurfoundation.org.

RESEARCH ASSOCIATE AND POSTDOCTORAL POSITIONS in Cancer Population Genetics and Genomics, Memorial Sloan-Kettering Cancer Center. Starting fall 2010. Focus on inherited susceptibility to cancers of the breast, ovary, colon, prostate, and lymphoma. Methodologies include whole genome association studies, candidate gene association, and full sequencing approaches (see PubMed identifiers 19567420, 19287384, 19497887, 18326623). Applicant must have strong background in population genetics and laboratory experience with high throughput genotyping. Send applications and three letters of reference to: **Kenneth Offit, M.D., M.P.H., Clinical Genetics Service, Memorial Sloan-Kettering Cancer Center, 1275 York Avenue, Box 192, New York, NY 10021. Fax: 646-888-4081; e-mail: offitk@mskcc.org.** *Memorial Sloan-Kettering Cancer Center is an Equal Opportunity Employer with a strong commitment to enhancing the diversity of its faculty and staff. Women and applicants from diverse racial, ethnic, and cultural backgrounds are encouraged to apply.*

POSTDOCTORAL POSITION Harvard Medical School Computational Biology and Bioinformatics. Qualifications: (i) Ph.D. in bioinformatics, biostatistics, computer science, or related fields; (ii) familiarity with molecular biology and genomics; (iii) strong programming skills (R, C++, Python); and (iv) proficiency in microarray software Bioconductor, dChip, and GenePattern. Working at the interface of biology, statistics, and computing, the candidate will analyze high throughput gene expression microarray data in cancer genomics. The goal is to develop novel data analysis algorithms and software and to identify genomics signatures in cancer patients and tumor-bearing mice. Please send curriculum vitae, a career statement, and three letters of reference to: **Dr. A.I. Kassis, HMS, Armenise Building, 200 Longwood Avenue, Boston, MA 02115. E-mail: amin_kassis@hms.harvard.edu.** *An Equal Opportunity/Affirmative Action Employer.*

We are looking for highly motivated **POSTDOCTORAL** candidates who are interested in metal-induced oxidative stress, carcinogenic signal transduction, and cancers of the lung, skin, and colon. Our research focuses on: (1) the molecular mechanisms of metal toxicity and carcinogenesis and (2) the antioxidant properties of various naturally occurring compounds and to develop them as chemopreventive agents. Please send your curriculum vitae and names of three references to **e-mail: zzhand@uky.edu** with the subject Reply to Postdoctoral Ad.

Positions of **POSTDOCORAL/RESEARCH ASSOCIATES** are available in the mechanism-based cancer prevention and molecular mechanisms of chemical carcinogenesis in the laboratory of **Xianglin Shi**, University of Kentucky. Send curriculum vitae to **e-mail: xianglin.shi@uky.edu.**

The World Is Your Lab on a Postdoc or Sabbatical Abroad

Graduate students dream of it and tenured professors get a shot at it every seven years. The chance to work abroad, either for postdoctoral training or a sabbatical, is "one of the unique opportunities we have in science," says Joel Rothman, who did a postdoctoral fellowship in Cambridge, England, and a sabbatical leave in Paris, France. Scientists who have done a foreign postdoc or sabbatical say it's the experience of a lifetime, and are eager to offer encouragement and advice. By Chris Tachibana

Kate Jackson removing a snake from a net in a swamp in the Republic of Congo.

"I went for the animals, and didn't expect to have any interest in the people, but now I feel like I'm needed by the animals *and* the people."

Doing research in a foreign country begins with finding a suitable lab. Professors looking for an overseas sabbatical lab can rely on their established network, but graduate students looking for a postdoc abroad must create a connection to the international community. Talking at an international meeting makes you visible, and may even get you an offer on the spot. **Elke Küster-Schöck** was a graduate student at Friedrich-Alexander-Universität Erlangen-Nürnberg, when she attended a Cold Spring Harbor Laboratory meeting in New York. "It was a small enough conference to really meet people," she says. "I presented my graduate work, and actively participated in the discussions. I was approached by Alan Grossman, who organized a ride to Boston for me, where I interviewed for a postdoc position in his lab at MIT [Massachusetts Institute of Technology]. I got the offer before I even went back to Germany!"

If the international community comes to you, take advantage of it. As a graduate student at the University of Oregon, **Joel Rothman,** chair of Molecular, Cellular and Developmental Biology at the University of California Santa Barbara (UCSB), had been considering a postdoc at the Medical Research Council (MRC) in the United Kingdom, so when a seminar speaker came from the MRC, Rothman took him out for a drink. After a long, late-night conversation, he decided that when he met the MRC's requirement that postdocs bring their own funding, he would go. "Living in another country for a while is a fabulous experience," he says. "The social and scientific interactions are different from what you get from just passing through at a conference."

ADVANCE PREPARATION

Working abroad means confronting a country's immigration system, and this often comes with at least a little bureaucracy. Küster-Schöck, who moved to Montreal, Canada, after her postdoc in the United States says, "Each country confronts newcomers with a dazzling array of administrative hurdles to pass." Start gathering the necessary documents and forms as soon as you know where you are going, and if you will be working at a large university or research institution, contact its international services office. Be prepared for paperwork, and waiting periods of weeks or months. **Robert Eisenman** recently took a sabbatical from Fred Hutchinson Cancer Research Center to work at the University of Tokyo in Japan. He says, "There were a lot of forms to fill out, but it's the same everywhere. I got no sympathy from the foreigners in my lab who had been though the US immigration process." While waiting for your work permits and visas, read about your new home, and if you don't know the language, do your best to learn it. Eisenman recommends, "Know as much as you can of the history and the language of the place you're going to. You need to at least try, or you won't get much out of it."

Scientists doing a sabbatical abroad may have a house and a family to consider. To help pay the mortgage at home and rent in another country, Rothman recommends services like sabbaticalhomes.com, which can help you rent your home, find a place in your new city, or even swap with another professor continued »

UPCOMING FEATURES

Postdoc Survey—August 27

Faculty: Small vs. Large Universities—September 10

Focus on Germany—September 24

CREDITS: (FROM TOP) KATE JACKSON (TAKEN WITH KATE'S CAMERA BY CONGOLESE VILLAGER; ©ISTOCKPHOTO.COM/TRIFONOV_EVGENIY

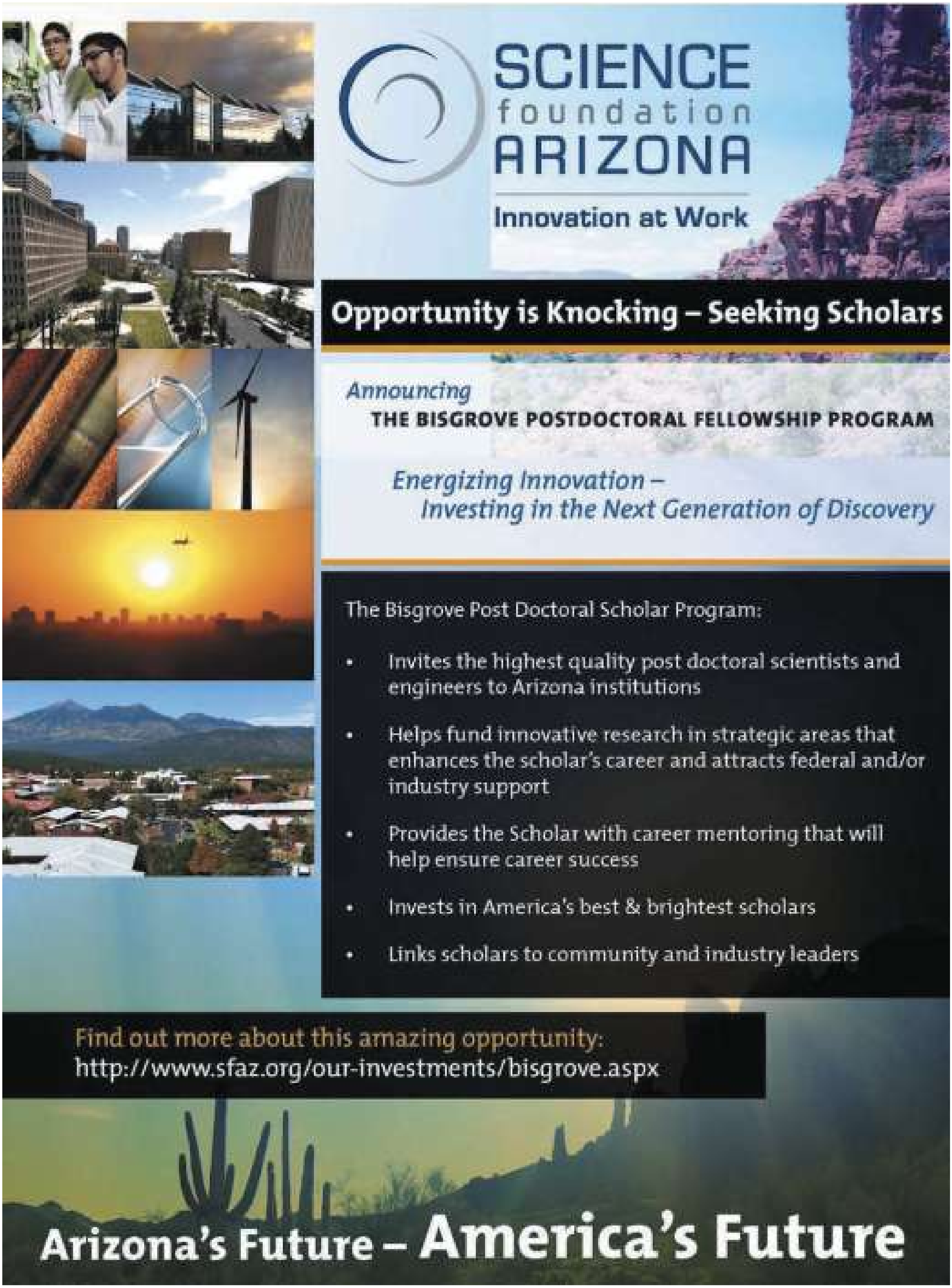
SCIENCE
foundation
ARIZONA
Innovation at Work
Opportunity is Knocking – Seeking Scholars
Announcing
THE BISGROVE POSTDOCTORAL FELLOWSHIP PROGRAM
Energizing Innovation –
Investing in the Next Generation of Discovery
The Bisgrove Post Doctoral Scholar Program:
• Invites the highest quality post doctoral scientists and engineers to Arizona institutions
• Helps fund innovative research in strategic areas that enhances the scholar's career and attracts federal and/or industry support
• Provides the Scholar with career mentoring that will help ensure career success
• Invests in America's best & brightest scholars
• Links scholars to community and industry leaders
Find out more about this amazing opportunity:
http://www.sfaz.org/our-investments/bisgrove.aspx
Arizona's Future – America's Future

"Each country confronts newcomers with a dazzling array of administrative hurdles to pass."

— Elke Küster-Schöck

whose sabbatical plans mirror your own. Be prepared to spend some time searching for a place to live, and don't be afraid to ask for advice. A good resource for informal help is your new lab, where someone might be willing to recommend neighborhoods, or even to look through ads.

Rothman and his wife Molly took two children, ages 8 and 14, along on their French sabbatical at the Jacob Monod Institute, and they acknowledge the move was initially stressful for the kids. "We saw some tears in the first month," he says, "but by the time we left, they didn't want to leave Paris." Finding a school is the first task for getting kids settled, and again, the locals in the lab you are visiting may be able to offer advice. Rothman adds, "If you are going to a country where you don't speak the language, try to find a bilingual school. The one our kids went to had a lot of visiting students, and knew how to give them a positive experience."

If you've been a tourist in the country where you are moving, working there will be less romantic and more realistic, but also more rewarding. Rothman says, "Living in a place is a very different experience from falling in love with it as a tourist, because you're dealing with day-to-day life. But that's one of the reasons to do it, to experience the real life of another culture." Küster-Schöck had traveled in the United States as a student but said, "living there required 'adult' skills, like renting a house, paying taxes, opening a bank account, and getting insurance. Finding new friends is hard work, and not any easier if you don't know the unwritten social rules in the new place. But we did find some very good friends."

LIFE AS A FOREIGNER

To get the most out of your time abroad, explore your new culture and see the sights. This doesn't necessarily mean traveling, though. It might mean just going out the front door. Eisenman says, "Japan had all these places we had always wanted to see, but in the end, we thought, 'why live out of suitcases when we have this great place in Tokyo?' By staying in our neighborhood, we got to know the people and the shops in our area, and saw what life on our street was like."

Chris Nomura also recommends diving into your new country, and welcoming the everyday surprises. He did a postdoc at the RIKEN Institute in Tokyo after getting a Ph.D from Penn State University. "Enjoy the cultural differences," he advises. As a fourth-generation Japanese American who had never been to Japan, he confronted a special set of these differences. "Most people assumed that I was Japanese, so when I told people, like train conductors, that I couldn't read a map, they would shake their head and say something like, 'kids these days....'" Still, he says, "You should try to learn the language. Even though my Japanese was less than stellar, just trying was appreciated."

Eisenman agrees. "Whenever I said something in Japanese, they'd laugh and I'd think I'd said something wrong, but then I realized they were laughing because they were surprised and pleased." Still, foreign scientists should be prepared for daily miscommunications. Eisenman says that misunderstandings occurred all the time, whether he was trying out his Japanese, or speaking in English, even though, in theory, everyone in the department he was visiting spoke English. "Sometimes I'd be talking to someone, thinking we were on the same page, but we weren't even in the same book!" he says.

STAYING IN TOUCH, AND GETTING AWAY

On the other hand, talking with colleagues at home was "almost too easy," says Eisenman. Global connectedness means professors on sabbatical can have daily contact with their lab, but may never truly get away. "Lab supervision was all by e-mail and Skype," he says. "Actually, 30 percent of my time in Tokyo was spent working on stuff for my lab in Seattle. People on sabbatical in my lab also say they spend a lot of time working on projects from home."

Kate Jackson also uses the reach of the Internet to connect with her research group. It is in the Republic of Congo, while her faculty office is in the United States. Jackson studies the amphibians and reptiles of Central Africa, so for her, sabbaticals abroad are absolutely necessary. Her multiple trips to the Congo are both inspiring and alarming to traveling scientists.

From Whitman College in Walla Walla, Washington, Jackson supervises herpetology graduate students at the Université Marien-Ngouabi in Brazzaville, Congo. Like Eisenman, she uses e-mail and Skype to keep in touch, long-distance. Fortunately, "the students can do a lot on their own," she says, and they'll need to. Jackson was slowed by malaria in 2008, and in 2009, she suffered spinal cord damage from "a virus I picked up in the Congo." She's currently working with a physical therapist so she can return to her Congolese group in summer 2010. This is only the latest hurdle she has overcome in doing research abroad. "How do I manage? By making every mistake possible," she says, "from mundane things like not having a specimen-collecting permit, to having to be evacuated by medical transport with a badly infected wound, to being bitten by a cobra. There was also a civil war once." Still, her advice is to persevere, because "it always seems to work in the end."

And it's absolutely worth it, she says. If you are interested in doing field science in a remote area, she says, "Just go there, that's how I learned." Like Jackson, you might make a connection that brings you back. She says, "I went for the animals, and didn't expect to have any interest in the people, but now I feel like I'm needed by the animals *and* by the people."

Even if you are not looking for an Indiana Jones experience, a sabbatical or postdoc overseas can be an adventure. continued »

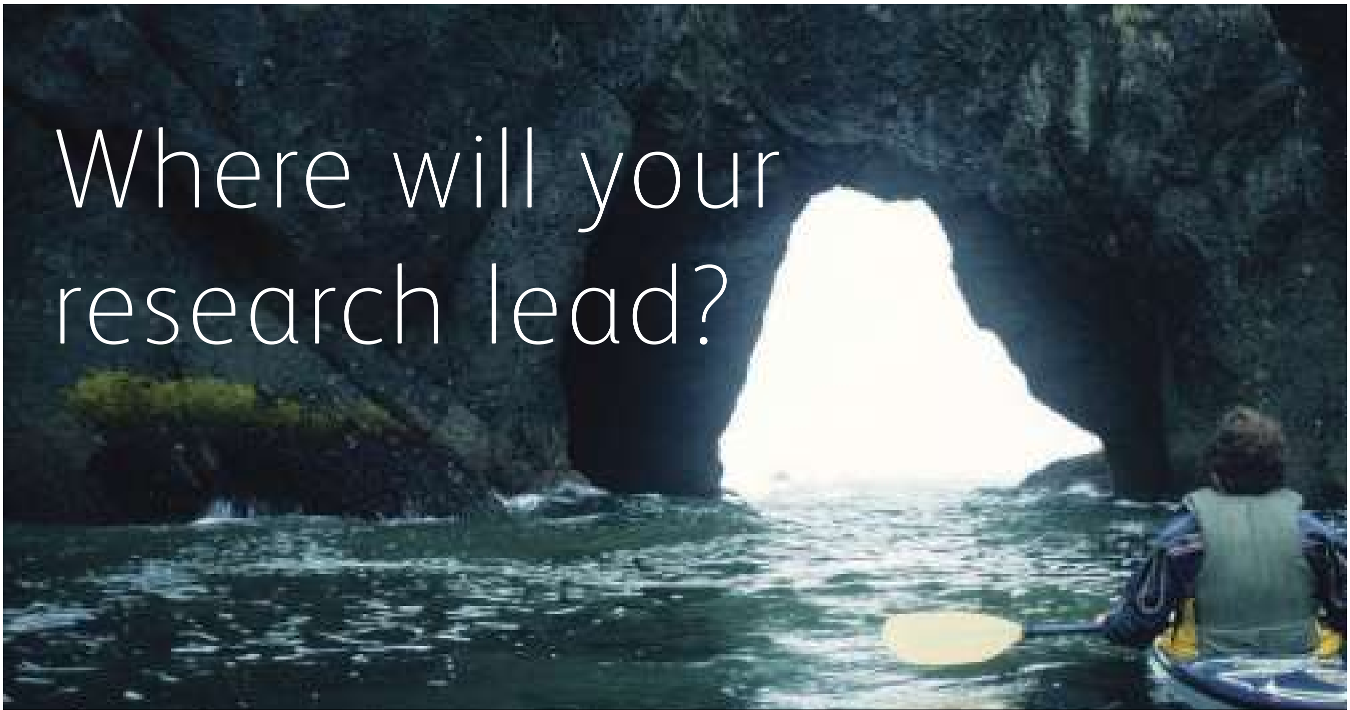

Postdoctoral Program

The Pfizer Research and Development organization is launching an ambitious postdoctoral training program that encompasses its Research, Biotech, and Technology Units. We are recruiting highly motivated Ph.D. recipients with a demonstrable track record of scientific productivity during their graduate training. Ideal candidates will express a passion for creative research that facilitates the translation of novel biological or technological advances into innovative therapies for human diseases. Postdoctoral positions are available in the following areas:

INFLAMMATION AND IMMUNOLOGY
METABOLIC DISEASES
OLIGONUCLEOTIDE-BASED THERAPIES
HIGH-CONTENT CELL-BASED SCREENING
ANTIBODY-PROTEIN ENGINEERING
VACCINE RESEARCH
ONCOLOGY
PHARMACEUTICAL SCIENCES
PROTEOMICS
MUSCULOSKELETAL BIOLOGY
STRUCTURAL BIOLOGY
PHARMACOKINETICS, DYNAMICS AND METABOLISM
MEDICINAL/ORGANIC CHEMISTRY
NEUROSCIENCE

The Pfizer Research and Development organization strives to deliver innovative medicines that improve the lives of patients world-wide. Our postdoctoral program is designed to provide the research foundation that will lead to future improvements in disease therapy, while at the same time offering our trainees an exceptional career-building experience in the biomedical sciences. Our trainees perform cutting-edge research leading to publications in top-tier journals, attend high-profile scientific meetings, and interact with well-known academic labs worldwide.

You may explore and apply for specific opportunities by visiting us online at: **www.pfizer.com/careers**

We are proud to be an equal opportunity employer and welcome applications from people with different experiences, backgrounds and ethnic origins.

Pfizer

Working together for a healthier world™

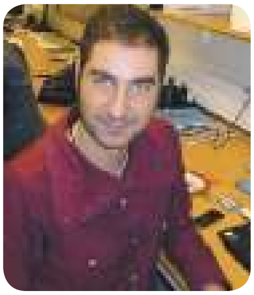

"We never really discussed going back, although sometimes during the winter, we question our choice."
— Gianni Panagiotou

FEATURED PARTICIPANTS

Danish Technical University
www.dtu.dk/English.aspx

European Institute of Business Administration
www.insead.edu

Fred Hutchinson Cancer Research
www.fhcrc.org

McGill University
www.mcgill.ca

Medical Research Council
www.mrc.ac.uk

MIT
www.mit.edu

Northwestern University
www.northwestern.edu

State University of New York
www.suny.edu

Université Marien-Ngouabi
www.univ-mngb.net (in French)

University of Tokyo
www.u-tokyo.ac.jp

Living in a new country, whether in an actual or an urban jungle, takes courage and persistence. "Doing a postdoc is hard work wherever you do it," says Küster-Schöck. "You will be a newcomer to the lab, the institution, and maybe the field and techniques. Throw in a new city, country, and culture, and it can be pretty tough. But, as clichéd as it may sound, getting through that can be one of the best learning experiences of your life."

COMING HOME…

Postdocs who want to return to their home country can easily apply for jobs online, although interviewing takes a little advance planning. From his postdoc in Japan, Nomura found a faculty position in the United States, at the State University of New York, College of Environmental Science and Forestry. "I either went to interviews in the United States after attending a conference there, or was flown out by the university to interview," he says. "I do believe, though, that it is extremely difficult to get an interview in the United States if you are based overseas, unless you have something that your employer really wants." In general, though, overseas applicants are not at a disadvantage. Rothman says, "Having run faculty searches for many years here at UCSB, I don't think it matters where you are coming from."

That said, Rothman notes that working in England meant he missed out on some practical training about US science that he would have gotten at an American university, like how to write an effective US grant application, and how graduate students are funded. However, he says, "That was far outweighed by the richness of my experience as a postdoc."

…OR NOT COMING HOME

Especially for postdocs, a temporary move can turn permanent. Nomura met his wife in Japan, and says he would have stayed for the right job opportunity. After doing postdoctoral fellowships in the United States, Küster-Schöck and her husband expected to go back to Germany, but instead went to McGill University in Canada, where he got a faculty position, and she did a second postdoc before becoming manager of the university's proteomics and genomics facilities. This meant another international move, this time with a baby, but Küster-Schöck is now settled into her second new home. "At this point, I would probably have trouble fitting in, in Germany," she says.

No one has embraced a new country as thoroughly as **Gianni Panagiotou,** who visited the Danish Technical University (DTU) as a Ph.D. student from the National Technical University of Athens, Greece. Originally attracted by the state-of-the-art laboratory facilities, he found that Scandinavia suited him, and he stayed for his postdoc. He is now an associate professor at DTU, where his girlfriend, **Irene Kouskoumvekaki,** is an assistant professor. She is also from Greece, although the couple first met in Denmark. "We never really discussed going back," says Panagiotou, "although sometimes during the winter, we question our choice." To adapt to a new land, Kouskoumvekaki says, "Don't judge things in the new country based on where you came from. It's a new situation and you can't make comparisons." Scientists moving temporarily abroad may be tempted to stay, advises Panagiotou, so just in case, "have a big party with all your friends and family before you leave."

CREATIVE BENEFITS

No matter where you end up, working abroad may have subtle scientific and personal benefits. Researchers at Northwestern University in the United States and INSEAD (European Institute of Business Administration) business school in France found that people who had lived abroad and successfully adapted to the foreign culture showed enhanced creativity in problem solving. Returning postdocs and sabbatical professors may find that overcoming the challenge of living in a new society ends up boosting their creative skills, inside and outside of the lab. "Working in another country gives you ideas and experiences that you can't get by staying in one place," says Kouskoumvekaki. Some things will be stressful, she notes, but "the excitement is bigger than any of the negatives, so just go for it."

Chris Tachibana is a science writer based in Seattle, USA, and Copenhagen, Denmark.

DOI: 10.1126/science.opms.r1000092


life

IASS
Institute for Advanced Sustainability Studies e.V., Potsdam, Germany

Two Post-doctoral Positions at the IASS

(IASS/2010/PhD/EEE)

Closing date: September 10th, 2010

The Institute for Advanced Sustainability Studies (IASS) is a newly formed Institute located in Potsdam and engaged in fundamental Energy and Environmental Research both from the theoretical and the experimental perspectives. One of its main activities will be the creation of the Earth, Energy and Environment (E^3) section under the responsibility Prof. Carlo Rubbia, the recently appointed IASS Scientific Director.

Among the scientific programmes on Energy and Environmental Research which will be hosted in IASS under the E^3 tasks, will feature (a) the transformation of natural gas into hydrogen without CO_2 emissions, (b) the production of synthetic methanol as a substitute to oil for transport, (c) the properties and applications of natural methane calthrates, (d) advanced concepts of concentrating solar energy (CSP) and (e) the development of very long superconducting electric lines carrying electricity especially from distant, renewable energy sources.

We invite hereby applications for **two post-doctoral positions** within the international environment of the IASS Institute. Successful candidates are expected to operate in very close cooperation with the Scientific Director and support him in the creation of the teams for the five above mentioned specific subjects (a) to (e), each of them comprising several research fellows and in collaboration with other Institutions worldwide.

Required skills for candidates are **a PhD in physics and/or in chemistry** and a strong interest and eventually previous experiences in fields related to the above E^3 subjects. Good knowledge in nuclear and atomic physics, chemistry, instrumentation and computing are desirable.

The first candidate is expected to have an applied physicist training, having already acquired a significant role in the development of alternatives in the field of the future energy transformations with the aim toward effective de-carbonisation processes. Previous experience both in renewable energies for electricity production (d) and alternatives to transport (e) will be considered an asset. The candidate must also be fluent in the computer programming analysis and capable of using or eventually expanding sophisticated computer codes.

The second candidate is expected to have a training in chemistry, with the ability of developing in a quantitative and practical way models and scenarios with specific focus on the constituents involved in future de-carbonized alternatives, with special consideration of the afore mentioned activities (a) and (b). Previous experience will be considered an asset. He or she must demonstrate a great amount of flexibility and ingenuity in assessing various alternate options, like for instance the ones of (a) hydrogen from natural gas without CO_2 emissions, in order to produce (b) new methods for liquid de-carbonized substitutes to gasoline, eventually combined with already processed CO_2, in alternative to CCS (Carbon Capture and Sequestration). The candidate should also be fluent in thermo-dynamical data computing simulations of specific compounds.

Both candidates may contribute to the different aspects of the above mentioned novel activity related to (c), properties and applications of natural methane calthrates.

Both candidates should jointly play the role of an effective interface between the IASS Scientific Director and the E^3 related teams and the research fellows which will be successively be hired and eventually with other collaborating Institutions.

They will work as team-players in a stimulating international environment in this small and newly formed Scientific Organization, giving excellent opportunities for new initiatives and innovative research.

Salary and benefits are according to the German public service pay scale E 14 TVöD Bund (annual gross income: €42.000-€60.000 depending on employment scale). The contracts are initially limited to three years with the possibility of extension. Excellent knowledge of English is required, German language is welcome, but it is not a necessary prerequisite, since most of the professional activities will be pursued at the international level. The Institute For Advanced Sustainability Studies (IASS) is an equal opportunity employer.

Interested applicants should send an application letter including curriculum vitae, list of publications, a statement on research interests and two letters of recommendation, to arrive not later than Friday, September 10th, 2010 at the following address (both in hard copy and e-mail):

IASS, Institute for Advanced Sustainability Studies e.V.
Kleist-Villa, Berliner Str. 130, 14467 Potsdam
T. +49(0)331-20194-19
e-mail: delia.salmieri@cern.ch
(application documents will only be returned if a postpaid envelope is attached)

For further information regarding the position please contact Dr. Delia Salmieri (delia.salmieri@cern.ch), T. +41 22 7676338.

UNIVERSITY OF LIVERPOOL

Faculty of Science and Engineering
School of Physical Sciences
Department of Chemistry

Postdoctoral Researcher (Molecular Electronics)

£30,747 - £35,646 pa

You will join an interdisciplinary team to carry out a wide-ranging study of the effect of the environment on the properties of metal / single molecule / metal junctions, employing scanning tunnelling microscopy-based methods developed by the group. You should have a PhD in experimental physical chemistry and experience of scanning tunnelling microscopy, and/or of single molecule electrical property determination. You will have demonstrated the ability to produce high quality published scientific work. Excellent verbal and written communication skills would be an advantage, as would some familiarity with theoretical methods employed in this field. The post is available for 2 years.

Job Ref: R-572886/S **Closing Date: 1 September 2010**

For full details, or to request an application pack, visit www.liv.ac.uk/working/job_vacancies/ or e-mail jobs@liv.ac.uk Tel 0151 794 2210 (24 hr answerphone) please quote job ref in all enquiries.

COMMITTED TO DIVERSITY AND EQUALITY OF OPPORTUNITY

Stonewall DIVERSITY CHAMPION

POSITIVE ABOUT DISABLED PEOPLE

Work that makes a difference.

Opportunities that expand your horizons.

Teammates who share your values.

Are you ready for what's next in your career? At Booz Allen Hamilton, our ability to help clients solve their most challenging problems and achieve success in their most critical missions hinges on our people. Which is why we hire staff with great minds and a passion for making a difference, and provide them with ongoing learning opportunities, a vibrant team-based culture, a comprehensive rewards package, and the chance to make an impact in our firm, in our communities, and for our nation.

If you have strong problem-solving and consulting skills, deep technical knowledge, and a dedication to client service, Booz Allen could be what's next in your career.

The following opportunities—and many others—are available in Washington, DC:

- Alternative Energy Specialists
- Energy Efficiency Engineers
- Energy Storage Specialists
- Grid/Smart Grid Engineers
- Microbiologists
- Power Electronics Engineers

If you're ready for what's next in your career, e-mail your resume to Kimberly Douthit at douthit_kimberly@bah.com.

Ready for what's next. www.boozallen.com/careers

We are proud of our diverse environment, EOE/M/F/D/V. Applicants selected will be subject to a security investigation and may need to meet eligibility requirements for access to classified information.

Booz | Allen | Hamilton

strategy and technology consultants

NATIONAL RESEARCH COUNCIL

OF THE NATIONAL ACADEMIES

Research Associateship Programs

Graduate, Postdoctoral and Senior Research Awards

offered for research at

US Government Laboratories and affiliated institutions

Opportunities for graduate, postdoctoral and senior research in all areas of science and engineering

- Awards for independent research at over 100 participating laboratory locations
- 12-month awards renewable for up to 3 years
- Annual stipend $42,000 to $75,000 - higher for senior researchers; graduate entry level stipend is $30,00 and higher for additional experience
- Relocation, professional travel, health insurance
- Annual application deadlines Feb. 1, May 1, Aug. 1, Nov. 1
- Open to US and non-US citizens

Detailed program information, including instructions on how to apply online, is available on the NRC Web site at :

www.nationalacademies.org/rap

Applicants must establish dialogue with Advisors at the Lab(s) prior to application deadline.

Questions should be directed to the :

National Research Council

TEL: (202) 334-2760

E-MAIL: rap@nas.edu

Qualified applicants will be reviewed without regard to race, religion, color, age, sex or national origin.

THE NATIONAL ACADEMIES

Advisers to the Nation on Science, Engineering, and Medicine

SIR HENRY WELLCOME POSTDOCTORAL FELLOWSHIPS

Sir Henry Wellcome Postdoctoral Fellowships provide a unique opportunity for the most promising newly qualified postdoctoral researchers to work in the best laboratories in the UK and overseas.

Awards provide £250 000 over four years.

To apply, you must have no more than 12 months' postdoctoral experience on submission of a full application.

Preliminary applications must be received by 1 November 2010.

Further information is available at **www.wellcome.ac.uk/shwpf/science**

Applications are now invited.

The Wellcome Trust is a global charity dedicated to achieving extraordinary improvements in human and animal health (a charity registered in England and Wales, no. 210183).

wellcometrust

SANFORD HEALTH

Postdoctoral Fellow Positions
The Sanford Project

The Sanford Project, an emerging translational research center focused on type 1 diabetes (T1D), seeks postdoctoral fellows to join their team at Sanford Research/University of South Dakota. Concentrating on beta cell regeneration and autoimmunity, the Sanford Project (*Nature Reviews Drug Discovery,* **9:** 187-188, 2010; *Science,* **327:**520-521, 2010) is funded by Sanford Health, a $400 million gift to Sanford Health by Denny Sanford, a $10 million donation from the Todd & Linda Broin family, and by extramural funding. The positions are located at the new Sanford Research Center (300,000 sq ft) in Sioux Falls, SD. An established collaboration with the Sanford-Burnham Institute for Medical Research in La Jolla, CA provides for an integrated, world class, academic research environment.

Postdoctoral Fellows in **Dr. Zhiguang Guo's** laboratory will study disease underlying autoimmune and beta cell regenerative mechanisms in mouse models of T1D (*Endocrinology*, **151:**3049-3060, 2010) and investigate the molecular mechanisms involved in human beta cell regeneration in a transplanted mouse models. A Ph.D. or M.D. degree with background in immunology, beta cell regeneration, or cellular and molecular biology is required. Experience in T1D research, autoimmunity, beta cell biology, or islet transplant models are a definite plus.

Postdoctoral Fellows in **Dr. Chen-Shian Suen's** laboratory will be involved in designing, evaluating and developing novel therapies for T1D that target several novel G protein-coupled receptors (GPCRs) involved in the regulation of incretin and insulin secretion, beta cell regeneration, and autoimmune and inflammatory processes. A Ph.D. with experience in cellular endocrinology and/or *in vivo* pharmacology is required along with the ability to conduct independent research and the understanding of incretin hormone actions.

Postdoctoral Fellows funded by DOD and NIH grants in **Dr. Da-Qing Yang's** laboratory will study translational regulation of the p53 tumor suppressor in response to DNA damage (*Oncogene,* **25:** 4613-9, 2006; *Gene,* **395:**1-7, 2007; Pubmed keywords, Yang DQ and translation). Experience in studying insulin signal transduction and/or animal models of cancer and diabetes is a plus. The successful candidates should have a Ph.D. in biomedical sciences or related areas.

Additional information and position details can be requested by contacting the respective Principle Investigator. Zhiguang Guo (**Zhiguang.Guo@sanfordhealth.org**), Dr. Chen-Shian Suen (**Chen.Suen@sanfordhealth.org**) and Dr. Da-Qing Yang (**Daqing.Yang@sanfordhealth.org**).

Application materials should include: detailed curriculum vitae; cover letter; experience and expertise; and the names and contact information of three references. All applicants need to apply online at **https://sanfordhealthcareers.silkroad.com/** and refer to job **#216617** for **Dr. Guo's position**, **#216834** for **Dr. Suen's** position and **#216582** for **Dr. Yang's position**.

www.sanfordproject.org
www.sanfordhealth.org/Research/ResearchCenters/SanfordProject

SysCODE Systems-based Consortium for Organ Design & Engineering

The Systems-based Consortium for Organ Design and Engineering (**http://www.SysCODE.org**) is an NIH-funded Interdisciplinary Research Consortium that is using systems biology to build organ parts from stem cells. It involves scientific collaborations between stem cell biologists, genomicists, computational scientists, and tissue engineers. A joint, 2-year interdisciplinary postdoctoral fellowship position is available in the laboratories of Richard Maas, M.D, Ph.D. and Martha Bulyk, Ph.D., in the Division of Genetics, Department of Medicine at Brigham and Women's Hospital and Harvard Medical School. The goal is to use an ES cell directed differentiation system as a source of genomic data to construct transcriptional regulatory networks that can provide "instructions" for organ building. Applicants should have a strong background in cell and molecular biology, with experience in stem cell biology and/or ChIP-Seq or other types of genomic analyses.

Interested applicants should submit a cover letter, brief description of research interests, and CV to **Dr. Irina Agoulnik**: **Irina@SysCODE.med.harvard.edu**.

Brigham and Women's Hospital is an EEO, AA and VEVRAA Employer.

Postdoctoral Associate
Rewiring of Gene Expression in the Meiotic State

Stony Brook University's Center for Yeast Molecular Genetics and Cell Biology has postdoctoral associate positions available for work on a multi-investigator project to study the reprogramming of gene expression during meiosis and sporulation in the yeasts S. cerevisiae and S. pombe.

Possible research topics include:

- Antisense RNA regulation and the control of mRNA stability (Dr. Janet Leatherwood)
- Developmentally programmed changes in chromatin structure (Drs. Rolf Sternglanz and Aaron Neiman)
- Regulation of transcription factors by meiotic kinases (Dr. Nancy Hollingsworth)
- Rewiring of cell cycle transcriptional regulation from vegetative to meiotic cells; Mechanisms of cell cycle regulation and cell size control; co-ordination of energy metabolism and cell cycle progression. (Dr. Bruce Futcher).

For a full position description, application procedures, or to apply online, visit *www.stonybrook.edu/jobs* (JOBS Reference #: WC-S-6408-10-07-S, WC-S-6409-10-07-S, WC-S-6410-10-07-S and WC-S-6411-10-07-S)

Stony Brook University/SUNY is an equal opportunity/affirmative action employer.

STONY BROOK

UNIVERSITY OF ALBERTA
EDMONTON, ALBERTA, CANADA

www.careers.ualberta.ca

Professor and Scientific Director – Nano-Enabled Biomaterials for Sustainable Living Accelerator

The Faculty of Engineering, University of Alberta, in collaboration with the National Research Council National Institute for Nanotechnology (NINT), with $36.8 million in funding over six years through Alberta Innovates – Technology Futures, seeks a Scientific Director to define and lead a transformative research initiative in Nano-Enabled Biomaterials for Sustainable Living (NEBSL). The mandate is to advance and apply nanotechnology in order to create new biomaterials that can be used to address challenges and opportunities of significance to Alberta and globally. These materials may result from the programmed assembly of biomaterials, biomass conversion, and/or the utilization of naturally occurring biomaterials. This could lead to the development of environmentally compatible, high performance, nano-biomaterials for environmental sensing and remediation, energy conversion, catalysis, health monitoring and regulation, bio-refining and conversion, and value-added applications.

The Scientific Director will be the key leader of the NEBSL initiative and be responsible for defining, implementing and executing the overall research and commercialization programs. Responsibilities include providing overall leadership and management of the NEBSL initiative, teaching at the undergraduate and graduate levels, conducting, publishing and commercializing research, and supervising graduate students and research, technical and administrative staff.

The successful candidate will have demonstrated success in defining and leading initiatives of this magnitude, an internationally-recognized proven record of research achievement including significant accomplishments in the commercialization of nanotechnology advances, and hold a PhD degree in a discipline appropriate to the NEBSL initiative.

The successful candidate will be appointed at the rank of Professor with tenure in an appropriate Department within the Faculty of Engineering at the University of Alberta and will also be considered for nomination for a Canada Research Chair (Tier I) position. The NEBSL Scientific Director will have a formal association with NINT.

The University of Alberta and NINT offer extensive nanotechnology facilities and laboratories in an advanced nanotechnology research and educational environment representing an investment in excess of $250 million. The co-location of NINT on the University of Alberta campus enables seamless collaborations among faculty, industrial partners, postdoctoral fellows, and students on basic research through to commercialization outcomes.

Applications, including a statement of interest and vision, a curriculum vitae, a description of research and teaching interests, and the names and addresses (including email) of three referees, should be sent to:

Dr. David T. Lynch, Dean
Faculty of Engineering
E6-050 ETLC
University of Alberta
Edmonton, Alberta T6G 2V4
Canada
Email: nanobio@engineering.ualberta.ca

Review of applications will begin on September 1, 2010. However, the competition will remain open until the position is filled.

All qualified candidates are encouraged to apply; however, Canadians and permanent residents will be given priority. The University of Alberta hires on the basis of merit. We are committed to the principle of equity in employment. We welcome diversity and encourage applications from all qualified women and men, including persons with disabilities, members of visible minorities, and Aboriginal persons.

Alberta's TOP 50 EMPLOYERS 2010

MichiganTech

Faculty positions in Health

Michigan Technological University invites applicants for new tenure-track positions at any rank in the broad areas of health sciences and engineering. This campus-wide Strategic Faculty Hiring Initiative (SFHI) is projected to bring up to ten new faculty members to campus over a two year period to strengthen the key focus areas of biochemistry, bioengineering, bioethics, biomaterials, biomechanics, human factors, medical informatics, cell biology, physiology, and statistical genetics.

Faculty hired through this initiative are expected to establish a vigorous, nationally competitive research program and to be committed to excellence in both undergraduate and graduate education. The application review process will begin on October 1, 2010. Details on the SFHI and application instructions are available at **www.mtu.edu/sfhi**. More general information on Michigan Technological University is available at **www.mtu.edu**.

Michigan Tech is an internationally renowned doctoral research university located in Michigan's scenic Upper Peninsula, on the south shore of Lake Superior. Houghton provides a unique setting where natural beauty and exceptional year-round outdoor activities, culture, education, and a diversity of residents from around the world come together to share a superb living and learning experience. As part of its strategic focus, Michigan Tech is experiencing remarkable growth in research. In the last five years, research expenditures have doubled, up to $60M in 2008. The university has also recently initiated efforts to advance health-related research capabilities with the establishment of animal facilities and the formation of the Departments of Biomedical Engineering and Exercise Science, Health and Physical Education.

Michigan Tech is an ADVANCE institution, one of a limited number of universities in receipt of NSF funds in support of our commitment to increase diversity and the participation and advancement of women in STEM.

Michigan Technological University is an Equal Opportunity, Affirmative Action Employer/Educational Institution. Applications from women and minorities are encouraged.

VET TES TAM EN NOV VM
DEI SVB NVMINE VIGET

Faculty Position
Department of Molecular Biology
Princeton University

The Molecular Biology Department at Princeton University invites applications for a tenure-track faculty position at the Assistant Professor level in Developmental Biology. We are seeking an outstanding investigator using multicellular model systems to address fundamental questions in cell signaling, gene regulation, pattern formation, morphogenesis and/or pathogenesis. The University has a strong commitment to interdisciplinary studies, especially in the areas of systems biology, imaging, genomics, biophysics and neuroscience. The department has high level computing and microscope facilities, DNA array and high through-put sequencing technologies, mass spectrometry, modern transgenic mouse facilities and state of the art vivarium.

Applicants must have an excellent record of research productivity and demonstrate the ability to develop a rigorous research program. All applicants must have a Ph.D. or equivalent degree and a commitment to teaching at the undergraduate and graduate levels.

Applications must be submitted online at **http://jobs.princeton.edu**, requisition **#1000527**, and should include a cover letter, curriculum vitae, a two-page research description, and contact information for three references. All materials must be submitted as PDF files. For full consideration, applications should be received by **November 1, 2010**.

Princeton University is an Equal Opportunity Employer and complies with applicable EEO and affirmative action regulations.

NIMS ICYS

Research Position at ICYS, NIMS, Japan

The International Center for Young Scientists (ICYS) of the National Institute for Materials Science (NIMS) is now seeking a few researchers. Successful applicants are expected to pursue innovative research on broad aspects of materials science using most advanced facilities in NIMS **(http://www.nims.go.jp/eng/index.html).**

In the ICYS, we offer a special environment that enables young scientists to work independently based on their own idea and initiatives. All management and scientific discussions will be conducted in English. An annual salary between 5.03 and 5.35 million yen (level of 2009) will be offered depending on qualification and experience. The basic contract term is two years and may be renewed to one additional year depending on the person's performance. A research grant of 2 million yen per year will be supplied to the ICYS researcher.

All applicants must have obtained a PhD degree within the last ten years. Applicants should submit an application form, which can be downloaded from our web site, together with a resume (CV) and a list of publications. A research proposal on an interdisciplinary or integrated area related to the materials science should also be submitted. The application letter should reach the following address via e-mail or air mail by **October 15, 2010**. Visit our website for more details **(http://www.nims.go.jp/icys/newicys/).**

ICYS Administrative Office,
National Institute for Materials Science
Sengen 1-2-1, Tsukuba, Ibaraki 305-0047, Japan
E-mail: icys-recruit@nims.go.jp

UNIVERSITY OF WASHINGTON

Bacteriology Search: Tenure Track or Tenured Faculty
Department of Microbiology

The Department of Microbiology at the University of Washington in Seattle is conducting a search for an Assistant or Associate Professor in the fields of bacterial-host interactions and/or bacterial physiology. We are looking for an innovative investigator who currently has or will develop an independent research program studying bacterial pathogenesis, bacterial interactions with the immune system, mutually beneficial relationships between microbes and hosts, or bacterial physiology relevant to a variety of microbial systems. The position is a 12-month, full-time, tenure track position in the School of Medicine. In addition to research, the new faculty member will support the department's teaching mission, including teaching at the undergraduate or graduate level. All University of Washington Faculty engage in teaching, research and service.

Salary and benefits are competitive and will be commensurate with the qualifications and experience of the applicant. Applications from female and minority candidates are especially encouraged. Expanding opportunities for women and other underrepresented groups in the faculty is an important goal of the department.

Applicants with a Ph.D., 1-2 years postdoctoral experience and a strong publication record should send their CV, a one or two page statement of research interests and the names and contact information for three references to: **Chair, Bacteriology Search Committee, Department of Microbiology, Box 357242, Room K357B, University of Washington, 1705 N.E. Pacific Street, Seattle WA 98195**. Application materials may also be sent by email **c/o Bonnie Hightower** at **bbh@uw.edu**. Applications should be submitted by **September 15, 2010**, but search will remain open until the position is filled.

The University of Washington is an Affirmative Action, Equal Opportunity Employer and has built a culturally diverse faculty. Applications from female and minority candidates are especially encouraged.

Department of the Army
U.S. Army Medical Research and Materiel Command
U.S. Army Medical Research Institute of Chemical Defense

Science Director
$123,758 – 155,500

The U.S. Army Medical Research Institute of Chemical Defense (USAMRICD), the Department of Defense's premier research Institute for medical defense against chemical warfare agents and toxins located in the Edgewood Area of the Aberdeen Proving Ground, Maryland, is seeking to fill the new position of Science Director serving as the **DEPUTY COMMANDER FOR RESEARCH, GS-1301-15**. You will serve as the civilian scientific programmatic advisor to the Commander and will assist the Commander in setting the strategic direction and priorities for the Institute. In addition, you will be responsible for integrating the Institute's scientific and consultative activities with the growing interagency medical chemical defense programs for national defense by interfacing with DOD and other external agencies as required. The Deputy Commander for Research will be responsible for ensuring USAMRICD's continued leadership role in the field of chemical defense by facilitating the identification of the scientific staffing, infrastructure, and capital equipment investments required to support the scientific needs of a state-of-the-art, multidisciplinary research organization. Position may require up to 15% national/international travel.

Qualifications: A doctoral degree in Medicine, Veterinary Medicine, or related biomedical sciences, and at least 2 years direct research experience, and at least 10 years relevant experience in leading or developing a world-class research organization is required. Able to obtain and maintain a Secret Clearance. A successful candidate must be a U.S. citizen who is a recognized expert or global leader in one core area of biological research, yet must have a broad understanding of the biomedical sciences. Must have strong process orientation with the ability to understand the strategic and tactical links between basic research and early product development. Must have strong business and scientific perspectives, demonstrated ability to deliver results in a structured organization, and a solid background in the management of a technical organization. Excellent communication skills, both written and oral, strong project management skills, outstanding interpersonal relationship skills, and the ability to work cooperatively in a collaborative, multidisciplinary research environment must be demonstrated.

Interested applicants should apply at: **https://cpolwapp.belvoir.army.mil/public/vabSelfNom/index.jsp** AND send all of the following: a Curriculum Vitae with list of publications; copies of three major publications; a summary of research accomplishments; a statement describing their scientific management philosophy; and three letters of recommendation POSTMARKED BY **30 Sept 2010** to **LTC Deborah Whitmer, c/o DCR Search Committee, USAMRICD – 3100 Ricketts Point Road, Aberdeen Proving Ground, MD 21010-5400**.

Visit us on the web at: **http://usamricd.apgea.army.mil**. Visit APG: **http://www.apg.army.mil/apghome/sites/local**. RECRUITMENT and RELOCATION incentives. PCS is authorized.

Equal Opportunity Employer.

Tenure Track Positions (4th Term)
Nanoscience and Nanotechnology Research Center
Osaka Prefecture University, Osaka, Japan

Osaka Prefecture University is seeking application for two tenure track positions at the Nanoscience and Nanotechnology Research Center. This recruitment is being carried out under the "Leading University in the Region as a Base for Human Resource Development in Nanoscience and Nanotechnology" program. Applicants should hold a PhD degree acquired within the past 10 years; a track record of three or more years as an assistant professor, postdoctoral fellow or an equivalent title as of April 1, 2011; and excellent research achievements in the fields of nanoscience or nanotechnology.

- **Number of tenure track positions available:** Two tenure-track special lecturers.
- **Research areas:** A wide range of research areas related to nanoscience and nanotechnology.
- **Appointment duration:** From April 1, 2011 to March 31, 2016.
- **Annual salary:** Approximately 8,000,000 yen**.**
- **Research fund:** During the first fiscal year, 10,000,000 yen will be provided as a start-up fund, and from the second year onward, 5,000,000 yen per annum will be ensured.
- **Promotion to tenured associate professors:** Tenure track lecturers hired through this recruitment program will be promoted to tenured associate professors of Osaka Prefecture University—or tenured full professors if they have shown an excellent record of accomplishment—starting from April, 2016 after successfully passing the final evaluation. In such cases, those who have been promoted may be positioned to their preferred department and faculty at the university.
- **Submission deadline:** September 29, 2010, 5 p.m. Japan Standard Time. All documents must be submitted online through our website by the deadline, with hard-copy documents to follow.

*Please refer to our official website below for a complete description of the position and application information.

http://www.nanosq.21c.osakafu-u.ac.jp/
http://www.nanosq.21c.osakafu-u.ac.jp/en/

One focus: join our shared commitment to improve the lives of cancer patients worldwide.

The innovative science of a leading American biopharmaceutical company plus the global assets of Takeda, Japan's largest pharmaceutical company, equal one global commitment to oncology.

Millennium: The Takeda Oncology Company is developing an extensive pipeline — among the top in oncology worldwide — with more than 17 compounds for a broad range of solid and hematological cancers.

Come to where lifesaving science meets lifechanging opportunities. At Millennium, you'll help develop breakthrough treatments that can make a difference in patients' lives. All in a dynamic, collaborative environment where you can be yourself — and do your best science. To learn more or apply, visit us at **millennium.com**.

Millennium has opportunities in the following areas:

- Clinical Development
- Clinical Quality Assurance
- International Regulatory
- Oncology Clinical Research
- Pharmacovigilance
- Regulatory CMC
- Regulatory Labeling & Compliance
- Regulatory Submission Management
- Regulatory Therapeutics
- Translational Medicine

Takeda MILLENNIUM THE TAKEDA ONCOLOGY COMPANY

Science 2009 TOP EMPLOYER

THE GEORGE WASHINGTON UNIVERSITY MEDICAL CENTER
WASHINGTON DC

THE GEORGE WASHINGTON UNIVERSITY SCHOOL OF MEDICINE AND HEALTH SCIENCES

FACULTY POSITION IN DEVELOPMENTAL NEUROSCIENCE

INSTITUTE FOR NEUROSCIENCE AND DEPARTMENT OF PHARMACOLOGY AND PHYSIOLOGY

The newly formed Institute for Neuroscience and the Department of Pharmacology and Physiology are accepting applications for a tenure-eligible faculty member at the rank of Assistant or Associate Professor with expertise in the field of Developmental Neuroscience. This position will be one of five added to the existing community of GWU neuroscientists as part of an initiative to expand research in developmental disorders including autism. We seek an investigator whose research focuses on development and plasticity of cerebral cortical circuitry. This individual will participate in medical and graduate education in the Department of Pharmacology and Physiology as well as the Institute for Biomedical Sciences.

Basic Qualifications: A terminal degree (Ph.D. or M.D.) in an appropriate discipline and substantial accomplishments in biomedical research as demonstrated by a significant number of first and/or senior author publications in outstanding peer-reviewed journals as well as initial success in obtaining external research support.

Preferred Qualifications: Preference will be given to candidates with a growing research program focused on cortical circuit assembly at the structural and physiological level in mouse or other genetically manipulatable mammalian models of human neuro-developmental disorders, or in mice with mutations of genes known to compromise cortical development and function. Integration of genetic analysis with optical imaging and physiological methods is encouraged. The successful candidate will participate in Institute for Neuroscience research activities including development of multi-investigator projects for extramural funding. Salary and start up funds will be commensurate with experience.

Application Procedure: Please send a complete curriculum vitae plus names and contact information for 3 references electronically to Anthony-Samuel LaMantia, Ph.D., Professor of Pharmacology and Physiology, Director, GWU Institute for Neuroscience at **phmasl@gwumc.edu**. PDF format is preferred and only complete applications will be considered.

Review of Applications will begin on September 1, and will continue until the position is filled.

The George Washington University, is an Equal Opportunity/Affirmative Action Employer.

Duke University School of Medicine

Tenure-track Faculty Position (Assistant/Associate/Full Professor)

Institute for Genome Sciences and Policy

Departments of Medicine and Molecular Genetics and Microbiology, Duke University Medical Center

Applications are invited for a tenure-track position at Duke University Medical Center. The position is a partnership of the Institute for Genome Sciences and Policy and the Departments of Medicine and Molecular Genetics and Microbiology. We are currently seeking individuals studying infectious diseases via the application of genome sciences to the host, microbial pathogens or commensals, or both. Existing areas of strength in the institute and departments include:

(1) infectious diseases and global health
(2) microbial pathogenesis (bacteriology, virology, mycology)
(3) mechanisms of host-pathogen interactions and innate immunity
(4) genomics and genetics of the host-pathogen interaction
(5) genomic signatures of infection.

Areas of particular interest include analysis of the microbiome in health and disease and the application of genetics and genomics to define mutations that confer resistance or susceptibility to infection or modulate therapeutic responses in humans.

Applications should include a curriculum vitae, a description of research accomplishment and plans for future research, and reprints of three representative publications. Applicants should also arrange to have three letters of recommendation submitted on their behalf. Application materials should be emailed as pdf files to: **IGSP.DOM.MGMSearch2010@duke.edu**

The deadline for receipt of applications is **October 15, 2010**.

Women and minorities are encouraged to apply. Duke University is an Equal Opportunity/Affirmative Action Employer.

St. Jude Children's Research Hospital
ALSAC • Danny Thomas, Founder
Finding cures. Saving children.

FACULTY POSITIONS DEPARTMENT OF HEMATOLOGY

The Department of Hematology, at St. Jude Children's Research Hospital, is seeking to fill faculty positions at the level of ASSISTANT and/or ASSOCIATE MEMBER. We are specifically seeking applicants whose research program is or will be focused on laboratory-based research in Hematology. Candidates with interests in erythropoiesis, stem cell biology, gene therapy, iron metabolism, or other areas in molecular hematopoiesis are encouraged to apply. Research plans that are either basic or translational science will be considered. An MD, PhD, or a combined degree is required.

The Hematology Department currently consists of ten faculty members who are engaged in clinical and laboratory research in sickle cell disease, thalassemia, hemophilia disorders, stem cell biology, gene therapy for blood and immune cell disorders, and other aspects of molecular hematopoiesis.

St. Jude offers a rich academic environment for laboratory-based research in Hematology with state-of-the-art resources for genomics, molecular bioinformatics, genetic animal models, cell and animal imaging, cell sorting and flow cytometry. We also have an active GMP-manufacturing facility, and other strong clinical resources. Numerous opportunities exist for interdisciplinary academic collaborations, both within the Department of Hematology and within the institution.

Interested individuals should send their CV and a brief description of their research plans to:

Brian Sorrentino, MD – Chair, Search Committee Chair
Hematology Faculty Search Committee, Department of Hematology
St. Jude Children's Research Hospital
262 Danny Thomas Place – MS #341
Memphis, TN 38105-3678
E-mail: Brian.sorrentino@stjude.org
Ph: (901) 595-2727

St. Jude is an Equal Opportunity Employer and a Drug-Free Workplace.

www.stjude.org

NATIONAL CENTRE FOR CELL SCIENCE

(An autonomous Institution of the Department of Biotechnology, Government of India)
NCCS Complex, Pune University Campus, Ganeshkhind, Pune - 411007,
Maharashtra, India.

Website : www.nccs.res.in Email: infonccs@giaspn01.vsnl.net.in
Ph: 25708000 Fax: 91(020)25692259

Advertisement No. Admn-2-2010

RESEARCH SCIENTISTS

National Centre for Cell Science (NCCS), Pune, invites applications from outstanding researchers at the level of Scientist D to pursue cutting edge research in the areas of Stem Cell Biology / Regenerative Biology / Neurobiology / Developmental Biology / System Biology / Translational Medicine / Computational Biology (for Computational Biologist position, preference will be given to candidates having experience in Cluster Computing & Management). The successful candidate is expected to have research interests that complement those of the NCCS's faculty, and to develop interdisciplinary research.

The incumbent must hold 1st class MTech / MD / MVSc / MPharm / MBiotech or PhD/ Corresponding degrees in other disciplines with original work as evidenced by patents or publications. Evidence of leadership with about 8 years experience in R & D.

For detailed advertisement and application format, please visit our website **www.nccs.res.in/admn-02A-2010.html**

Interested applicants holding Indian Citizenship may send their applications with CV and three reference letters to the following address.

The Director
National Centre for Cell Science
NCCS Complex, Ganeshkhind
Pune – 411 007
Maharashtra, India.
Phone : 91 20 25708121
Fax : 91 20 25692259
Email : gcmishra@nccs.res.in

The application, strictly in the prescribed format with all supporting documents, should reach NCCS within 6 weeks from the date of appearance of this advertisement.

Want to learn more about exciting and rewarding careers outside of academic/industrial research? View a roundtable discussion that looks at the various career options open to scientists across different sectors and strategies you can use to pursue a nonresearch career.

Now Available On Demand
www.sciencecareers.org/webinar

Nontraditional Careers: Opportunities Away From the Bench

Webinar

Produced by the *Science*/AAAS Business Office.

Science Careers
From the journal *Science* AAAS

BCM
Baylor College of Medicine

CHAIR
Department of Neuroscience

Baylor College of Medicine, a leader in academic medical research, seeks nominations and applications for the position of Chair of the Department of Neuroscience. This dynamic basic science department is comprised of 19 tenured and tenure track faculty focused on basic research programs in molecular, cellular, and systems plasticity, behavioral human brain imaging, learning, memory, and addiction using computational, electrophysiological and optical approaches. A multidisciplinary interdepartmental joint faculty currently has ~10 million/yr NIH funding and local philanthropy. The faculty are actively involved in major aspects of neurosensory function, CNS-imaging, neurogenetics, neurodevelopment, and neurobiology of disease. The College is looking for an outstanding scientist with an exciting vision for the future who will expand upon the tradition of excellence in research and medical, graduate and post graduate education in neuroscience. Leadership and the ability to create and sustain innovative collaborations with other basic and clinical departments in the College will be an important factor in the selection process.

Baylor College of Medicine is a private medical College with $335 million of federal research support, 14 active Ph.D. granting programs and multiple interdepartmental academic units that integrate both clinical and research missions. The College has undergone substantial growth in the past decade and has new leadership with a comprehensive plan to accelerate the next phase of growth and accomplishment.

Applicants should send a cover letter and curriculum vitae to: **Bert O'Malley, M.D., Chair, Neuroscience Chair Search Committee, c/o Rebecca Vahabzadeh, Office of the Senior Vice President & Dean of Research, Baylor College of Medicine, MS: BCM 109, One Baylor Plaza, Houston, TX 77030; Email: vahabzad@bcm.edu.**

Baylor College of Medicine is an Equal Opportunity/Affirmative Action Employer.

MEETINGS

6TH ANNUAL MEETING OF THE OLIGONUCLEOTIDE THERAPEUTICS SOCIETY

October 20-23, 2010

LAGUNA CLIFFS RESORT
DANA POINT | SOUTHERN CALIFORNIA

REGISTER NOW FOR EARLY BIRD PRICING!

Save $100 off the registration fee before September 8

www.otsannualmeeting.com

ABSTRACT SUBMISSION DEADLINE — AUGUST 27

Student Travel Grants Available

Send your abstract to: ots@eventinnovations.com

SESSIONS

- Aptamers
- Clinical Applications
- Genome-wide definition of the human transcriptome and posttranscriptional and posttranslational regulation of protein abundance
- Immunomodulatory Oligonucleotides
- Novel Approaches for RNA Targeting Oligonucleotide Applications: Non-coding and microRNAs
- Oligonucleotides and Stem Cells
- Preclinical Applications
- RISC-Based Mechanisms
- RNaseH-Based Mechanisms
- Splicing Applications

Visit www.otsannualmeeting.com for the full meeting agenda

OTS

CO-ORGANIZERS: Brett P. Monia, Isis Pharmaceuticals & John Rossi, City of Hope

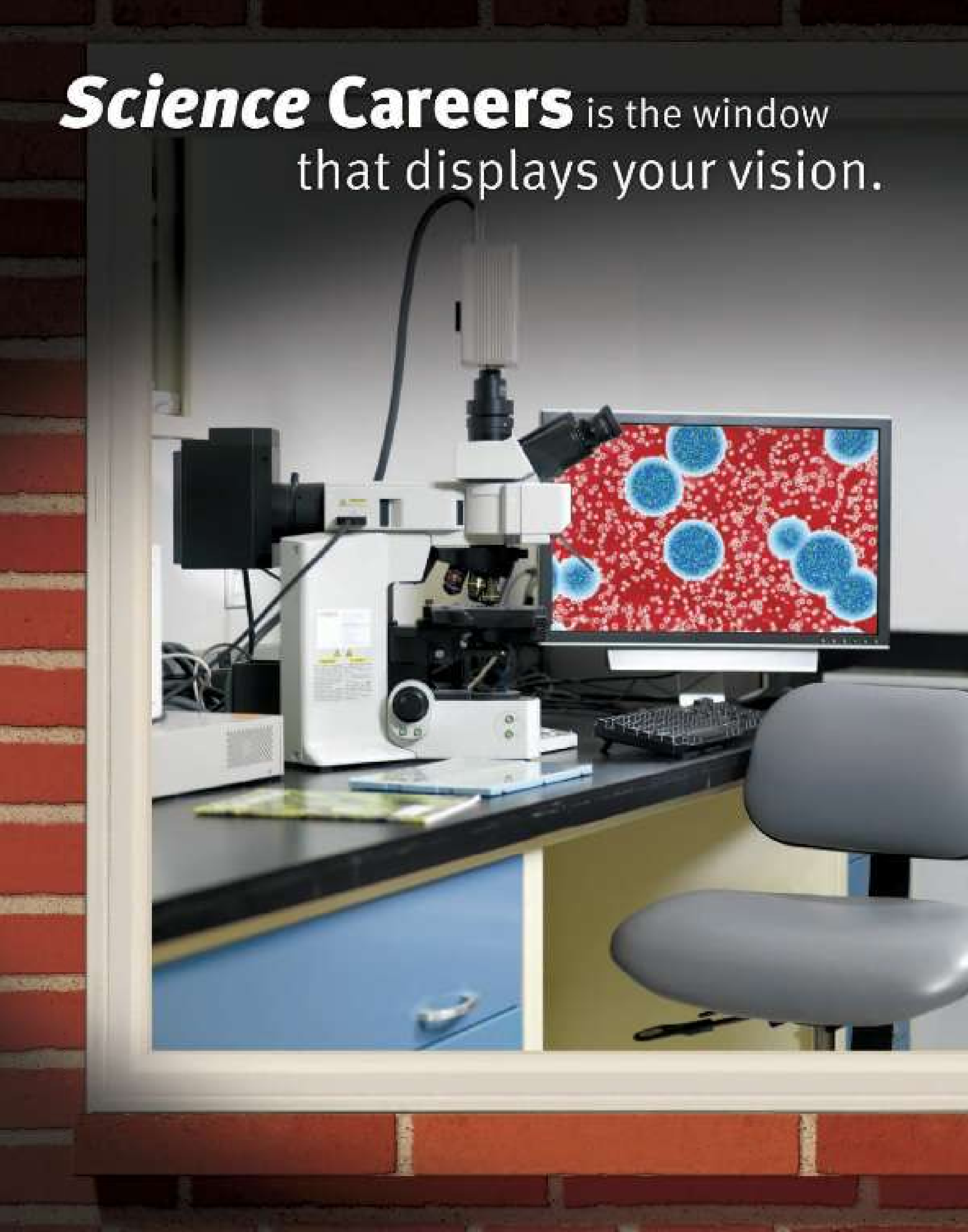
Science Careers is the window
that displays your vision.

POSTDOCTORAL OPPORTUNITIES

A **POSTDOCTORAL POSITION** is available in **Dr. Xiaolu Yang**'s laboratory at the University of Pennsylvania School of Medicine. The focus of the research is on apoptosis, tumor suppression, the promyelocytic leukemia nuclear bodies, and their relations to human disease (Recent publications: *Nature Cell Biology* **8:855**; *Molecular Cell* **31:415**; *Molecular Cell* **37:668**). Please send your curriculum vitae and contact information of three references to **e-mail: xyang@mail.med.upenn.edu.**

SIDNEY KIMMEL COMPREHENSIVE CANCER CENTER
Johns Hopkins University School of Medicine
Tumor Immunology/Immunotherapy

Two **POSTDOCTORAL FELLOWSHIP** positions are available in the laboratory of **Dr. Hyam Levitsky** (Departments of Oncology, Medicine, Urology, Immunology, and Cellular and Molecular Medicine). The first fellowship, supported by a newly funded National Cancer Institute (NCI) Center of Cancer Nanotechnology Excellence (CCNE), focuses on magnetic resonance imaging as a tool for the development of novel cancer vaccine strategies (**C.M. Long et al.,** *Cancer Research* **69(7):**3180–7, 2009). Close collaboration between immunologists, cell biologists, bioengineers, and radiologists provides a unique opportunity for career growth.

The second fellowship, supported by an NCI Program Project Grant in Bone Marrow Stem Cell Transplantation, focuses on modulation of anti-tumor immunity during immune reconstitution following BMT (**I.M. Borrello et al.,** *Blood* **114(9):**1736–45, 2009; **P. Mirmonsef et al.,** *Blood* **111(4):**2112–21, 2008). Basic mechanisms of host anti-tumor immunity as well as clinical translational objectives will be emphasized.

Successful candidates are required to have a recent Ph.D. in immunology, bioengineering, or related fields with a track record of publication in peer-reviewed journals and excellent verbal and written English skills. Experience with in vivo models of immunity preferred. Candidate with previous knowledge of in vivo imaging of cellular trafficking is not required but would be a plus. Please send a cover letter and curriculum vitae to **e-mail: hy@jhmi.edu.** *Equal Opportunity Employer.*

PLANT CELL WALL RESEARCH OPPORTUNITIES

The Center for Lignocellulose Structure and Formation (CLSF), an Energy Frontiers Research Center of the Department of Energy, announces several competitive awards (stipend and project costs) to support innovative, interdisciplinary **POSTDOCTORAL** research on plant cell walls in CLSF laboratories. Candidates are invited to develop a collaborative research project in conjunction with the CLSF research team which includes plant and microbial molecular biologists, biochemists, bio- and materials scientists, microscopists, and computational modelers at Pennsylvania State University, North Carolina State University, and Virginia Tech. Candidates must have a Ph.D. in life or physical sciences or related engineering discipline and a compelling research idea advancing CLSF research topics, which include: (a) how the cellulose synthase complex produces the cellulose microfibril, (b) how cellulose interacts with matrix polymers to make a strong network, and (c) how macroscale properties of the cell wall emerge from its nanoscale structure. See **website: http://www.lignocellulose.org** for more information about CLSF, its participating faculty, and how to apply for these research awards.

POSTDOCTORAL POSITION
Leukemia Stem Cell Genetics

Postdoctoral position available immediately at the University of Rochester, Department of Pathology, to investigate the genetics of leukemia stem cell function using a lentiviral shRNA screen, for which funding was just received. This is a great opportunity for a highly motivated young scientist to learn about high throughput screens to uncover critical pathways in leukemia stem cells. Please send curriculum vitae and names of three references to **A.S. Perkins**, M.D., Ph.D., at **e-mail: archibald_perkins@urmc.rochester.edu.**

POSITIONS OPEN

ASSOCIATE PROFESSOR
Tenure-track Research Position
Department of Ophthalmology
Hamilton Eye Institute
University of Tennessee Health Science Center

The Department of Ophthalmology at the University of Tennessee Health Science Center is seeking a research faculty to join our vision research group at the Hamilton Eye Institute. We are seeking an enthusiastic scientist that will fit into our current areas of strength: genomics, molecular biology of ocular trauma, glaucoma, or inherited eye diseases. Exceptional candidates in other appropriate fields will also be considered. The candidate should demonstrate a successful, vigorous, independent research program with extramural funding. Recruited faculty will receive generous startup support including ample research laboratory space. Applicants must have Ph.D. or M.D. degree and have completed postdoctoral training. Send curriculum vitae, statement of research interests, and the names of three references to: **Ophthalmology Recruiting Committee, c/o Mary Douglas, Department of Ophthalmology, 930 Madison Avenue, University of Tennessee HSC, Memphis, TN 38163.**

The University of Tennessee is an Affirmative Action/Equal Opportunity Employer and is an Equal Employment Opportunity/Affirmative Action/Title VI/Title IX/Section 504/ADA/ADEA Institution in the provision of its education and employment programs and services.

FACULTY POSITION
in Diabetes or Obesity

The Vanderbilt Diabetes Center and the Department of Medicine in the Vanderbilt University School of Medicine, is recruiting a tenure-track or tenured scientist (M.D. or Ph.D.) at the **ASSISTANT PROFESSOR, ASSOCIATE PROFESSOR,** or **PROFESSOR** level to conduct in vivo investigation in humans on diabetes, metabolism, or obesity. Vanderbilt has outstanding resources available for diabetes and obesity research, including the Vanderbilt Diabetes Research and Training Center and the new Vanderbilt Institute for Obesity and Metabolism. The Vanderbilt Institute for Clinical and Translational Research provides outstanding infrastructure support for translational research in humans. An extensive system of core laboratories is available to all investigators. Applicants should submit curriculum vitae and a concise statement of research plans. Please send information or direct any inquiries to:

Vanderbilt Diabetes Center
Telephone: 615-322-7990
E-mail: dc.brown@vanderbilt.edu

Vanderbilt University is an Equal Opportunity Employer. Women and minorities are encouraged to apply.

FACULTY POSITION

The Saint James School of Medicine, an international medical school (**website: http://www.sjsm.org**), invites applications from candidates with teaching and/or research experience in any of the basic medical sciences for its Caribbean campuses. Senior faculty positions are currently available in anatomy, pathology, and physical diagnosis. Applicants should be M.D., D.O., and/or Ph.D.

Teaching experience in the U.S. system is desirable but not required. Retired persons are encouraged to apply. Attractive salary and benefits. Submit curriculum vitae by **e-mail: info@sjsm.org** or mail to: **Human Resources Development Services Inc., 1480 Renaissance Drive, Suite 300, Park Ridge, IL 60068.**

RESEARCH ASSOCIATE
Cellular Technology, Ltd.

Research Associate, experience required. Send resume to **Resumes, Cellular Technology Ltd., 20521 Chagrin Boulevard, Shaker Heights, OH 44122.** Must refer to job code **LABGLP.**

Equal Opportunity Employer.

POSITIONS OPEN

LABORATORY MANAGER/GENETICIST

Laboratory manager needed for rapidly-growing, Boston-based company. Genetics, molecular biology experience required. Model organism/*Drosophila* experience preferred. Management/computer background a plus. Send curriculum vitae and references to **e-mail: geneticsmanagement@gmail.com.**

RESEARCH SCIENTIST/ENGINEER
Hitachi Chemical Research Center, Inc.

Hitachi Chemical Research Center, Inc. (HCR) is a research and development company directed toward novel technology platforms and related bio- or biomimetic materials for life sciences. HCR is a subsidiary of Hitachi Chemical Company, Ltd., a chemical manufacturer producing innovative technologies in the areas of electronics related products and advanced performance products.

In this multifaceted role as a researcher, you will utilize your technical skills and knowledge to create, develop, and direct your own project in the nanotechnology or nanomaterial fields. The goal is to develop polymer-based functional materials/composites to support human health and the environment. With the support of the business development group, you will understand the market value of your project and help guide it to commercialization.

HCR is hiring two Research Scientists with a background in biochemistry, polymer chemistry (including synthetic chemistry), and material sciences. In addition, we are looking for candidates with the following qualifications: a Ph.D.; an independent researcher who has demonstrated scientific creativity and technical proficiency in his/her field as evidenced by publications in top-tiered journals and presentations of work at relevant scientific conferences; advanced problem solving skills, excellent communication skills, and sound scientific judgment of complex issues; a strong background working with polymers/polymer composites. HCR offers competitive benefits and salary. Interested candidates can electronically send resumes to: **Ms. Lisa Osborn** at **e-mail: recruiting@hcrcenter.com** or **fax: 949-725-2727.**

Equal Opportunity Employer.

MARKETPLACE